RAMAN STUDIES OF THE CADMIUM CHLORIDE-ALKALI METAL CHLORIDES, LEAD CHLORIDE-CESIUM CHLORIDE AND LITHIUM CARBONATE-CESIUM CARBONATE SYSTEMS

JIANFANG WANG

RAMAN STUDIES OF THE CADMIUM CHLORIDE-ALKALI METAL CHLORIDES, LEAD CHLORIDE-CESIUM CHLORIDE AND LITHIUM CARBONATE-CESIUM CARBONATE SYSTEMS

by

© Jianfang Wang, B.Sc.

A thesis submitted to the School of Graduate
Studies in partial fulfillment of
requirements for the degree of
Doctor of Philosophy

Department of Chemistry
Memorial University of Newfoundland
St. John's, Newfoundland

November 1992

Abstract

Raman studies have been performed on following systems: $CdCl_2/CsCl$ and $CdCl_2/RbCl$ solids and melts; $CdCl_2/KCl$ solids; $PbCl_2/CsCl$ solids and melts; Li_2CO_3/Cs_2CO_3 solids; and Li_2CO_3/LiCl and Li_2CO_3/K_2CO_3 melts. The phase diagrams suggested by this work are in excellent agreement with the literature and the framework of the phase diagram for the Li_2CO_3/Cs_2CO_3 binary system has been reported for the first time.

The Raman spectra of the compounds with known structures have been discussed in terms of factor group analysis. It has been possible to characterize the Raman spectra for the discrete octahedrally coordinated cadmium, $CdCl_6^{4-}$ in Rb_4CdCl_6 and K_4CdCl_6 and the discrete tetrahedrally coordinated $CdCl_4^{2-}$ in Cs_3CdCl_5 and the high temperature phase of Cs_2CdCl_4. The Raman studies of the solids have provided useful reference frequencies to assist the analysis of the Raman studies of the molten salts.

In the $CdCl_2/CsCl$ binary system, a total of five compounds have been identified, three congruent: Cs_3CdCl_5, Cs_2CdCl_4, $CsCdCl_3$, and two incongruent: $Cs_3Cd_2Cl_7$ and $CsCd_5Cl_{11}$. Cs_3CdCl_5 is isostructural with Cs_3CoCl_5 and thermodynamically stable only above 390°C. Below 390°C Cs_3CdCl_5 decomposes into a mixture of Cs_2CdCl_4 and $CsCl$, but the sample quenched to room temperature from the melt may give a metastable Cs_3CdCl_5. Cs_2CdCl_4 has the K_2NiF_4 structure in the LTP (low temperature phase), but the salt undergoes a SPT (structural phase transition) at about 435°C to a β-K_2SO_4 type HTP (high temperature phase). The transition takes place over a temperature range from 435°C up to just below the melting point. At any temperature within this temperature range Raman bands for each of the separate phases may be detected simultaneously with relative intensities that are dependent of the temperature. Relative intensity measurements of bands characteristic of each cadmium coordination as a function of temperature indicated an equilibrium distribution. The enthalpy and entropy associated with the change of coordination were of the order of those usually observed on fusion. These large values

are consistent with the major structural rearrangement from a network octahedral structure to a discrete tetrahedral coordination. $Cs_3Cd_2Cl_7$ decomposes into $CsCdCl_3$ and Cs_2CdCl_4 at temperatures above 450°C. Raman spectra suggest that the Cd atom has octahedral coordination within a network structure for solids $Cs_3Cd_2Cl_7$ and $CsCd_5Cl_{11}$. $CsCdCl_3$ is hexagonal and there is no SPT from 25°C to the melting point.

For the $CdCl_2/RbCl$ and $CdCl_2/KCl$ solid systems, six compounds: Rb_4CdCl_6, Rb_2CdCl_4, $Rb_3Cd_2Cl_7$, $Rb_4Cd_3Cl_{10}$, $RbCdCl_3$ and $RbCd_5Cl_{11}$ in the $RbCl$ system; and two compounds: K_4CdCl_6 and $KCdCl_3$ in the KCl system have been identified. Both K_4CdCl_6 and Rb_4CdCl_6 contain discrete octahedral $CdCl_6^{4-}$ species. The other compounds have network structures with $CdCl_6$ local units and chloride bridges. Unlike $KCdCl_3$ and $CsCdCl_3$, the anhydrous $RbCdCl_3$ gave no intense peaks in the Cd-Cl stretching region of the Raman spectra and probably has an octahedral structure. When $RbCdCl_3$ was opened to the atmosphere it gave a different structure which is isostructural with NH_4CdCl_3 and $KCdCl_3$. The discrete tetrahedral $CdCl_4^{2-}$ structure is favored by larger and more polarization alkali cations and higher temperature.

In the $CdCl_2/CsCl$, $CdCl_2/RbCl$ and $PbCl_2/CsCl$ melts, the tetrahedral structure was indicated. As the $Cl^-/M^{2+} \geq 4$ ($M^{2+} = Cd^{2+}$ and Pb^{2+}) the discrete tetrahedral MCl_4^{2-} species were the principle species present, while as $Cl^-/M^{2+} < 4$ short-lived tetrahedral units with bridge structures were suggested. Exchange processes were too fast to permit detection of separate peaks for the discrete tetrahedron and the bridge species. Raman spectra indicate that the bond strength between Pb^{2+} and Cl^- ions is much weaker than that between Cd^{2+} and Cl^- ions.

For the Li_2CO_3/Cs_2CO_3 system, only a congruent compound $LiCsCO_3$ has been identified and the compound forms eutectic mixtures with Li_2CO_3 or Cs_2CO_3. This compound $LiCsCO_3$ undergoes a SPT at about 435°C. The quenched sample from the melt to room temperature may give a metastable HTP which is stable for a long time at room temperature or even 77K. Unlike the SPT in Cs_2CdCl_4, there is no dynamic equilibrium

between the HTP and the LTP, but the transition is kinetically sluggish. Raman analysis indicates that the SPT in $LiCsCO_3$ is associated with the rotation of CO_3^{2-} in the primitive unit cell. The carbonate ion in molten alkali metal carbonates was found to be relatively unperturbed by the cations.

Dedication

To my parents and my son

ACKNOWLEDGEMENTS

I would like to express my warmest gratitude to my supervisor, Dr. Murray H. Brooker, for his helpful guidance and timely encouragement through the course of my research.

I am grateful to Dr. R.W. Davis, Dr. R.A. Poirier and Dr. F.R. Smith for their kind advice with my work. Sincere thanks to Gary Hancock, Bernie Rice and Jerome Johnson for their kind help in my studies.

I am most grateful to my parents for their encouragement and help to look after my son.

The financial support in the form of a Memorial graduate fellowship is grately acknowledged.

Table of contents

Abstract ..... (i)

Acknowledgements ..... (vi)

List of tables ..... (xi)

List of figures ..... (xiv)

Chapter 1 Introduction ..... (1)

1.1 Systems and Purposes ..... (1)

1.1.1 MX_2/AX ionic mixtures ..... (2)

1.1.2 A_2CO_3/B_2CO_3 ionic mixtures ..... (3)

1.2 General Analytical Methods ..... (5)

1.2.1 Determination of compound formation and phase equilibrium ..... (5)

1.2.2 Studies of structural phase transitions in solids ..... (9)

1.2.3 Studies of molten salts ..... (10)

1.3 Comparison with diffraction methods ..... (12)

Chapter 2 Theory ..... (14)

2.1 Raman scattering in non-interacting molecule ..... (14)

2.2 Raman scattering in crystals ..... (23)

Chapter 3 Experiments ..... (28)

3.1 Preparation of samples ..... (28)

3.1.1 $CdCl_2/ACl$ (A = Cs, Rb, K) and $PbCl_2/CsCl$ systems ..... (28)

3.1.2 $A_xB_{(1-x)}CO_3$ systems ..... (28)

3.2 Raman spectroscopic measurements ..... (29)

3.2.1 Solids ..... (29)

3.2.2 Temperature dependence of solids ..... (30)

3.2.3 Melts ..... (30)

Chapter 4 Raman studies on the structures and properties of the compounds formed in the $CdCl_2$/$CsCl$ binary system ..... (34)

4.1 Introduction ..... (34)

4.2 Results and discussion ..... (37)

4.2.1 Compound formation ..... (37)

4.2.2 Structures and properties ..... (40)

4.2.2.1 Compound Cs_2CdCl_4 ..... (40)

4.2.2.2 Compound $CsCdCl_3$ ..... (42)

4.2.2.3 Compound Cs_3CdCl_5 ..... (43)

4.2.2.4 Compounds $CsCd_5Cl_{11}$ and $Cs_3Cd_2Cl_7$ ..... (45)

Chapter 5 Raman studies of a dynamic phase equilibrium in solid Cs_2CdCl_4 ..... (58)

5.1 Introduction ..... (58)

5.2 Results and discussion ..... (59)

5.3 Conclusion ..... (70)

Chapter 6 Raman studies of the complex halides in the solid $CdCl_2$/$RbCl$ and $CdCl_2$/KCl systems ..... (79)

6.1 Introduction ..... (79)

6.2 Results and discussion ..... (81)

6.2.1 Compound formation ..... (81)

6.2.1.1 $CdCl_2$/$RbCl$ system ..... (81)

6.2.1.2 $CdCl_2$/KCl system ..... (84)

6.2.2 Structures and properties ..... (85)

6.2.2.1 K_4CdCl_6 and Rb_4CdCl_6 ..... (85)

6.2.2.2 Rb_2CdCl_4 ..... (87)

6.2.2.3 $KCdCl_3$ and $RbCdCl_3$ ..... (88)

6.2.2.4 $Rb_3Cd_2Cl_7$ ..... (91)

6.2.2.5 $Rb_4Cd_3Cl_{10}$ and $RbCd_5Cl_{11}$ ..... (93)

6.3 Summary ..... (93)

Chapter 7 Raman studies of the $CdCl_2$/CsCl and $CdCl_2$/RbCl molten systems ..... (112)

7.1 Introduction ..... (112)

7.2 Results and discussion ..... (114)

7.2.1 $CdCl_2$/CsCl melts ..... (114)

7.2.2 $CdCl_2$/RbCl melts ..... (119)

7.2.3 Pure $CdCl_2$ melt ..... (120)

7.3 Conclusion ..... (122)

Chapter 8 Raman studies of the $PbCl_2$/CsCl solid system ..... (138)

8.1 Introduction ..... (138)

8.2 Results and discussion ..... (140)

8.2.1 Compound formation ..... (140)

8.2.2 Structures and Properties ..... (142)

8.2.2.1 Cs_4PbCl_6 ..... (142)

8.2.2.2 $CsPbCl_3$ ..... (143)

8.2.2.3 $PbCl_2$ ..... (145)

Chapter 9 Raman studies of the $PbCl_2$/$CsCl$ molten system ..... (157)

9.1 Introduction ..... (157)

9.2 Results and discussion ..... (159)

9.2.1 $x \geq 0.67$ systems ..... (159)

9.2.2 Pure $PbCl_2$ and $x < 0.67$ systems ..... (162)

Chapter 10 Structural phase transition in $LiCsCO_3$ and phase equilibrium in the Li_2CO_3/Cs_2CO_3 system ..... (172)

10.1 Introduction ..... (172)

10.2 Results and discussion ..... (174)

10.2.1 Compound formation ..... (174)

10.2.2 Phase transition in $LiCsCO_3$ ..... (175)

10.2.2.1 Temperature dependent spectra of $LiCsCO_3$ ..... (176)

10.2.2.2 Raman spectra of the stable and metastable $LiCsCO_3$ at low temperature ..... (177)

10.2.3 Phase transition in $LiCsCO_3$ with excess Li_2CO_3 or Cs_2CO_3 ..... (180)

10.3 Conclusion ..... (181)

Chapter 11 Raman studies of the molten Li_2CO_3/LiCl and Li_2CO_3/K_2CO_3 systems ..... (205)

11.1 Introduction ..... (205)

11.2 Results and discussion ..... (206)

11.2.1 Li_2CO_3/LiCl melt ..... (206)

11.2.2 Li_2CO_3/K_2CO_3 melt ..... (207)

References ..... (221)

List of Tables

Table 4.1 The compounds suggested by several previous studies in the $CdCl_2$/CsCl binary system ..... (47)

Table 4.2 The Raman frequencies (cm^{-1}) of the characteristic bands in the Cd-Cl stretching regions and the corresponding suggested compounds in the $CdCl_2$/CsCl systems ..... (48)

Table 4.3 The vibrational frequencies (cm^{-1}) and tentative assignments of the bands observed for Cs_2CdCl_4 and Cs_3CdCl_5 ..... (49)

Table 4.4 The vibrational frequencies (cm^{-1}) of the bands for compounds $CsCdCl_3$ and $CsCd_5Cl_{11}$ ..... (50)

Table 5.1 Raman frequencies (cm^{-1}) and assignments for the different phases of Cs_2CdCl_4 ..... (71)

Table 5.2 The equilibria constants calculated from relative Raman intensities for the structural phase transition in solid Cs_2CdCl_4 ..... (72)

Table 6.1 The compounds identified by several previous studies on the $CdCl_2$/RbCl binary system ..... (95)

Table 6.2 The Raman frequencies (cm^{-1}) of the characteristic bands in the Cd-Cl stretching regions and the corresponding suggested compounds in the $CdCl_2$/RbCl systems ..... (96)

Table 6.3 The correlation diagram for K_4CdCl_6 ..... (97)

Table 6.4 The frequencies (cm^{-1}) of the bands observed from solids K_4CdCl_6, Rb_4CdCl_6, $Rb_3Cd_2Cl_7$, $KCdCl_3$ and $RbCdCl_3$ (II) at room temperature ..... (99)

Table 6.5 The Raman frequencies (cm^{-1}) for the bands in Rb_2CdCl_4 and

Cs_2CdCl_4 at room temperature ..... (100)

Table 6.6 The center frequencies (cm^{-1}) of the most intense bands and structures for some coordination compounds in the $CdCl_2/ACl$ (A = K, Rb, Cs) systems at room temperature ..... (101)

Table 7.1 The center frequencies (cm^{-1}) and the FWHH of the ν_1 and ν_3 bands, and the values of the calculated vibrational lifetimes of the complex ions for the $CdCl_2$/CsCl and $CdCl_2$/RbCl molten systems ..... (123)

Table 7.2 Several Cd-Cl symmetrical vibrational frequencies of possible coordinational states in the cadmium chloride alkali metal chloride binary system ..... (124)

Table 8.1 The Raman frequencies (cm^{-1}) of solid Cs_4PbCl_6 and $CsPbCl_3$ at several temperatures ..... (147)

Table 8.2 The Raman frequencies (cm^{-1}) of solid $PbCl_2$ ..... (148)

Table 9.1 The center frequencies (cm^{-1}) and FWHH based on the isotropic spectra of the polarized intense bands for the $PbCl_2/CsCl$ molten system ..... (165)

Table 9.2 The unperturbed vibrational frequencies (cm^{-1}) of isotopic CCl_4 ..... (166)

Table 9.3 The frequencies (cm^{-1}) of a model tetrahedral MCl_4 molecules obtained from the normal mode calculations based on the force constants of the CCl_4 molecule ..... (166)

Table 10.1 Raman frequencies (cm^{-1}) in the ν_1 region for the Li_2CO_3/Cs_2CO_3 binary system at 300K ..... (183)

Table 10.2 Raman frequencies (cm^{-1}) for $LiCsCO_3$ in the LTP and the

metastable HTP at 77K, 300K, 703K (LTP) and 713K (HTP) ..... (184)

Table 10.3 The phase transition temperatures for the compound $LiCsCO_3$ in the Li_2CO_3/Cs_2CO_3 binary systems ..... (185)

Table 11.1 The Raman frequencies (cm^{-1}) of the molten Li_2CO_3/LiCl and Li_2CO_3/K_2CO_3 mixtures ..... (209)

List of Figures

Fig. 1.1 The phase diagram of the $CdCl_2/KCl$ binary system ..... (8)

Fig. 3.1 The diagram of the Raman furnace ..... (32)

Fig. 3.2 The schematic representation of an experimental arrangement for Raman scattering from molten salts ..... (33)

Fig. 4.1 Examples of the structures of the three major possible coordination types of Cd^{2+} with Cl^- ions ..... (51)

Fig. 4.2 The phase diagram of the $CdCl_2/CsCl$ system ..... (52)

Fig. 4.3 Raman spectra obtained for the $CdCl_2/CsCl$ binary system with mole fractions of $CsCl$ 0.80, 0.75, 0.67, 0.60, 0.50 and 0.40 respectively ..... (53)

Fig. 4.4 Raman spectra obtained for the $CdCl_2/CsCl$ binary system with mole fractions of $CsCl$ 0, 0.14, 0.17, 0.20, 0.22, 0.25 and 0.33 respectively ..... (54)

Fig. 4.5 Raman spectra obtained for Cs_3CdCl_5 and Cs_2CdCl_4 in various phases ..... (55)

Fig. 4.6 Raman spectra observed for $Cs_3Cd_2Cl_7$ and $CsCdCl_3$ obtained with different cooling rates ..... (56)

Fig. 4.7 Raman spectra obtained from fast and slow cooled samples respectively for the x = 0.20, 0.17 and 0.14 samples ..... (57)

Fig. 5.1 Raman spectra obtained for pure Cs_2CdCl_4 at the temperatures indicated ..... (73)

Fig. 5.2 Raman spectra obtained for samples at different temperatures from the mixture Cs_2CdCl_4 + 1 $CsCl$ ..... (74)

Fig. 5.3 Raman spectra obtained for samples at different temperatures from the mixture $Cs_2CdCl_4 + 2CsCl$ ..... (75)

Fig. 5.2 Raman spectra obtained from the mixture Cs_2CdCl_4 +0.5CsCl at the temperatures indicated ..... (76)

Fig. 5.5 Raman spectra in the R(ω) format at selected temperatures to illustrate the baseline employed for the relative intensity calculations. ..... (77)

Fig. 5.6 The plot of ln JQ vs. 1/T for the phase transition of pure Cs_2CdCl_4 and mixtures with CsCl ..... (78)

Fig. 6.1 Phase diagram of the $CdCl_2/RbCl$ binary system ..... (102)

Fig. 6.2 Raman spectra observed for the $CdCl_2/RbCl$ solid systems with x from 0.80 to 0.56 ..... (103)

Fig. 6.3 Raman spectra observed for the $CdCl_2/RbCl$ solid systems with x from 0.50 to 0.17 ..... (104)

Fig. 6.4 Raman spectra observed for the slow and fast cooled samples with x = 0.80 and 0.56 to show the peaks due to incongruent compounds Rb_4CdCl_6 and $Rb_4Cd_3Cl_{10}$ ..... (105)

Fig. 6.5 Raman spectra observed for the slow and fast cooled samples with x = 0.63 and 0.60 to show the peaks due to incongruent compound $Rb_3Cd_2Cl_7$ ..... (106)

Fig. 6.6 Raman spectra of $RbCdCl_3$ (I) and (II) ..... (107)

Fig. 6.7 Raman spectra observed for the $CdCl_2/KCl$ binary system ..... (108)

Fig. 6.8 Raman spectra for samples at different temperatures for the compound Rb_2CdCl_4 ..... (109)

Fig. 6.9 Raman spectra for solids $CsCdCl_3$, $RbCdCl_3$, and $KCdCl_3$ at 25°C ..... (110)

Fig. 6.10 Raman spectra for solids $CsCdCl_3$, $RbCdCl_3$, and $KCdCl_3$ at 77K ..... (111)

Fig. 7.1 I(ν) Raman spectra for the molten $CdCl_2/CsCl$ system ..... (125)

Fig. 7.2 $R(\nu)$ Raman spectra for the molten $CdCl_2/CsCl$ system ..... (126)

Fig. 7.3 Isotropic Raman spectra for the molten $CdCl_2/CsCl$ system ..... (127)

Fig. 7.4 An example of the method used to obtain the isotropic spectrum (the example is for the Cs_2CdCl_4 melt) ..... (128)

Fig. 7.5 Raman spectra for the $AlCl_3/KCl$ melts [Φye 1971] ..... (129)

Fig. 7.6 Band resolution for the isotropic and depolarized spectra for the Cs_2CdCl_4 melt ..... (130)

Fig. 7.7 Band resolution for the isotropic spectra of the $CdCl_2/CsCl$ melts with x = 0.60, 0.56 and 0.50 ..... (131)

Fig. 7.8 I(ν) Raman spectra for the molten $CdCl_2/RbCl$ system ..... (132)

Fig. 7.9 $R(\nu)$ Raman spectra for the molten $CdCl_2/RbCl$ system ..... (133)

Fig. 7.10 Isotropic Raman spectra for the molten $CdCl_2/RbCl$ system ..... (134)

Fig. 7.11 Plots of FWHH vs. compositions for the $CdCl_2/CsCl$ and the $CdCl_2$/RbCl molten systems ..... (135)

Fig. 7.12 Raman spectra, $I(\nu)$, for solid $CdCl_2$ at different temperatures ..... (136)

Fig. 7.13 Raman spectra, $R(\nu)$, for solid $CdCl_2$ at different temperatures ..... (137)

Fig. 8.1 The phase diagram of the $PbCl_2$/CsCl binary system [Strukturbericht 1952] ..... (149)

Fig. 8.2 Raman spectra observed for the $PbCl_2/CsCl$ solid system (x = 0.83 to 0.60) ..... (150)

Fig. 8.3 Raman spectra observed for the $PbCl_2/CsCl$ solid system (x = 0.50 to 0) ..... (151)

Fig. 8.4 Raman spectra of the compounds Cs_4PbCl_6 and $CsPbCl_3$ at 25°C and 77K ..... (152)

Fig. 8.5 Raman spectra of Cs_4PbCl_6 at different temperatures ..... (153)

Fig. 8.6 Raman spectra of $CsPbCl_3$ at different temperatures ..... (154)

Fig. 8.7 Raman spectra, $I(\nu)$, of $PbCl_2$ at different temperatures ..... (155)

Fig. 8.8 Raman spectra, $R(\nu)$, of $PbCl_2$ at different temperatures ..... (156)

Fig. 9.1 Raman spectra observed from the $PbCl_2/CsCl$ molten system ..... (167)

Fig. 9.2 The $R(\nu)$ Raman spectra for the $PbCl_2/CsCl$ molten system ..... (168)

Fig. 9.3 Isotropic reduced Raman spectra for the $PbCl_2/CsCl$ molten system ..... (169)

Fig. 9.4 The plot of the characteristic vibrational frequencies of tetrahedral MCl_4 molecules verse the M-Cl distance ..... (170)

Fig. 9.5 The band resolution of the isotropic Raman spectra for the $PbCl_2$/CsCl melts with x = 0.50, 0.60 and 0.67 ..... (171)

Fig. 10.1 Raman spectra in the ν_1 region for the Li_2CO_3/Cs_2CO_3 binary system ..... (186)

Fig. 10.2 The framework of the phase diagram for the Li_2CO_3/Cs_2CO_3 binary system ..... (187)

Fig. 10.3 The plot of the intensity of the ν_1 band due to the LTP during SPT in $LiCsCO_3$ vs. time. ..... (188)

Fig. 10.4 Raman spectra obtained from the stable and metastable $LiCsCO_3$ at 77K ..... (190)

Fig. 10.5 Raman spectra obtained from the stable and metastable $LiCsCO_3$ at 25°C ..... (192)

Fig. 10.6 Raman spectra in the external mode region for the $LiCsCO_3$

system at different temperatures ..... (193)

Fig. 10.7 Raman spectra in the ν_1 region for the $LiCsCO_3$ system at different temperatures ..... (194)

Fig. 10.8 Raman spectra in the ν_3 region for the $LiCsCO_3$ system at different temperatures ..... (195)

Fig. 10.9 Raman spectra in the ν_4 region for the $LiCsCO_3$ system at different temperatures ..... (196)

Fig. 10.10 Raman spectra obtained from $LiCsCO_3$ at 430 and 440°C respectively ..... (198)

Fig. 10.11 Raman spectra in the ν_3 region for $LiCsCO_3$ in the LTP and the metastable HTP at 77K and 298K respectively ..... (199)

Fig. 10.12 Raman spectra in the ν_4 region for $LiCsCO_3$ in the LTP and metastable HTP at 77K and 298K respectively ..... (200)

Fig. 10.13 Raman spectra in the external mode region for $LiCsCO_3$ in the LTP and the metastable HTP at 77K and 298K respectively ..... (201)

Fig. 10.14 Raman spectra in the external mode region for the $LiCsCO_3 + Cs_2CO_3$ mixture ..... (202)

Fig. 10.15 Raman spectra in the ν_1 and ν_4 regions for the $LiCsCO_3 + Cs_2CO_3$ mixture ..... (203)

Fig. 10.16 Raman spectra in the ν_3 region for the $LiCsCO_3 + Cs_2CO_3$ mixture ..... (204)

Fig. 11.1 Raman spectra ($I_{\parallel}$, $I_{\perp}$ and I_{iso}) of the molten Li_2CO_3/LiCl mixture ..... (211)

Fig. 11.2 Raman spectra ($R_{\parallel}$, $R_{\perp}$ and R_{iso}) of the molten Li_2CO_3/LiCl mixture ..... (213)

Fig. 11.3 Curvefit for the isotropic (R_{iso}) and anisotropic (R_{aniso}) components of the ν_1 band for the Li_2CO_3/LiCl melt by a Lorentzian function ..... (214)

Fig. 11.4 The ten times scale expanded reduced Raman spectra of the molten Li_2CO_3/LiCl and Li_2CO_3/K_2CO_3 melts ..... (215)

Fig. 11.5 Raman spectra ($I_{\parallel}$, $I_{\perp}$ and I_{iso}) of the molten Li_2CO_3/K_2CO_3 mixture ..... (217)

Fig. 11.6 Raman spectra ($R_{\parallel}$, $R_{\perp}$ and R_{iso}) of the molten Li_2CO_3/K_2CO_3 mixture ..... (219)

Fig. 11.7 Curvefit for the isotropic (R_{iso}) and anisotropic (R_{aniso}) components of the ν_1 band for the Li_2CO_3/K_2CO_3 melt by a Lorentzian function ..... (220)

Chapter 1

INTRODUCTION

1.1 Systems and Purposes

Vibrational spectroscopic studies of inorganic materials have several major purposes: 1) the identification of ionic or molecular species in a particular environment; 2) the determination of the structure of such species; 3) the deduction of qualitative and quantitative information about intramolecular and intermolecular forces related to physical and chemical properties of the materials. The frequencies, intensities, bandshapes and polarization characteristics of the bands are usually measured as a function of concentration, temperature, and pressure. Often, the interpretation of the spectra may be aided by studies of the same system in the solid, glassy, molten, vapor and aqueous phases. In this thesis, the Raman spectroscopic studies for some ionic mixtures in the solid and molten phases will be discussed.

Two or more ionic crystals can be fused together into new, mixed ionic materials which may have totally different structures and properties from the original members. The new materials may have interesting and potentially useful physical and electro-optic properties, such as fast ionic conductivity, superconductivity and non-linear electro-optic behavior. For example, certain ionic crystals can be mixed together under special conditions and compositions to become high temperature superconductors. The development of new materials with characteristic structures and properties under specific conditions has always been an interesting subject of investigation.

The ionic mixtures studied in this program were limited to those made from two ionic crystals with a common anion. Further, according to whether or not there are the same number of net charges for two cations, only two types of the ionic mixtures, MX_2/AX and A_2CO_3/B_2CO_3, were studied, where A and B are alkali metals ions, X

chloride, M cadmium or lead ion.

In the MX_2/AX systems the Raman spectra can be interpreted primarily in terms of metal chloride vibrations whereas the Raman spectra of the carbonate mixtures must be interpreted in terms of changes to the spectra of carbonate ion due to different environments.

1.1.1 MX_2/AX ionic mixtures

The structures for these mixtures, especially those rich in AX, have been interpreted basically in terms of compound formation. Complex ions may be formed as discrete species in certain solid compounds and molten states.

In a molten MX_2/AX mixture the M^{2+} and A^+ cations will be surrounded by the common anions X^-. For mixtures dilute in MX_2 there will be an excess of the A^+ cations and the probability of having M^{2+} as a second nearest neighbor is small. The probability will be further diminished if the electrostatic forces in competition for the common anion are different. Usually the M^{2+} ion has stronger polarizing power than the alkali metal ion so that the favorable configuration is M - X $\cdots$ A [Lumsden 1961, Forland 1964]. In this case, the second neighbor of the M^{2+} cation will be A^+ alone and the local structure may be considered as a complex MX_n^{2-n}. If the lifetime of the complex is long it is reasonable to consider the isolated species or complex ion model in the interpretation of the spectrum. If the interaction with the second neighbor A^+ ions is sufficiently strong, the formation of a discrete complex may be perturbed. Many short-lived configurations may exist simultaneously. On the other hand when the concentration of the MX_2 component is increased, the probability of M^{2+} as a second neighbor increases. The local structure in the melt will change. The coordination number of the complex ion may be decreased (e.g. AlF_6^{3-} to AlF_4^-); a new binuclear complex may be formed (e.g. $AlCl_4^-$ to $Al_2Cl_7^-$); many short-lived configurations with a range of coordination numbers with fast exchange may be observed.

Since the local structure of the melt is dynamic, the apparent structure will depend on the method of investigation. Vibrational spectroscopy is a fast detection method and any local structure that persists for 10^{-11} or 10^{-12} second (i.e. the time for several vibrational periods) may be detected. On the other hand NMR is a slower process (10^{-6} sec.) and species that exist for times between 10^{-6} and 10^{-12} second would be unresolved. Finally X-ray and elastic neutron diffraction methods are very slow processes (measured over hours) and time-averaged structures are obtained. Full understanding of the molten state will only come from the interpretation of each complementary method. The Raman method is important because the detection time is of the order of diffusion times (picoseconds). An entity that exists long enough to diffuse or transport several atomic distances is able to vibrate several times and has the potential to give Raman intensity.

When a molten mixture is cooled to a solid state, complex compounds may form. In the MX_2/AX system the most common compounds have the formula AMX_3, $A_3M_2X_7$, A_2MX_4 and A_4MX_6 with several different coordination types for the central M atom. Some may contain discrete complex species, such as tetrahedral or the octahedral structure, e.g. $MgCl_4^{2-}$ in Cs_2MgCl_4 [Brooker 1975] and $CdCl_6^{4-}$ in K_4CdCl_6 [Bergerhoff 1956, Wells 1962]. In other cases network structures may form. In contrast to the molten state, the local structure of species in the solid state is kinetically stable. The structure of the complex compound will be affected by ion size, concentration, temperature, pressure, purity and the preparational methods. It is important to study the effect of these factors on the properties of the materials, e.g. conductivity, linear, non-linear optical properties.

1.1.2 A_2CO_3/B_2CO_3 ionic mixtures

In these systems complex ions already exist. Ion-pairs may form in molten salts or aqueous solutions. The mixed crystals may give new compounds and new phases. Although sulfates and nitrates have been extensively studied there has been little work on the carbonates.

An important application of this study is to develop new materials. For example, in recent years $KLiSO_4$ has been under extensive investigation as the prototype member of a new $ABSO_4$ family of ferroelectrics [Hiraishi 1976, Teeters 1982a, 1982b, Fonseca 1983, Xie 1983, Li 1984]. Evidence of a superlattice to incommensurate transition at 743K was suggested by Raman studies [Zhang 1987]. Also Cach et al. [Cach 1985] showed that the phase transition was strongly dependent upon the thermal history of the sample. Several studies have shown that other $ABSO_4$ crystals undergo phase transitions and exhibit ferroelectric and ferroelastic properties [Tanisaki 1980, Rangaprasad 1978, Shiroishi 1976].

Another important application of these studies is that they may help to deduce useful information about the structures and properties of the pure compounds. For example, as early as in 1950's , potassium nitrate was reported by Sawada et al. [Sawada 1958] to be ferroelectric in phase III. Many studies have been performed on this compound [Yoshida 1960, Sawada 1961, Tanisaki 1961, Shinnaka 1962, Dork 1964]. In order to further understand the ferroelectric behavior, $A_xB_{1-x}NO_3$ mixed crystals were studied, e.g. $(NH_4)_xK_{1-x}NO_3$ [Yanagi 1963, 1965] and $Rb_xK_{1-x}NO_3$ [Kawabe 1964, 1965] et al. These studies were designed to answer a question why ferroelectricity appeared only in potassium nitrate and not in other nitrates. The results suggested that the crystal structure and ionic radii play important roles in the appearance of ferroelectricity in KNO_3 type ferroelectrics.

The study of mixed systems may give important information about the effect of the different cations on the structures and properties of the materials in both the solid and molten states. For example, vibrational spectroscopic studies [Sharma 1979, Sahni 1976, Narayanan 1973, Teeters 1982c, Ramakrishnan 1985] showed the effect of the crystal field from different A^+ and B^+ ions on the perturbation of the SO_4^{2-} ions in the family of $ABSO_4$ crystals.

In this program Raman measurements have been performed on several mixed binary systems in both the solid and molten states which include $CdCl_2/ACl$ (A = Cs, Rb, K),

$PbCl_2/CsCl$, Li_2CO_3/B_2CO_3 (B = Na, K, Rb, Cs), and K_2CO_3/Na_2CO_3 mixtures (Only the Li_2CO_3/Cs_2CO_3 solids and Li_2CO_3/K_2CO_3 melt will be discussed in this thesis). The major purposes of these studies are:

a) to develop Raman spectroscopy as a method complementary to thermal (DSC, TGA) and diffraction methods (X-ray, neutron) for structural analysis.

b) to detect compound formation and to study phase equilibria and structural phase transitions.

c) to identify possibly discrete species in both the solid and molten states and to study their structures and properties.

d) to deduce intramolecular and intermolecular forces from probe species in various phases.

1.2 General Analytical Method

1.2.1 Determination of compound formation and phase equilibria

Phase equilibria and compound formation in binary or multiple component systems can usually be studied by the methods of differential thermal analysis and X-ray diffraction. Laser Raman spectroscopy provides a very good complementary method for these tasks. In principle, each compound and every different phase of a compound will exhibit a distinct spectrum. Discrete polyatomic ions may be identified by characteristic bands and small changes in these bands may be used to distinguish among different compounds of the polyatomic ions.

If two ionic compounds are fused together, the mixture may form an eutectic mixture, a solid solution, or one or two new compounds depending on the composition. The new phases formed may be identified in the following ways from characteristic Raman spectra.

For a simple eutectic system, each component salt exhibits its own characteristic spectrum. Two sets of Raman bands may be observed at frequencies close to those of the

pure components. The relative intensity of each mode is proportional to the mole fraction of each component. The frequency of each mode will be almost independent of composition of the component.

In a solid solution, there is only one phase. The local environment of probe species will change with the molar fraction of each component. Both the intensity and frequency of each mode may vary with composition. If a solid solution consists of two compounds with common probe species, there may be only one set of bands with frequencies which vary continuously with the composition from the mode frequencies of one component to that of the other.

If new compounds form in a fused binary system, Raman spectra will depend on the composition of the system. For example, in the $CdCl_2/KCl$ system, the phase diagram [Cristol 1978] as shown in fig. 1.1 was suggested. For the x = 0.50 or 0.80 sample (x, mole fraction of KCl), only one set of bands will be present due to the compound $KCdCl_3$ (x = 0.50) or the compound K_4CdCl_6 (x = 0.80). For the $0 < x < 0.50$ samples, two sets of bands will be detected due to the presence of both compounds $CdCl_2$ and $KCdCl_3$. For the $0.5 < x < 0.8$ samples, two sets of bands due to the compounds K_4CdCl_6 and $KCdCl_3$ will be observed. For the $x > 0.8$ samples, two sets of bands due to the compounds K_4CdCl_6 and KCl are presented. Although first order Raman scattering is not allowed for KCl [Agrawal 1975, Wilkinson 1973], weak second order scattering will be observed.

It is also possible to determine if a new compound is an incongruently or congruently melting compound. Again for the $CdCl_2/KCl$ system (fig. 1.1), when the molten system with composition x = 0.80 is cooled to temperature T', the following peritectic reaction begins to occur:

$$\text{melt}_{(l)} + \text{KCl}_{(s)} = K_4CdCl_{6\,(s)}$$

The extent of the reaction depends on the time that the sample remains at the peritectic temperature. If the cooling rate is very low, the equilibrium state will be obtained and

only K_4CdCl_6 will be formed. If the cooling rate is very high the non-equilibrium solid mixture of K_4CdCl_6 and $KCdCl_3$ will result. Raman peaks due to K_4CdCl_6 and $KCdCl_3$ permit identification of the compounds in the mixed system. Therefore, Raman spectra observed from the quenched and the slowly cooled samples from the melts may be used to determine whether or not an incongruent compound forms.

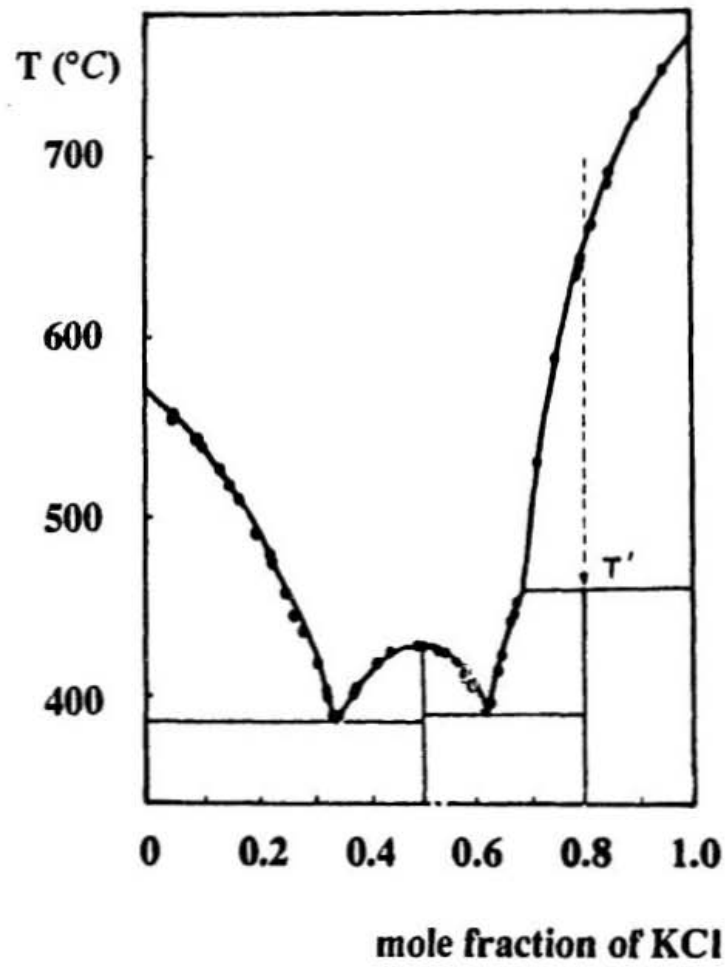

Fig. 1.1

The phase diagram of the $CdCl_2/KCl$ binary system. Redrawn from Ref. [Cristol 1978].

1.2.2 Studies of structural phase transitions in solids

Studies of structural phase transitions provide information about the subtle forces that control the packing of ions and molecules in a solid. Various spectroscopic techniques have been employed, such as Raman, infrared, neutron scattering, EPR, NQR, X-ray and ultrasonic analysis. Raman spectroscopy provides a simple and good method for this task. The probe species in different phases will generate different Raman spectra. Usually the frequencies of the bands decrease and the halfwidths increase gradually due to anharmonic effects as temperature increases in the absence of a structural phase transition. However, if a structural phase transition takes place, the characteristic Raman spectrum will change. The frequencies of bands may shift abruptly, bands may disappear and new bands appear.

An early work to introduce the Raman method to the studies of structural phase transitions was reported by Raman and Nedugadi in 1940 [Raman 1940]. They found the trigonal-hexagonal structural phase transition in quartz at ~573°C. The work was based on a study of the 220 cm^{-1} line which broadened greatly and shifted towards the exciting line as the transition temperature was approached. This was explained as due to the increasing deformation of the atomic arrangement to induce the transformation from the α to β phase.

Another early work was a Raman study of a ferroelectric phase transition of SbSI by Perry and Agrawal [Perry 1970]. SbSI was the first known ferroelectric photoconductor and has a Curie temperature (T_c) of about 288K. Above T_c, SbSI was found to have an orthorhombic structure with the space group D_{2h}^{16}, but as temperature decreased the paraelectric phase transformed into a ferroelectric phase with space group C_{2v}^{9}. The temperature dependent Raman spectra showed a frequency softing of the transverse A mode as T approached T_c from below.

Studies of structural phase transitions by Raman methods have been performed on many systems. Two excellent, very readable reviews are available on this subject [Scott

1974, 1983].

1.2.3 Studies of molten salts

Raman spectroscopy provides a good method to study molten salts because i) in principle discrete species will generate unique spectra; ii) vibrational spectroscopy is a fast process and is able to detect the symmetry of a local structure with a lifetime as short as a picosecond.

Two excellent examples to illustrate the use of Raman spectroscopy for studies of molten salts are the studies of the $AlCl_3$ - $nACl$ (A = alkali metal) system [Torsi 1970, Φye 1971, Rytter 1973] and those of Gilbert et al. for the AlF_3 - nAF system [Gilbert 1974, 1975].

For $AlCl_3$ - $nACl$ melts, Raman results indicated that:

1) For $n \geq 1$, the $AlCl_4^-$ tetrahedral species predominates.

2) For $n < 1$, the relative intensities of the bands due to $AlCl_4^-$ decreased upon addition of $AlCl_3$, while new bands were detected due to a species identified as $Al_2Cl_7^-$. The structure of $Al_2Cl_7^-$ was considered to be two distorted $AlCl_4$ tetrahedra with a bridging Cl^-. In the composition range of n < 1, there was an equilibrium between $AlCl_4^-$ and $Al_2Cl_7^-$ i.e.

$$2AlCl_4^- \rightleftharpoons Al_2Cl_7^- + Cl^-$$

For AlF_3 - nAF melts, changes in Raman spectra with temperature and melt composition reflected an equilibrium between the species AlF_4^- and AlF_6^{3-}, i.e.

$$AlF_6^{3-} \rightleftharpoons AlF_4^- + 2F^-$$

The AlF_6^{3-} ion was detected in AF rich melts while AlF_4^- was observed as the value of n $\rightarrow$ 1. Spectra could not be obtained for melts with n < 1. The discrete AlF_6^{3-} species has an octahedral coordination; while the AlF_4^- species has a tetrahedral structure. Quantitative analysis of the intensity ratio of the ν_1 bands of AlF_4^- and AlF_6^{3-} as a function of the

composition of the melt gave an approximate value of the stoichiometric dissociation constant $K = X_{AlF_3} \cdot X_{F^-}^3 / X_{AlF_6^{3-}}$ [Gilbert 1975].

These two examples demonstrate the two major types of complex equilibria i.e. formation of polynuclear species and change of coordination number. An excellent review on the vibrational spectroscopy of molten salts was published by Brooker and Papatheodorou [Brooker 1983].

In many cases Raman spectra are less than ideal; peaks are often broad, overlapped or of low intensity. One possible method to assist interpretation of spectra from molten salts is the use of Raman studies of the same system in the solid state or solution. Studies of intensity and bandshape as a function of the concentration and temperature can also be employed. Furthermore, results from other techniques must be considered and critically assessed.

X-ray and neutron diffraction are excellent methods to study the structures and properties for materials in different states. Recent development of a isotope different method for neutron diffraction studies of molten salts has provided excellent structural information. The determination of the partial structure factor and partial radial distribution function by thermal neutron scattering from molten states of different isotopic composition was first suggested in 1966 by Enderby et al. [Enderby 1966]. The method was based on the fact that the neutron scattering length and cross section, a property of the nucleus, may vary considerably between different isotopes. Molten NaCl was the first melt studied by this method [Edwards 1975], but many molten salts have now been studied, e.g. $RbCl$ [Mitchell 1976], $BaCl_2$ [Edwards 1978], $CaCl_2$ [Biggin 1981a], $ZnCl_2$ [Biggin 1982b], $SrCl_2$ [McGreevy 1982, Margaca 1984] and MCl_2 ($M = Mg$, Ca, and Sr) [Bunten 1984]. It has been suggested [Biggin 1981a, 1981b] that the dominant contribution to the structural properties of ionic melts with a common anion is the size of the cations and not their electronic structure. In a recent study in 1989, the structure of molten $CdCl_2$ has been investigated by X-ray diffraction [Takagi 1989]. The tetrahedral

configuration $CdCl_4$ was confirmed from the first and second peaks of the radial distribution function. For mixed binary systems, the structure of $LiAlCl_4$ [Biggin 1986] has been investigated by neutron diffraction of isotopically enriched samples. The results indicated a tetrahedral distribution of Cl^- ions about Al^{3+} ion.

1.3 Comparison with diffraction methods

In contrast to the diffraction methods, the advantages of the Raman method may be:

a) Raman spectroscopy is a fast process and able to detect the symmetry of a local structure with a lifetime as short as picoseconds. Diffraction methods give only time averaged nuclear positions.

b) The Raman method can identify discrete species in different phases and possibly provides information on the various kinetic processes and thermodynamic equilibria in a system.

c) Analysis of intensity, shape and polarization properties of Raman bands can provide information about specific interactions among species, intramolecular forces within species and the nature of diffusing species.

d) The Raman method can produce good results even when a small quantity of an impurity is also present in a system.

e) The Raman method is relatively easy. Sample preparation is relatively easy and high temperatures present no serious problems. Most samples can be contained in quartz tubes or windowless cells.

The disadvantages of the Raman method may be:

a) In the solid state, even a single crystal, the assignment of Raman bands usually requires a knowledge of the diffraction results.

b) It is difficult to determine the state of the probe species in a disordered solid system, or in those systems where first order Raman scattering is not allowed.

c) In the molten state, if the vibrational relaxation time is very short (possibly due to exchange) Raman bands will be very broad and will not give any information about geometry. The Raman method does not give the coordination number directly.

d) Usually, the Raman method fails to measure colored samples.

e) Some samples are easily decomposed by the laser.

Chapter 2

THEORY

2.1 Raman Scattering in Non-interacting Molecules

When monochromatic radiation of wavenumber ω_0 is incident on a system, some scattering of the radiation may occur, the frequencies of the scattered radiations will be observed at wavenumber ω_0 associated with the incident radiation (Rayleigh scattering) and pairs at new wavenumbers $\omega_0 \pm \omega_k$ (Raman scattering). The energy difference ω_k may be associated with difference in rotational, vibrational, or electronic energy state of the molecule.

Classical descriptions of the vibrational Raman effect have been developed by Raman and Plazcek etc. [Raman 1928, Placzek 1934, Long 1977]. When light of a given polarization impinges on a molecule it induces an oscillating dipole moment

$$\vec{P} = \alpha \vec{E} + \beta \vec{E}^2 + \gamma \vec{E}^3 + \cdots \tag{2.1}$$

where α represents the polarizability tensor; $\vec{E}$ is the electric vector; β, γ are the hyper-polarizabilities. Spontaneous Raman scattering arises due to the linear term in Eq. (2.1).

The components of the induced moment vector are related to the electric vector as follows if we consider only the linear term in Eq. (2.1):

$$\begin{aligned} P_x &= \alpha_{xx} E_x + \alpha_{xy} E_y + \alpha_{xz} E_z \\ P_y &= \alpha_{yx} E_x + \alpha_{yy} E_y + \alpha_{yz} E_z \\ P_z &= \alpha_{zx} E_x + \alpha_{zy} E_y + \alpha_{zz} E_z \end{aligned} \tag{2.2}$$

where the coefficients α_{ij} $(i,j = x, y, z)$ are the components of the polarizability tensor. In general, the polarizability will be a function of the nuclear coordinates. The variation of

the polarizability with vibrations of the molecule can be expressed by expanding each component α_{ij} of the polarizability tensor in a Taylor series with respect to normal coordinates of vibrations:

$$\alpha_{ij} = (\alpha_{ij})_0 + \sum_k (\frac{\partial \alpha_{ij}}{\partial Q_k})_0 Q_k + \frac{1}{2} \sum_{k,l} (\frac{\partial^2 \alpha_{ij}}{\partial Q_k \partial Q_l})_0 Q_k Q_l + \cdots \tag{2.3}$$

where $(\alpha_{ij})_0$ is the value of α_{ij} at the equilibrium configuration; Q_k, Q_l ... are normal coordinates of vibration associated with vibrational frequencies ω_k, ω_l ...; and the summations are over all normal coordinates. The coefficients of the second term in Eq. (2.3) are of special importance and are the derivatives of the polarizability tensor components with respect to changes in normal coordinate, α'_{ij}. They are defined as:

$$(\alpha'_{ij})_k = (\frac{\partial \alpha_{ij}}{\partial Q_k})_0 \tag{2.4}$$

The linear induced dipole $\vec{P}$ has three distinct frequency components:

$\vec{P}(\omega_0)$— for Rayleigh scattering;

$\vec{P}(\omega_0 - \omega_k)$— for Stokes Raman scattering;

$\vec{P}(\omega_0 + \omega_k)$— for anti-Stokes Raman scattering.

The amplitudes of the induced dipoles associated with Stokes and anti-Stokes Raman scattering to the incident electric field are:

$$\begin{aligned}
P_{x_0}(\omega_0 \pm \omega_k) &= \{(\alpha'_{xx})_k E_{x_0} + (\alpha'_{xy})_k E_{y_0} + (\alpha'_{xz})_k E_{z_0}\} Q_{k_0} \\
P_{y_0}(\omega_0 \pm \omega_k) &= \{(\alpha'_{yx})_k E_{x_0} + (\alpha'_{yy})_k E_{y_0} + (\alpha'_{yz})_k E_{z_0}\} Q_{k_0} \\
P_{z_0}(\omega_0 \pm \omega_k) &= \{(\alpha'_{zx})_k E_{x_0} + (\alpha'_{zy})_k E_{y_0} + (\alpha'_{zz})_k E_{z_0}\} Q_{k_0}
\end{aligned} \tag{2.5}$$

It is clear from Eq. (2.5) that the condition for Raman activity is that at least one of the

components of the polarizability tensor derivative $(\alpha'_{ij})_k$ is non-zero. If the mechanical and electrical anharmonicities are taken into account, overtone and combination bands should be considered. Since $(\alpha'_{ij})_k$ is unaffected by the mechanical anharmonicity, the selection rule of the fundamental can be applied to the overtones ($\omega_0 \pm 2\omega_k$, combinations ($\omega_0 \pm (\omega_k \pm \omega_l)$) due to the mechanical anharmonicity. But if electrical anharmonicity is taken into account, the third and higher terms in the equation (2.3) must be considered. Therefore the selection rule for overtone and combination bands due to electrical anharmonicity is that at least one of the components $(\frac{\partial^2 \alpha_{ij}}{\partial Q^2_k})_0$, $(\frac{\partial^2 \alpha_{ij}}{\partial Q_k \partial Q_l})_0$, ... is non-zero.

Similar results can be obtained by a quantum mechanical treatment. According to the quantum theory, radiation is emitted or absorbed as a result of a system making a downward or upward transition between two discrete energy levels; and the radiation itself is also quantized with the energy in discrete photons. The quantum theory treats the radiation and molecule together as a complete system, and explores how energy may be transferred between the radiation and the molecule as a result of their interaction.

In the quantum mechanical treatment, if a transition from an initial state i to a final state f is induced by incident radiation of frequency ω_0, the amplitude of the transition moment is given by

$$[\bar{P}_0]_{fi} = \langle \Psi_f | \alpha | \Psi_i \rangle \bar{E}_0 \tag{2.6}$$

where Ψ_i and Ψ_f are the time-independent wave functions of the initial and final states. The components of the transition moment are:

$$\begin{aligned}
[P_{x_0}]_{fi} &= [\alpha_{xx}]_{fi} E_{x_0} + [\alpha_{xy}]_{fi} E_{y_0} + [\alpha_{xz}]_{fi} E_{z_0} \\
[P_{y_0}]_{fi} &= [\alpha_{yx}]_{fi} E_{x_0} + [\alpha_{yy}]_{fi} E_{y_0} + [\alpha_{yz}]_{fi} E_{z_0} \\
[P_{z_0}]_{fi} &= [\alpha_{zx}]_{fi} E_{x_0} + [\alpha_{zy}]_{fi} E_{y_0} + [\alpha_{zz}]_{fi} E_{z_0}
\end{aligned} \tag{2.7}$$

where

$$[\alpha_{ij}]_{fi} = \langle \Psi_f | \alpha_{ij} | \Psi_i \rangle \tag{2.8}$$

are the matrix elements of the polarizability tensor. After separation of vibrational and rotational transitions, each component of the pure vibrational transition polarizability tensor can be expanded as a Taylor series in terms of the normal coordinates.

$$\alpha_{v'v} = (\alpha_{v'v})_0 + \sum_k (\frac{\partial \alpha_{v'v}}{\partial Q_k})_0 Q_k + \frac{1}{2} \sum_{kl} (\frac{\partial^2 \alpha_{v'v}}{\partial Q_k \partial Q_l})_0 Q_k Q_l + \cdots \tag{2.9}$$

In the approximation of electrical and mechanical harmonicity the condition for a Raman active mode is that only one vibrational quantum number changes by unity, i.e, $\Delta v_k = \pm 1$. The second condition is that at least one of the elements of the derived polarizability tensor is non-zero.

The complex, apparently random internal motions of a vibrating molecule are the result of the superposition of a number relatively simple vibrational motions known as the normal vibrations. Each of these has its own fixed frequency. In a molecule consisting of **n** atoms there is **3n** degrees of freedom, but only **3n - 6** remain to be combined into genuine vibrational motions (**3n - 5** for a linear molecule), the rest of the freedom corresponds to translational and rotational motions of the whole molecule.

For a free molecule, the symmetry types of the normal modes can be determined by point group theory from a knowledge of the molecular symmetry and have been well discussed by many authors [for example, Cotton 1963, Herzberg 1945] and will not be discussed here.

According to the Placzek theory [Placzek 1934, Woodward 1967, Person 1982], α' is a key quantity required to determine the intensity and state of polarization of a Raman line. It can be divided into a symmetric and an asymmetric part. The symmetric part can be described by the mean derived polarizability invariant $\overline{\alpha'}$ as defined by

$$\overline{\alpha'} = \frac{1}{3}(\alpha'_{xx} + \alpha'_{yy} + \alpha'_{zz}) \tag{2.10}$$

and the anisotropy part is:

$$(\beta')^2 = \frac{1}{2}[(\alpha'_{xx} - \alpha'_{yy})^2 + (\alpha'_{yy} - \alpha'_{zz})^2 + (\alpha'_{zz} - \alpha'_{xx})^2 + 6(\alpha'^2_{xy} + \alpha'^2_{yz} + \alpha'^2_{zx})] \tag{2.11}$$

The quantum mechanical expression in the Schrödinger representation [Placzek 1934] for the differential scattering section into a solid angle Ω and frequency range $d\omega$ about ω_0 is:

$$\frac{d^2\sigma}{d\Omega d\omega} = \lambda_s^{-4} \sum_{i,f} |\langle i|\hat{\varepsilon}_i \cdot \boldsymbol{\alpha} \cdot \hat{\varepsilon}_s|f\rangle|^2 \rho_i \delta(\omega - \omega_{fi}) \tag{2.12}$$

where λ_s is the wavelength of the scattered light, $\hat{\varepsilon}_i$ and $\hat{\varepsilon}_s$ are unit vectors defining the polarization directions of the incident and scattered lights, and $\boldsymbol{\alpha}$ is the polarizability tensor of the scattering medium. The initial and final states of the system with energy E_i and E_f are i and f; and ρ_i is the probability that the system is in initial state i.

If $E_f > E_i$, Raman lines occur at lower frequencies (Stokes line) than the incident exciting line; if $E_f < E_i$ the Raman lines occur at higher frequencies (anti-Stokes lines) than the incident exciting line.

The intensity of a Stokes Raman band associated with a shift ω_k is given by

$$I_k = C\, d_k \frac{(\omega_0 - \omega_k)^4}{\omega_k} [(1 - exp(-h\omega_k/kT)]^{-1} [45(\overline{\alpha'_k})^2 + 7(\beta_k')^2] \tag{2.13}$$

where C is a constant, d_k is the degeneracy of Q_k , k is the Boltzmann constant and T is the temperature in Kelvin.

Experimentally and theoretically the scattered intensity may be divided into two parts, polarized and depolarized. When $\hat{\varepsilon}_i$ and $\hat{\varepsilon}_s$ are perpendicular only the depolarized

component appears (Eq. 2.14) and when $\hat{\varepsilon}_s$ and $\hat{\varepsilon}_l$ are parallel both components appear (Eq. 2.15).

$$\frac{d^2\sigma\ depol}{d\Omega d\omega} \equiv \frac{1}{10}\frac{d^2\sigma}{d\Omega d\omega_\perp} \tag{2.14}$$

$$\frac{d^2\sigma\ pol}{d\Omega d\omega} \equiv \frac{d^2\sigma}{d\Omega d\omega_\parallel} - \frac{4}{6}\frac{d^2\sigma}{d\Omega d\omega_\perp} \tag{2.15}$$

The time dependent polarizability tensor can be considered as a scalar part α and a traceless anisotropic part β. Then the following equations in terms of intensities can be obtained:

$$\begin{aligned} I_\alpha(\omega) &= I_{iso}(\omega) = I_{pol}(\omega) \\ &= I_\parallel(\omega) - \frac{4}{3} I_\perp(\omega) \end{aligned} \tag{2.16}$$

$$I_\beta(\omega) = I_{aniso}(\omega) = I_{dep}(\omega) = I_\perp(\omega) \tag{2.17}$$

A Taylor series like Eq. (2.3) can be obtained by expanding the scalar part α and traceless anisotropic part β with respect to the normal vibrational coordinates. $\frac{\partial\alpha}{\partial Q_k}$ is independent of molecular orientation, but $\frac{\partial\beta}{\partial Q_k}$ depends on molecular reorientation. Therefore $I_\alpha(\omega)$ ($I_{iso}(\omega)$) is identified with the part of the scattered intensity due to pure vibrational relaxation, and I_β ($I_{aniso}(\omega)$) with a convolution of vibrational and reorientational relaxation. According to Eqs. 2.16 and 2.17, I_α and I_β can be obtained by Raman measurements of $I_\parallel$ and $I_\perp$ spectra which normally are measured as I_{VV} and I_{VH} for 90° scattered light. Where VV means the incident laser light and the scattered light are both polarized in the vertical plane, while VH indicates the scattered light is polarized in the horizontal plane.

The intensity of a particular Raman band and its dependence on the scattering geometry is the result of the polarization property of the band and is related to the symmetry of

the vibration. The depolarization ratio of the Raman light scattered at right angle to the incident direction of polarized exciting laser light is:

$$\rho_l = \frac{I_\perp}{I_\parallel} = \frac{3\,(\beta')^2}{45\,(\bar{\alpha}')^2 + 4\,(\beta')^2} \tag{2.18}$$

The intensity $I_\perp$ and the depolarization ratio ρ are determined by the symmetry of the corresponding vibration. Therefore the bands from modes of different symmetry types may be distinguished in the Raman spectra of gases, liquids (include melts), solutions and single crystals by determining the depolarization ratio for every band.

According to Eq. (2.13), the Raman intensity depends on the molar scattering efficiency $S_{(i)}$ which is given by $45(\overline{\alpha'})^2 + 7(\beta'_k)^2$. The molar scattering efficiency is the quantity of real interest in the Raman experiment [Brooker 1986]. A $R_2(\omega)$ reduction function has been defined to get the reduced intensity spectrum and to give relative value of $S_{(i)}$ directly. The $R_2(\omega)$ function is defined as:

$$R_2(\omega) = I(\omega)\,(\omega_0 - \omega_k)^{-4}\,\omega_k\,B \tag{2.19}$$

where ω_0 is the absolute frequency of the laser excitation line; ω_k is the Raman shift of the k^{th} normal mode; and B is the Bose-Einstein temperature factor for which the Boltzman distribution gives a good approximation. The molar scattering efficiency $S_{(i)}$ can be obtained directly by integration (Eq. 2.13).

$$S_{(i)} = \int_{band} R_2(\omega)\,d\omega \tag{2.20}$$

In recent years, the reduction function has been proven to be useful in the analysis of Raman spectra [Shuker 1971, Lund 1978, Snyder 1980, Perrot 1970, Brooker 1981, 1988 and 1989, Nielsen 1981, Murphy 1989]. The major advantage [Murphy 1989] of the reduction procedure is to transform the observed spectra to a common basis for

comparison under differing sample conditions (exciting line, temperature). Certain forms of the reduced Raman spectra can be compared directly with infrared absorption spectra.

The quantitative study of I_a and I_β may provide useful information about vibrational reorientational relaxation processes through time correlation function methods [Long 1977, Gordon 1968, Brooker 1986]. For example, the vibrational correlation function $G_v(t)$ is defined as:

$$G_v(t) = < Q_i(0) \cdot Q_i(t) > \tag{2.21}$$

Where Q_i is the i^{th} vibrational normal coordinate. $G_v(t)$ provides a direct probe of vibrational dephasing and can be obtained from the Fourier transform of the normalized isotropic Raman profile.

$$G_{iso} = G_v(t) = \int I_a(\omega) exp(-i\omega t) d\omega) \tag{2.22}$$

Where ω represents the frequency measured from the band center, ω_0.

By the same way, the Raman reorientational correlation function G_{2R} may be obtained by the deconvolution of the vibrational contribution with the G_{aniso} function.

$$G_{aniso} = G_v(t) \cdot G_{2R}(t) = \int I_\beta(\omega) exp(-i\omega t) d\omega \tag{2.23}$$

For narrow bands the slit correlation function should also be deconvoluted from the observed bandshape [Kato 1978].

Although the various correlation times can be obtained from the integration

$$\tau = \int_{-\infty}^{\infty} G(t)\, d\tau \tag{2.24}$$

very good approximations of the correlation times can be obtained from the halfwidths of the bands. If the correlation function $G(t)$ follows an exponential decay with time

$$G(t) = A \exp t/\tau \tag{2.25}$$

where τ is the correlation time, the band profile in frequency space will have a Lorentzian shape with a full width at half height $\Gamma(cm^{-1})$ that is related to the correlation time as:

$$\Gamma^{-1} = \pi c \tau \tag{2.26}$$

For a totally symmetric vibration, the vibrational and reorientational correlation times τ_V and τ_R can be determined from the halfwidths of the isotropic and anisotropic spectra i.e

$$\Gamma_{iso} = \Gamma_V \approx \Gamma_{\parallel} \tag{2.27}$$

$$\Gamma_{aniso} = \Gamma_{\perp} = \Gamma_V + \Gamma_R \tag{2.28}$$

$$\tau_V^{-1} = \pi c \Gamma_V \tag{2.29}$$

$$\tau_R^{-1} = \pi c \Gamma_R = \pi c (\Gamma_{aniso} - \Gamma_{iso}) \tag{2.30}$$

However, the analysis of the bandshape is complicated. For example, the contribution to isotropic Raman I_{iso} spectrum may include:

energy relaxation (lifetime broadening);

pure dephasing;

resonance energy transfer;

and chemical exchange reactions (fast exchange).

Also, if two, or several bands overlap, possibly due to several species or a continuous distribution of bond strength (e.g. hydrogen bonds in H_2O), a very broad band profile will be observed. In this case it is difficult to get accurate relaxation information.

2.2 Raman scattering in crystals

The vibrational spectrum of a molecule in a solid phase will be different from that of the molecule in gas or liquid. In a crystal, molecules are in close proximity to other molecules. The intermolecular interactions may have a significant effect on the vibrational modes and vibrational transitions. Usually the internal vibrational frequencies of molecules in crystals are not very different from the corresponding frequencies of the free molecules. This persistence of the molecular identity in a solid is a consequence of the fact that the interaction forces within the molecules are much stronger than the forces acting between molecules. Nevertheless the vibrational selection rules are changed. The fundamental vibrational modes of the molecule may be split into additional bands and a number of new bands may be observed [Sherwood 1972]. Several major effects are:

a) static field effects (site group splitting)

Static field effect is a measure of the influence which the surrounding crystal structure exerts on the molecule. Non-degenerate internal vibrations may be shifted in frequency, degenerate internal vibrations may be split if the lower local symmetry of the crystal is no longer consistent with degeneracy, and inactive fundamentals may become active.

b) correlation field splitting effects

These effects are due to interaction with internal vibrations of the other molecules in the same unit cell of the crystal. Both degenerate and non-degenerate internal vibrations may be split since the potential energy may be different according to whether or not the internal vibrations are in phase or out of phase in the unit cell.

c) Transverse/Longitudinal (TO/LO) splitting

TO/LO splitting is due to the long range electrostatic forces in a non-centric crystal. Short range forces can also lead to anisotropy of force constants causing a different frequency for different crystal directions.

As a result of the periodic nature of the ordered crystal, a range of possible vibrations occur when the atoms (many crystals do not contain molecules, e.g. Rb_2CdCl_4, $CsCdCl_3 \cdots$ etc.) and/or molecules in adjacent unit cells move in phase or partly out of phase. The energy difference between such vibrations can be described by a perturbation of a molecular system, because intramolecular forces are much stronger than intermolecular forces. The energy difference between such vibrations would be expected to be appreciable for external vibrations which completely depend upon intermolecular and/or interatomic or interionic forces and such vibrations can be considered as a wave propagating through the crystal structure.

The phase relationship between the wavelike motions of atoms (phonons) in adjacent cells may be specified by the wave vector, $k = \frac{2\pi}{\lambda}$ where λ is the wavelength of the crystal wave motion and corresponds to the distance over which motions of atoms are in phase. The wave vectors of an infrared photon (~1000 cm^{-1}), or a visible photon in a Raman experiment (~ 20000 cm^{-1}) are small compared to 10^8 cm^{-1}, and since energy and wave vector must be conserved in the interaction only $K \approx 0$ phonons will be allowed in infrared and Raman experiments. This selection rule greatly simplifies the treatment of the vibrational spectra of crystals because it means that selection rules can be deduced on the basis of the unit cell (factor) group symmetry.

The normal modes of vibrations or phonons propagating in a solid can be predicted by theories based on the unit cell group (factor group) analysis [Cotton 1963, Schonland 1965, Johnston 1960, Jones 1969, Heine 1960, Tinkham 1964, Wilson 1955, Bhagavantam 1969, Horning 1948, Winston 1948, Halford 1946, Zbinden 1964, Sherwood 1972]. If a primitive cell contains **n** atoms there will be **3n** degrees of freedom or **3n** normal modes, of which three will represent acoustic modes, which leaves **3n-3** optical modes at $k \approx 0$. The equivalent particles in the crystal structure move in identical phase for these modes of oscillation. In other words, all the unit cells of the lattice are in the same phase throughout the period of execution of the fundamental optical modes. The symmetry

classification of the $k \approx 0$ modes of vibrations can be therefore accomplished by taking into consideration of the factor group of the crystal, instead of the entire crystal. There are several methods by which the unit cell may be analyzed and the selection rules determined [Rousseau 1981].

The first method is the factor group analysis of the unit cell [Bhagavantam et al. 1939, 1941, 1962] by which the number of normal modes is determined by applying all of the symmetry operations of the factor group (unit cell group) for each atom in the unit cell to obtain an reducible representation. The number of normal modes belonging to each irreducible representation of the factor group may then be determined.

The second method is the correlation molecular site group method based on the unit-cell group correlation [Halford 1946, Hornig 1948, Winston 1949, Fateley 1971, 1972, and Ferraro 1975]. By this method the symmetry properties are determined first for the unit of interest as an isolated species (molecule) and then correlated to the site symmetry of the unit which is centered on one of the lattice sites and finally in terms of factor group symmetry.

The third method [Mathieu 1945] is simply a generalization of the correlation method carried out on every atom in the unit cell.

The vibrational modes predicted from the unit cell group analysis may be assigned by several Raman measurements from an ordered crystal oriented in different directions because of the directional and polarization properties of Raman scattering. The values of depolarization ratios are determined by symmetry properties of the derived polarizability tensor, which itself reflects the symmetry of the mode of vibration [Long 1977]. For example [Long 1977], calcite has a trigonal structure, with two molecules per unit cell. The calcium ions and the carbon atoms of the carbonate ions all lie on the trigonal axis (z - axis), and the orientations of the two carbonate ions are staggered relative to each other. The A_{1g} and E_g modes of the D_{3h} symmetry are Raman active. The scattering tensor for the A_{1g} and E_g modes are:

$$A_{1g}: \quad \begin{matrix} a & 0 & 0 \\ 0 & a & 0 \\ 0 & 0 & b \end{matrix}$$

$$E_g: \quad \begin{matrix} c & 0 & 0 \\ 0 & -c & d \\ 0 & d & 0 \end{matrix} \quad \text{and} \quad \begin{matrix} 0 & -c & -d \\ -c & 0 & 0 \\ -d & 0 & 0 \end{matrix}$$

For the scattering geometry Y(XY)X (Porto notation [Damen 1960, 1966], the four symbols define the propagation direction of the incident radiation (Y), the direction of the electric vector of the incident radiation (X), the direction of the electric vector of the scattered radiation being examined (Y), and the direction of the propagation of the scattered radiation (X) in the order Y(XY)X respectively.), the scattered power is proportional to α_{xy}^2, and since this is non-zero only for one component of each of the E_g modes, only the E_g vibrations will be observed for this experimental arrangement. For scattering geometry Z(XX)Y, all the Raman active modes will be observed.

Examples to illustrate the determination of the normal modes by group theory will be given in following chapters in the analysis of the Raman spectra for the molecules concerned.

However unit cell group analysis will not always predict the correct number of active fundamentals. For a linear lattice, the motion of the atoms is restricted to a line and only transverse motion is considered. In three dimensions, transverse motion will be possible in two dimensions and additional longitudinal displacement of the atoms must also be considered. In certain special directions the normal vibrations will be strictly transverse and/or longitudinal because of symmetry, since the vibrations involve restriction of the motion of the particles to a plane. For a Face-centered cubic crystal, the two transverse optical modes will be degenerate, but the longitudinal optical mode will occur at

higher frequency at $K \approx 0$ because such vibrations are associated with a finite macroscopic electrostatic field. The difference in frequency between the transverse and longitudinal modes is the transverse/longitudinal splitting.

Crystal samples frequently contain impurities, disorder, distortion [Hodges 1969] and stacking faults [Christian 1970], and these can cause striking macroscopic effects. Small amounts of impurity may result in different crystal structures from those of pure materials. Major faults destroy the translational symmetry of the crystal hence changing the normal modes from their usual plane wave form and breaking down the conservation of the wave vector rule. The phonons of a branch will still have similar energy over a continuous distribution and broad bands will be observed. These bands actually represent a range of frequencies of all the vibrational modes over a range of environments.

Chapter 3

EXPERIMENTS

3.1 Preparation of Samples

3.1.1 $CdCl_2$/ACl (A = Cs, Rb, K) and $PbCl_2$/CsCl systems

Anhydrous $CdCl_2$ (or $PbCl_2$)and alkali metal chlorides were dried at ~100°C for a few hours under vacuum, the temperature was slowly raised to ~250°C, then the samples were further dried for at least 48 hours. The dried solids were handled in a dry box filled with nitrogen gas dried by P_2O_5. Proper amounts of $CdCl_2$ (or $PbCl_2$) and ACl were weighed carefully and mixed well in a mortar, then transferred into 8 mm i.d. quartz tubes. The mixture of solids was further dried at ~250°C for 2 hours under same conditions as described above before slowly heating it to the melt. The molten mixture was quenched to room temperature. The sample was then transferred into a 6 mm i.d. quartz tube and dried again at ~180°C for two hours before being sealed under vacuum. Additional slowly cooled or quenched samples were further prepared directly in the 6 mm i.d. quartz tube.

3.1.2 $A_xB_{(1-x)}CO_3$ systems

Anhydrous alkali carbonates were dried at about 100°C for a few hours under vacuum, then further dried at about 250°C for at least 48 hours. Proper amounts of dried A_2CO_3 and B_2CO_3 were weighed carefully and mixed well in a dry box filled with nitrogen gas dried by P_2O_5. The solid mixture was transferred into a nickel crucible. The nickel crucible with the sample was put into a quartz tube and dried for at least 1 hour at ~250°C and further dried at ~400°C for about half an hour under approximately 1 atm of CO_2 gas. The sample was heated slowly to the melt under dry CO_2 gas, then cooled very slowly. The fused sample was transferred into a 6 mm i.d. quartz tube and was dried for at least two hours at ~200°C then sealed under a pressure of 200 mmHg dried CO_2 gas.

The quenched samples from the high temperature solids and the melts were directly prepared in the 6 mm i.d. quartz tubes.

All of the materials used to prepare these samples were analytical grade reagents.

3.2 Raman Spectroscopic Measurements

3.2.1 Solids

All Raman spectra of solids at room temperature were obtained directly from samples in 6 mm i.d. quartz tubes. Raman spectra were measured with a Coderg PHO Raman spectrometer. Usually the 488.0 nm line of the argon ion laser was used to excite the sample, sometimes the 514.5 nm line was also used to reduce the intensity of fluorescence for some samples. The power level at the sample was about 0.3 W. Plasma lines were removed with a narrow-band-pass interference filter. A solution of 0.5 M $Pr(EDTA)^-$ complex as a post sample filter was used to reduce stray-light and ghosts. Peak positions were calibrated against the laser plasma lines. The standard 90° scattering geometry was used. The slit widths of the double monochromator were set at 2 cm^{-1} usually, but sometimes were reduced to 1 cm^{-1} or 0.5 cm^{-1} as required for resolution. The photomultiplier tube was cooled to $-20°C$. Usually the scan rate was 50 cm^{-1} min^{-1}, for special cases 10 cm^{-1} min^{-1}.

The Raman scattering light was detected with a PMT cooled to -20°C, integrated with a photon counter and processed with a home-built box-car averager interfaced to the Memorial university computer. Two data points were collected per wavenumber. At least two sets of data were collected for each spectrum. Spectra were signal-averaged and smoothed with a three-point Savitsky-Golay smoothing function. A baseline program was applied which corrected the measured intensity for the fourth power frequency factor and then set the lowest data point to zero and the highest data point to 999 on a relative intensity scale. This form of data is defined as the $I(\omega)$ spectrum. The same baseline program was applied with the option of correcting for the fourth power scattering factor, the

Bose-Einstein temperature factor, $B = [1 - \exp(-hc\omega/kT)]$ and frequency factor, ω, to give the reduced or $R(\omega)$ spectrum which is directly proportional to a point-by-point relative scattering activity, $S_Q(\omega)$ in terms of mass-weighted normal coordinates, Q in the double harmonic approximation. The relationship between the $I(\omega)$ and $R(\omega)$ forms of the spectra is given by following equation:

$$S_Q(\omega) \propto R_Q(\omega) = I(\omega) \cdot \omega \cdot B$$

3.2.2 Temperature Dependence for Solids

Raman spectra of solids at different temperatures were obtained from samples in 6 mm i.d. quartz tubes heated in an insulated furnace (fig. 3.1) with a proportional temperature controller. The temperature was monitored with a chromel-alumel thermocouple and the quoted temperature at the sample was constant to about one degree and accurate to about five degrees. The spectrometer settings used to obtain the spectra from high temperature solids were similar to those for room temperature solids.

3.2.3 Melts

The 6 mm i.d. quartz tubes were still used to contain the molten $CdCl_2$/ACl and $PbCl_2$/CsCl samples, while a graphite windowless cell was used for the molten carbonate samples. The windowless cell with sample was contained in a quartz tube under a pressure of 0.8 atm of dried CO_2.

The schematic representation of an experimental arrangement for Raman scattering from molten salts is presented in fig. 3.2. Polarization of the incident beam was controlled by a half-wave plate and the 90 ° scattered light was analyzed with a polaroid film placed before the monochromator slit. Depolarization measurements for all the melts were made by analyzing the scattered light parallel ($I_{\parallel}$) and perpendicular ($I_{\perp}$) to the incident laser light. Usually the slit widths of the double monochromator were set at 2 cm^{-1}. For the $PbCl_2$/CsCl sample and the pure $PbCl_2$ melt, a lower intensity of incident

laser light was employed to get better spectra. Spectra of the $PbCl_2/CsCl$ or pure $PbCl_2$ systems were found to have a higher intensity of noise under high intensity excitation. Perhaps the higher noise arose from the decomposition of the sample.

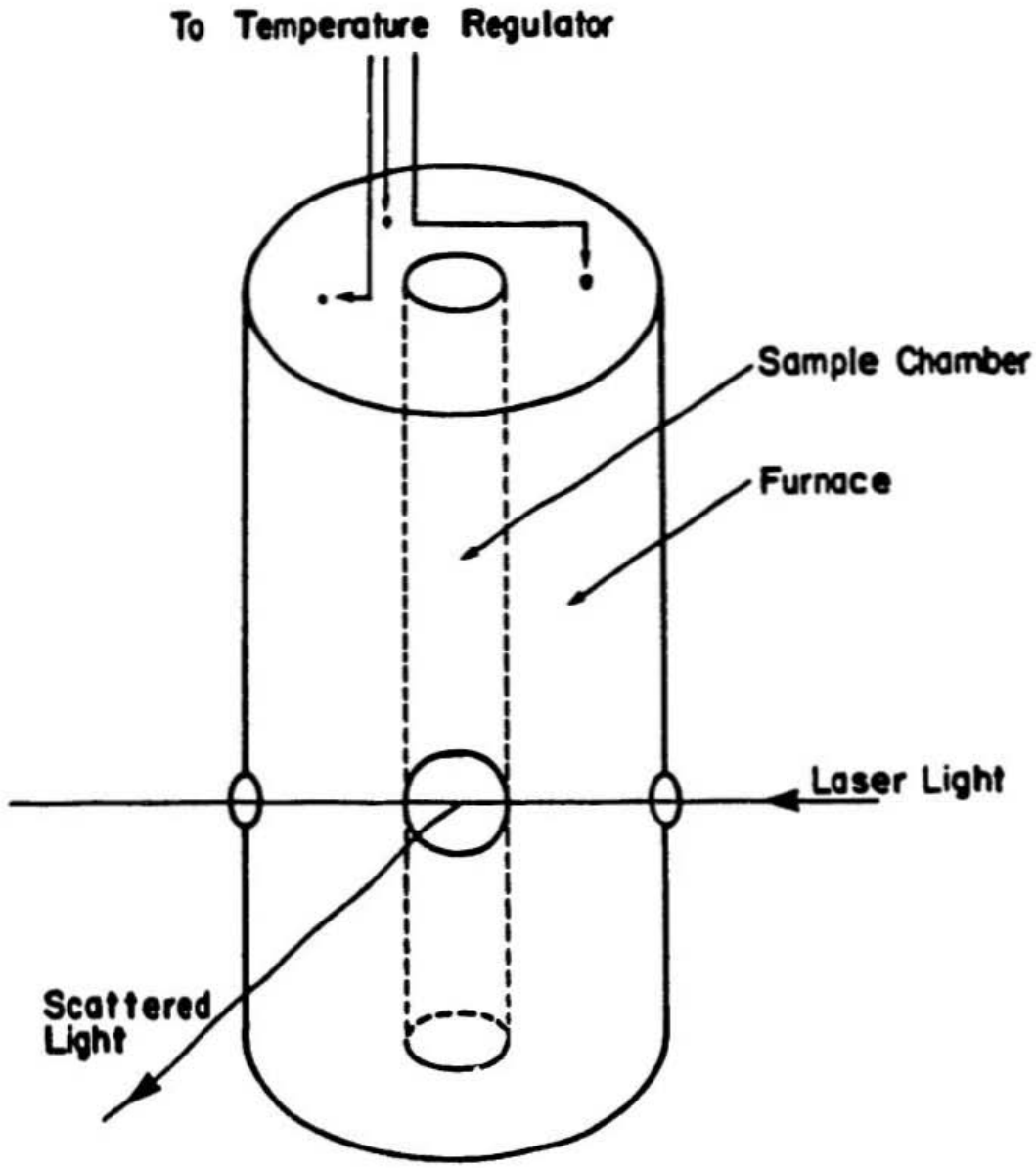

Fig. 3.1
The diagram of the Raman furnace

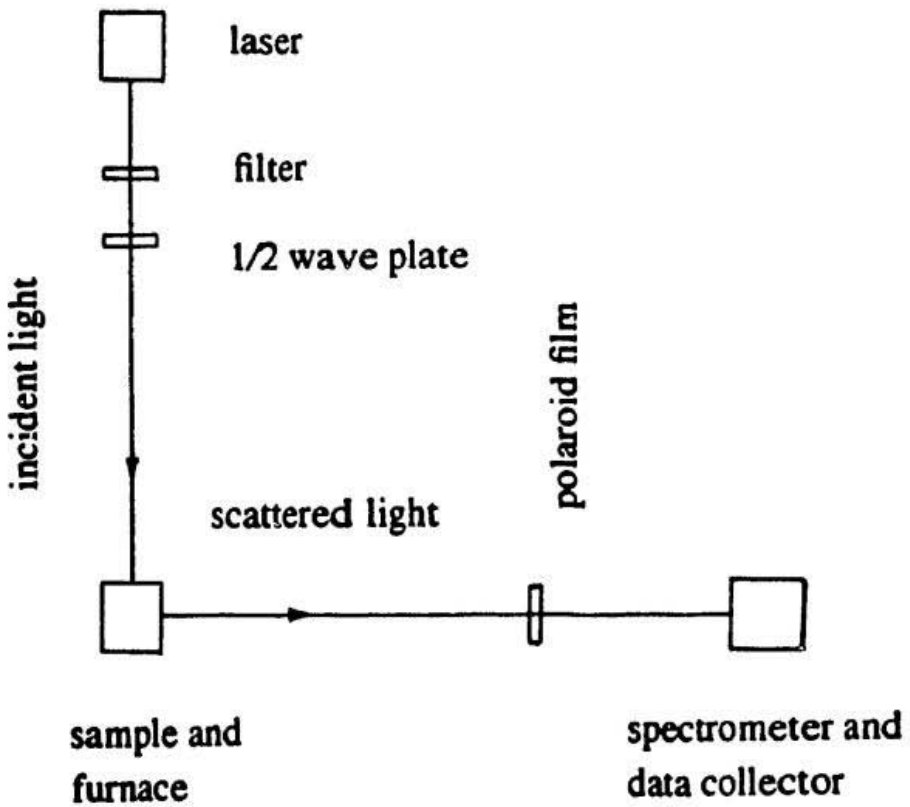

Fig. 3.2

The schematic representation of an experimental arrangement for Raman scattering from molten salts.

Chapter 4

RAMAN STUDIES ON THE STRUCTURES AND PROPERTIES OF THE COMPOUNDS FORMED IN THE $CdCl_2$/CsCl BINARY SYSTEM

4.1 Introduction

A major part of this project is the studies of phase equilibria of mixed binary salts of divalent metal and alkali metal chlorides in an attempt to identify possible complex formation in the molten mixtures and then to follow the formation of solid compounds as the melts are cooled. The cadmium chloride - alkali metal chloride system is interesting because:

i) Cadmium has been shown to form compounds with a wide range of coordination types due to the intermediate size of the Cd^{2+} ion. The coordination number of the Cd atom may not be equal to the apparent coordination number "m" in the compound A_nCdCl_m. The coordination number is strongly dependent on the other cation and the temperature. The possible coordination of Cd in solids are found to be:

a) discrete octahedral $CdCl_6^{4-}$ species

For example X-ray diffraction studies of K_4CdCl_6 and Rb_4CdCl_6 [Bergerhoff 1956, Wells 1962] indicated the presence of discrete octahedral $CdCl_6^{4-}$ species as shown in fig. 4.1a. Raman spectra indicate a characteristic Cd-Cl symmetric stretching vibration at 229 cm^{-1} [Clarke 1972a] or 230 cm^{-1}* and 221 cm^{-1}* respectively.

b) discrete tetrahedral $CdCl_4^{2-}$ species

For example Raman studies indicated that $[NEt_4]_2CdCl_4$ contains discrete $CdCl_4^{2-}$ species [Davis 1971]. The characteristic Raman band due to the ν_1 mode is at 265 cm^{-1}

* Refer to this work

[Davies 1971]. The discrete $CdCl_4^{2-}$ ion was found to be present in the high temperature solid Cs_2CdCl_4 (above 435 °C) as shown in fig. 4.1b with the ν_1 frequency at 269 cm^{-1}*). The metastable compound Cs_3CdCl_5 at room temperature and the stable form of Cs_3CdCl_5 at temperatures above 390°C contain discrete tetrahedral $CdCl_4^{2-}$ species with the ν_1 frequencies about 275 cm^{-1}* and 268 cm^{-1}* respectively. In the molten salts rich in ACl the tetrahedral $CdCl_4^{2-}$ species was found to be the dominant species and the ν_1 band was centered at 261 cm^{-1}*.

c) octahedral network structure

The room temperature solids Cs_2CdCl_4 and Rb_2CdCl_4 are isostructural with K_2NiF_4 with an octahedral network structure as shown in fig. 4.1c. The Cd-Cl stretching frequencies are 198* and 207 cm^{-1}* for Cs_2CdCl_4 and Rb_2CdCl_4 respectively.

ii) The number of the compounds formed and the corresponding compositions in the solid states are strongly dependent on the alkali ion. Usually large cations stabilize large anions but the solids formed in the alkali metal chloride cadmium chloride systems provide anomalous examples. In the $CdCl_2/KCl$ system, K_4CdCl_6 is a stable compound but K_2CdCl_4 can not be formed. In the $CdCl_2/CsCl$ system, Cs_2CdCl_4 can be prepared but not Cs_4CdCl_6. In the $CdCl_2/RbCl$ system, both Rb_4CdCl_6 and Rb_2CdCl_4 are stable compounds.

iii) Even compounds with the same formula (A_nCdCl_m) and similar crystal class may have structures that are very different for different cations. The effect of the alkali cation on the coordinational structure of the Cd atom is complicated. For example, the $ACdCl_3$-type compounds $KCdCl_3$ and $RbCdCl_3$ were suggested to be isostructural with NH_4CdCl_3 [Brasseur 1938, MacGillavry 1939]; $CsCdCl_3$ grown from solution was suggested to be hexagonal (space group $p6_3/mmc$) and has two crystallographically distinct types of cadmium ions with a complicated chain structure containing strings of pairs of linked $CdCl_6$ octahedra [Brasseur 1938, MacGillavry 1939]; NMe_4CdCl_3 [Adams 1971]

is isostructural with NMe_4NiCl_3 which has a single chain of $CdCl_6$ octahedra linked by opposite faces [Stucky 1968]. The structures of $CsCdCl_3$ and $RbCdCl_3$ were found to be dependent on the preparation method of the crystals grown from melts or aqueous solutions [Siegel 1964, Chang 1975, Møller 1977]. The different structures of these compounds with different cations exhibited different characteristic Raman spectra. Raman spectra of NH_4CdCl_3 have shown two intense bands at 244 and 219 cm^{-1} [Bergerhoff 1956] (or 244 and 222 cm^{-1} [Adams 1971]) at 25°C in the Cd-Cl stretching region. However Raman spectra showed a single symmetric stretching band at 249 cm^{-1}* for $CsCdCl_3$ and a band at 251 cm^{-1} for NMe_4CdCl_3 at 25°C [Adams 1971].

The effect of alkali ion, temperature and other factors on the structures and properties of the complex compounds and their mixtures have been systematically studied in the present work. In this chapter the phase equilibria, compound formation and the structures and properties of the compounds formed in the $CdCl_2/CsCl$ binary system will be discussed. A special structural phase transition in Cs_2CdCl_4 will be described in chapter 5. The structures and properties of the $CdCl_2/RbCl$ (KCl) fused binary systems and the $CdCl_2$/ACl (A = Cs, Rb and K) molten states will be discussed in chapters 6 and 7 respectively.

There is an additional reason to study the $CdCl_2/CsCl$ binary system. Although the phase diagram for this system has been reported many times [Dergurov 1949, Seifert 1965, 1968, 1979, 1986, Filippov 1973, Belyaev 1972, Iskandarov 1976], the results are not in full agreement. Table 4.1 lists results for seven studies reported by several authors from 1965 to 1986. Except for the compounds Cs_2CdCl_4 and $CsCdCl_3$, there are arguments about the other compounds. Fig. 4.2 presents a recently reported phase diagram by Seifert and Thiel [Seifert 1986]. Five compounds, $CsCd_5Cl_{11}$, $CsCdCl_3$, $Cs_3Cd_2Cl_7$, Cs_2CdCl_4 and Cs_3CdCl_5 were identified.

4.2 Results and Discussion

4.2.1 Compound Formation

Raman spectra obtained from solid samples of different compositions at room temperature are presented in fig. 4.3 (mole fraction of CsCl from x = 0.80 to 0.40) and fig. 4.4 (x = 0.33 to 0). The frequencies of the peak maxima for the most characteristic bands and the corresponding compounds suggested are listed in table 4.2. Five compounds, Cs_3CdCl_5, Cs_2CdCl_4, $Cs_3Cd_2Cl_7$, $CsCdCl_3$ and $CsCd_5Cl_{11}$ have been identified.

Cs_3CdCl_5:

The compound with this formula forms from the melt but is only stable above 390°C. It has a strong peak at 268 cm^{-1} characteristic of a discrete tetrahedral $CdCl_4^{2-}$ species. At 390°C the compound decomposed into a mixture of Cs_2CdCl_4 and $CsCl$ and exhibited the similar spectrum to that of pure Cs_2CdCl_4 at room temperature (fig. 4.5b). The fast cooled sample gave a metastable form at low temperature with a characteristic Cd-Cl frequency at 275 cm^{-1} (fig. 4.5a). The solid corresponding to a mixture with composition x = 0.80 was found to be a mixture of $CsCl$ and Cs_3CdCl_5 when cooled from the melt and kept above 390°C and a mixture of $2CsCl$ and Cs_2CdCl_4 from 390°C to room temperature (fig. 4.3). The increased intensity in the 150 cm^{-1} region with the increase of $CsCl$ can be attributed to weak second order scattering from solid $CsCl$.

Cs_2CdCl_4:

Slowly cooled samples of the composition x ≥ 0.67 exhibited similar spectra at room temperature with a characteristic intense band at 198 cm^{-1} except that samples with composition x > 0.67 showed additional weak bands in the 100 - 150 cm^{-1} region due to second order scattering from CsCl [Agrawal 1975] (fig. 4.3, x = 0.80, 0.75, 0.67). These results suggest the formation of a stable room temperature compound Cs_2CdCl_4. The similarity of the spectra observed for both the slowly and fast cooled Cs_2CdCl_4 suggests a congruent compound. This compound was observed to have a high temperature phase

with a transition which started at about 435°*C* but was not complete until 460°*C*. The high temperature phase of Cs_2CdCl_4 has a strong peak at 268 cm^{-1} characteristic of the discrete tetrahedral $CdCl_4^{2-}$ (fig. 4.5e).

$CsCdCl_3$:

The sample of the composition x = 0.50 gave a unique spectrum and a characteristic intense band at 249 cm^{-1} (fig. 4.3, 0.50). This peak (249 cm^{-1}) can be identified in the spectra for the slowly cooled x = 0.40, 0.33, 0.25, 0.22 and 0.20 samples and the fast cooled x = 0.60 sample (fig. 4.3, x = 0.40 and fig. 4.4, x = 0.33, 0.25, 0.22 and 0.20). These results suggest the formation of a compound with the formula $CsCdCl_3$. It is also a congruent compound.

$Cs_3Cd_2Cl_7$:

The Raman spectrum for the x = 0.60 sample was strongly dependent on the cooling rate when it was prepared. For the quenched sample there were two intense bands at 198 and 249 cm^{-1}, and a very weak band at 221 cm^{-1} (fig. 4.6a). When the cooling rate was moderately low as 1°*C*/min, the relative intensity of the 221 cm^{-1} band was slightly increased. However, if the cooling rate was very low (a few degrees per day in the temperature range 440 - 450°*C*) the 221 cm^{-1} band was much stronger and the band at 249 cm^{-1} became very weak as shown in fig. 4.6b. This observation is in agreement with Seifert's result [Seifert 1979] which indicated a solid-solid reaction between $CsCdCl_3$ and Cs_2CdCl_4 to form the incongruent compound $Cs_3Cd_2Cl_7$ at about 450°*C*. The band at 221 cm^{-1} is attributed to this compound $Cs_3Cd_2Cl_7$. The bands at 198 cm^{-1} and 249 cm^{-1} were assigned to Cs_2CdCl_4 and $CsCdCl_3$ that resulted because the cooling rate was still not low enough.

$CsCd_5Cl_{11}$:

For the samples with the composition 0.17 < x < 0.50, there were bands at 249 and 215 cm^{-1}, and a broader shoulder centered at about 196 cm^{-1}, while for the x = 0.17

sample there were only two bands at 215 and 196 cm^{-1} (fig. 4.4). For the x < 0.17 sample a new peak was observed at 231 cm^{-1} which was assigned to $CdCl_2$. These results suggest the formation of the compound $CsCd_5Cl_{11}$ on the $CdCl_2$ rich side. In fig. 4.7 three pairs of spectra are illustrated to show the results obtained from the fast and slowly cooled samples with x = 0.20, 0.17 and 0.14. The relative intensity of the band at 231 cm^{-1} depends strongly on the cooling rate. The peak is intense for the fast cooled x = 0.17 sample (fig. 4.7 $CsCd_5Cl_{11}$ **F**), but has almost disappeared for the slowly cooled sample (fig. 4.7 $CsCd_5Cl_{11}$ **S**). The result indicates that $CsCd_5Cl_{11}$ is an incongruent compound and the peritectic reaction is:

$$CsCd_5Cl_{11_{(s)}} = CdCl_{2_{(s)}} + liquid$$

The weak shoulder centered at 231 cm^{-1} for the slowly cooled 0.17 (fig. 4.7 $CsCd_5Cl_{11}$ **S**) sample may be due to a small error in the composition or a cooling rate that was not low enough in the peritectic temperature range.

For the x < 0.17 samples, the relative intensity of the band at 231 cm^{-1} increased as the concentration of $CdCl_2$ increased. The intense band at 231 cm^{-1} was assigned to the A_{1g} mode of $CdCl_2$ with space group $R\bar{3}m$ (D_{3d}^5) [Donnay 1963]. The result is in good agreement with previous Raman studies [Anderson 1981] which indicated the intense A_{1g} band at 233 ± 1 cm^{-1}.

The analysis described above indicates that the present Raman results are in excellent agreement with Seifert's [1979, 1986] results regarding compound formation. However, these are not in full agreement about the structural phase transition in Cs_2CdCl_4. This structural phase transition was reported to occur at about 459°C [Seifert 1986]. The present study indicates that the structural phase transition takes place over a wide temperature range from 435°C to just below the melting point with a dynamic equilibrium between the two solid phases.

4.2.2 Structures and Properties

4.2.2.1 Compound Cs_2CdCl_4

Cs_2CdCl_4 is a congruent compound. Raman spectra measured for samples over a range of temperatures indicate a structural phase transition which occurs over a wide temperature range from $435°C$ to just below the melting point. At any temperature within this temperature range the high and low temperature phases coexist and have an equilibrium distribution which is dependent on the temperature. A study of the structural phase transition and the solid-solid phase equilibrium will be discussed in the next chapter.

The room temperature solid Cs_2CdCl_4 is tetragonal [Siegel 1964], a = b = 5.26 Å and c = 16.88 Å, and isostructural with K_2NiF_4 [Balz 1953]; space group I_4/mmm (D_{4h}^{17}): two formula per unit cell and one per primitive cell. Each cadmium atom is bonded to six chloride neighbours in an octahedral configuration, and each octahedron shares four corners with other octahedra. Factor group analysis based on the D_{4h} group has been given in detail by Brooker [Brooker 1975] for K_2NiF_4 type compounds in the Raman studies of the solid K_2MgCl_4. The vibrational modes are:

$$\Gamma_{vib} = 2A_{1g} + 4A_{2u} + 2E_g + 5E_u + B_{2u}$$

The two A_{1g} and two E_g modes are Raman active. The totally symmetric vibration of A_{1g} should appear in the XX, YY, ZZ components of the scattering tensor, and the doubly degenerated E_g modes in the ZX and ZY components in the Raman spectrum of a single crystal. Four bands have been detected (fig. 4.5d) and assigned (table 4.3) by comparison with the peak position and relative intensity of the corresponding band in the polarized Raman spectrum of a single crystal of Rb_2CdCl_4 [Aleksandrov 1985a] which is isostructural with Cs_2CdCl_4. The most intense band in the spectrum of Cs_2CdCl_4 occurs at 198 cm^{-1} which corresponds to a similar band at 208 cm^{-1} in Rb_2CdCl_4. The present Raman results are in good agreement with the predictions from factor group analysis based on the known crystal structure from the X-ray studies [Siegel 1964]. In previous Raman

studies of this compound [Clarke 1972a] two bands observed at 251 and 231 cm^{-1} in the symmetric Cd-Cl stretching region have not been detected in the present study. Only an intense band at 198 cm^{-1} was observed in this region. Careful Raman studies indicated that there was no large frequency shift of the band at 198 cm^{-1} in a temperature range 25 - 435°C. At 435°C a structural phase transition took place.

The high temperature solid Cs_2CdCl_4 is isostructural with β-K_2SO_4 [Seifert 1986] which has an orthorhombic pseudohexagonal unit, four formula units per primitive cell; space group Pnma (D_{2h}^{16}) [Wyckoff 1965b]. Discrete $CdCl_4^{2-}$ tetrahedral species are present. The Cs^+ ions and $CdCl_4^{2-}$ ions sit on positions with m (c_s) symmetry. The correlation diagram for the internal modes of $CdCl_4^{2-}$ in this type of structure has been discussed in detail by Brooker [Brooker 1975]. The 36 internal modes are:

$$\Gamma_{internal} = 6A_g + 6B_{1g} + 3B_{2g} + 3A_u + 3B_{1u} + 6B_{2u} + 6B_{3u} + 3B_{3g}.$$

and the 45 external modes are:

$$\Gamma_{external\ rotatory} = A_g + B_{1g} + 2B_{2g} + 2B_{3g} + 2A_u + 2B_{1u} + B_{2u} + B_{3u},$$

$$\Gamma_{external\ translatory} = 6A_g + 6B_{1g} + 3B_{3g} + 3A_u + 3B_{1u} + 6B_{2u} + 6B_{3u}.$$

Although the 24 lattice modes are theoretically Raman active, the combination of high temperature and Rayleigh wing scattering preclude the possibility of detecting the weak broad external vibrations. Band overlap due to broadening by thermal motion at high temperature also severely limits detection of the site and correlation field effects of the internal modes of the $CdCl_4^{2-}$ ion.

The Raman spectrum obtained at about 450°C is shown in fig. 4.5e and the frequencies of the bands observed and their assignments are listed in table 4.3. The results are consistent with the factor group analysis and X-ray result [Seifert 1986]. Two bands at 268 and 102 cm^{-1} can be assigned to the ν_1 and ν_4 modes of the tetrahedral $CdCl_4^{2-}$ species based on the D_{2h} factor group. The shoulders at about 85 and 250 cm^{-1} on the

low frequency sides of the bands at 102 and 268 cm^{-1} respectively are due to the ν_2 and ν_3 vibrations. Since there is a dynamic equilibrium between the high and low temperature solids Cs_2CdCl_4, the four weak bands at 40, 65, 92 and 194 cm^{-1} observed in the spectrum are attributed to the low temperature Cs_2CdCl_4 solid phase.

4.2.2.2 Compound $CsCdCl_3$

Several X-ray studies have been reported for $CsCdCl_3$. Ferrari and Baroni [Ferrari 1927] suggested a cubic, perovskite type structure, while Náray-Szabo [Náray 1947] indicated a monoclinic symmetry. Siegel and Gebert [Siegel 1964] reported that crystals grown from the melts developed with hexagonal symmetry, but those grown from solution are predominantly hexagonal with small amounts of a cubic modification present. Chang and Mcpherson [Chang 1975] have confirmed that the compound crystallizes in the hexagonal space group $P6_3/mmc$ and has two crystallographically distinct types of cadmium ions. One of the Cadmium ions, Cd(1), occupies a site having D_{3d} symmetry, while the other, Cd(2), exhibited C_{3v} site symmetry. This structure was considered as intermediate between the $CsNiCl_3$ structure which consists of infinite linear arrays of octahedral sharing faces and the perovskite structure which consists of a three-dimensional network of octahedra sharing corners. Further, Møller [Møller 1977] found that the compound grown from a dilute solution of CsCl and $CdCl_2$ formed birefringent white crystal which is different from crystal grown from the melt. Further, when a precipitate of composition $CsCdCl_3$ was left for about three months in the mother liquor, it lost its birefringence and had formed an ideal cubic perovskite structure. On heating crystals of $CsCdCl_3$ with the perovskite structure to about 230 °C the crystals gradually became birefringent, and X-ray results showed that both the cubic and the hexagonal forms were present. This solid state transformation was reported to be very sluggish. The presence of a trace amount of water appears to stabilize a cubic perovskite structure which is different from the hexagonal structure of the crystal grown from the melt.

Factor group analysis based on the $P6_3/mmc$ space group [Chang 1975] predicts 87 optical modes of vibrations with 33 Raman active modes [Gorban 1990].

$$5A_{1g} + 6E_{1g} + 8E_{2g}$$

The Raman spectrum from polycrystalline $CsCdCl_3$ is presented (fig. 4.6d) with the frequencies and assignments given (table 4.4). The polarized Raman spectra of a hexagonal single crystal $CsCdCl_3$ have been recently studied by Gorban et al. [Gorban 1990] at 300, 77 and 2K, and by Kuok [Kuok 1983]. The present results are in good agreement with the previous studies. However, the band at 208 cm^{-1} observed by Kuok [Kuok 1983] was not detected in present study or in that of Gorban et al. Further a band at 196 cm^{-1} was observed and assigned to the E_{2g} mode by Gorban. Although the band appeared in our spectrum, it might be due to the Cs_2CdCl_4 impurity not $CsCdCl_3$. The spectrum (fig. 4.6c) for the quenched sample showed an intense band at 249 cm^{-1}, and a weak band at 197 cm^{-1}. But for a slowly cooled sample, the band at 197 cm^{-1} became very very weak (fig. 4.6d) and a new weak band at 221 cm^{-1} appeared which indicates that a solid-solid reaction took place between the compounds Cs_2CdCl_4 (197 cm^{-1}) and $CsCdCl_3$ (249 cm^{-1}) to form a new compound $Cs_3Cd_2Cl_7$ (221 cm^{-1}).

The present studies indicate that $CsCdCl_3$ is a congruent compound. Measurements of Raman spectra for samples at temperatures from room temperature up to the melting point indicated that there were no structural phase transitions over this range.

4.2.2.3 Compound Cs_3CdCl_5

The compound Cs_3CdCl_5 is unusual. DTA and X-ray patterns [Seifert 1979] indicated that it is not stable below 395°C at which temperature it decomposes into a mixture of Cs_2CdCl_4 and $CsCl$. The sample quenched from the melt to room temperature could give a metastable form at room temperature. The Raman spectra observed for this compound in both the stable (390°C) and metastable forms (25°C) are shown in fig. 4.5.

Cs_3CdCl_5 is tetragonal [Seifert 1979], isostructural with Cs_3CoCl_5, with four formula units in the unit cell and two per primitive cell; space group I_4/mcm (D_{4h}^{18}). Each Cd atom is tetrahedrally surrounded by four Cl atoms as discrete species. The other chloride atoms have only cesium neighbors which surround them octahedrally. Factor group analysis for optic modes of vibrations of the tetrahedral $CdCl_4^{2-}$ was given in detail by Brooker [Brooker 1980] for an isostructural compound Cs_3MgCl_5. There are 54 normal modes:

$$\Gamma_{total} = 3A_{1g} + 3A_{2g} + 2B_{2g} + 4B_{2g} + 6E_g + 2A_{1u} + 6A_{2u} + 3B_{1u} + B_{2u} + 9E_u.$$

Since the $CdCl_4^{2-}$ ion has a D_{2d}' site symmetry, the internal and external modes of $CdCl_4^{2-}$ are:

$$\Gamma_{CdCl_4^{2-}\,internal} = 2A_{1g} + B_{1g} + 2B_{2g} + 2E_g + A_{1u} + 2A_{2u} + 2B_{1u} + 2E_u$$

$$\Gamma_{CdCl_4^{2-}\,external\ translatory} = B_{2g} + E_g + A_{2u} + E_u$$

$$\Gamma_{CdCl_4^{2-}\,external\ rotatory} = A_{2g} + E_g + B_{2u} + E_u$$

The Raman spectrum of the metastable crystalline Cs_3CdCl_5 at room temperature (fig. 4.5a) indicated the presence of the $CdCl_4^{2-}$ tetrahedral species. Peak frequencies and tentative assignments (table 4.3) are in excellent agreement with the factor group prediction based on the X-ray result [Seifert 1979]. The ν_1 band observed at 275 cm^{-1} is consistent with the ν_1 frequencies for $CdCl_4^{2-}$ in the stable high temperature solid (268 cm^{-1} in Cs_2CdCl_4) and in the molten state (261 cm^{-1}). Two components were detected in the ν_4 region at about 103 and 110 cm^{-1}, while only one component was observed for ν_2 at 77 cm^{-1}. The ν_3 band appeared at 261 cm^{-1} on the low frequency side of the ν_1 band. It seems very probable that the 261 cm^{-1} band is due to the A_g factor group component of ν_3 in Fermi resonance with the A_g component of ν_1. Raman depolarization measurements for $CdCl_4^{2-}$ in the molten phase confirmed that ν_1 and ν_3 are almost coincident. Four weak external lattice modes were detected below 70 cm^{-1} and although difficult to assign

they provide strong evidence to indicate that the Cs_3CdCl_5 has the Cs_3CoCl_5 crystal structure.

The stable form of the sample with the composition Cs_3CdCl_5 at room temperature is a mixture of Cs_2CdCl_4 and $CsCl$. The spectrum for the sample with the composition $Cs_2CdCl_4 \cdot CsCl$ at room temperature is also shown in fig. 4.5. The relative intensities, peak positions, and the number of the bands observed are the similar as those in the spectrum obtained from Cs_2CdCl_4 at the same temperature except for a little difference due to the second order scattering of $CsCl$ in the 150 cm^{-1} region.

4.2.2.4 Compounds $CsCd_5Cl_{11}$ and $Cs_3Cd_2Cl_7$

The Raman spectrum of solid $CsCd_5Cl_{11}$ at room temperature is shown (fig. 4.4, x = 0.17) and the band positions are collected in table 4.4. The Raman spectrum (fig. 4.4, x = 0.17) shows a strong band at 215 cm^{-1} and a broader low frequency shoulder centered at about 196 cm^{-1} in the Cd-Cl stretching region. The relative intensities of the two bands at 196 and 215 cm^{-1} are independent of the cooling rate of the sample from the melt (fig. 4.7 $CsCd_5Cl_{11}$ **F. S**). Therefore both the bands are attributed to the same compound $CsCd_5Cl_{11}$. The frequency for the broader shoulder (196 cm^{-1}) is very close to the Cd-Cl stretching frequency for Cs_2CdCl_4 (198 cm^{-1}). The presence of two relatively strong peaks in the Cd-Cl stretching region may indicate two different crystallographic sites and two different types of octahedral cadmium.

The compound $Cs_3Cd_2Cl_7$ is stable only at temperatures below 450°C. In this work the pure compound has not been prepared because the reaction between the two solid phases is very slow. The Raman spectrum obtained for this compound containing Cs_2CdCl_4 and $CsCdCl_3$ impurities is shown in fig. 4.6. The characteristic band at 221 cm^{-1} in the Cd-Cl stretching region is attributed to this compound. The frequency of this band suggests that the Cd atom may have an octahedral coordination geometry since the band position at 221 cm^{-1} is in the range of octahedral $CdCl_6$ stretching frequencies from

198 cm^{-1} (Cs_2CdCl_4) to 249 cm^{-1} ($CsCdCl_3$). This agrees with the X-ray result [Seifert 1986] which suggested that the compound $Cs_3Cd_2Cl_7$ is isostructural with $Rb_3Mn_2Cl_7$ which has octahedral coordination of the Mn atom.

Table 4.1

The compounds suggested by previous studies in the $CdCl_2/CsCl$ binary system.

Seifert (1965)		Cs_3CdCl_5	Cs_2CdCl_4	$Cs_3Cd_2Cl_7$	$CsCdCl_3$	$CsCd_5Cl_{11}$	
Seifert (1968)		Cs_3CdCl_5	Cs_2CdCl_4	$Cs_3Cd_2Cl_7$	$CsCdCl_3$	$CsCd_5Cl_{11}$	
Belyaev (1972)		Cs_3CdCl_5	Cs_2CdCl_4		$CsCdCl_3$		
Filippopv (1973)			Cs_2CdCl_4	$Cs_3Cd_2Cl_7$	$CsCdCl_3$		
Ilyasov (1976)	Cs_4CdCl_6		Cs_2CdCl_4		$CsCdCl_3$		$\alpha - + \beta - CdCl_2$
Seifert (1979)		Cs_3CdCl_5	Cs_2CdCl_4	$Cs_3Cd_2Cl_7$	$CsCdCl_3$	$CsCd_5Cl_{11}$	
Seifert (1986)		Cs_3CdCl_5	Cs_2CdCl_4	$Cs_3Cd_2Cl_7$	$CsCdCl_3$	$CsCd_5Cl_{11}$	

Table 4.2

The Raman frequencies (cm^{-1}) of the characteristic bands in the Cd-Cl stretching regions and the corresponding suggested compounds in the $CdCl_2$/CsCl system.

composition	frequency	compound
0.80	198 (s)*	Cs_2CdCl_4
0.75	198 (s)	Cs_2CdCl_4
0.67	198 (s)	Cs_2CdCl_4
0.60	221 (s)	$Cs_3Cd_2Cl_7$
0.50	249 (s)	$CsCdCl_3$
0.40	196 (br)	$CsCd_5Cl_{11}$
	215 (m)	$CsCd_5Cl_{11}$
	249 (s)	$CsCdCl_3$
0.33	196 (br)	$CsCd_5Cl_{11}$
	215 (s)	$CsCd_5Cl_{11}$
	249 (s)	$CsCdCl_3$
0.25	196 (br)	$CsCd_5Cl_{11}$
and	215 (s)	$CsCd_5Cl_{11}$
0.22	249 (w)	$CsCdCl_3$
0.20	196 (br)	$CsCd_5Cl_{11}$
	215 (s)	$CsCd_5Cl_{11}$
	249 (vw)	$CsCdCl_3$
0.17	196 (br)	$CsCd_5Cl_{11}$
	215 (s)	$CsCd_5Cl_{11}$
	231 (vw)	$CdCl_2$
0.14	196 (br)	$CsCd_5Cl_{11}$
	215 (s)	$CsCd_5Cl_{11}$
	231 (s)	$CdCl_2$
0	231	$CdCl_2$

* s - strong, w - weak, m - medium, br - broad, vw - very weak

Table 4.3

The vibrational frequencies (cm^{-1}) and tentative assignments of the bands observed for Cs_2CdCl_4 and Cs_3CdCl_5.

Cs_2CdCl_4			Cs_3CdCl_5			
LTP*		HTP	metastable		stable	assignments**
I_4/mmm		P_{nma}	I_4/mcm			
(D_{4h}^{17})		(D_{2h}^{16})	(D_{4h}^{18})			
(298K)		(723K)	77K	(298K)	(668K)	
42(vw)	E_g			39(vw)	37.5(w)	lattice
69(w)	E_g		44(vw)	43.5(vw)		
92(w)	A_{1g}		60(w)	59.5(w)		
198(s)	A_{1g}		68(w)	67.5(w)		
		85(w)	78.5(m)	77(br)	79(br)	ν_2
		102(w)	104(m)	103(m)	104(br,m)	ν_4
			112.5(m)	110(m)		ν_4
		250(w)	264.5(m)	261(w)		ν_3
		268(s)	278.5(m)	275(s)	268(s)	ν_1

* LTP - low temperature phase; HTP - high temperature phase

** Assignments for the tetrahedral $CdCl_4^{2-}$ in the Cs_3CdCl_5 and the HTP of Cs_2CdCl_4.

Table 4.4

The vibrational frequencies (cm^{-1}) of the bands for compounds $CsCdCl_3$ and $CsCd_5Cl_{11}$.

$CsCdCl_3$				$CsCd_5Cl_{11}$
	$P6_3/mmc$			unknown
b	this work	c	assignments	
		30	E_{2g}	
46	44(vw[a])	45	A_{1g}	41.5(m)
52	58(vw)	52	E_{2g}	45(w)
71	68.5(w)	69	E_{2g}	54(w)
85	82(vw)	83	E_{1g}	59(m)
115	116(s)	116	A_{1g}	64.5(m)
128	129(s)	129	E_{2g}	73(s)
156	164(vw)	163	E_{2g}	98(m)
170		196	E_{2g}	108(br)
208				129(m)
248	249(vs)	249	A_{1g}	145(br)
				196(br)
				215(s)

a - vs (very strong), s (strong), vw (very weak), w (weak), br (broad), m (medium).

b - Ref. [Kuok 1983]

c - Ref. [Gorban 1990]

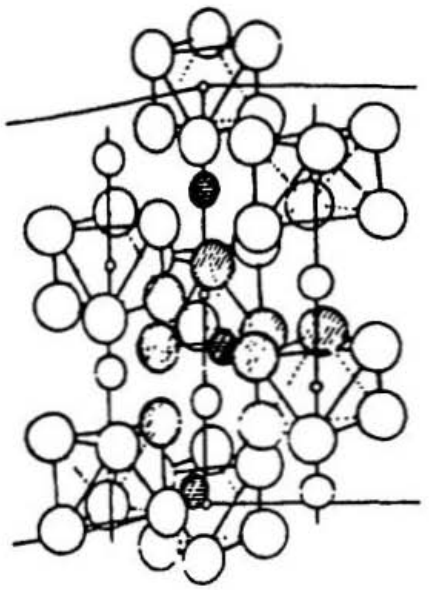

(a)

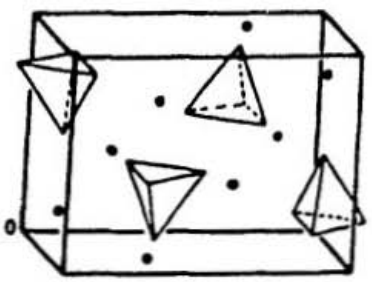

(b) (c)

Fig. 4.1

Examples of the structures of the three major coordinations types of Cd^{2+} with Cl^- ions. (a): discrete $CdCl_6^{4-}$ species in K_4CdCl_6 [Bergerhoff 1956]; (b): discrete $CdCl_4^{2-}$ species in the high temperature solid Cs_2CdCl_4 [Cs_2MgCl_4, Brooker 1983]; (C): linked $CdCl_6$ octahedral units in the low temperature solid Cs_2CdCl_4 [K_2MgCl_4, Brooker 1983].

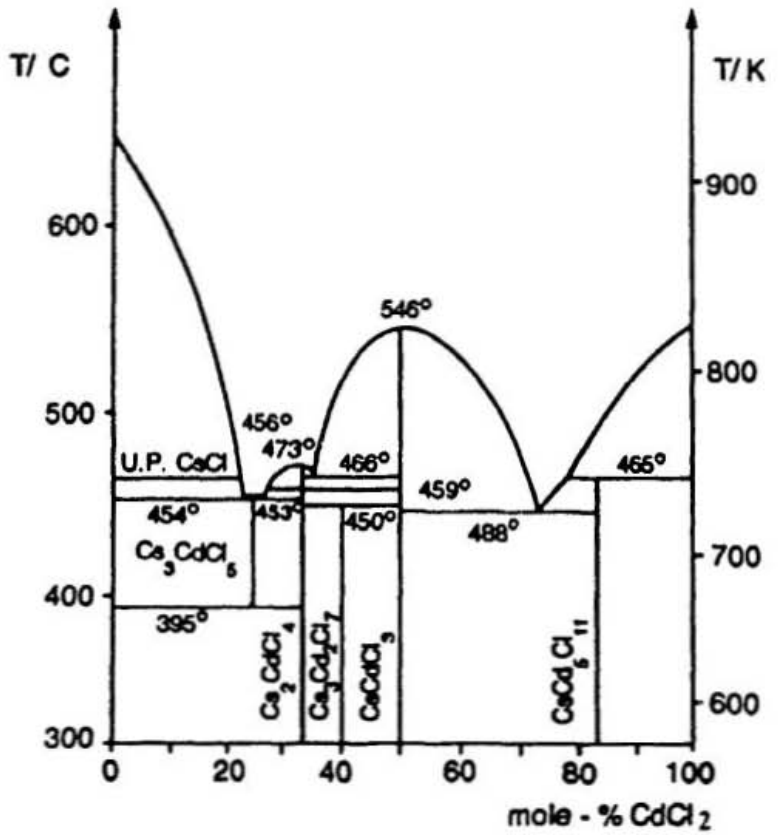

Fig. 4.2

The phase diagram of the $CdCl_2$-$CsCl$ system. Redrawn from Ref. [Seifert 1986].

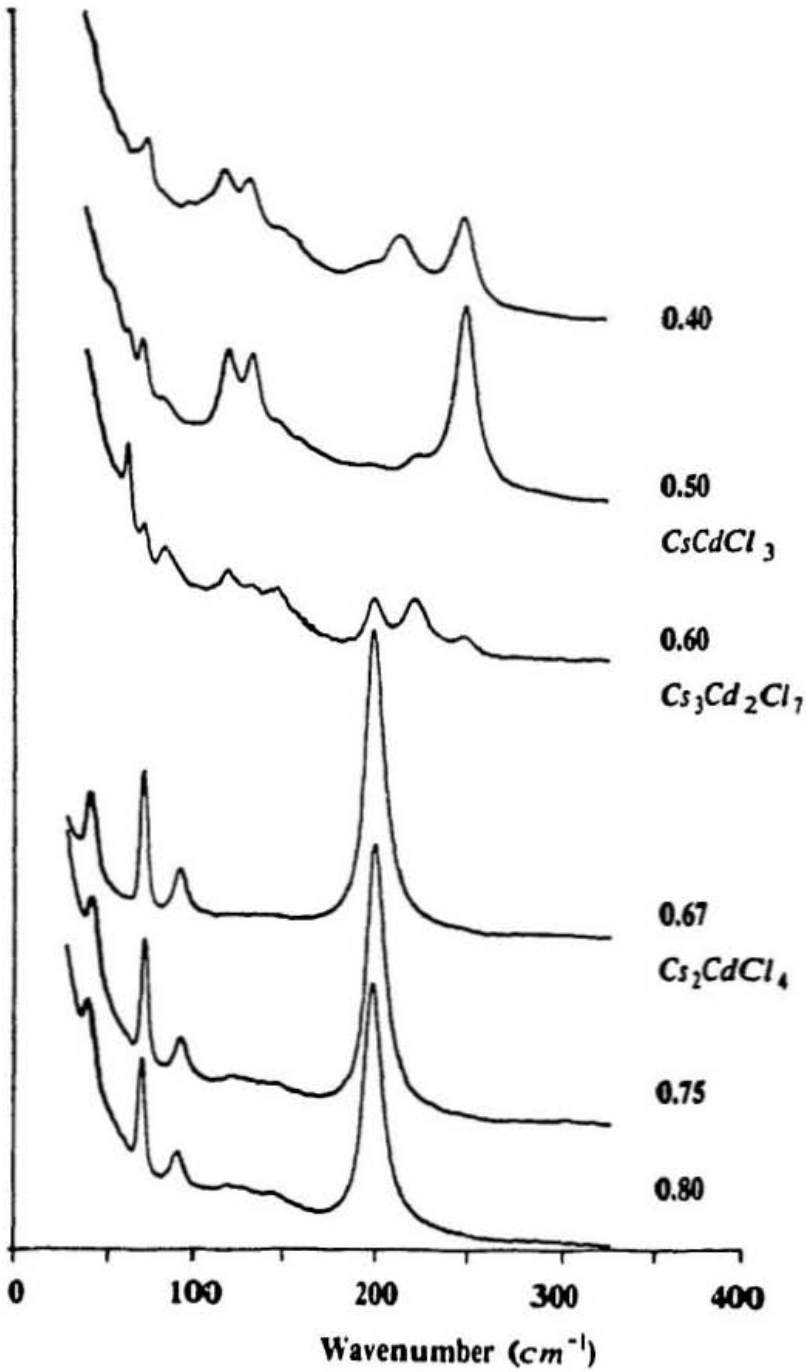

Fig. 4.3

Raman spectra obtained for the $CdCl_2/CsCl$ binary system with mole fraction of $CsCl$ 0.80, 0.75, 0.67, 0.60, 0.50, and 0.40 respectively. Temperature 25°C; Slits 2 cm^{-1}.

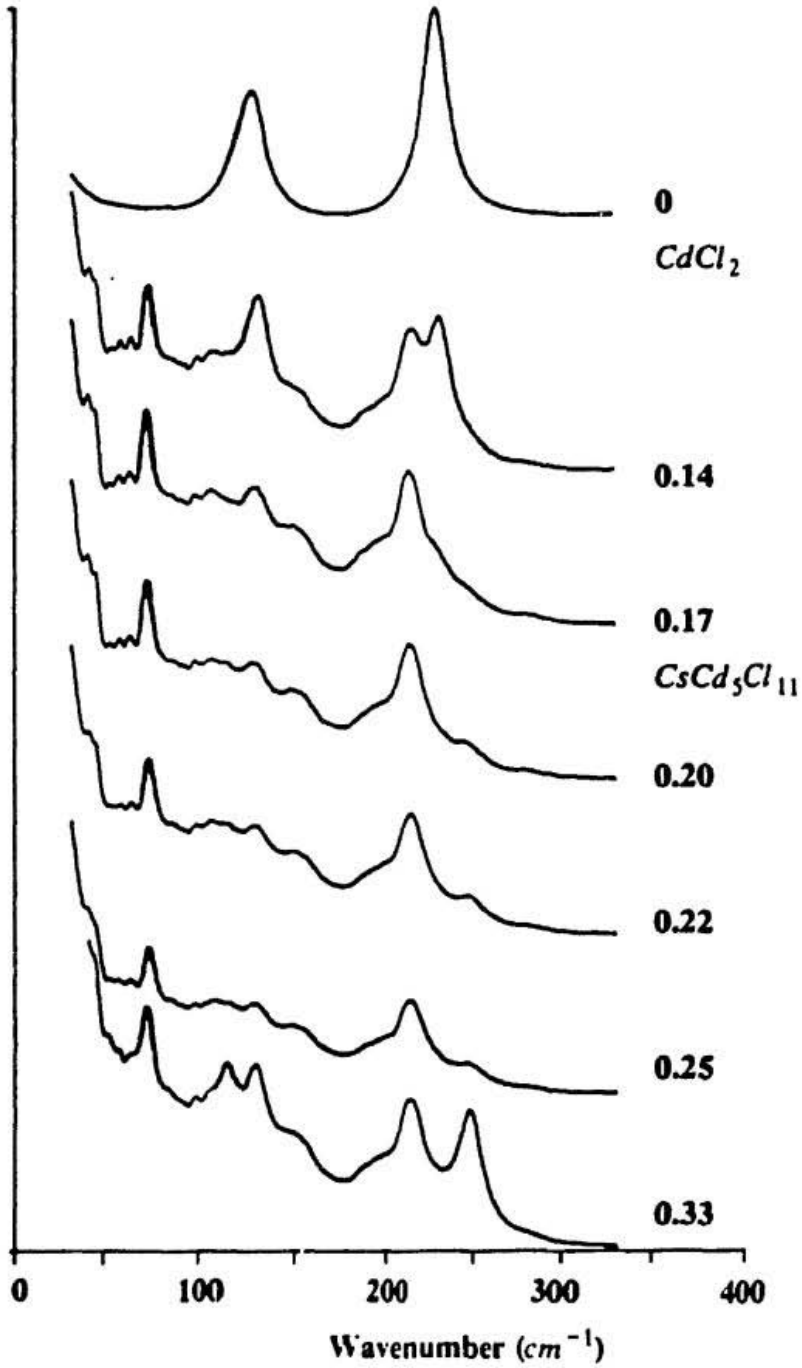

Fig. 4.4

Raman spectra obtained for the $CdCl_2/CsCl$ binary system with mole fraction of $CsCl$ 0, 0.14, 0.17, 0.20, 0.22, 0.25, and 0.33, respectively. Temperature 25°C. Slits 2 cm^{-1}.

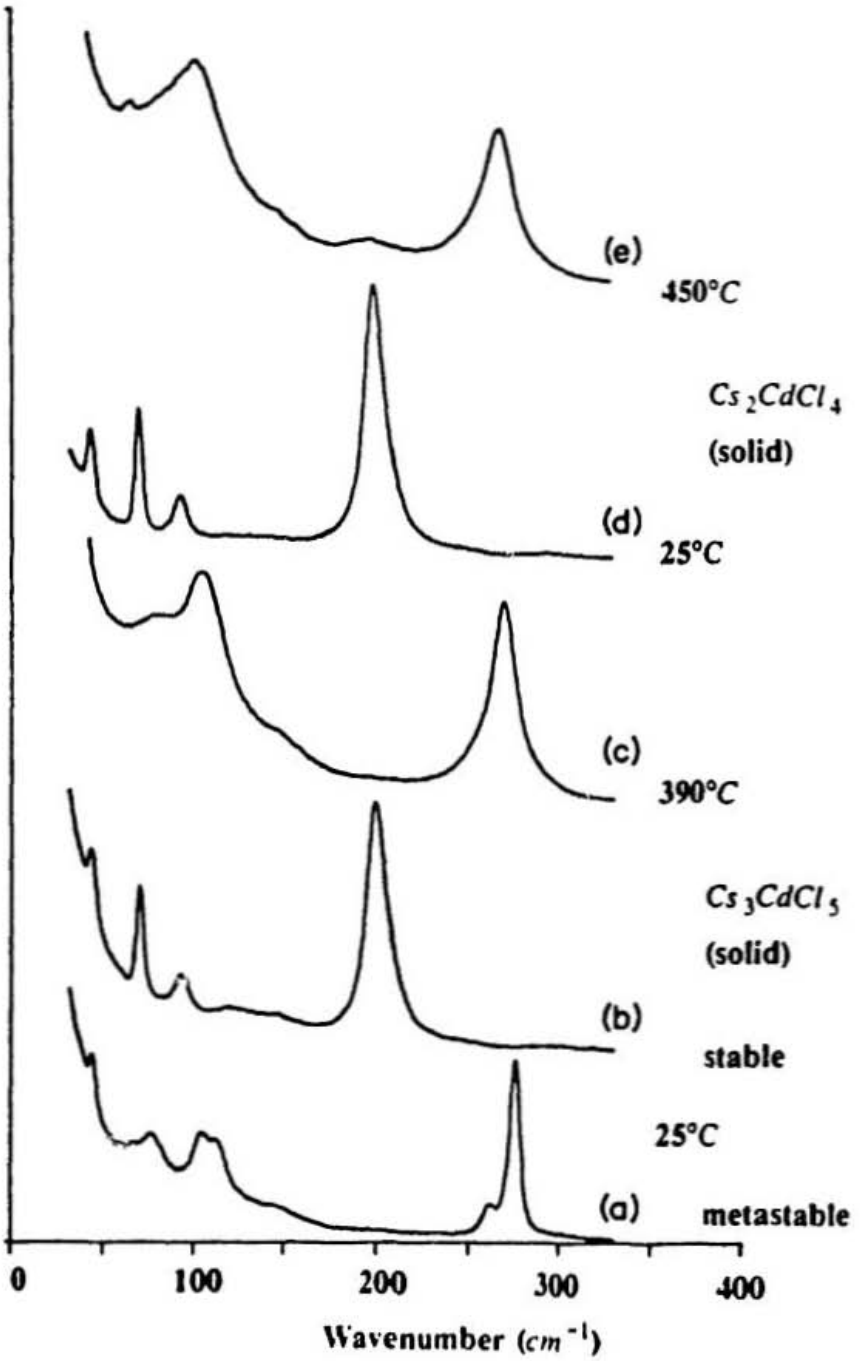

Fig. 4.5

Raman spectra obtained for Cs_3CdCl_5 and Cs_2CdCl_4 in various solid phases. Slits 2 cm^{-1}.

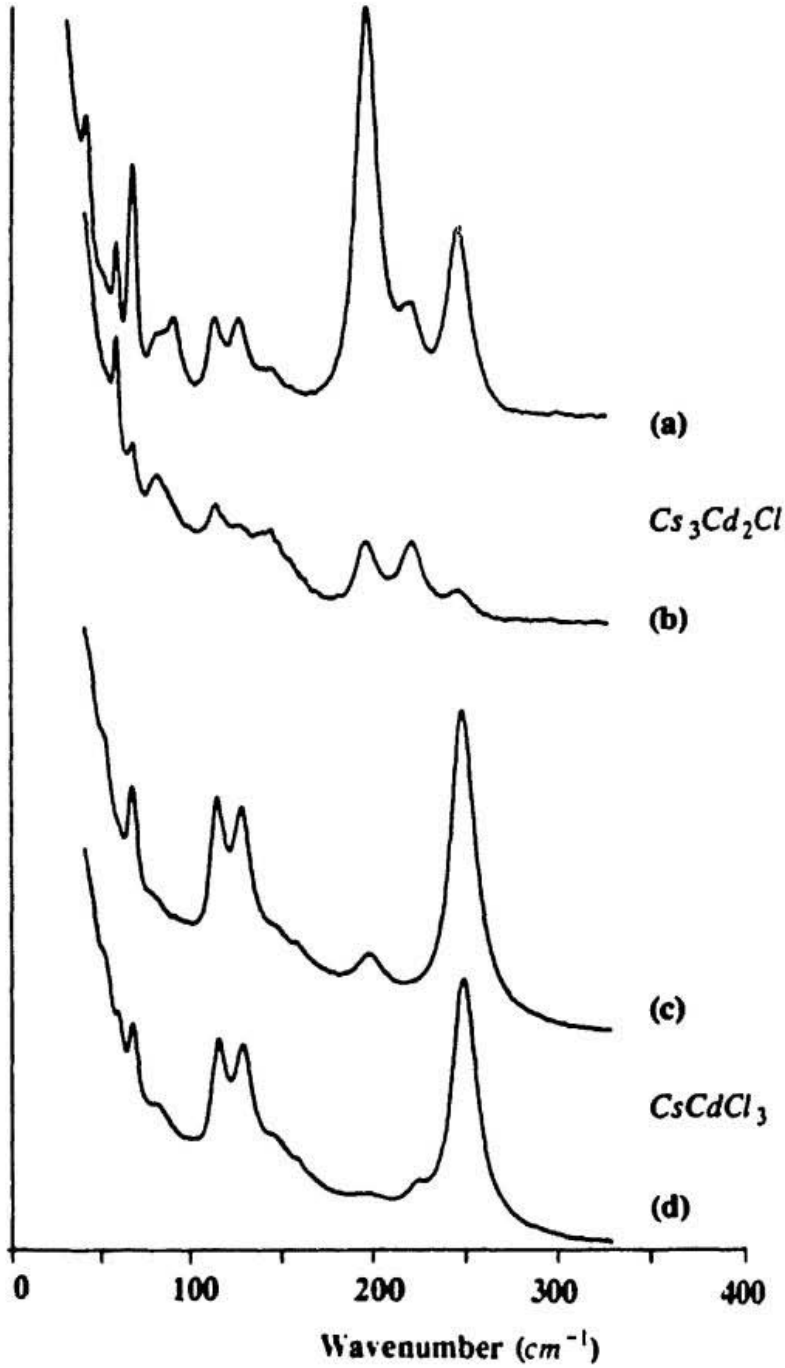

Fig. 4.6

Raman spectra obtained for $Cs_3Cd_2Cl_7$ and $CsCdCl_3$. $Cs_3Cd_2Cl_7$: (a) cooling rate 1°C/min; (b) a few degrees per day in the range 440 - 450°C. $CsCdCl_3$: (c) quenched; (d) slow cooled. Temperature 25°C. Slits 2 cm^{-1}.

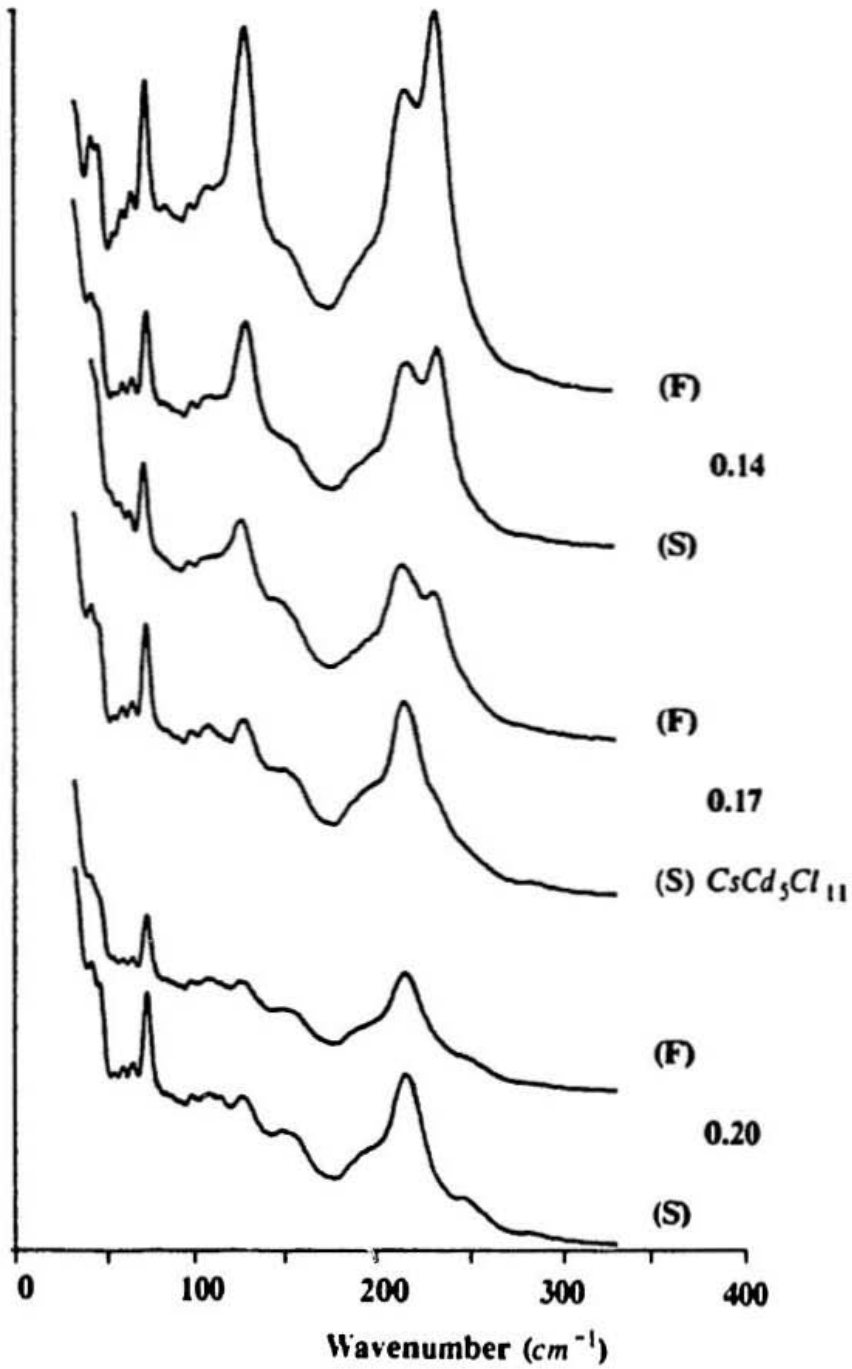

Fig. 4.7

Raman spectra obtained from fast (F) and slow (S) cooled samples respectively for the x = 0.20, 0.17 and 0.14 samples. Temperature 25°C. Slits 2 cm^{-1}.

Chapter 5

RAMAN STUDIES OF A DYNAMIC PHASE EQUILIBRIUM IN SOLID Cs_2CdCl_4

5.1 Introduction

In the last chapter, the compound formation and the structural properties of the compounds formed in the $CdCl_2$/CsCl binary system have been discussed. In this chapter, a special structural phase transition in solid Cs_2CdCl_4, one of the compounds identified in the $CdCl_2$/CsCl system, will be discussed in detail.

Structural phase transitions in the crystals of perovskite families have been widely investigated by many methods. The symmetry aspect of the structural phase transition in perovskite-like crystals was reviewed by Aleksandrov [Aleksandrov 1978] in 1978. Scott [Scott 1974, 1983] also described these phase transitions in reviews of light scattering. Most previously reported phase transitions were detected below or near room temperature. Relatively few high temperature transitions have been studied. Most of the structural phase transitions in layered perovskite-like A_2MX_4 crystals of the K_2NiF_4-type were observed in compounds with large organic cations and alkali metal A^+ ions [Aleksandrov 1985]. These structural phase transitions were found to be associated with the re-ordering of cations, rotation and distortion of MX_6 units with retention of octahedral coordination.

The low temperature solid Cs_2CdCl_4 belongs to the family of the K_2NiF_4-type crystals [Siegel 1964]. The present study on the structural phase transition in Cs_2CdCl_4 is unusual because:

i) There is a change in coordination number as the structure transforms from array octahedra to discrete tetrahedra in the solid state. Usually the array network structure will only be broken at the melting temperature but in the Cs_2CdCl_4 crystal the coordination number changes from six to four at a temperature far below the melting temperature.

ii) The phase transition is associated with a dynamic equilibrium between two coordinations of cadmium over a range of temperatures. The transition was found to start at about 435°C and continued until essentially completed at about 459°C which is just below the melting point of 473°C.

iii) The formation of a compound Cs_3CdCl_5 from the reaction of CsCl with Cs_2CdCl_4 was also found to occur over a range of temperatures. The reaction began at about 365°C and was completed at 395°C. For mixtures of Cs_2CdCl_4 and Cs_3CdCl_5 at temperatures above 395°C the Cs_2CdCl_4 (phase-II) appeared to dissolve in the Cs_3CdCl_5 to form a solid solution in which the cadmium is in the form of $CdCl_4^{2-}$ ions.

The structural phase transition in the Cs_2CdCl_4 crystal has been reported before by Seifert and Thiel [Seifert 1986] from X-ray and DTA studies. However, they reported a phase transition point at 459°C which is not in full agreement with present result. The dynamic equilibrium between the two solid phases has not been reported previously.

5.2 Results and Discussion

Raman spectrum for Cs_2CdCl_4 at room temperature is presented in fig. 5.1. An intense band at 198 cm^{-1} and three weaker bands at 42, 69 and 92 cm^{-1} have been observed (table 5.1). The spectrum is similar with that obtained from the isostructural compound Rb_2CdCl_4 as a single crystal [Aleksandrov 1985] which has four corresponding bands at 46, 85, 89 and 209 cm^{-1}. The vibrational spectrum of Cs_2CdCl_4 is in good agreement with the prediction based on X-ray studies [Seigel 1964]. Cs_2CdCl_4 is isostructural with K_2NiF_4; space group I_4/mmm (D_{4h}^{17}). Each cadmium atom is bonded to six chloride neighbors with an octahedral local unit. Each octahedral unit is linked by sharing four corners with other octahedra.

The effect of temperature on the Raman spectra for the compound Cs_2CdCl_4 has been measured very carefully from 25°C to above the melting point (Fig. 5.1, table 5.1). Frequencies decreased, and bandwidths increased smoothly as temperature increased to

435°C. At about 435°C a new set of bands appeared at 85, 102, 250 and an intense band at about 269 cm^{-1} (table 5.1). These have been assigned to the ν_4, ν_2, ν_3 and ν_1 modes of a discrete tetrahedral $CdCl_4^{2-}$ ion respectively (table 5.1). A further increase in temperature caused the relative intensity of the new bands to increase relative to the bands due to the low temperature phase. The two sets of bands coexisted in a temperature range from 435°C up to about 460°C. At about 473°C the sample began to melt and the pairs of bands at 85 and 102 cm^{-1} and 250 and 268 cm^{-1} coalesced into two broad bands centered at 105 and 261 cm^{-1} (table 5.1). At the melting point the halfwidth of the ν_1 symmetric stretching mode of $CdCl_4^{2-}$ increased from about 18 cm^{-1} to 35 cm^{-1}. The experiments strongly suggest that a structural phase transition took place in the temperature range from 435 to 460°C and the phase change was complete before the sample melted. The spectrum of the high temperature solid of Cs_2CdCl_4 is similar with that of Cs_2MgCl_4 which contains the discrete $MgCl_4^{2-}$ species [Brooker 1975]. Further the similarity of the Raman spectra observed for the high temperature solid phase and the melt suggests that the similar tetrahedral complex species existed in these two phases. These results indicate that the structure of the Cs_2CdCl_4 crystal transformed from the K_2NiF_4 type network structure to a structure with discrete tetrahedral $CdCl_4^{2-}$ species. The new bands have been attributed to the $CdCl_4^{2-}$ ions in the new solid phase (table 5.1). The ν_1 frequency of the totally symmetric vibration with tetrahedral symmetry is 268 cm^{-1} at 452°C in the solid phase, while it is 261 cm^{-1} in the melt.

The phase transition in Cs_2CdCl_4 has been reported before by Seifert and Thiel [Seifert 1986] from the X-ray and DTA studies. The compound was found to have a transition point at 459°C. It was proposed that the K_2NiF_4-structure type with connected $CdCl_6$-octahedra transformed to the β-K_2SO_4 type, space group $Pnma$ (D_{2h}^{16}), with isolated tetrahedra. The measured transition enthalpy was reported to be of the same magnitude as the melting enthalpy although numerical values were not reported. It was reported that the melt undercooled by 14°C (melting point 473°C) and at 459°C the low

temperature modification crystallized directly. Therefore, the structural phase transition temperature was taken as 459°C for the compound Cs_2CdCl_4 as indicated on the phase diagram [Seifert 1986] (Fig. 4.2).

The major results of the present study are essentially in agreement with the work of Seifert and Thiel. Since DTA scans speeds are normally relatively fast. The relatively slow solid state equilibrium could be easily missed. Furthermore, X-ray powder pattern would be less sensitive to the more disordered high temperature phase.

Raman measurements in the present study indicated that almost all of the low temperature phase transformed to the high temperature phase at 459°C, but that the transition took place over a temperature range from 435°C up to 460°C. A dynamic equilibrium between the two solid phases (two coordinations of cadmium) was indicated by the variation of the relative intensity of the characteristic bands due to the two solid phases as a function of temperature. The low temperature phase did not transform completely to the high temperature phase at intermediate temperatures no matter how long the sample remained at a specific temperature within the temperature range. For example, identical spectra have been observed for the sample monitored over 16 hours at an intermediate temperature of 440°C. As the temperature increased the relative intensities of the bands at 40, 65, 92 and 194 cm^{-1} due to the network low temperature phase decreased and the bands at 268 cm^{-1} and about 100 cm^{-1} due to the new phase increased. The pattern reversed as the temperature decreased. These experiments indicated that the equilibrium was a function of temperature.

Many studies for the structural phase transitions in A_2MX_4 and AMX_4 perovskite layer-type crystals have been performed in recent years, and mechanisms have been proposed. Blinc et al. [Blinc 1978] have proposed a model to describe the structural phase transition in the $(CH_3NH_3)_2CdCl_4$ compound as an orientational order-disorder transition of the CH_3NH_3 groups. Each CH_3NH_3 group has four possible equilibrium orientations in the cavities between corner-sharing $CdCl_6$ octahedra. Kind et al. [Kind 1978] reported

that $NH_3(CH_2)_3NH_3MnCl_4$ underwent two discontinuous structural phase transitions at 336 and 305 K which were governed by the rotational motion of the rigid chains around their long axis. Hidaka et al. have explained the structural phase transitions in compounds $AFeF_4$ (A = Rb, Cs) [Hidaka 1979a] and KMF_4 (M = Fe, V, Ti) [Hidaka 1979b] as the rotations of MF_6 octahedra about the [100] and [010] axes. A EPR study by Aleksandrov [Aleksandrov 1985a, 1985b] et al. suggested that Rb_2CdCl_4 underwent a structural phase transition near 133K. The structural phase transition was connected with tilts and additional distortion of $CdCl_6$ octahedra. In all these cases the mechanisms were described as orientations of cations and/or the rotation and distortion of MX_6 octahedra around one or several symmetry axes in the network structures. In present case, the structural phase transition in Cs_2CdCl_4 is unusual. This compound is the first one in the family of the K_2NiF_4-type crystals to have the network structure broken in the solid state at a temperature far below the melting point, and a change in coordination number from six to four for the divalent metal cation.

In the normal phase transition [Denbeigh 1968], such as those described above, there is a discontinuous change of entropy or volume over a very small temperature interval. Since entropy and volume are first derivatives of the chemical potential with respect to pressure and temperature this type of transition has been classified as first order. An important criterion of the first order transition is the fact that the observable physical properties show no sign of the impending drastic structural change. Ehrenfest [Denbeigh 1968] and others have proposed the possibility of higher order transitions associated with second and third derivatives of the chemical potential but even true second order transitions have been difficult to document. A number of "second order type" transitions have been reported and characterized by a gradual increase in the heat capacity up to the transition temperature followed by a rapid decline when the heat capacity falls to the value of the high temperature phase. It is usually difficult to determine whether or not the heat capacity reaches a finite maximum (true second order transition) or rises to infinity. This

type of transition has been labelled a lambda transition because of the shape of the heat capacity versus temperature plot. There is strong evidence to indicate that in the pretransition temperature region of the lambda transition the low temperature phase and the high temperature phase are able to co-exist along a temperature pressure equilibrium curve rather than just at a particular temperature and pressure [Denbeigh 1968]. The lambda transition of $NaNO_3$ at about 275°C provides a good example [Reinsborough 1967, Mustajoki 1957, Brooker 1978 and Newns 1966]. Heat capacity measurements [Reinsborough 1967 and Mustajoki 1957] have shown that the rise in heat capacity associated with the order-disorder transition begins well below the transition temperature, perhaps as low as room temperature. Mustajoki [Mustajoki 1957] reported an enthalpy and entropy of transition for $NaNO_3$ based on the arbitrary assumption that the phase transition started at 170°C. Reinsbourough and Wetmore [Reinsbourough 1967] were reluctant to calculate a transition enthalpy from their data because of the uncertainty in the temperature at which the transition started and the inability to show that the heat capacity was finite over the transition temperature (275°C). Diffraction [Lefebvre 1984] and spectroscopic [Brooker 1978] measurements have shown that the characteristic disorder of the high temperature phase co-exists in dynamic equilibrium within the ordered lattice of the low temperature phase. The fraction of the NO_3^- ions in disordered positions increases with temperature until the inter-ionic forces can no longer support an ordered lattice and the NO_3^- ions become disordered over two equivalent lattice sites.

The results of the present Raman study indicated that Cs_2CdCl_4 has a lambda type transition that started about 435°C and was essentially complete at 460°C. Between 435 and 460°C the low temperature phase with Cd^{2+} in an octahedral site co-existed in dynamic equilibrium with the high temperature phase with Cd^{2+} in tetrahedral sites.

In order to further understand the structural phase transition, mixtures of Cs_2CdCl_4 with $CsCl$ and $2CsCl$ have been studied (See phase diagram, Fig. 4.2). The mixture of Cs_2CdCl_4 + $1CsCl$ forms the compound Cs_3CdCl_5 above 390°C but may exist in a

metastable form at room temperature [Seifert 1986 and chapter 4 in this thesis]. The compound Cs_3CdCl_5 is isostructural with Cs_3CoCl_5 and contains discrete $CdCl_4^{2-}$ species. On heating the metastable compound to about 200°C, it decomposed into a mixture of Cs_2CdCl_4 and $CsCl$. Further heating of the mixture to 395°C gave the stable form of the compound Cs_3CdCl_5.

Raman spectra which illustrate the temperature dependence for the $Cs_2CdCl_4 \cdot CsCl$ and $Cs_2CdCl_4 \cdot 2CsCl$ mixtures are presented in figs. 5.2 and 5.3 respectively. In the temperature range from room temperature to 365°C, these spectra are similar with those of the pure compound Cs_2CdCl_4 at a corresponding temperature. At 365°C, a new set of bands appeared due to $CdCl_4^{2-}$ in the high temperature phase, Cs_3CdCl_5. The relative intensities of the new bands increased and old bands decreased as the temperature increased similar to the spectra obtained from pure Cs_2CdCl_4. The two sets of the bands coexisted over a temperature range from 365 to about 390°C when the bands due to the low temperature phase of Cs_2CdCl_4 disappeared completely. The appearance of the Raman bands characteristic of $CdCl_4^{2-}$ can be attributed to the reaction of CsCl with Cs_2CdCl_4-II to form the stable compound Cs_3CdCl_5.

Raman spectra which illustrate the temperature dependence for the Cs_2CdCl_4 + 0.5CsCl mixture are presented in fig. 5.4. When the sample temperature was 395°C all the excess CsCl reacted with Cs_2CdCl_4 to produce Cs_3CdCl_5 and the sample consisted of a mixture of Cs_2CdCl_4-II and Cs_3CdCl_5. Above 395°C the relative intensity of the bands due to the $CdCl_4^{2-}$ continued to increase which suggests that more $CdCl_4^{2-}$ is produced. It would appear that the Cs_2CdCl_4 dissolves to form a solid solution with the cadmium in the form of the tetrahedral $CdCl_4^{2-}$. When the sample temperature reached 435°C the remainder of the Cs_2CdCl_4-II gradually converted to Cs_2CdCl_4-I in a similar manner to that of the pure Cs_2CdCl_4.

In order to confirm the unusual two coordination equilibrium for Cs_2CdCl_4 a sample prepared with excess $CdCl_2$ was studied. A mixture of 3 CsCl and 2 $CdCl_2$ can be

synthesized into an incongruent compound $Cs_3Cd_2Cl_7$ (Fig. 4.2) under carefully controlled conditions just below 450°C. Normal cooling of this mixture usually results in a mixture of Cs_2CdCl_4, $CsCdCl_3$ and a small amount of $Cs_3Cd_2Cl_7$. Raman spectra obtained from this mixture at elevated temperatures indicated that the Cs_2CdCl_4 portion of the solid exhibited the same characteristic phase transition as the pure compound. For instance, at 440°C the characteristic peaks for $CsCdCl_3$, Cs_2CdCl_4 (I) and Cs_2CdCl_4 (II, low temperature phase) were identified at 248, 268 and 196 cm^{-1} respectively.

Studies of the intensities of the characteristic bands may further provide some quantitative information about the structural phase transition and the dynamic phase equilibrium. The relative intensities of the intense bands at 194 and 268 cm^{-1} due to the two phases of Cs_2CdCl_4 were measured for samples over the temperature range of the transition. The spectra were treated in both the $I(\omega)$ and $R(\omega)$ forms as a check on internal consistency because of potential errors due to baseline construction. For the $I(\omega)$ spectrum level baseline was achieved by numerical subtraction of a linear baseline as shown (Fig. 5.4, 410°C for example). The spectrum in the $R(\omega)$ format had a much more level background (Fig. 5.5) but it was also necessary to subtract a linear baseline. The relative intensities were calculated by numerical integration and checked by the weight of paper traces. The spectra were also curvefit to two product functions in order to provide assurance that proper baselines had been chosen and to provide an assessment of the extent of bands overlap. When the relative intensities measured for the $I(\omega)$ spectra were corrected for the frequency and temperature factors the two set of data gave the same values (within 10%). The relative intensity data corrected for temperature and frequency factors (Table 5.2) provide an assessment of the relative concentrations of the octahedral and tetrahedral cadmium as a function of temperature.

At any time within the crystal it appears that the coordination of any cadmium ion can switch from octahedral to tetrahedral with a temperature dependent rate constant. The rate constants have not been measured but from the approximate time required for the

intensity ratio to stabilize at a fixed temperature it was possible to infer that the rate constants were of the order of minutes at near 390°C and of the order of seconds near 450°C. At a given temperature there was an equilibrium concentration of the two sites. The following ideal equilibrium was assumed:

$$Cd_{(I)} \underset{k'}{\overset{k}{\rightleftharpoons}} Cd_{(II)} \tag{5.1}$$

where $Cd_{(I)}$ represents the state of the Cd^{2+} ion with octahedral coordination in the network structure, $Cd_{(II)}$ represents the state of Cd^{2+} with tetrahedral coordination in the high temperature phase, k and k' are rate constants. The intensity of a Raman band is given by I = JC, where J is the intrinsic molar scattering coefficient and C is the concentration of the species. At a given temperature the intensity ratio reflects a concentration ratio (5.2).

$$\frac{I_{(268\,5cm^{-1})}}{I_{(194cm^{-1})}} = \frac{J_{(II)}C_{Cd_{(II)}}}{J_{(I)}C_{Cd_{(I)}}} = JQ \tag{5.2}$$

Where $Q = C_{Cd_{(II)}} / C_{Cd_{(I)}}$ is a pseudo-equilibrium constant (reaction quotient) of the structural phase transition; and $J = J_{(II)} / J_{(I)}$ is a constant.

From a kinetic viewpoint, the rate constants can be expressed as

$$k \propto exp(-G/RT) \tag{5.3}$$

$$k' \propto exp(-G'/RT) \tag{5.4}$$

and

$$Q = k/k'$$

$$= exp(-\Delta G^0/RT) \tag{5.5}$$

ΔG is a thermodynamic constant which reflects the standard change in free energy that accompanies the reaction between the two kinds of coordinations referred to some

standard state of the substances involved. Essentially this treatment leads to a form of the Gibbs-Helmholtz equation and suggests that a plot of lnJQ against 1/T should be linear. There are a number of problems with this type of treatment for an equilibrium in a solid phase. It was not possible to define a standard state or to evaluate activity coefficients since it was not possible to alter an equilibrium position at a constant temperature by a variation of concentration. Furthermore the value of J, the ratio of the relative molar scattering factor, can not be easily evaluated although a value of about unity can be estimated from a comparison of the relative intensity of pure phase I compared to pure phase II. Nevertheless some insight about the nature of the phase transition may be inferred.

The value of JQ at each temperature was determined from the ratio of the integrated intensities for the two bands at 268.5 and 194 cm^{-1} (Table 5.2). A plot of lnJQ versus 1/T was not linear but had an S shape (Fig. 5.6). The shape of the curve is reasonable since below 435°C there is only phase II and above 460°C there is only phase I and the value of lnJQ should go to negative and positive infinity at these temperatures.

For the mixtures of Cs_2CdCl_4 and 0.5CsCl in the temperature range 390 to 440°C the plot was almost linear and a linear regression of the six points gave value of 4.8 ± 0.3 K for the slope and 8.5 ± 0.5 for the intercept. If the heat capacity, C_p was constant over this temperature range it would be possible to estimate values of ΔH and ΔS. For the value of ΔS, it was also necessary to assume that J was unity since lnJ contributes to the value of the intercept. The values for ΔH (40 ± 3 kJ mol^{-1}) and ΔS (70 ± 4 J $mol^{-1}K^{-1}$) obtained in this way were too large since they are as large as normal heats and entropies [Newns 1966 and Holm 1973]. The value of ΔS obtained from $\Delta H/T$ for a transition temperature of 460°C (55 ± 5J mol^{-1} K^{-1}) is also too large. The assumption that the heat capacity would be constant is unreasonable and inconsistent with previous studies of second order phase transitions. In fact, second order phase transitions are accompanied by a significant increase in the value of C_p up to the transition point at which temperature the value of C_p usually returns over a small temperature interval to low normal values. The

ΔC_p term for the reaction would tend to decrease the values of ΔH and ΔS estimated from the values of lnJQ. The S type curve for the plot of lnJQ versus 1/T can be considered the spectroscopic equivalent to the lambda shape of the C_p versus T plot. Although in the present case it seems reasonable to conclude that the enthalpy and entropy of transition are probably of the same order of magnitude as those of melting as reported by Seifert and Thiel [Seifert 1986], the limitations on the evaluation of these parameters preclude unambiguous evaluation. The Raman method suffers from the same problem (i.e. the pre-transition increase in C_p) that precludes the calculation of precise enthalpy and entropy of transition from C_p versus T data.

The large enthalpy change reflects the major structural rearrangement from the network octahedral coordination of the low temperature phase to the discrete $CdCl_4^{2-}$ molecular ion of the high temperature phase.

The value of ΔS is also large by comparison to entropies for many phase transitions [Newns 1966]. For example the entropy change is only 2.3 J/(mol K) for the displacive phase transition of Rb_2CdCl_4 which involves a simple tilt of the octahedra [Aleksandrov 1985a, 1985b]. Newns and Staveley [Newns 1966] have listed the values of ΔS for the phase transitions of 58 inorganic salts. The average value of ΔS was close to 10 J/(mol K) although values as high as 33 J/(mol K) were found. Solids with large entropies of phase transition were found to have correspondingly small entropies of fusion (and visa versa). Newns and Staveley [Newns 1966] associated large entropies of transition with the onset of orientation disorder in the high temperature phase. The magnitude of ΔS_{trans} was related to the number, n, of equivalent distinguishable orientations available to the molecule or molecular ion, i.e. ΔS = Rln n. The small values for enthalpies of fusion result because the orientation disorder normally presents only in the liquid state was already present in the solid. Similarly Timmermans [Timmermans 1961] has identified a class of orientationally disordered solids composed of rigid, compact molecules of approximately spherical shape (globular molecules) and with entropies of fusion below

20 J/(mol K). Since many of these orientationally disordered solids flow under stress they have also been called plastic crystals. The term "premelting" has been used to describe the change associated with the transition to the orientationally disordered phase. The high temperature phases of $NaClO_4$ [Toupry 1978], $KClO_4$ [Toupry 1983], $NaNO_3$ [Newns 1966, Brooker 1978] and KNO_3 [Newns 1966, Brooker 1978] have been identified as orientationally disordered crystals.

On the basis of the measured enthalpies and entropies of transition it would appear that the high temperature phase of Cs_2CdCl_4 is orientationally disordered. The discrete tetrahedral $CdCl_4^{2-}$ ion sits in the cavity created by the Cs^+ ions in a structure that in certain ways resembles the room temperature K_2SO_4 but without apparent order in the orientation of the Cd-Cl bond direction. The $CdCl_4^{2-}$ ions are not free to rotate but rapidly interchange among several distinguishable but energetically equivalent positions. The fact that the Raman bands for the $CdCl_4^{2-}$ ions are relatively broad together with high intensity and lack of structure in the Rayleigh wing further suggests disorder of the tetrahedra.

It is interesting to note that local order increased around the cadmium ion in the transition from the low temperature to the high temperature phase although the measured overall entropy increased. The frequency of the Cd-Cl stretching vibration increased from 194 to 268 cm^{-1} when the coordination changed from octahedral to tetrahedral which implies that the bond strength is greater and the bond length is shorter for the Cd-Cl bond in the tetrahedral coordination. In addition the halfwidth of the band at 194 cm^{-1} (29 cm^{-1}) is much greater than the halfwidth of the band at 268 cm^{-1} (16 cm^{-1}). Since the halfwidth of a band may be inversely related to the range of environments and perhaps thermal amplitudes it can be concluded that there is a greater distribution of bond lengths for the octahedrally coordinated cadmium. Nevertheless the overall order of the crystal decreases because of the change in the Cs^+ sub-lattice and the orientational disorder of the $CdCl_4^{2-}$ ion.

5.3 Conclusion:

Raman spectra for Cs_2CdCl_4 measured for samples over a wide range of temperature from the room temperature solid to the molten salt revealed the presence of an unusual second order phase transition. The transition occurred over a range of temperature from 435 to 460°C and between these temperatures the two solid phases co-existed in dynamic equilibrium. The transition is associated with the re-arrangement of the coordination about the cadmium ion from an array type octahedron at low temperature to a discrete tetrahedral $CdCl_4^{2-}$ polyatomic ion at high temperature. Measurement of the entropy of transition indicated that the high temperature phase was orientationally disordered.

Table 5.1

Raman frequencies (cm^{-1}) and assignments[a] for the different phases of Cs_2CdCl_4.

Phase II 298K D_{4h}^{17}	Phase I 723K D_{2h}^{16}	melt 743K
42 E_g		
69 E_g		
	85 (sh) ν_4	
92 A_{1g}		
	102 (m) ν_2	
		105 (m) $\nu_2 + \nu_4$
198 A_{1g}		
	~250 (w) ν_3	
	268 (vs) ν_1	261 (vs) $\nu_1 + \nu_3$

a Assignments for phase II are based on the unit cell group analysis by analogy to Rb_2CdCl_4 [Aleksandrov 1985a] while the assignments for phase II and the melt are for the discrete $CdCl_4^{2-}$ tetrahedral ion.

Table 5.2

The equilibrium constants calculated from relative Raman intensities for the structural phase transition in pure solid Cs_2CdCl_4 and mixtures with CsCl.

lnJQ [a]				T (K)
Cs_2CdCl_4	+0.5CsCl	+1.0CsCl	2.0CsCl	
	-∞	-∞	-∞	633
		-0.33	-1.63	638
	-2.65	1.75	-0.36	643
	0.01	2.90	1.41	6.48
	0.82	3.8	3.0	653
	1.0			658
	1.19	4.0	3.7	663
		+∞	+∞	668
	1.25			673
	1.42			683
	1.51			693
-∞	1.62			703
0, -2.45				708
-0.64, -1.51	1.66			713
-0.36, -0.52				715
0.23, 0.37				718
0.88				721
1.15, 1.06				723
	2.54			725
2.72				729
2.73				731
+∞	+∞			732

a Obtained from intensity ratio for spectra corrected for the temperature and frequency factors, i.e. the $R(\omega)$ spectra.

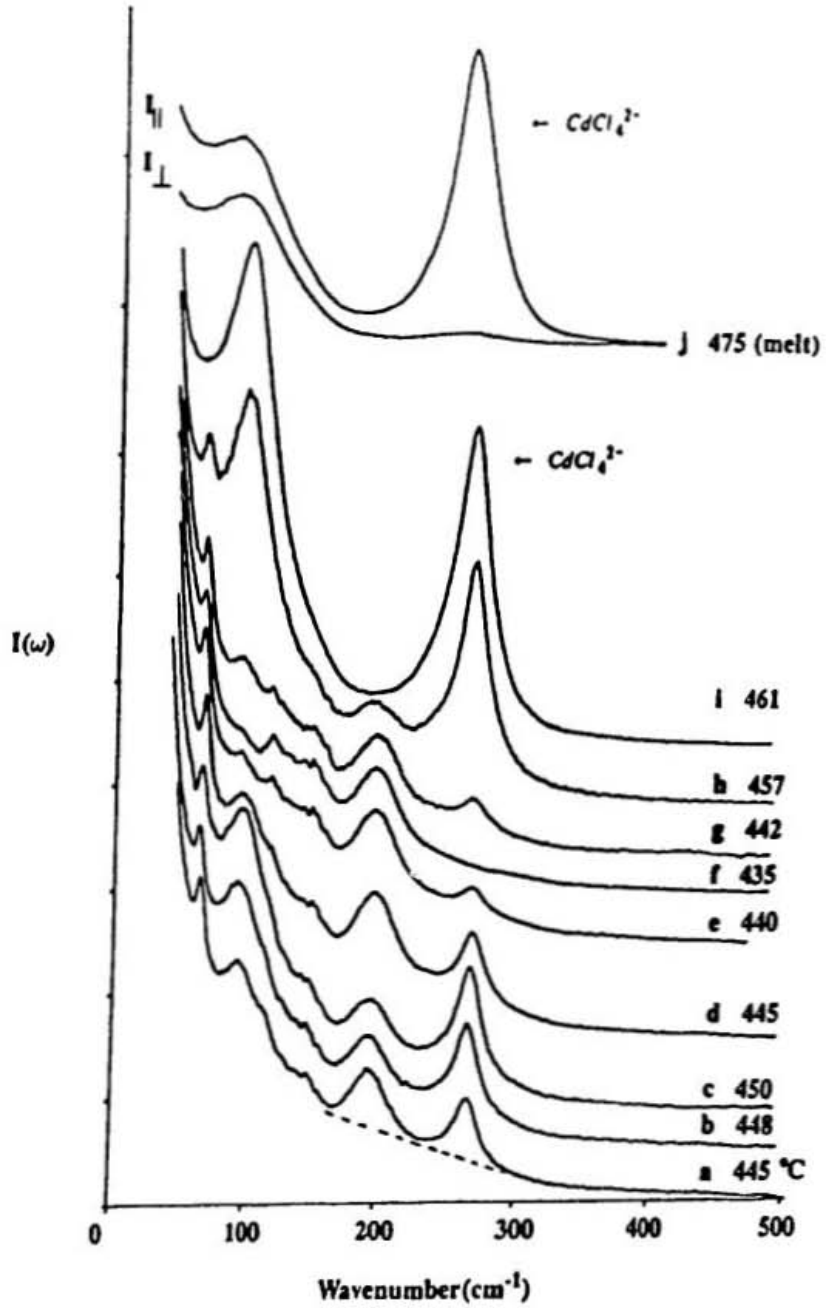

Fig. 5.1

Raman spectra obtained for pure Cs_2CdCl_4. Spectra a→ c are for the sample heated to the listed temperature; d→ f for the sample cooled to the listed temperature; g→ i for the sample again heated to the listed temperature and j for molten phase.

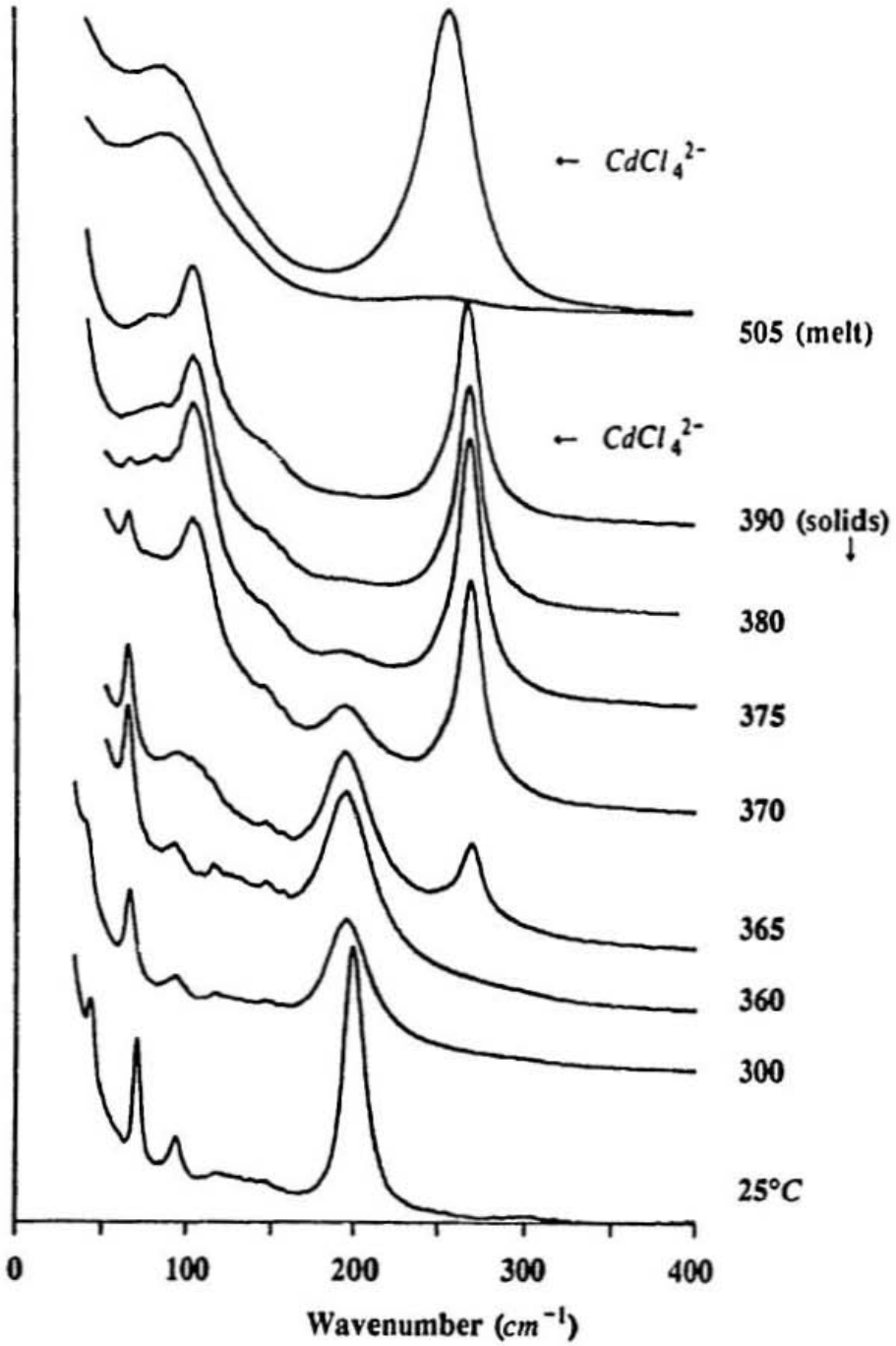

Fig. 5.2

Raman spectra obtained for samples at different temperatures from the mixture Cs_2CdCl_4 + 1 $CsCl$. Cs_3CdCl_5 is formed above 390°C. Slits 2 cm^{-1}.

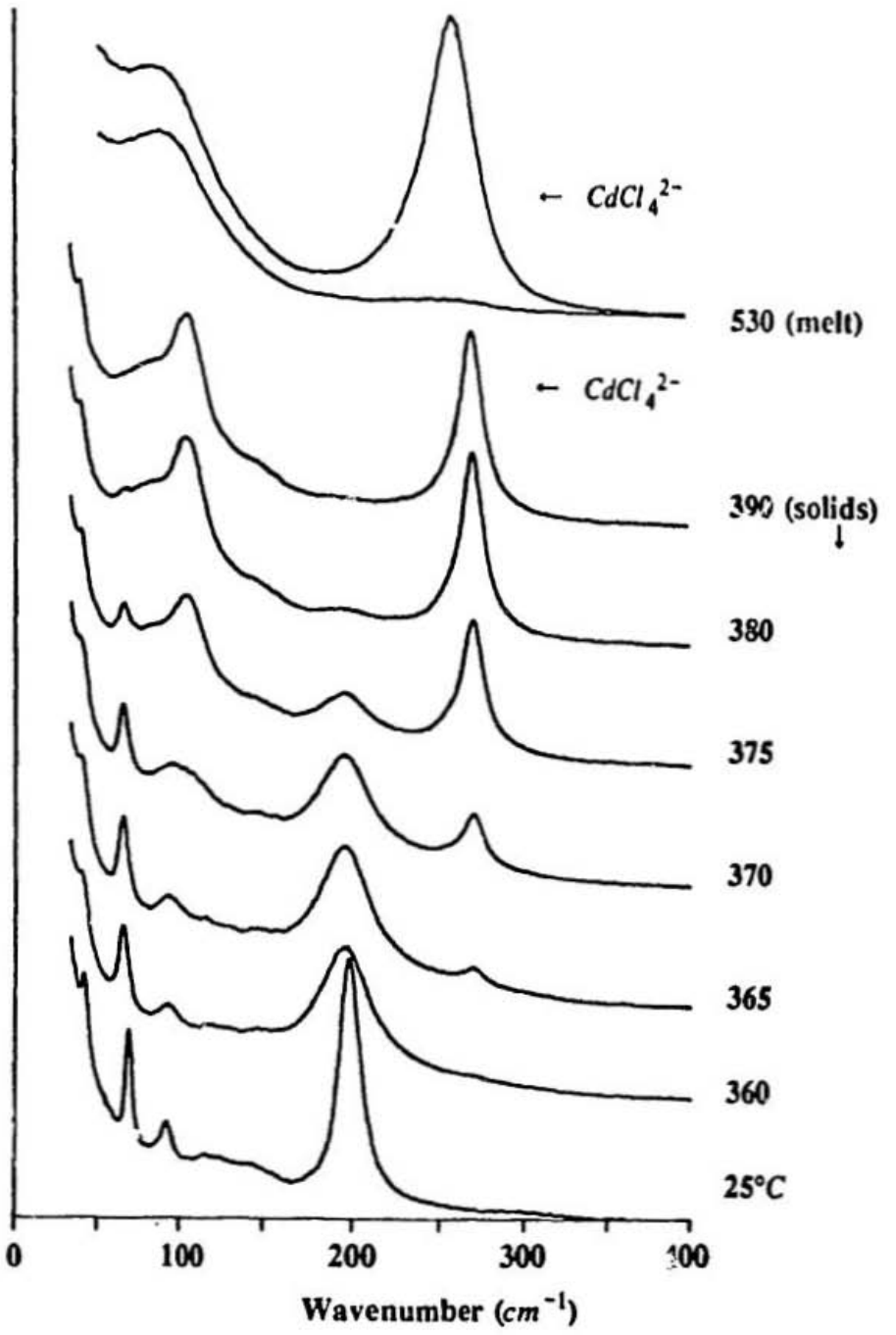

Fig. 5.3

Raman spectra obtained for samples at different temperatures from the mixture Cs_2CdCl_4 + 2 $CsCl$. Cs_3CdCl_5 is formed above 390°C. Slits 2 cm^{-1}.

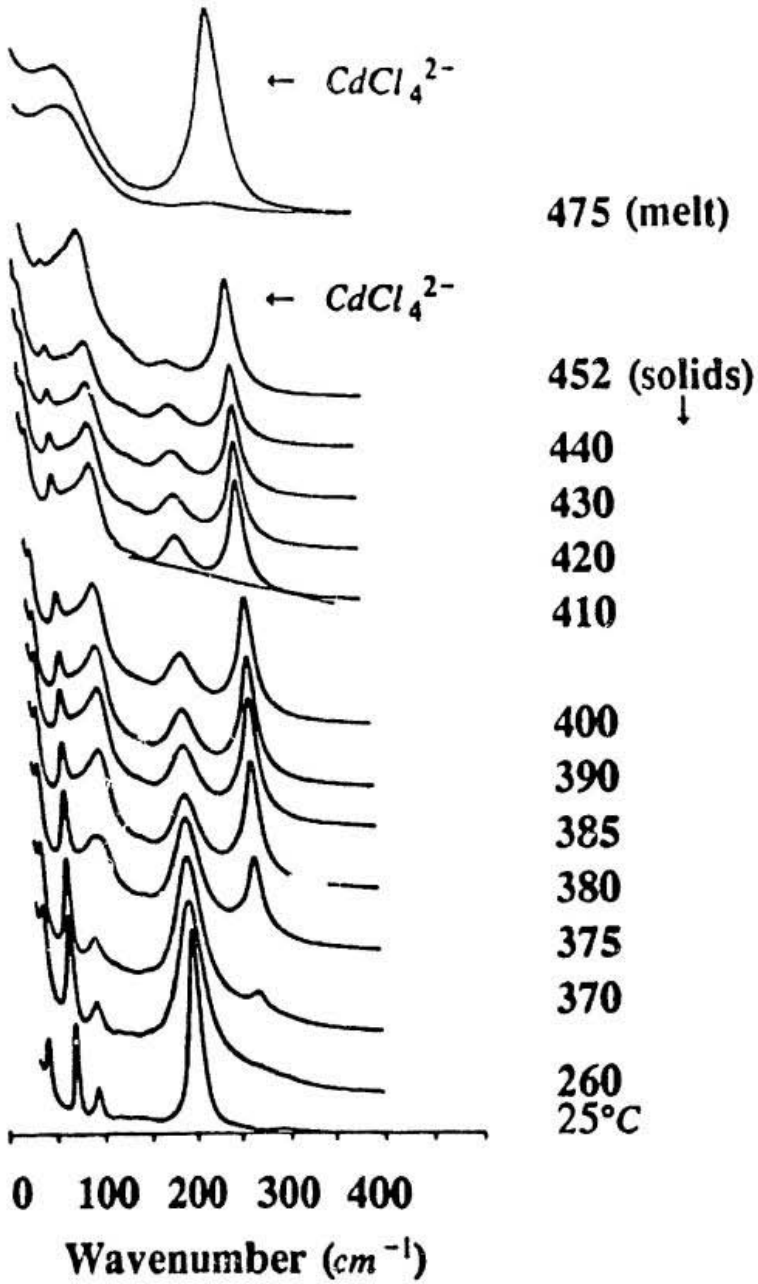

Fig. 5.4
Raman spectra obtained for samples at different temperatures from the compound Cs_2CdCl_4 at the temperatures as indicated. Slits 2 cm^{-1}.

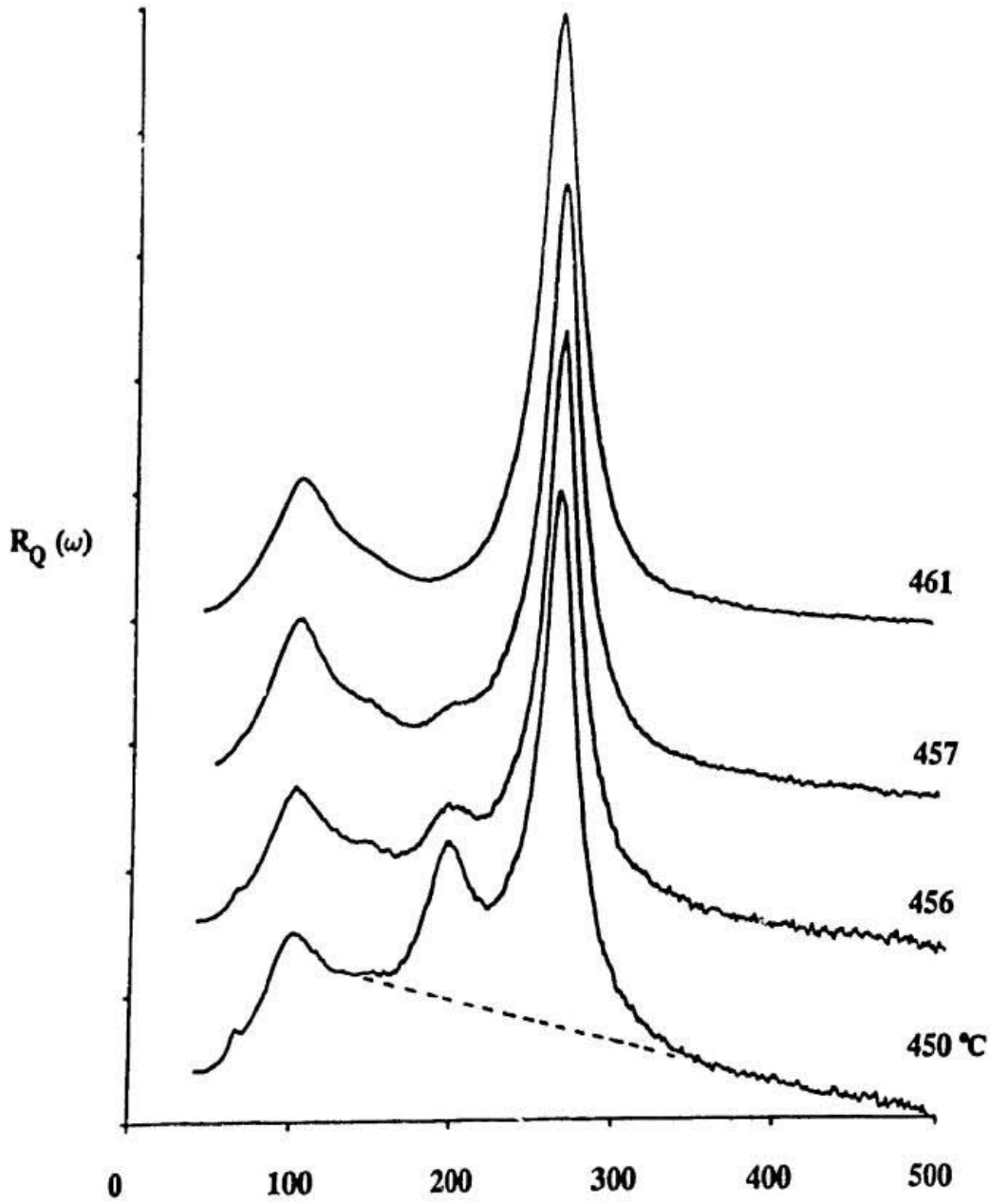

Fig. 5.5 Raman spectra in the R(ω) format at selected temperatures to illustrate the baseline employed for the relative intensity calculations. The sample temperatures of the spectra are: 461, 457, 456 and 450°C in the order from top to bottom.

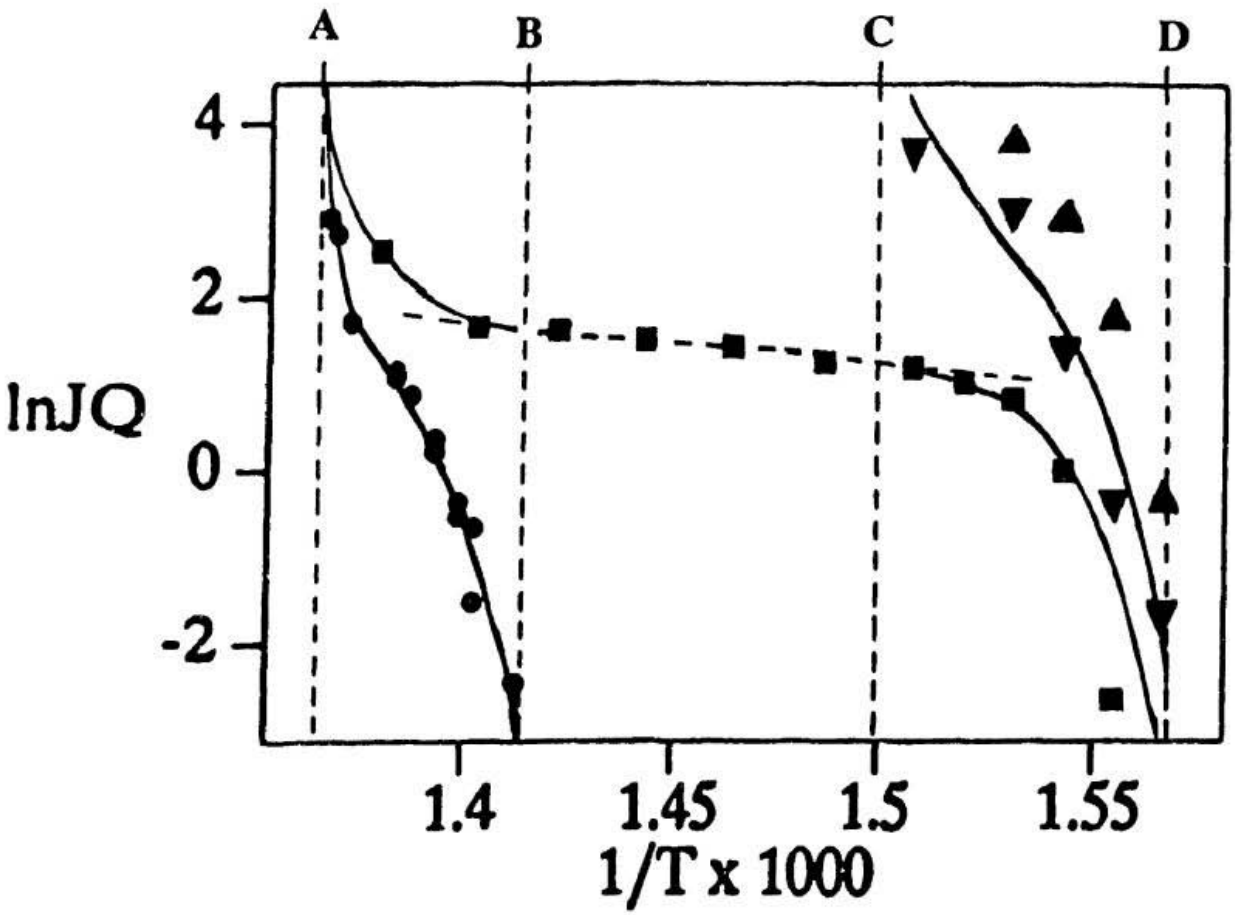

Fig. 5.6

The plot of lnJQ vs. 1/T for the phase transition in pure Cs_2CdCl_4 and mixtures with CsCl. A: Above 459°C the transition to Cs_2CdCl_4-I is complete and all the cadmium is tetrahedrally coordinated. B: Below 435°C the cadmium is all octahedrally coordinated in pure Cs_2CdCl_4-II. C: Above 395°C the reaction of CsCl with Cs_2CdCl_4 is complete. D: Below 365°C all the cadmium is octahedrally coordinated as Cs_3CdCl_5 reverts to Cs_2CdCl_4-II and CsCl.

Chapter 6

RAMAN STUDIES OF THE COMPLEX HALIDES IN THE SOLID $CdCl_2$/RbCl AND $CdCl_2$/KCl SYSTEMS

6.1 Introduction

The structures and properties of the compounds formed in the $CdCl_2/CsCl$ system have been discussed in chapters four and five. Five compounds, Cs_3CdCl_5, Cs_2CdCl_4, $Cs_3Cd_2Cl_7$, $CsCdCl_3$ and $CsCd_5Cl_{11}$ have been identified. At room temperature the metastable compound Cs_3CdCl_5 contains discrete tetrahedral $CdCl_4^{2-}$ species; while others have octahedral network structures. Unusually the larger and the more polarizing Cs^+ ion stabilizes the compound with lower chloride number in contrast to the Rb^+ and K^+ ions. In this chapter Raman studies of the $CdCl_2/RbCl$ and $CdCl_2/KCl$ systems will be discussed in order to understand the effect of the temperature, alkali metal ions and other factors on the structures and properties of the compounds formed in these systems.

The compound Cs_2CdCl_4 was found to undergo a structural phase transition from a K_2NiF_4 type layered perovskite-like low temperature phase with linked local $CdCl_6$ units into a structure with discrete tetrahedral $CdCl_4^{2-}$ species in a temperature range from about $435°C$ to below the melting point. A dynamic equilibrium between the low and high temperature solid phases in the temperature range was discovered by Raman measurements. The relative concentration of the two solid phases depended on the temperature only within the temperature range. Rb_2CdCl_4 is isostructural with Cs_2CdCl_4. The question arises whether or not there is a similar structural phase transition in solid Rb_2CdCl_4. Since different alkali metal cations exhibit different effects on the coordination structures of complex ions MX_n^{2-n} in the MX_2/AX systems, one can not simply predict the structural properties for these complex ions, especially in the solid states. In the $MgCl_2/ACl$ (A = alkali metal ion) systems, the discrete tetrahedral $MgCl_4^{2-}$ ions were

found in Cs_2MgCl_4 solid at room temperature, but not in K_2MgCl_4 or Rb_2MgCl_4 [Brooker 1980]. For the $CdCl_2/ACl$ systems, one would predict that the ability of Rb^+ to stabilize a tetrahedral species in solid must be weaker than Cs^+ and stronger than K^+. At room temperature Rb_2CdCl_4 should not contain discrete tetrahedral species. Even if the $CdCl_4^{2-}$ species were stable in Rb_2CdCl_4 in the high temperature solids, similar to Cs_2CdCl_4, we would predict that the phase transition should occur at a higher temperature compared to that in Cs_2CdCl_4.

Reports of compound formation in the $CdCl_2/RbCl$ system are inconsistent. P. Bohac [Bohac 1973] reviewed nine references from 1875 to 1973 including his own work (table 6.1) [Godeffroy 1875, Rimbach 1902, Hofmann 1926, Dergunov 1949, Gromakov 1950, Seifert 1968, Drobasheva 1971, Belyaev 1972]. Most recently Seifert et al. [Seifert 1979] reported six compounds, i.e. Rb_4CdCl_6, Rb_2CdCl_4, $Rb_3Cd_2Cl_7$, $Rb_4Cd_3Cl_{10}$, $RbCdCl_3$ and $RbCd_5Cl_{11}$ (table 6.1). The phase diagram suggested by Seifert et al. [Seifert 1979] is presented in fig. 6.1. The compound formation of this system was reexamined in this work.

Only two compounds, incongruent K_4CdCl_6 and congruent $KCdCl_3$, were identified in the $CdCl_2/KCl$ system [e.g. Cristol, 1978]. The phase diagram is presented in fig. 1.1. The compound formation was restudied in a composition range x = 0.50 to 0.80 (x - mole fraction of KCl) in this study to find out that whether or not there is a compound K_2CdCl_4 (similar to Rb_2CdCl_4 and Cs_2CdCl_4 in the RbCl and CsCl systems).

In the $CdCl_2/ACl$ (A =Cs, Rb and K) systems, the compounds with common formula $ACdCl_3$ have been reported. Although it has been suggested that the crystals are isostructural the results are not consistent. The effect of alkali metal cation size may affect the structure. The structure of $RbCdCl_3$ was reported to depend on the method of preparation. Crystal grown from a melt was found to have a different structure from that grown from a aqueous solution [MacGillavry 1939, Wyckoff 1965a, Swanson 1967, Natarajan 1971, 1978, Barr 1974, Seifert 1979].

6.2 Results and Discussion

6.2.1 Compound formation

6.2.1.1 $CdCl_2$/RbCl system

The Raman spectra obtained from several samples in different compositions for the $CdCl_2/RbCl$ system at room temperature are presented in fig. 6.2 (mole fraction of RbCl, x, from 0.80 to 0.56) and fig. 6.3 (x from 0.50 to 0.17). The characteristic peak frequencies in the most intense region and the corresponding compounds identified are listed in table 6.2. The present Raman results based on the analysis of the characteristic bands in the Cd-Cl stretching region are in excellent agreement with the Seifert's work [Seifert 1979]. Six compounds, Rb_4CdCl_6, Rb_2CdCl_4, $Rb_3Cd_2Cl_7$, $Rb_4Cd_3Cl_{10}$, $RbCdCl_3$ and $RbCd_5Cl_{11}$ have been identified.

Rb_4CdCl_6:

The Raman spectrum for the sample with x = 0.80 was dependent on the cooling rate of the sample from the melt (figs. 6.4a, 6.4b). For the quenched sample two intense bands at 208.5 and 218 cm^{-1} were observed (fig. 6.4b). But for the slowly cooled sample only one band centered at 220 cm^{-1} characteristic of the discrete octahedral $CdCl_6^{4-}$ species (fig. 6.4a). The result suggests that Rb_4CdCl_6 is an incongruent compound. The band at 220 cm^{-1} is due to this compound. The band at 208.5 cm^{-1} for the quenched sample is attributed to the compound Rb_2CdCl_4.

Rb_2CdCl_4:

The compound of this composition exhibited a unique spectrum at room temperature with a characteristic intense band at 208 cm^{-1} (fig. 6.2, 0.67 sample). The result suggests the formation of a compound Rb_2CdCl_4. The similarity of the spectra obtained from both the fast and slowly cooled samples at room temperature suggests a congruent compound. The present Raman result is not in full agreement with the X-ray and DTA studies

[Seifert 1979] which suggested an incongruent compound. However, if the peritectic temperature is very close to the melting point and the concentration of the other phase is low in the fast cooled sample, it would be hard to tell whether or not a compound is an incongruent compound by the method which described in chapter 1 in this thesis. However, in principle, careful Raman measurements for a full range of conditions, especially in the peritectic temperature region should distinguish between an incongruent and a congruent compound.

There is no evidence to suggest the formation of the Rb_3CdCl_5 compound [Gromakov 1950]. The Raman spectrum indicates that the x = 0.75 sample is a mixture of Rb_4CdCl_6 and Rb_2CdCl_4 (fig. 6.2, 0.75 sample).

$Rb_3Cd_2Cl_7$:

The Raman spectrum for the x = 0.60 sample was strongly dependent on the cooling rate (fig. 6.5). Two intense bands at 232 cm^{-1} and 207 cm^{-1} were observed for the fast cooled sample (fig. 6.5b), while only one band at 232.5 cm^{-1} was detected in this region for the slowly cooled sample (fig. 6.5a). The result suggests formation of an incongruent compound $Rb_3Cd_2Cl_7$. The intense band at 232 cm^{-1} is attributed to this compound. The band at 207 cm^{-1} is due to Rb_2CdCl_4. In comparison to $Cs_3Cd_2Cl_7$, pure $Rb_3Cd_2Cl_7$ was much easier to prepare although both compounds are incongruent melting. A relatively pure $Rb_3Cd_2Cl_7$ crystal was prepared in this work. $Cs_3Cd_2Cl_7$ is formed by a solid-solid reaction between Cs_2CdCl_4 and $CsCdCl_3$ and it is difficult to prepare the pure compound. $Rb_3Cd_2Cl_7$ is formed by a peritectic reaction: $Rb_3Cd_2Cl_7 = Rb_4Cd_3Cl_{10}$ + liquid (fig. 6.1) [Seifert 1979]. The frequency of the intense band at 232 cm^{-1} for the fast cooled $Rb_3Cd_2Cl_7$ was slightly lower than the corresponding band at 232.5 cm^{-1} for the slowly cooled sample. A small amount of $Rb_4Cd_3Cl_{10}$ (229 cm^{-1}) may be present in the fast cooled sample.

$Rb_4Cd_3Cl_{10}$:

A sample with the exact composition of this compound $Rb_4Cd_3Cl_{10}$ (x = 0.57) was not prepared but the Raman spectrum for the sample with x = 0.55 provides evidence for its formation. Raman spectrum depended on the cooling rate of this sample from the melt (figs. 6.4c, 6.4d). Only one band at 229 cm^{-1} in the Cd-Cl stretching region was observed (fig. 6.4c) for the slowly cooled sample, but two bands at 232 and 209 cm^{-1} for the fast cooled sample were detected (fig. 6.4d). The presence of the band at 229 cm^{-1} for the slowly cooled sample suggests an incongruent compound. The bands at 232 and 209 cm^{-1} for the fast cooled sample are due to $Rb_3Cd_2Cl_7$ and Rb_2CdCl_4 respectively. The disappearance of the band at 229 cm^{-1} and the appearance of the band at 209 cm^{-1} due to the Rb_2CdCl_4 in the fast cooled sample indicate a lower peritectic temperature of $Rb_4Cd_3Cl_{10}$ compared to that of $Rb_3Cd_2Cl_7$. These results are in excellent agreement with Seifert's work (fig. 6.1) [Seifert 1979].

$RbCdCl_3$:

The compound formed from the melt exhibited a spectrum with no intense characteristic band in the Cd-Cl stretching region. The formation of this compound is suggested by the fact that the samples with composition $0.50 < x < 0.57$ (fig. 6.2) gave a band at 229.5 cm^{-1} ($Rb_4Cd_3Cl_{10}$); the samples for $0 < x < 0.50$ (fig. 6.3) gave a band at 215 cm^{-1} ($RbCd_5Cl_{11}$), only for x = 0.50 was there no intense band in the Cd-Cl stretching region (fig. 6.3, 0.50 sample). The result suggests that the compound $RbCdCl_3$ grown from the melt has a cubic symmetry [Fernández 1978] and no allowed Raman bands or it may have a disordered structure. The similarity of the spectra for both the fast and slowly cooled samples indicates a congruent compound.

The compound $RbCdCl_3$ is unusual. The crystal grown from the melt (phase I) absorbs a trace amount of water (0.1%) [Bohac 1973] in air and transforms into an ordered structure (phase II) which is isostructural with NH_4CdCl_3 and $KCdCl_3$. The

amount of water absorbed is not sufficient for a true hydrate. $RbCdCl_3$ (II) gave a unique spectrum with two characteristic intense bands at 247.5 and 217 cm^{-1} in the Cd-Cl stretching region (fig. 6.6b). When the sample was dried at 200°C for a few hours the phase II structure changed back to the phase I structure and the two characteristic bands at 247.5 and 217 cm^{-1} disappeared completely (fig. 6.6c).

$RbCd_5Cl_{11}$:

Raman spectrum of this compound was dependent on the cooling rate of the sample from the melt. It has a strong peak at 215 cm^{-1} which has the same value as the corresponding band observed from $CsCd_5Cl_{11}$ (fig. 6.3). For the fast cooled sample a band at 233 cm^{-1} due to pure $CdCl_2$ appeared. The result suggests an incongruent compound formation. The peritectic reaction is:

$$RbCd_5Cl_{11_{(s)}}\ (215cm^{-1}) = CdCl_{2_{(s)}}\ (233cm^{-1}) + liquid$$

This compound has been identified before by Seifert et al. [Seifert 1968, 1979]. The present measurements on two different sets of samples with different compositions showed that the composition of this compound is about x = 0.3. Perhaps the error is due to the sublimation of $CdCl_2$ at high temperatures.

6.2.1.2 $CdCl_2$/KCl system

Several previous Raman studies [Bues 1955, Tanaka 1963, Maroni 1970a, Cristol 1978] have been performed on this system. The Raman spectra obtained from three samples with x = 0.50, 0.67 and 0.80 (x, mole fraction of KCl) at room temperature are presented in fig. 6.7. The peak frequencies in the Cd-Cl stretching region and the compounds identified are listed in table 6.4. Two compounds K_4CdCl_6 and $KCdCl_3$ have been identified in this composition region.

$KCdCl_3$:

The compound gave a unique spectrum with two characteristic intense bands at 248.5 and 221.5 cm^{-1} (fig. 6.7d). The identical spectra observed from both the fast and slowly cooled samples suggest a congruent compound.

K_4CdCl_6:

The Raman spectrum for the sample with x = 0.80 was strongly dependent on the cooling rate of the sample (figs. 6.7a, 6.7b). For the quenched sample there were two intense bands at 248.5 and 226.5 cm^{-1} (fig. 6.7b). For the slowly cooled sample there was only one band at 230 cm^{-1} (fig. 6.7a) characteristic of the discrete $CdCl_6^{4-}$ species. The peritectic reaction is:

$$K_4CdCl_{6(s)} = KCl_{(s)} + liquid$$

The peritectic reaction rate is very low. Great care must be exercised in the preparation of this compound. Even with a cooling rate as low as 0.2-1.0°C/min the pure compound was not obtained in the present work, but a mixture of K_4CdCl_6, $KCdCl_3$ and KCl. The compound was prepared by very slowly cooling the sample from the melt, especially in the temperature range of the peritectic reaction. The temperature was maintained at about 450°C for ten hours for the preparation of a relatively pure sample.

Unlike the CsCl and RbCl systems, there is no evidence to suggest formation of a compound with formula K_2CdCl_4. The sample with x = 0.67 was found to be a mixture of K_4CdCl_6 and $KCdCl_3$ (fig. 6.7c). These results are in good agreement with the most recent work by Cristol etc. [Cristol 1978].

6.2.2 Structures and properties

6.2.2.1 K_4CdCl_6 and Rb_4CdCl_6

K_4CdCl_6 is rhombohedral with a bimolecular pseudocubic cell [Bergerhoff 1956]; isostructural with K_4MnCl_6. The space group is D_{3d}^6 ($R\bar{3}c$). Discrete $CdCl_6^{4-}$ octahedral

units are present. The cadmium atoms sit on the positions (2b) with C_{3i} symmetry; K(1) on (2a) (D_3); K(2) on (6e) (C_2); and Cl on (12f) (C_1) respectively. Factor group analysis based on the D_{3d} group predicts 63 optic normal modes of vibrations. The correlation diagram is shown in table 6.3. The mode distribution is:

$$\Gamma_{3n} = 4\,A_{1g} + 6\,A_{2g} + 5\,A_{1u} + 7\,A_{2u} + 10\,E_g + 12\,E_u$$

$$\Gamma_{acoustic} = A_{2u} + E_u$$

$$\Gamma_{internal\ CdCl_6^{4-}} = 2\,A_{1g} + 2\,A_{2g} + 4\,E_g + 3\,A_{1u} + 3\,A_{2u} + 6\,E_u$$

$$\Gamma_{external} = 2\,A_{1g} + 4\,A_{2g} + 6\,E_g + 2\,A_{1u} + 3\,A_{2u} + 5\,E_u$$

Both the A_{1g} and E_g are Raman active; A_{2u} and E_u are infrared active; A_{2g} and A_{1u} are both Raman and Infrared inactive. The Raman spectrum of K_4CdCl_6 at 25°C is presented in fig. 6.7. The characteristic spectrum suggests that the crystal K_4CdCl_6 contains discrete $CdCl_6^{4-}$ octahedral species. The peak positions and tentative assignments are listed in table 6.4. An octahedral species has three Raman active normal modes, ν_1 (A_{1g}), ν_2 (E_g) and ν_5 (F_{2g}). Usually the frequencies of these modes increase in the order $\nu_5 < \nu_2 < \nu_1$. In solid state, the degenerate ν_2 and ν_5 modes are usually split by crystal field forces and overlap. The most intense band at 230 cm^{-1} was assigned to the symmetrical stretching ν_1 vibration of the $CdCl_4^{2-}$ ion. Four bands centered at 124, 134, 146 and 156.5 cm^{-1} were assigned to the ν_2 vibrations. The band at 104.5 cm^{-1} was due to the ν_5 mode (table 6.4). The present Raman studies are in good agreement with the prediction from the factor group analysis based on the known structure from X-ray studies [Cristol 1978] and are in excellent agreement with the previous Raman studies [Clarke 1972a]. The frequency of the ν_1 mode was reported to be 229 cm^{-1}.

The Raman spectrum of the compound Rb_4CdCl_6 is presented in fig. 6.4a. The similarity of the spectra of K_4CdCl_6 and Rb_4CdCl_6 at room temperature suggests that Rb_4CdCl_6 is isostructural with K_4CdCl_6. Octahedral $CdCl_6^{4-}$ species are present. The ν_1 peak was centered at about 220 cm^{-1}; the ν_2 modes at 137, 150 and 158 cm^{-1}; and the ν_5

at 116 cm^{-1} (table 6.4). In contrast to the spectrum of K_4CdCl_6 the bands in the ν_2 and ν_5 regions for Rb_4CdCl_6 are slightly broader.

Previous studies [Clarke 1972a] suggested that the central Cd atom of complex $CdCl_n^{2-n}$ with the alkali metal cations series has a tendency to have six coordination ligands in the solid state. The present studies indicate that both K_4CdCl_6 and Rb_4CdCl_6 contain discrete $CdCl_6^{4-}$ species. It seems that if a pure compound A_4CdCl_6 forms in the $CdCl_2/ACl$ system, the crystal will contain the discrete octahedral $CdCl_6^{4-}$ species.

It can be seen that the ν_1 frequency of the symmetric vibration in the $CdCl_6^{4-}$ species has a higher value for a lighter alkali metal ion, 230 cm^{-1} for K_4CdCl_6 and 220 cm^{-1} for Rb_4CdCl_6. The same trend has been observed for A_2CdCl_4 compounds. The frequency of the most intense band is about 198 cm^{-1} for Cs_2CdCl_4, while 207 cm^{-1} for Rb_2CdCl_4. However, in the molten states the tendency of the peak maximum of the ν_1 mode in the $CdCl_4^{2-}$ species was reported to go to an opposite direction. The center frequency of the ν_1 band decreased regularly along the series $Cs^+ > K^+ > Na^+ > Li^+$ [Clarke 1972a]. The result was explained as due to a corresponding increase in the polarizing power of the surrounding alkali metal cations. Clearly there is a different effect of the alkali metal cations on the complex species in the solid and molten states. In solids, the vibrational frequency depends strongly on the packing form of the atoms. Usually, the symmetric frequencies for a probe anion have higher values for the lighter alkali metal cations. Another example is the ν_1 frequency of CO_3^{2-} in A_2CO_3 compounds which increases regularly from 1040 cm^{-1} for Cs_2CO_3 to 1090 cm^{-1} for Li_2CO_3.

6.2.2.2 Rb_2CdCl_4

Rb_2CdCl_4 is a well-known compound with K_2NiF_4-type crystal structure (space group I_4/mmm (D_{4h}^{17}), z = 2) at room temperature [Aleksandrov 1985a, 1985b], isostructural with Cs_2CdCl_4. The complete factor group analysis for this type of crystals has been worked out for the isomorphic K_2MgCl_4 structure [Brooker 1975], and has been

discussed in chapter four in the analysis of the spectrum of Cs_2CdCl_4.

The Raman spectrum of Rb_2CdCl_4 at room temperature is presented in fig. 6.2 (x = 0.67 sample). Peak frequencies are listed in table 6.5. Four bands have been observed. The results are in excellent agreement with the predictions from factor group analysis based on the D_{4h} group and are in good agreement with previous Raman studies [Aleksandrov 1985a, 1985b]. Two of the four bands (89 and 85 cm^{-1}) were observed and resolved in Aleksandrov's Raman spectra by means of polarization measurements. The two corresponding bands overlapped to give a broad band in our Raman spectrum obtained from a polycrystalline sample. Band resolution showed that the two components of these broad band centred at about 88 and 84 cm^{-1} respectively. The corresponding bands in the spectrum of Cs_2CdCl_4 are well separated, at 69 and 92 cm^{-1}.

In chapter five the structural phase transition of Cs_2CdCl_4 was discussed. The structure of Cs_2CdCl_4 transformed from K_2NiF_4 type to a structure with discrete $CdCl_4^{2-}$ species at about 435°C. Rb_2CdCl_4 is isostructural with Cs_2CdCl_4. ESR, X-ray and optical studies by Aleksandrov et al. [Aleksandrov 1985a, 1985b] indicated that Rb_2CdCl_4 undergoes a structural phase transition at about 142K. It was demonstrated that this phase transition only involved the distortion of $CdCl_6$ octahedral unit.

Raman measurements over a wide temperature range from room temperature to above the melting point have been performed (fig. 6.8). The result indicates that the compound Rb_2CdCl_4 did not show any high temperature phase transition even up to just below the melting point. In order to break the network structure and create the tetrahedral ion, a sufficiently large activation energy would be required. The activation energy needed in Cs_2CdCl_4 is much lower than it in Rb_2CdCl_4.

6.2.2.3 $RbCdCl_3$ and $KCdCl_3$

$KCdCl_3$ is orthorhombic [MacGillavry 1939, Brandenberger 1947, Wyckoff 1965a]. The space group is Pnma (D_{2h}^{16}) with four formula units in the cell. Each cadmium atom is

surrounded by a distorted octahedron of chlorine atoms. The structure as a whole can be represented as strings of pairs of these octahedra extending along the c_0 axis, the individual octahedron in a string sharing edges with one another. Factor group analysis based on the D_{2h} group has been discussed in detail for the isostructural molecule NH_4CdCl_3 by Adams et al. [Adams 1971]. 60 normal modes of which three are acoustic modes are predicted:

$$10A_g + 5B_{1g} + 10B_{2g} + 5B_{3g} + 5A_u + 10B_{1u} + 5B_{2u} + 10B_{3u}$$

All the A_g, B_{1g}, B_{2g} and B_{3g} modes are Raman active.

The Raman spectrum obtained from solid $KCdCl_3$ at room temperature is presented in fig. 6.7d. The peak frequencies are listed in table 6.4. Ten bands have been observed. A comparison of the spectrum of $KCdCl_3$ with that of NH_4CdCl_3 [Adams 1971] indicates that $KCdCl_3$ is isostructural with NH_4CdCl_3. Bands at 221.5 and 248.5 cm^{-1} in the Cd-Cl stretching region in the Raman spectrum of $KCdCl_3$ correspond to the bands at 222 and 244 cm^{-1} [Adams 1971] or 219 and 244 cm^{-1} [Clarke 1972] for NH_4CdCl_3.

The room temperature solid $RbCdCl_3$ was suggested to be isostructural with NH_4CdCl_3 and $KCdCl_3$ [MacGillavry 1939, Wyckoff 1965a, Swanson 1967, Natarajan 1971, 1978, Barr 1974, Seifert 1979], with the space group Pnma (D_{2h}^{16}). The structural parameters of the unit cell and the atomic positions were also reported in detail [Swanson 1967, Natarajan 1978]. The polarized Raman spectrum of a $RbCdCl_3$ single crystal [Natarajan 1978] exhibited two Raman bands in the Cd-Cl stretching region, at 220 and 250 cm^{-1}.

Figs. 6.9 and 6.10 present the spectra of the compounds $CsCdCl_3$, $RbCdCl_3$ and $KCdCl_3$, grown from the melts, at room temperature and 77K respectively. In the Cd-Cl stretching region there are two bands, at 248.5 and 221.5 cm^{-1}, for $KCdCl_3$, one band, at 249 cm^{-1}, for $CsCdCl_3$, and no intense band for $RbCdCl_3$ at room temperature. These results suggest strongly that $CsCdCl_3$, $RbCdCl_3$ and $KCdCl_3$ have different structures at

room temperature. The result is in disagreement with previous studies which suggested that these two compounds are isostructure. [MacGillavry 1939, Wyckoff 1965a, Swanson 1967, Natarajan 1971, 1978, Barr 1974, Seifert 1979]. Raman spectrum of $RbCdCl_3$ is presented in fig. 6.9b. The present Raman study is in disagreement with previous results. Bands at about 250 and 220 cm^{-1} [Natarajan 1978] were not observed in the spectrum of the $RbCdCl_3$ sample grown from the melt in the present study.

It was reported that the crystal of $RbCdCl_3$ grown from the melt had the tetragonal structure at room temperature which stayed unchanged for one month in a closed glass ampoul. However, after opening the ampoul in air the crystal became milky after four hours and completely changed to the orthorhombic modification after two weeks in air [Bohac 1973]. Seifert et al. [Seifert 1986] found that the crystal of $RbCdCl_3$ grown from the melt had a cubic perovskite structure. At room temperature this structure was reported to transform to the orthorhombic $GdFeO_3$-type with a transition temperature of 114°C. However the orthorhombic form was only metastable. After several weeks a stable modification was formed with the NH_4CdCl_3-structure (this crystal could be crystallized directly from an aqueous solution).

In order to study the unusual properties of this crystal, careful Raman studies have been performed in this work. The crystal of $RbCdCl_3$ (I) grown from the melt did not have the orthorhombic NH_4CdCl_3 or $KCdCl_3$ structure at room temperature. The Raman spectrum of this crystal did not show any intense bands in the Cd-Cl stretching region (fig. 6.6a). Even after at least one year the Raman spectrum remained the same and the crystal did not transform to a modification with NH_4CdCl_3 structure. The result is in disagreement with Seifert's work. However, when the quartz tube was opened to the air for one week the sample gave a different spectrum. Apparently the crystal absorbed a trace amount of water. It was reported that the content of the water absorbed was only 0.1% [Bohac 1973]. The water was an impurity which stabilized a different structure, $RbCdCl_3$ (II). The spectrum of the solid $RbCdCl_3$ (II) displayed two strong peaks at 217 and 247.5

cm^{-1} in the Cd-Cl stretching region at room temperature (fig. 6.6b, table 6.4). The spectrum of $RbCdCl_3$ (II) is similar with that of a single crystal $RbCdCl_3$ reported by Natarajan et al. [Natarajan 1978]. The result suggests that $RbCdCl_3$ (II) is isostructural with NH_4CdCl_3 and $KCdCl_3$. In order to confirm the result, the $RbCdCl_3$ (II) sample was dried at about 200°C for a couple of hours, then a spectrum was recorded at room temperature immediately. The peaks at 217 and 247.5 cm^{-1} disappeared completely (fig. 6.6c). As expected the NH_4CdCl_3-type structure, $RbCdCl_3$ (II), transformed back into an anhydrous room temperature structure, $RbCdCl_3$ (I). In our conclusion, the stable modification of this compound at room temperature does not have a NH_4CdCl_3-type structure; while the wet $RbCdCl_3$ (II) is isostructural with NH_4CdCl_3. The structure suggested by previous studies is really for $RbCdCl_3$ (II) which absorbed a trace amount of water.

6.2.2.4 $Rb_3Cd_2Cl_7$

X-ray measurements [Aleksandrov 1988] suggested that $Cs_3Cd_2Cl_7$ is isostructural with $Sr_3Ti_2O_7$ [Ruddlesden 1958]; space group I4/mmm (D_{4h}^{17}) with two formulas per unit cell. The atoms have been placed in the positions: Rb(1) 2b with D_{4h} symmetry; Rb(2) 4e C_{4v}; Cd 4e C_{4v}; Cl(1) 2a D_{4h}; Cl(2) 8g C_{2v} and Cl(3) 4e C_{4v}. Factor group analysis based on the D_{4h} group predicts seventy two normal modes. The mode distribution is [Shabana 1985]:

$$\Gamma_{Cl} = 2A_{1g} + 2E_g + 2A_{2u} + 2E_u$$

$$\Gamma_{Rb(1)} = 2A_{2u} + 2E_u$$

$$\Gamma_{Rb(2)} = 2A_{1g} + 2E_g + 2A_{2u} + 2E_u$$

$$\Gamma_{Cl(1)} = 2A_{2u} + 2E_u$$

$$\Gamma_{Cl(2)} = 2A_{1g} + 2B_{1g} + 4E_g + 2A_{2u} + 2B_{2u} + 4E_u$$

$$\Gamma_{Cl(3)} = 2A_{1g} + 2E_g + 2A_{2u} + 2E_u$$

$$\Gamma_{total} = 8A_{1g} + 2B_{1g} + 10E_g + 12A_{2u} + 2B_{2u} + 14E_u$$

$$\Gamma_{acoustic} = A_{2u} + E_u$$

All the g modes are Raman active, the A_{2u} and E_u infrared active and B_{2u} inactive. Raman spectrum of the crystal $Rb_3Cd_2Cl_7$ is presented in fig. 6.5a and the peak frequencies are listed in table 6.4. Five peaks have been observed. A Raman spectrum for an isostructural compound $Rb_3Mn_2Cl_7$ of a single crystal was reported [Briat 1984]. Six bands at 36, 78, 98, 115, 166 and 242 cm^{-1} were observed. The present work indicates that the spectrum for $Rb_3Cd_2Cl_7$ is similar with that for $Rb_3Mn_2Cl_7$. Therefore $Rb_3Cd_2Cl_7$ is isostructural with $Sr_3Ti_2O_7$ or $Rb_3Mn_2Cl_7$. The present work is consistent with the X-ray studies [Aleksandrov 1988].

It is interesting that the compounds $Rb_3Cd_2Cl_7$, Rb_2CdCl_4, $Cs_3Cd_2Cl_7$ and Cs_2CdCl_4 have the same tetragonal crystal structure (space group D_{4h}^{17}, two formula units per unit cell). $Cs_3Cd_2Cl_7$ and $Rb_3Cd_2Cl_7$ are incongruent compounds, while Cs_2CdCl_4 and Rb_2CdCl_4 are congruent compounds. Perhaps it is the similar crystalline structure for the incongruent $A_3Cd_2Cl_7$ and congruent A_2CdCl_4 that results in the difficult in the preparation of the pure incongruent compound $A_3Cd_2Cl_7$, especially for $Cs_3Cd_2Cl_7$. Actually there were similar problems for the preparation of the compounds for the similar systems [Katsumata 1982, Kohles 1982, Briat 1984, and Shabana 1985]. Briat et. al reported the preparational methods of the compounds Rb_2MnCl_4 and $Rb_3Mn_2Cl_7$, while the pure compound $Rb_3Mn_2Cl_7$ was not obtained by Shabana in his thesis work.

6.2.2.5 $Rb_4Cd_3Cl_{10}$ and $RbCd_5Cl_{11}$

The pure compound $Rb_4Cd_3Cl_{10}$ was not prepared in this work. However the characteristic frequency of the Cd-Cl stretching vibration was found to be about 229 cm^{-1} (fig. 6.4c, table 6.2). For $RbCd_5Cl_{11}$ the stretching mode centers at about 215 cm^{-1} (fig. 6.3, 0.67 sample; table 6.2).

Table 6.6 summarizes the structures and vibrational frequencies in the most intense regions for some compounds formed in the $CdCl_2/ACl$ (A = K, Rb, Cs) systems. These results indicate that:

a) the frequency decreases as the coordination number of the central Cd atom increases.

b) in the network structure with $CdCl_6$ local unit, the frequency decreases in the order of $ACdCl_3 > A_2CdCl_4$.

c) the frequency decreases as the mass of the alkaline metal cation increases.

The frequencies 229 ($Rb_4Cd_3Cl_{10}$) and 215 cm^{-1} ($RbCd_5Cl_{11}$) are just between the frequency region for $ACdCl_3$ (248 cm^{-1}) and A_2CdCl_4 (208 cm^{-1} for Rb_2CdCl_4 and 198 cm^{-1} for Cs_2CdCl_4). According to the analysis described above about the relationship between the coordinational structure and symmetrical stretching vibrational frequency, the Raman results suggest that the compounds $Rb_4Cd_3Cl_{10}$ and $RbCd_5Cl_{11}$ have network structures with local octahedral $CdCl_6$ units.

6.3 Summary

Until now we have discussed the structures and properties for the compounds formed in the $CdCl_2/ACl$ systems. It can be seen that the ability to stabilize the compound A_4CdCl_6 increases in the order $Cs^+ < Rb^+ < K^+$, but decreases for A_2CdCl_4 compound along this series. In the $CdCl_2/CsCl$ system there is no compound Cs_4CdCl_6, but Cs_2CdCl_4; in the $CdCl_2/RbCl$ system there are both Rb_2CdCl_4 and Rb_4CdCl_6; while in

the $CdCl_2/KCl$ system there is no K_2CdCl_4, but K_4CdCl_6. Both Cs_2CdCl_4 and Rb_2CdCl_4 have the same K_2NiF_4 type crystal structure with linked octahedra. Both K_4CdCl_6 and Rb_4CdCl_6 contain discrete $CdCl_6^{4-}$ species. The Cd atom in other compounds A_nCdCl_m have octahedral coordination structures except Cs_1CdCl_5 which contains discrete tetrahedral $CdCl_4^{2-}$ species in both the metastable low temperature phase and the stable high temperature phase.

Although Cd follows a favourite trend to form an octahedral coordination structure, the coordination number is still dependent on the alkali cation in case and the temperature. In summary:

a) In the solid state, the larger the size of the cation, the more stable the tetrahedral $CdCl_4^{2-}$ species, conversely for octahedral $CdCl_6$ unit. K_2CdCl_4 can not be formed; Rb_2CdCl_4 has the octahedral structure until melting; Cs_2CdCl_4 has octahedral structure at low temperatures but tetrahedral in the high temperature solid phase; while $[NEt_4]_2[CdCl_4]$ [Davies 1971] contains discrete tetrahedral $CdCl_4^{2-}$ species even at low temperatures.

b) There is a trend to stabilize the $CdCl_4^{2-}$ species at higher temperatures. The low temperature solid Cs_2CdCl_4 has an octahedral structure, but the high temperature phase contains discrete tetrahedral $CdCl_4^{2-}$ species. In the molten states tetrahedral coordination of cadmium is the normal form even in the pure $CdCl_2$ melt (melts will be discussed in chapter 7).

As mentioned before the formation of the complex compound of the cadmium ion with chlorides is unusual. Normally one expects large cations to stabilize large anions and one would expect Cs_4CdCl_6 rather than K_4CdCl_6. This unusual behavior can be related to the special coordination properties of the Cd atom. The A_4CdCl_6 structure is unusual but must result from the overall packing stability of the K^+ and Rb^+ salts.

Table 6.1

The compounds identified by several previous studies on the $CdCl_2/RbCl$ binary system.

Godeffroy (1895)			Rb_2CdCl_4				
Rimbach (1902)						$RbCdCl_3$	
Hofmann (1926)	Rb_4CdCl_6			$Rb_3Cd_2Cl_7$		$RbCdCl_3$	
Dergunov (1949)			Rb_2CdCl_4			$RbCdCl_3$	
Gromakov (1950)		Rb_3CdCl_5				$RbCdCl_3$	
Seifert (1968)	Rb_4CdCl_6		Rb_2CdCl_4	$Rb_3Cd_2Cl_7$	$Rb_4Cd_3Cl_{10}$	$RbCdCl_3$	$RbCd_4Cl_{11}$
Drobasheva (1971)	Rb_4CdCl_6					$RbCdCl_3$	
Bohac (1972)	Rb_4CdCl_6			$Rb_3Cd_2Cl_7$		$RbCdCl_3$	
Seifert (1973)	Rb_4CdCl_6		Rb_2CdCl_4	$Rb_3Cd_2Cl_7$		$RbCdCl_3$	
Seifert (1979)	Rb_4CdCl_6		Rb_2CdCl_4	$Rb_3Cd_2Cl_7$	$Rb_4Cd_3Cl_{10}$	$RbCdCl_3$	$RbCd_4Cl_{11}$

Table 6.2

The Raman frequencies (cm^{-1}) of the characteristic bands in the Cd-Cl stretching regions and the corresponding suggested compounds in the $CdCl_2/RbCl$ systems.

composition	frequencies(cm^{-1})		compounds	
x	fast cooled	slow cooled	fast cooled	slow cooled
RbCl				
0.80	208.5		Rb_2CdCl_4	
	218	220	Rb_4CdCl_6	Rb_4CdCl_6
0.75	208	208	Rb_2CdCl_4	Rb_2CdCl_4
	218	218	Rb_4CdCl_6	Rb_4CdCl_6
0.67	207	207	Rb_2CdCl_4	Rb_2CdCl_4
0.63	207.5	207	Rb_2CdCl_4	Rb_2CdCl_4
	233.5	233.5	$Rb_3Cd_2Cl_7$	$Rb_3Cd_2Cl_7$
0.60	207		Rb_2CdCl_4	
	232.5	232.5	$Rb_3Cd_2Cl_7$	$Rb_3Cd_2Cl_7$
0.56	209		Rb_2CdCl_4	
	232	229	$Rb_3Cd_2Cl_7$	$Rb_3Cd_2Cl_{11}$
0.50	---	---	$RbCdCl_3$	$RbCdCl_3$
0.33	215	215	$RbCd_2Cl_5$	$RbCd_2Cl_5$
	248	248	$RbCdCl_3$	$RbCdCl_3$
0.17	215	215	$RbCd_2Cl_5$	$RbCd_2Cl_5$
	232	232	$CdCl_2$	$CdCl_2$
KCl				
0.80	221		$KCdCl_3$	
	248.5		$KCdCl_3$	
	230	230	K_4CdCl_6	K_4CdCl_6
0.67	221	221	$KCdCl_3$	$KCdCl_3$
	248.5	248.5	$KCdCl_3$	$KCdCl_3$
	230	230	K_4CdCl_6	K_4CdCl_6
0.50	221	221	$KCdCl_3$	$KCdCl_3$
	248.5	248.5	$KCdCl_3$	$KCdCl_3$

Table 6.3
The correlation diagram for K_4CdCl_6

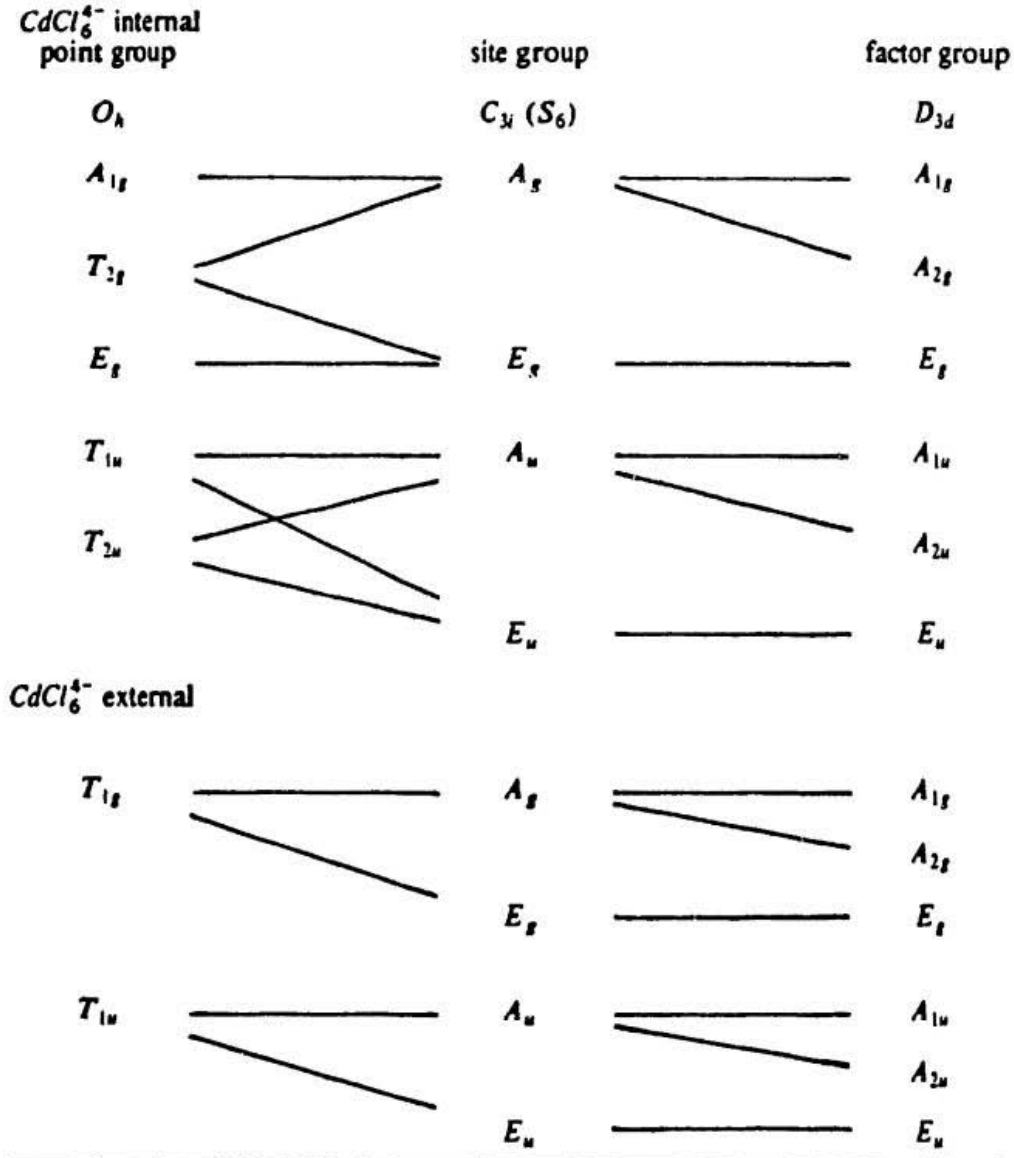

Table 6.3 (continued)

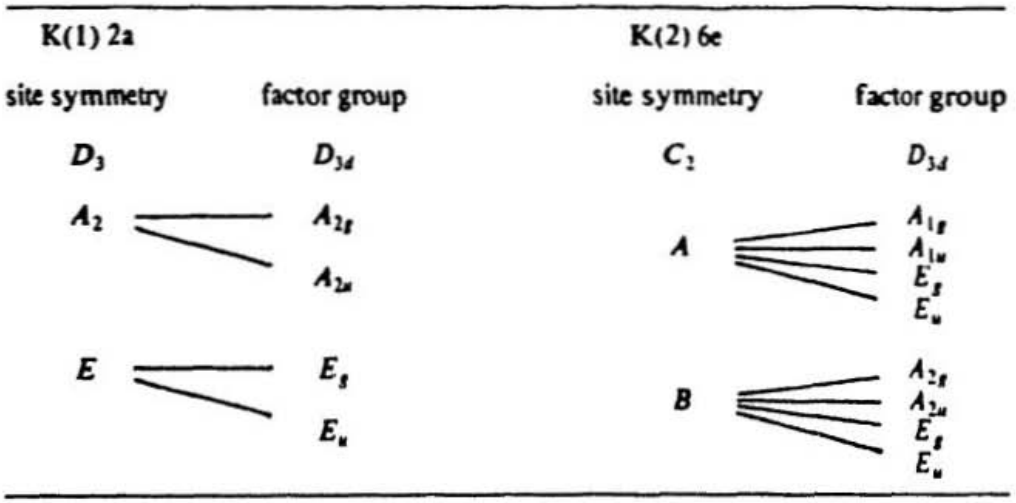

Table 6.4

The frequencies (cm^{-1}) of the bands observed from solids K_4CdCl_6, Rb_4CdCl_6, $Rb_3Cd_2Cl_7$, $KCdCl_3$ and $RbCdCl_3$ (II) at room temperature.

K_4CdCl_6	Rb_4CdCl_6	assignments	$Rb_3Cd_2Cl_7$	$KCdCl_3$	$RbCdCl_3$ phase (II)
					36(w)
67.5 (w)	52(w)		55.5(w)	52(m)	42.5(m)
			72(sh)	84.5(m)	81(m)
104.5 (m)	116(br)	ν_5			92.5(m)
			80(s)	101.5(m)	101(w)
124(m)	137(br)	ν_2			106.5(m)
134(m)	150(br)		143(m)	113.5(w)	114.5(w)
146(w)	158(br)		232.5(vs)	121(w)	122(w)
				137.5(w)	142(m)
156.5(s)				157(w)	158(w)
178(w)				163(w)	
185(w)				220.5(m)	217(m)
230(vs)	221(s)	ν_1		248.5(s)	247.5(s)

* w - weak; m - medium; br - broad; sh - shoulder; s - strong; vs - very strong

Table 6.5

The Raman frequencies for the bands in Rb_2CdCl_4 and Cs_2CdCl_4 compounds at room temperature

Rb_2CdCl_4		Cs_2CdCl_4	intensity
207	209*	198	strong
88	89	92	weak
84	85	69	weak
45	46	42	very weak

* Ref. [Aleksandrov 1985b]

Table 6.6

The center frequencies (cm^{-1}) of the most intense bands and structures for some coordination compounds in the $CdCl_2/ACl$ (A = K, Rb, Cs) systems at room temperature.

compounds	structure	frequency (cm^{-1})
Rb_4CdCl_6	$CdCl_6^{4-}$ species	221
K_4CdCl_6	$CdCl_6^{4-}$ species	229
Cs_3CdCl_5	$CdCl_4^{2-}$ species	275
Cs_2CdCl_4	$CdCl_4^{2-}$ species	268 (>435°C)
Cs_2CdCl_4	network	198
Rb_2CdCl_4	network*	209
$Cs_3Cd_2Cl_7$	network	221
$Rb_3Cd_2Cl_7$	network	232.5
$Rb_4Cd_3Cl_{10}$	network	229
$CsCdCl_3$	network	248
$RbCdCl_3$ (I)	network	-
$RbCdCl_3$ (II)	network	247.5 217
$KCdCl_3$	network	248.5 221.5
$CsCd_5Cl_{11}$	network	215
$RbCd_5Cl_{11}$	network	214

* network of linked octahedral $CdCl_6$ units.

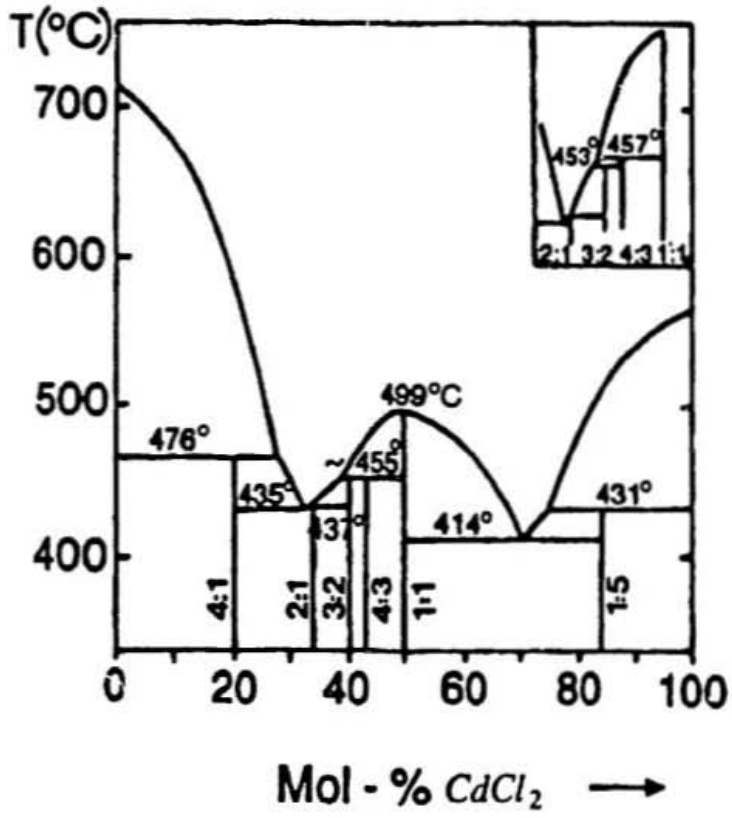

Fig. 6.1

Phase diagram of the $CdCl_2/RbCl$ binary system. Redrawn from Ref. [Seifert 1979].

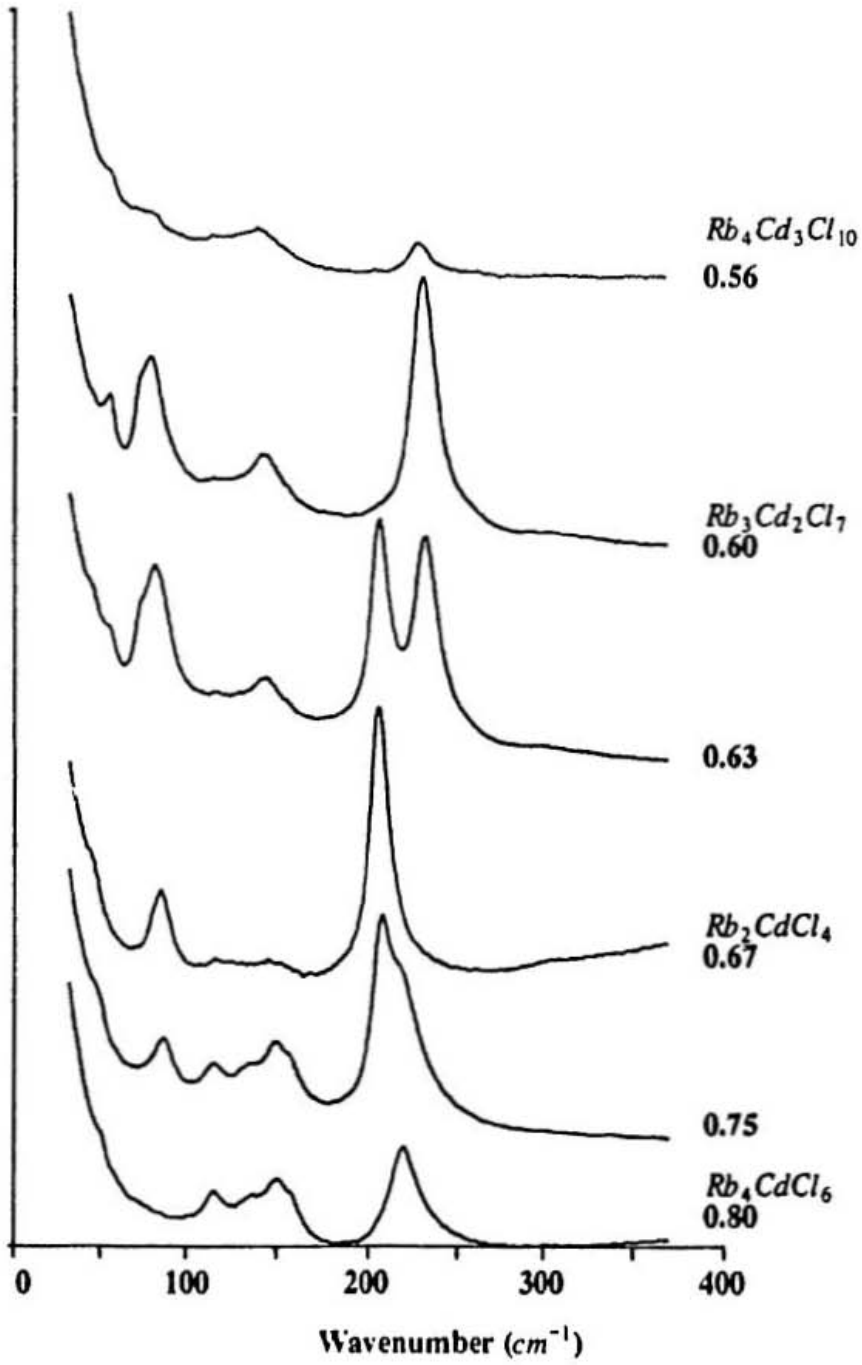

Fig. 6.2

Raman spectra observed for the $CdCl_2/RbCl$ solid systems with x from 0.80 to 0.56. Temperature 25°C; Slits 2 cm^{-1}.

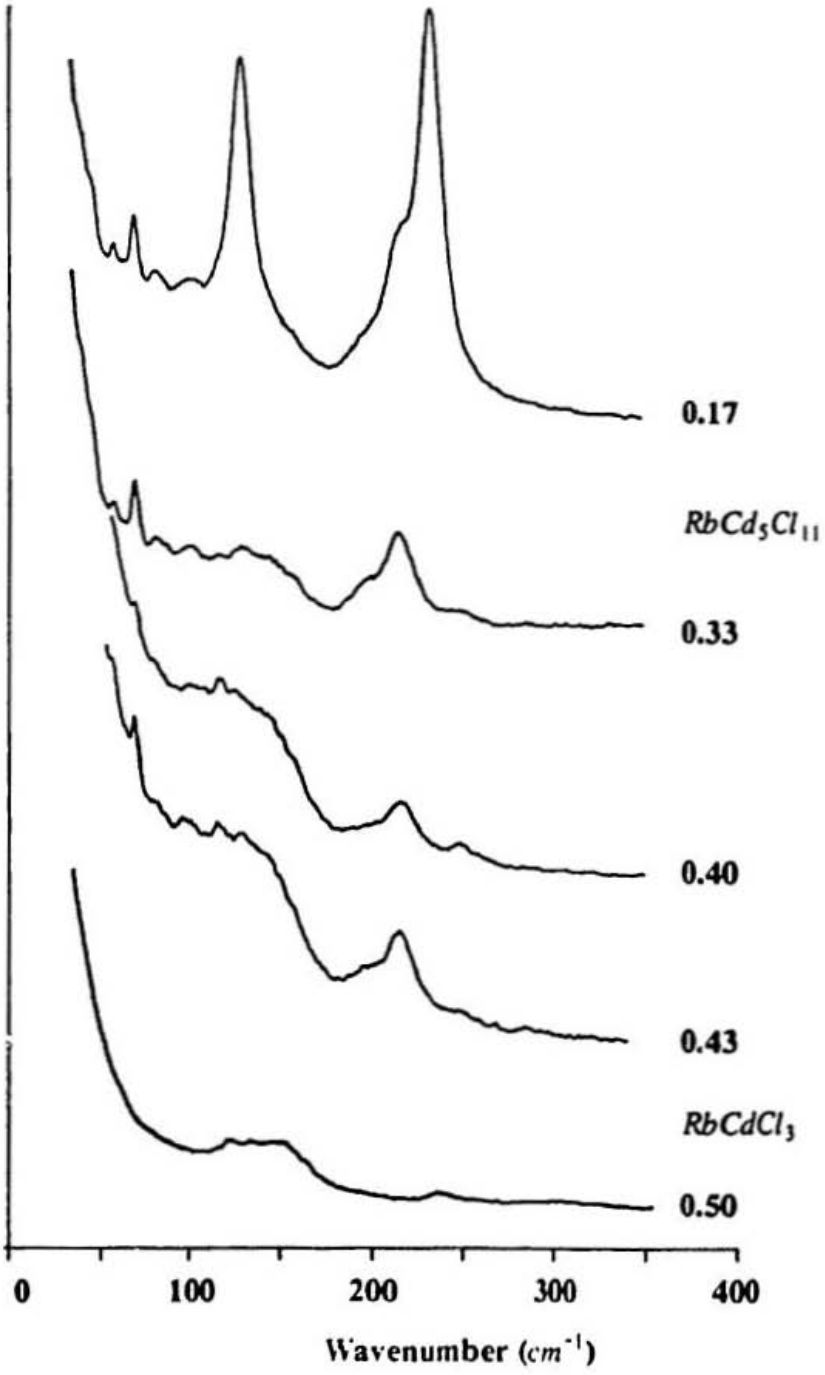

Fig. 6.3

Raman spectra observed for the $CdCl_2/RbCl$ solid systems with x from 0.50 to 0.17. Temperature 25°C; Slits 2 cm^{-1}.

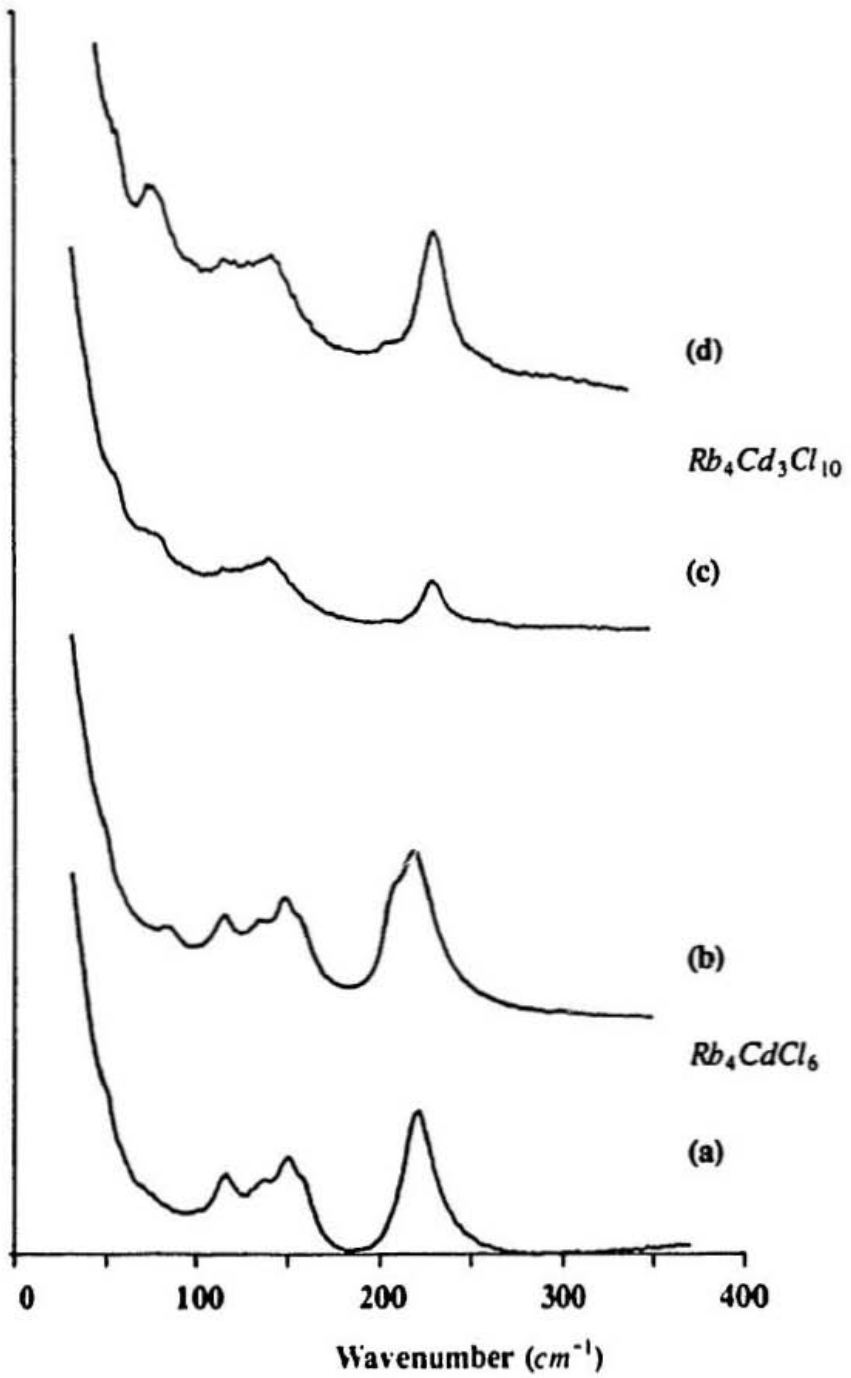

Fig. 6.4

Raman spectra observed for slow and fast cooled 0.80 and 0.56 samples to show the peaks due to incongruent compounds Rb_4CdCl_6 and $Rb_4Cd_3Cl_{10}$. Temperature 25°C; Slits 2 cm^{-1}. (a) slow cooled Rb_4CdCl_6; (b) fast cooled Rb_4CdCl_6; (c) slow cooled $Rb_4Cd_3Cl_{10}$; (d) fast cooled $Rb_4Cd_3Cl_{10}$.

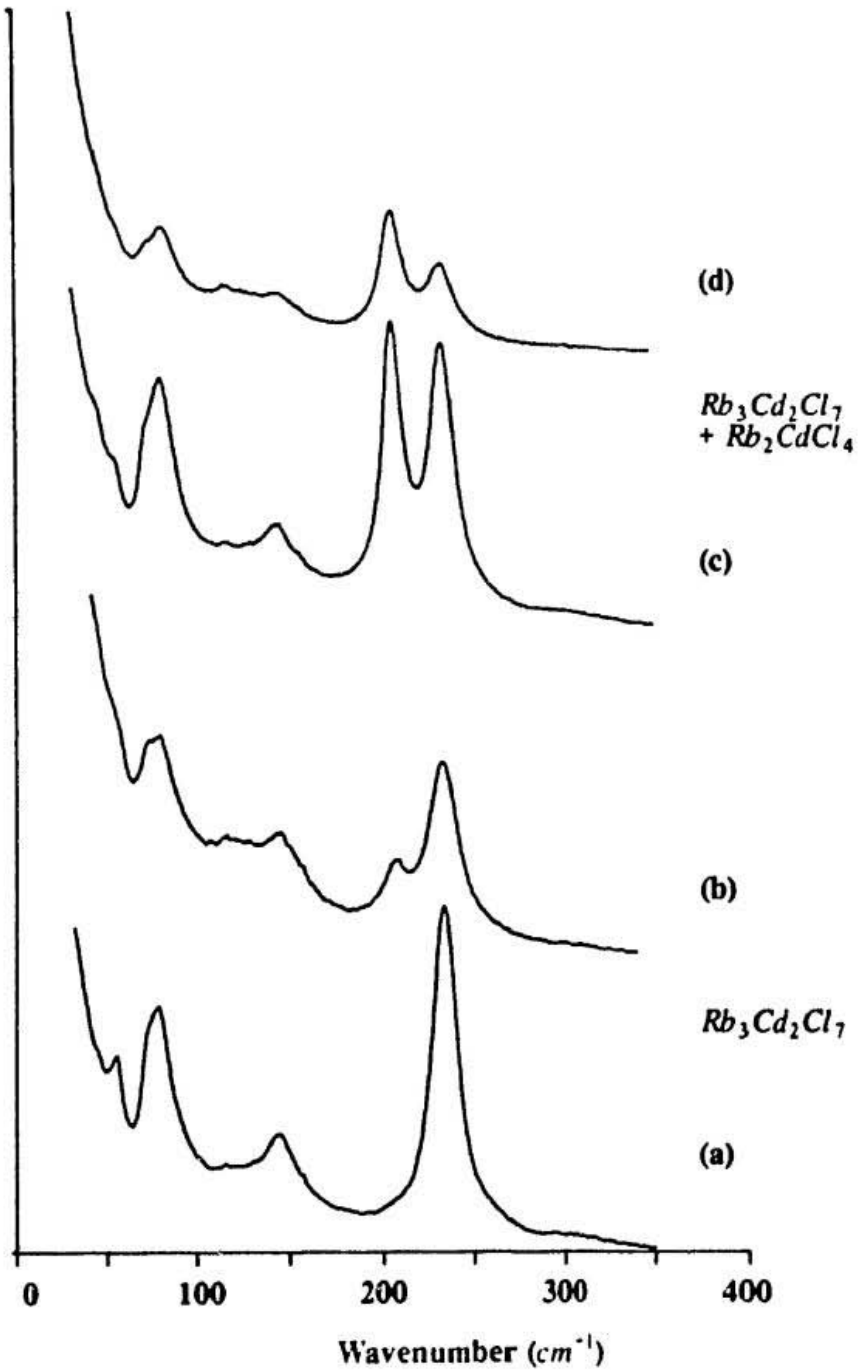

Fig. 6.5

Raman spectra observed for slow and fast cooled 0.63 and 0.60 samples to show the peaks due to incongruent compound $Rb_3Cd_2Cl_7$. Temperature 25°C; Slits 2 cm^{-1}. (a) slow cooled $Rb_3Cd_2Cl_7$; (b) fast cooled $Rb_3Cd_2Cl_7$; (c) slow cooled 0.63 sample; (d) fast cooled 0.63 sample.

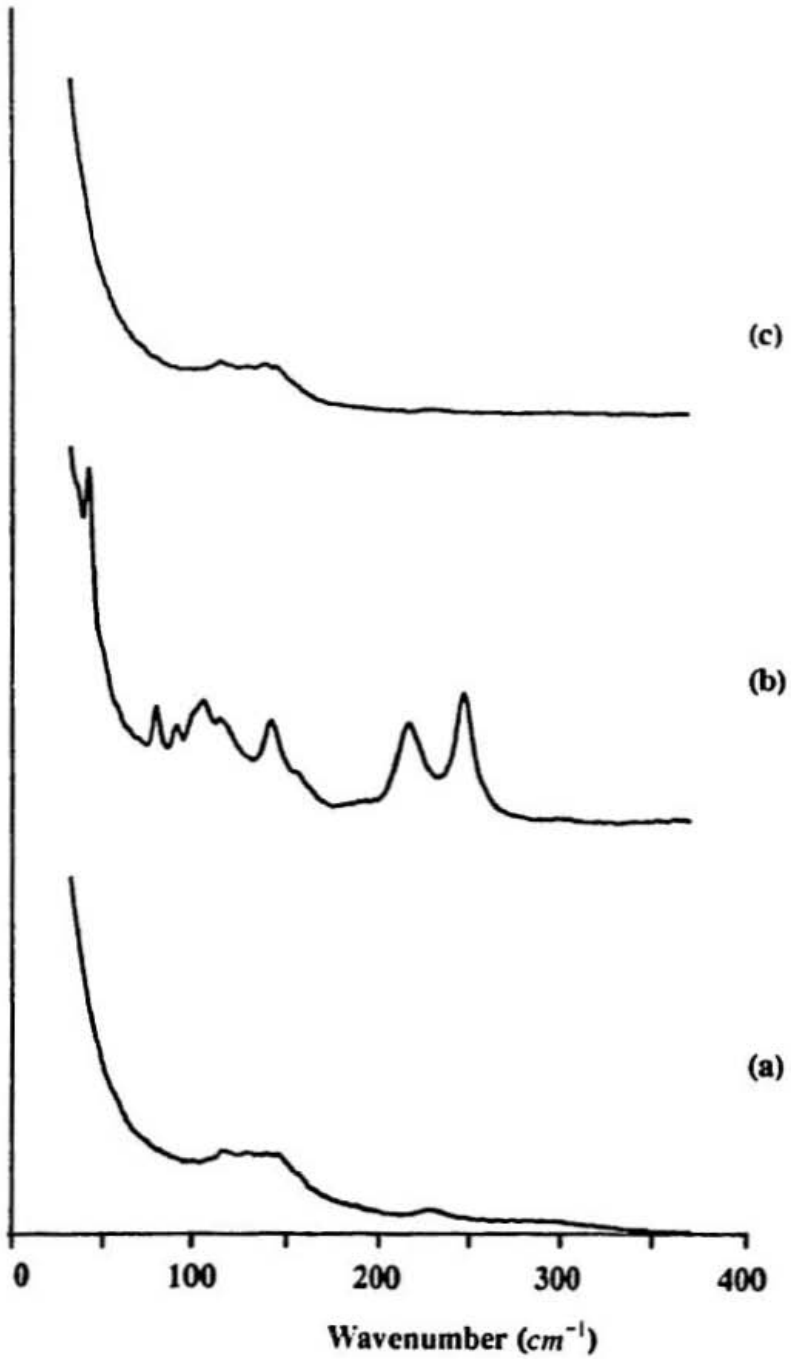

Fig. 6.6

Raman spectra of $RbCdCl_3$ (I) and (II). (a) $RbCdCl_3$ (I), before opening the quartz tube; (b) $RbCdCl_3$ (II), after opening the quartz tube for a week; (c) $RbCdCl_3$ (I), after drying the $RbCdCl_3$ (II). Temperature 25°C; Slits 2 cm^{-1}.

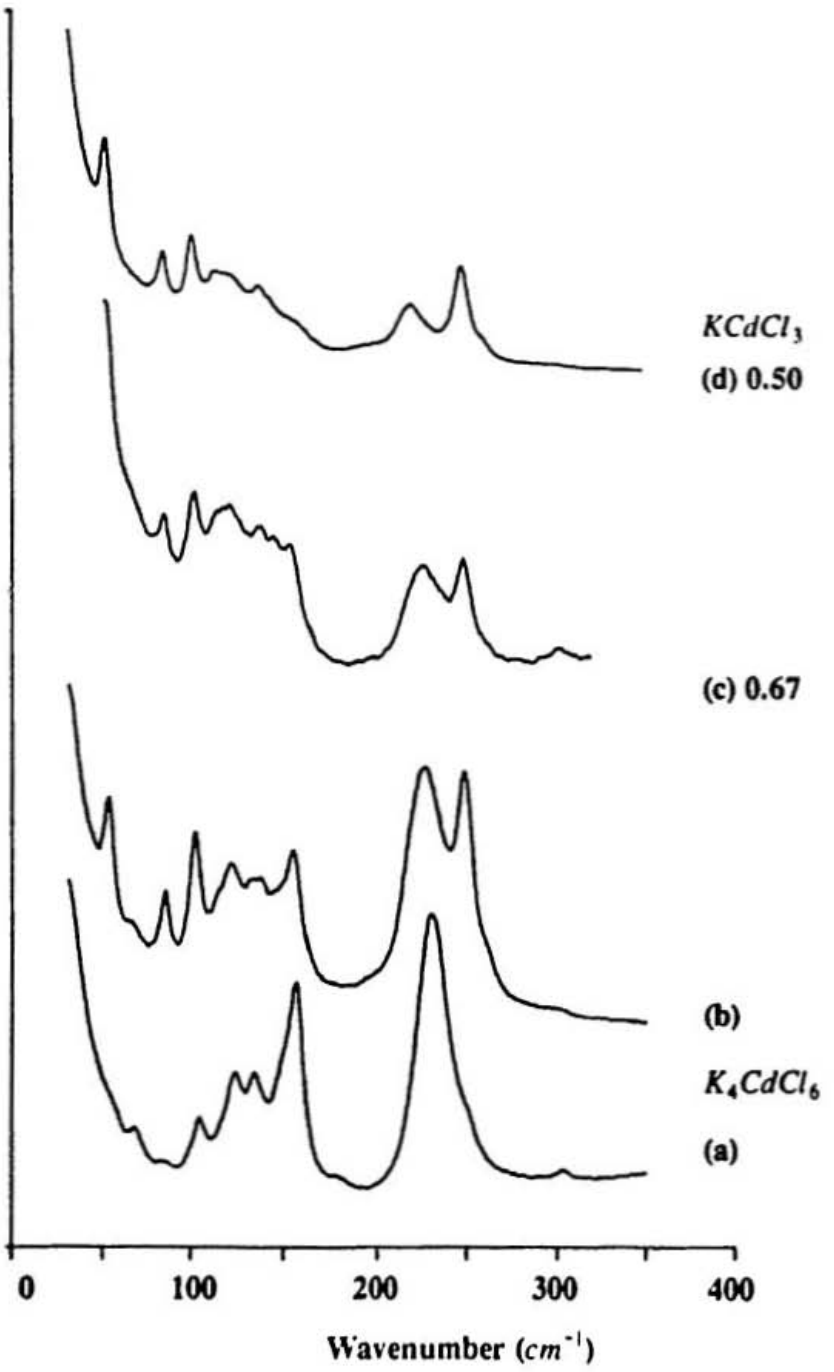

Fig. 6.7

Raman spectra observed for the $CdCl_2/KCl$ binary system. Temperature 25°C; Slits 2 cm^{-1}. (a) slow cooled K_4CdCl_6; (b) fast cooled K_4CdCl_6; (c) slow cooled 0.67 sample; (d) slow cooled $KCdCl_3$.

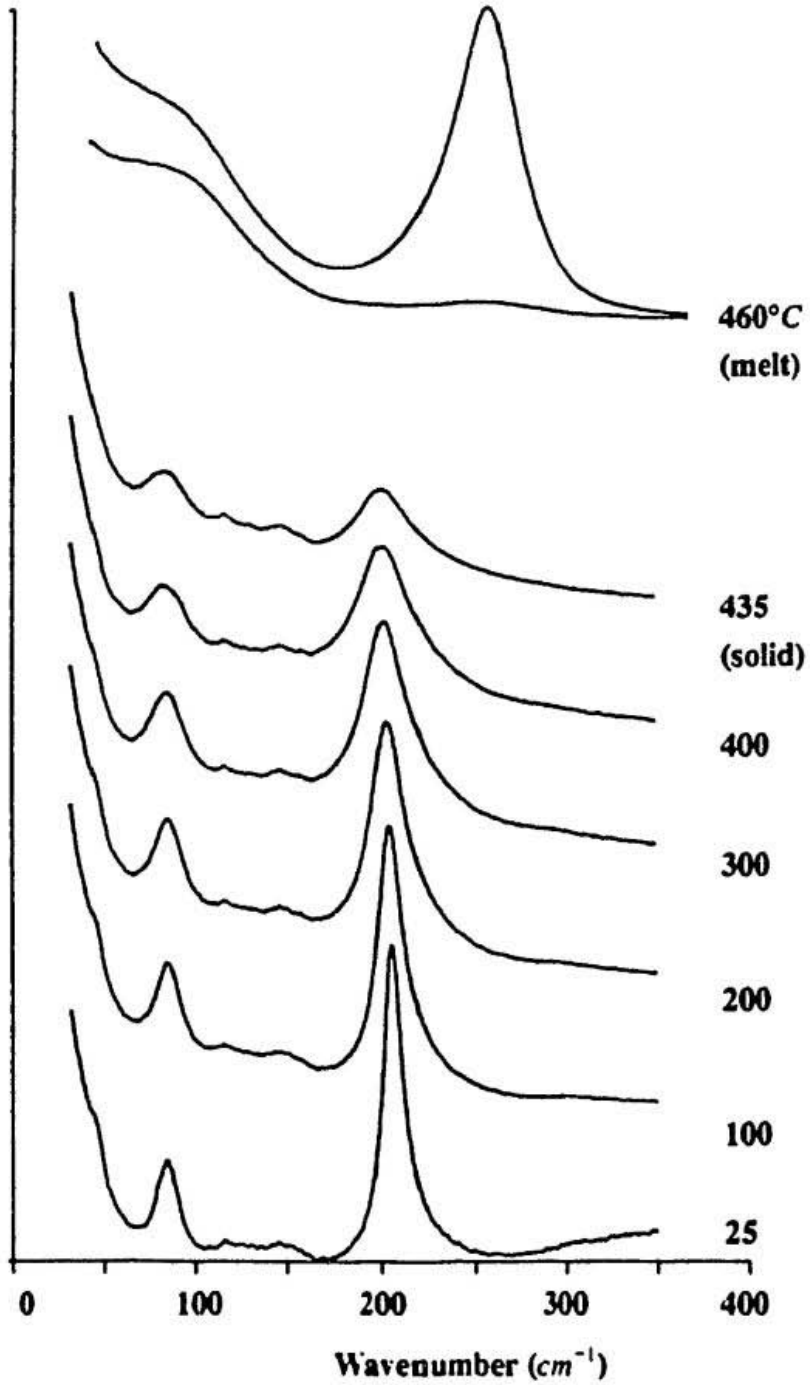

Fig. 6.8

Raman spectra for samples at different temperatures for the compound Rb_2CdCl_4 at the temperatures as indicated. Slits 2 cm^{-1}.

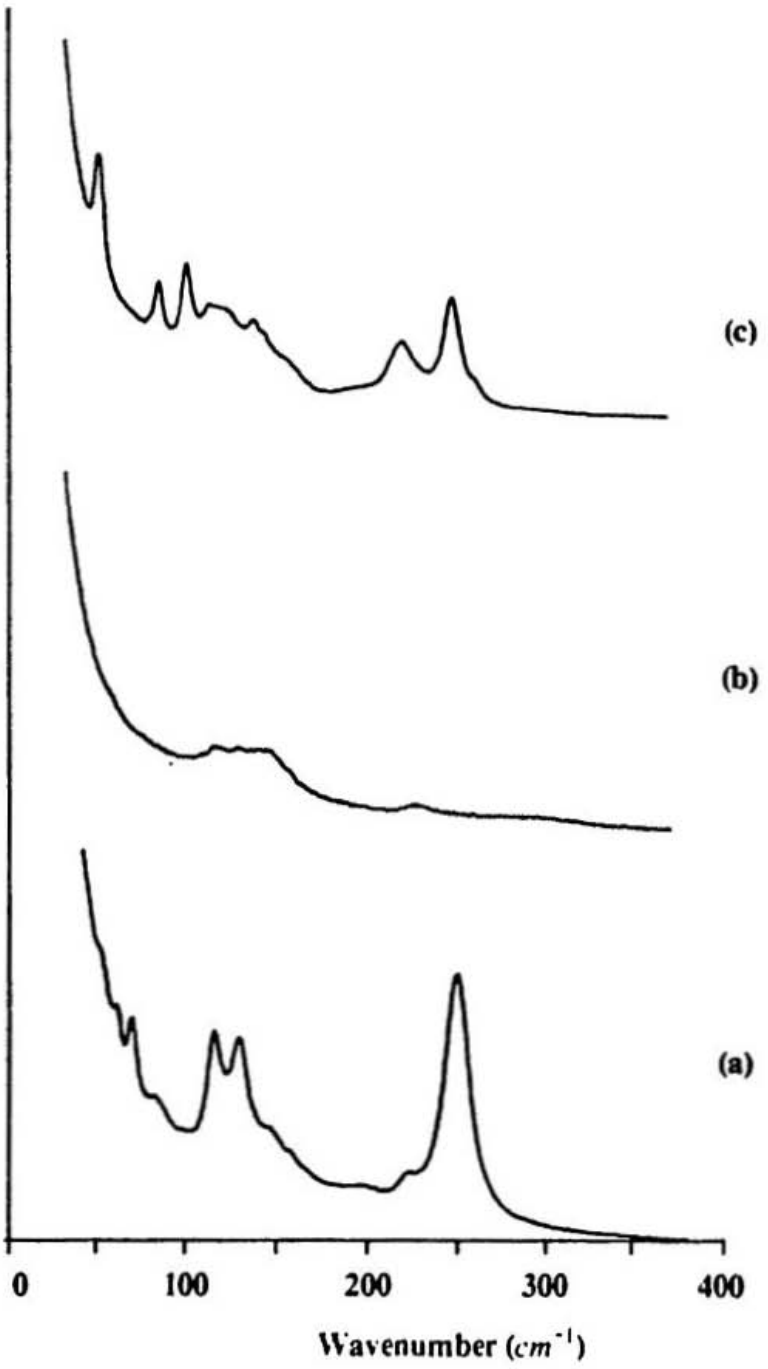

Fig. 6.9

Raman spectra for solids $CsCdCl_3$, $RbCdCl_3$, and $KCdCl_3$. Temperature 25°C; slits 2 cm^{-1}. (a) $CsCdCl_3$; (b) $RbCdCl_3$; (c) $KCdCl_3$.

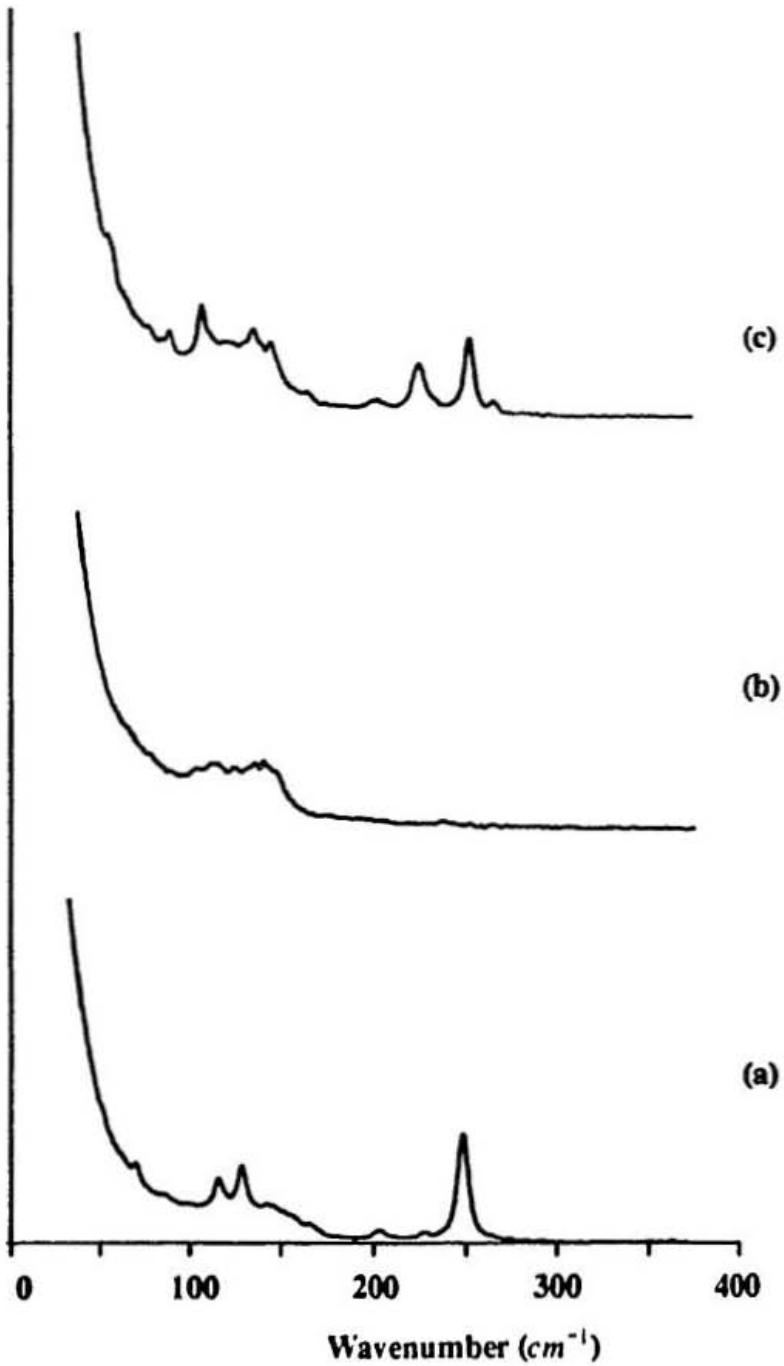

Fig. 6.10

Raman spectra for solids $CsCdCl_3$, $RbCdCl_3$, and $KCdCl_3$. Temperature 77K; Slits 2 cm^{-1}. (a) $CsCdCl_3$; (b) $RbCdCl_3$; (c) $KCdCl_3$.

Chapter 7

RAMAN STUDIES OF THE $CdCl_2$/CsCl AND $CdCl_2$/RbCl MOLTEN SYSTEMS

7.1 Introduction

In chapters four, five and six, Raman spectra of the $CdCl_2/ACl$ (A = Cs, Rb, K) solid systems have been discussed. The coordination property of the Cd atom depends on the type of the alkali cation in case and the sample temperature in the solid systems. Three types of coordination of the Cd complex dominate in the solid states i.e. discrete tetrahedron, discrete octahedron and linked octahedra. The larger the size of the cations and the higher the temperature, the more stable the tetrahedral configuration, conversely for the octahedral structure.

The coordination structure of a complex species in melt is much more complicated compared to the solid state. A species is under complicated thermal motions in the molten state. One must consider both the kinetic and thermodynamic (energies) stability of a species in the studies of the local structure. A discrete species must have both kinetic and thermodynamic stability. The lifetime of this species should be long enough to detect by some experimental methods but the apparent structure could depend on the method of investigation. Vibrational spectroscopy is a relatively fast detection method and any local structure that persists for 10^{-11} or 10^{-12} second may be detected. NMR is a relatively slow process and species that exist for times between 10^{-6} and 10^{-12} second would be unresolved. X-ray and elastic neutron diffraction are very slow processes and time-averaged structures are obtained.

In the $CdCl_2/ACl$ melts, there is strong evidence for the existence of the $CdCl_4^{2-}$ species in the ACl rich melts but there is much uncertainty about the coordination and structure of the $CdCl_2$ rich melts. Previous studies [Clarke 1974] indicated that at very

high temperature, in the molten state, the tetrahedral complex $CdCl_4^{2-}$ ion was found to exist predominantly in the ACl-rich mixtures. Even when the molten system was diluted by another molten solvent, like molten potassium tetrachloroaluminate, $CdCl_4^{2-}$ was still the most important cadmium complex species [Clarke 1974]. Recently X-ray studies [Takagi 1989] confirmed the tetrahedral configuration ($CdCl_4$) in the pure $CdCl_2$ melt. Furthermore, as early as in 1969, the calorimetric studies [Bredig 1969] have suggested strongly in favor of the stability of a tetrahedral $CdCl_4^{2-}$ ion in the molten state.

The $CdCl_3^-$ species was found in aqueous solutions [Davies 1968]. Raman spectroscopic studies [Clarke 1972b] and electrochemical measurements [Inman 1961, 1965] indicated that $CdCl_3^-$ existed in molten sodium nitrate-potassium nitrate solvents. In the molten $CdCl_2/ACl$ (A = Cs, K) system, Clarke et al. [Clarke 1972a] suggested that when either $CsCl$ or KCl was added to molten $CdCl_2$, the bandwidth of the Cd-Cl stretching band decreased vary rapidly and became symmetric. The peak frequency of the intense Cd-Cl stretching mode was reported to increase to a maximum value at $Cl^-/Cd^{2+} = 3$. These authors suggested that the structural unit involved might be $CdCl_3^-$ or else $CdCl_4^{2-}$ with two chlorides shared with neighboring cadmium ions in the $CsCdCl_3$ melt. No studies have confirmed whether or not the $CdCl_3^-$ species is a stable species in the $CdCl_2/ACl$ melts. Although in principle discrete species generate unique spectra, it is sometimes hard to identify the species. One of the methods to assist the interpretation of a Raman spectrum from the molten state is to study the same system in the solid, glassy, vapor and aqueous phases. In this chapter, an excellent example of this kind of studies will be provided. Interpretation of the spectra of the $CdCl_2/ACl$ (A = Cs, Rb) melts can be aided by the studies of the same systems in the solid states.

In this chapter the effect of the concentration of the alkali cations and different alkali cations on the coordination property in the $CdCl_2/ACl$ (A = Cs and Rb) molten systems will be also discussed.

7.2 Results and Discussion

7.2.1 $CdCl_2$/CsCl melts

Polarized and depolarized Raman spectra ($I(\nu)$) over a frequency range from 50 - 400 cm^{-1} for the molten $CdCl_2/CsCl$ systems in a composition range from x = 0 to 0.80 mole fraction of $CsCl$ are presented in fig. 7.1. The corresponding polarized and depolarized reduced spectra ($R(\nu)$) obtained by employing a reduction $R(\nu)$ function in fig. 7.2 and the isotropic spectra in fig. 7.3. A schematic representation of an experimental scattering geometry for the measurements of the polarized and depolarized spectra are shown in fig. 7.4. The isotropic spectra were generated from the corresponding reduced spectra, $R_{\parallel} - 1.33R_{\perp}$. Take the spectrum of the Cs_2CdCl_4 melt as an example. The procedure used to obtain an isotropic spectrum is shown (fig. 7.4). The center frequencies of the most intense bands in the $R_{\parallel}$ spectra, the values of the Fullwidth at Half Height (FWHH, Γ_{iso}) from the reduced isotropic spectra, the values of the Γ_{ν_1} from the $R_{\perp}$ spectra are also listed in table 7.1.

x ≥ 0.67

Almost identical spectra have been observed for the x ≥ 0.67 melts (fig. 7.1-7.3). The center frequencies and FWHH for the Cd-Cl stretching ν_1 mode have the same values (table 7.1). The result indicates that the three melts contain the same complex species. The fact that the Raman spectra for x ≥ 0.67 are essentially identical suggests that the maximum coordination number of the cadmium ion is four in the CsCl rich melts. This result is in excellent agreement with previous studies (e.g. ref. [Clarke 1974, 1972a, 1972b]) that suggested that the $CdCl_4^{2-}$ ion exists in the ACl rich mixtures.

The characteristic Raman spectra suggest that the complex species has a tetrahedral structure. For a tetrahedral species, the distribution of the normal modes is A_1 (ν_1) + E (ν_2) + $2F_2$ (ν_3, ν_4). All the four vibrations are Raman active. Usually the frequency of the ν_3 mode is higher than that of the ν_1 mode. For examples the ν_1 peak is at about 460

cm^{-1}, ν_3 at 762 cm^{-1} for the CCl_4 molecule in the liquid [Brooker 1986]; and the ν_1 at about 350cm^{-1}, ν_3 at 487 cm^{-1} for the tetrahedral $AlCl_4^-$ species in the $AlCl_3/KCl$ melts [Φye 1971] (fig. 7.5). For an octahedral molecule, three normal modes ν_1, ν_2 and ν_5 are Raman active, ν_3 and ν_4 are infrared active. Usually the frequencies of these Raman active modes increase in the order $\nu_5 < \nu_2 < \nu_1$. For example, the ν_1 peak centers at 373 cm^{-1}, ν_2 at 281 cm^{-1} and ν_5 at 175 cm^{-1} for $NbCl_6^-$ [Bues, 1973]; and ν_1 at 555 cm^{-1}, ν_2 at 390 cm^{-1} and ν_5 at 345 cm^{-1} for AlF_6^{3-} [Gilbert 1975].

The assignments of the bands of the tetrahedral species are based on the careful measurements of the polarized and depolarized spectra. It appears that the ν_2(E) and ν_4(F) bands normally expected for a tetrahedral species overlap and give rise to a broad depolarized band at 105cm^{-1}. The ν_1 and ν_3 modes appear to be almost coincident but may be differentiated by the small differences in peak frequency and large differences in halfwidth. The ν_1(A) mode in the R_{iso} spectrum has a peak maximum at 261 cm^{-1} and a halfwidth 35 cm^{-1} whereas the ν_3 mode in the $R_\perp$ has a peak maximum at 260 cm^{-1} and a halfwidth 63 cm^{-1}.

It appears that the ν_1 and ν_3 have similar frequencies. For a tetrahedral species, the frequencies of the ν_1 (A_1) and ν_2 (E) are independent and the ν_3 (F) and ν_4 (F) are dependent on the mass of the center atom. Normal coordination calculation, for a model MCl_4 with a fixed force constant, indicated that the frequencies of the ν_3 and ν_4 modes decrease with increase mass of M whereas the ν_1 and ν_2 modes remain at constant frequencies (the calculations will be discussed in detail in chapter 9). The mass of Cd is approximately that will give the $\nu_1 \approx \nu_3$ while for more heavy atoms $\nu_3 < \nu_1$. In fact the ν_3 may have a lower frequency than the ν_1 for a tetrahedral $CdCl_4^{2-}$ species in the solid state. The metastable Cs_3CdCl_5 contains discrete $CdCl_4^{2-}$ species with the characteristic ν_1 frequency 275 cm^{-1} and ν_3 261 cm^{-1} at 25°C [chapter 4 in this thesis]. A similar result was reported for $(NEt_4)_2CdCl_4$ solid for which the ν_1 mode centers at 265 cm^{-1} and ν_3 at 250

cm^{-1} [Davies 1971].

Band resolution (fig. 7.6) gave that the intensity ratio of the depolarized band at 260 cm^{-1} in $R_\perp$ and the polarized band at 261 cm^{-1} in $R_\parallel$ of the Cs_2CdCl_4 melt is about 0.083. The values of the relative intensities are 1468.85 ($R_\perp$) and 15111.7 (R_{iso}) respectively (fig. 7.6). Since $R_\parallel = R_{iso} + 1.33R_\perp$ then $R_\perp / R_\parallel = 0.083$. The large value of the ratio of the relative intensities is about that expected for the ν_3 mode of a tetrahedral species. The depolarization ratio of the ν_1 mode of a tetrahedral species is expected to be very small ($\rho \leq 0.01$).

The similarity between the Raman spectra of the high temperature solid and the melt of Cs_2CdCl_4 further supports the tetrahedral structure. Table 7.2 lists several Cd-Cl symmetrical stretching frequencies for the three possible coordination states in solids. The frequency of the ν_1 band for the $CdCl_4^{2-}$ species in melts is 261 cm^{-1} which is close to the ν_1 frequency 268 cm^{-1} for the discrete $CdCl_4^{2-}$ species in the high temperature solid Cs_2CdCl_4 at 452°C. X-ray measurements confirmed that the high temperature solid of Cs_2CdCl_4 contains the discrete tetrahedral $CdCl_4^{2-}$ species [Seifert 1986].

x < 0.67

For the x < 0.67 systems, the assignments of the species were based upon a close examination of the variation of the relative peak intensities, center frequencies and bandwidths with composition.

The Raman spectra (fig. 7.1-7.3) of the melts with different compositions indicated that:

i) As x decreases the frequency of the most intense band increases gradually to a maximum value 264.5 cm^{-1} at x = 0.50, then decreases gradually (table 7.1). The depolarized bands at ~265 - 282cm^{-1} and about 105 cm^{-1} are observed in these spectra.

ii) The FWHH of the ν_1 band increases gradually from 35 cm^{-1} for the x = 0.80, 0.75 and 0.67 melts to 123 cm^{-1} for the x = 0, the pure $CdCl_2$ melt (table 7.1).

iii) The ν_1 bands in the isotropic spectra (fig. 7.3) of all melts are symmetric.

The variation tendency of the bandshape with the composition suggests a tetrahedral configuration in all of these melts.

It was reported that the spectrum of the $CsCdCl_3$ melt might be explained by a tetrahedral $CdCl_4^{2-}$ species or a $CdCl_3^-$ species with D_{3h} symmetry [Clarke 1972a]. The present Raman studies indicate that there are at least two reasons to suggest that the $CdCl_3^-$ species is not the predominate species in the $CsCdCl_3$ melt.

i) The FWHH of the intense polarized band increases gradually as the concentration of $CdCl_2$ increases. For the x = 0.67, 0.60, 0.56 and 0.50 samples the values of the FWHH of this band are 35, 44, 50 and 61 cm^{-1} respectively (table 7.1, figs. 7.1-7.3). If the $CdCl_3^-$ species exists in the $CsCdCl_3$ melt, the melts with x = 0.56 and 0.60 should contain two species, i.e $CdCl_3^-$ and $CdCl_4^{2-}$ (discrete $CdCl_4^{2-}$ species exist in the x = 0.67 melt). The FWHH of the ν_1 band should be almost the same for these two samples and the value should be at least 61 cm^{-1} (the value of the FWHH of the ν_1 band for the $CsCdCl_3$ melt).

ii) The peak frequencies of the ν_1 bands for the x = 0.67, 0.60, 0.56 and 0.50 samples are 261, 262.5, 263, and 264.5 cm^{-1} respectively. If the $CdCl_3^-$ species was stable, the ν_1 band for the x = 0.56 and 0.60 samples should contain two components one due to $CdCl_3^-$ and another due to $CdCl_4^{2-}$. The relative intensities of these bands should change as the concentration of the $CdCl_2$ changes, i.e. as the relative concentration of the $CdCl_3^-$ and $CdCl_4^{2-}$ species changes. However both the isotropic spectra remain very symmetric (fig. 7.3) for all of these samples. Band resolution for the intense polarized band indicates that there is only one band for the x = 0.67, 0.60, 0.56 and 0.50 samples and that the shift in peak maximum is continuous (figs. 7.6 and 7.7). Raman spectra of the $KCl/AlCl_3$ melt [Φye 1971] showed two separated polarized peaks in the Al-Cl stretching region due to two discrete species, $AlCl_4^-$ and $Al_2Cl_7^-$ (fig. 7.5). The relative intensity of the bands

due to the $AlCl_4^-$ and $Al_2Cl_7^-$ species changed as the change of the concentration of KCl. Clearly there is no evidence to suggest the presence of a two species equilibrium in the $CdCl_2$/ACl melts with x ≤ 0.67. It seems very possible that the lifetime of the Cl^- ion on the Cd becomes too short for discrete species to be identified.

The vibrational and reorientational correlation times can be related to the FWHH of the isotropic and anisotropic spectra [Brooker 1986]. If the correlation function G(t) is exponentially decaying with time

$$G(t) = A \exp t/\tau$$

where τ is the correlation time, the band profile in frequency space will have Lorentzian shape with full width at half height (cm^{-1}) which is related to the correlation time as following equation.

$$\Gamma^{-1} = \pi c \tau$$

For a totally symmetric vibration, the vibrational and reorientational times Γ_v and Γ_R can be determined from the halfwidth of the isotropic and anisotropic spectra i.e.

$$\Gamma_{iso} = \Gamma_v \approx \Gamma_{\parallel}$$

$$\Gamma_{aniso} = \Gamma_{\perp} = \Gamma_v + \Gamma_R$$

$$\tau_v^{-1} = \pi c \Gamma_v$$

$$\Gamma_R^{-1} = \pi c \Gamma_R = \pi c (\Gamma_{\perp} - \Gamma_{\parallel})$$

The approximate values of the calculated Γ_{iso} are listed in table 7.1 (Since the depolarization ratio of the ν_1 band is very small and the presence of the ν_3 interferes it is difficult to measure the I_{aniso} of the ν_1 band to obtain the reorientational time.). The values of the Γ_{iso} of the species in the x = 0.80, 0.75 and 0.67 samples are the same as expected (0.38 ps). When the concentration of the CsCl decreases, the value of the Γ_{iso} decreases. The long lifetime (0.38 ps) indicates a discrete, stable $CdCl_4^{2-}$ species which gives a well defined, characteristic Raman spectrum of the tetrahedron. When the concentration of the

CsCl decreases the lifetime of the tetrahedral complex ions decreases. Many short-lived linked tetrahedral ions with fast exchange Cl^- between these ions appear to exist in these melts.

The analysis above suggests that the structure of the complex ion changes with the change of the composition of the melt from discrete $CdCl_4^{2-}$ species in the $x \geq 0.67$ melts to short lived, linked tetrahedral ions in the $x < 0.67$ melts and results in the shift of the characteristic vibrational frequencies. For example, the depolarized ν_3 mode shifts toward a higher frequency with the increase of $CdCl_2$. The continued presence of the ν_3 mode (higher than ν_1) indicates the retention of the tetrahedral coordination rather than octahedral.

7.2.2 $CdCl_2$/RbCl melts

Raman spectra of the $CdCl_2/RbCl$ melts are presented in figs. 7.8-7.10. The peak frequencies and values of the Γ_{iso}, Γ_{ν_1}, and τ_ν are listed in table 7.1. These results indicate that there is the same variation in the bandshape for different concentrations of the alkali metal ions in both the $CdCl_2/CsCl$ and $CdCl_2/RbCl$ melts. Similar analysis as described above for the $CdCl_2/CsCl$ melts suggests that there are the similar complex species structures in the $CdCl_2/RbCl$ melts as in the $CdCl_2/CsCl$ melts.

The comparison of the spectra obtained from the $CdCl_2/CsCl$ and $CdCl_2/RbCl$ systems gives information about the effect of the different alkali ions on the cadmium complex ions.

i) The central frequencies of the ν_1 modes for these two systems are of almost the same values in the corresponding compositions in the molten states, even for the discrete $CdCl_4^{2-}$ species (261 cm^{-1} for both CsCl and RbCl) or bridged $CdCl_4$ unit. The values are different in the solid states. For example, the central frequency of the most intense band is about 198 cm^{-1} for Cs_2CdCl_4, 207 cm^{-1} for the isostructural compound Rb_2CdCl_4 at room temperature. The result indicates that there is little effect on the

vibrational frequencies to replace the Cs^+ by Rb^+ in melts, but much larger effect in solids.

ii) Although the central frequency of the ν_1 mode of the complex ion does not shift for different alkali metal ions, the FWHH of this band is changed (table 7.1, fig. 7.11). For instance, for the x = 0.80 sample the halfwidth is 6 cm^{-1} greater for the rubidium sample than for the cesium sample. This difference continues for $x \leq 0.80$ but should approach zero for pure $CdCl_2$. The halfwidth of the ν_3 mode is almost unaffected.

The dependence of the bandwidths on the Rb^+ and Cs^+ ions reflects the magnitude of the interaction among the alkaline cations and the cadmium complex ions. The broadness of the bandwidths for the $CdCl_2/RbCl$ melts indicates a stronger interaction (greater range of environments) among the Rb^+ and the complex ions compared to that among the Cs^+ and the complex ions in the molten states. Meanwhile the same result was obtained for the solid state which has been discussed in the last chapter. The linked octahedra could be broken into discrete $CdCl_4^{2-}$ species in the high temperature solid Cs_2CdCl_4, but not in Rb_2CdCl_4. In conclusion, the interaction among the alkali metal cations and the Cd complex ions increases with decrease in size of the alkali cations in both the solid and molten states.

7.2.3 Pure $CdCl_2$ melt

Many previous studies have been performed on molten $CdCl_2$ by several methods, but the coordination structure of the cadmium ion suggested in molten $CdCl_2$ was inconsistent. An earlier Raman measurement by Bues [Bues 1955] suggested that $CdCl_2$ retained its layer structure in melt. A broad Raman band peaked at 215 cm^{-1} was reported. Clarke [Clarke 1972a] et al. found that the Cd-Cl stretching vibration had a complex bandshape which changed with temperature. They suggested that there were a number of different coordination geometries of Cd^{2+} in the $CdCl_2$ melt. A recent X-ray studies by Takagi et al. [Takagi 1989] indicated the tetrahedral configuration ($CdCl_4$).

Their Raman spectrum showed a single polarized band at 229 cm^{-1} which was in disagreement with other studies [Takagi 1989, Bues 1955, Tanaka 1963] at about 210 - 217 cm^{-1}.

Because of the high scattering intensity in the low frequency region, it is hard to analyze the $I(\nu)$ spectrum for this kind of melt. In order to deduce the structural information from the analysis of the bandshape, the reduced spectrum was obtained in the present study. The $I(\nu)$, $R(\nu)$ and isotropic Raman spectra for the $CdCl_2$ melt are presented in figs. 7.1, 7.2 and 7.3 (x = 0) respectively. The central frequency in the Cd-Cl stretching region in the $I(\nu)$ spectrum is about 215 cm^{-1} which is in good agreement with the most previous studies [Bues 1955, Tanaka 1963]. In the $R(\nu)$ spectrum the peak maximum shifts to about 238 cm^{-1} since the background scattering is reduced. Further there is a depolarized band at ~281 cm^{-1}. Like other spectra obtained from the $CdCl_2/CsCl$ and $RbCl$ melts, the intense band in the isotropic reduced spectrum of the $CdCl_2$ melt is symmetric. These results suggest that the basic tetrahedral $CdCl_4$ coordination structure is retained in the pure $CdCl_2$ melt.

Crystalline $CdCl_2$ has a typical layer structure with a corner-shared linked $CdCl_6$ octahedral unit. Raman measurements over a wide temperature range from 25°C to above the melting point (fig. 7.12 I(ν), fig. 7.13 R(ν)) indicated that no structural phase transition was observed in the solid states within this temperature range. The peak frequencies decreased and the bandwidths increased gradually with the increase of temperature. At about 560°C, a few degrees below the melting point (568°C), the frequency of the Cd-Cl stretching vibrational mode decreased to 228 cm^{-1}. However, when the temperature increased to about 580°C (above the melting point), the frequency of this band increased to 238 cm^{-1} in the molten state (fig. 7.14). Usually if a complex species has the same coordination in both the solid and molten states, the frequency of the intense band for the melt would have a lower value compared to that for the solid state. For example, as discussed in chapters four and five, the ν_1 frequency for the $CdCl_4^{2-}$ species is about 261

cm^{-1} in the Cs_2CdCl_4 melt (475°C), but 268 cm^{-1} in the high temperature solid Cs_2CdCl_4 at 452°C. The increase of the ν_1 frequency suggests that the coordination number of the Cd^{2+} decreases as the solid $CdCl_2$ melts. The result further supports the tetrahedral structure in the $CdCl_2$ melt.

The Raman studies indicate that molten $CdCl_2$ has the cadmium ions with tetrahedrally coordinated structure. The extent to which a Raman peak merges into a background scattering reflects the stability of a coordination sphere. Weak, broad Raman scattering superimposed on a broad Rayleigh wing is indicative of ill-defined, short-lived species. For example, only a weak shoulder can be observed on the Rayleigh line for molten $CaCl_2$, $SrCl_2$ and $BaCl_2$ in which no stable discrete complex species exist [Bunten 1984] However, a strong Raman band can be resolved for $MgCl_2$ [Bunten 1984, Huang 1976] in which it has been suggested that the Mg^{2+} ion also retains a basic tetrahedral coordination. The relatively high intensity for the peak centered at 215 cm^{-1} in molten $CdCl_2$ (fig. 7.13) indicates that the cadmium forms well defined complex species in the pure $CdCl_2$ melt.

7.3 Conclusion

The tetrahedral coordination is the favorable configuration of the cadmium ion in the $CdCl_2/ACl$ (A = Cs and Rb) melts. For the $x \geq 0.67$ melts discrete $CdCl_4^{2-}$ species are present. For the $x < 0.67$ melts (including the pure $CdCl_2$ melt) short-lived tetrahedrally coordinated complex ions persist (with Cd-Cl-Cd bridges). The short-lived local tetrahedral units have a continuous distribution of the Cd-Cl bond lengths due to the fast exchange of the bridged Cl^- ions among local $CdCl_4$ units. As a result the Cd-Cl stretching Raman band becomes very broad. The interaction between the cadmium-chlorides complex ions increases with the decreased size of the alkali metal ion.

Table 7.1

The center frequencies (cm^{-1}) and the FWHH of the ν_1 and ν_3 bands, and the values of the calculated vibrational lifetime of the complex ions for the $CdCl_2/CsCl$ and $CdCl_2/RbCl$ molten systems.

composition a mole fraction of ACl	$\nu_{1,iso}$ ν_3 (cm^{-1})	$\Gamma_{\nu_1,iso}$ Γ_{ν_3} (cm^{-1})	τ_v (ps)	(cm^{-1})	(cm^{-1})
CsCl					
0.80	261	35	0.30	260	63
0.75	261	35	0.30	260	63
0.67	261	35	0.30	260	63
0.60	262.5	44	0.24	265	66
0.56	263	50	0.21	270	70
0.50	264.5	61	0.17	276	73
0.40	261	78	0.14	281	85
0.33	254	100	0.11	282	104
0	238[b]	123	0.09	281	125
RbCl					
0.80	262	41	0.26	260	63
0.75	262	41	0.26	260	63
0.67	262	41	0.26	260	63
0.63	262	45	0.24	262	64
0.60	262.5	49	0.22	263	66
0.56	263	55	0.20	267	68
0.50	264	63	0.17	276	73

a Calculated from $\Gamma_{\nu_1,iso}$

b 215 cm^{-1} in $I(\nu)$ spectrum

Table 7.2

Several Cd-Cl symmetrical vibrational frequencies of possible coordinational states in the cadmium chloride aikali metal chloride binary system.

coordination state	compound	frequency (cm^{-1})	temperature (°C)
$CdCl_6^{4-}$	K_4CdCl_6	230	25
	Rb_4CdCl_6	221	25
$CdCl_4^{2-}$	Cs_3CdCl_5	275	25
		268	390
	Cs_2CdCl_4	268	452
linked octahedra	Cs_2CdCl_4	198	25
	Rb_2CdCl_4	209	25

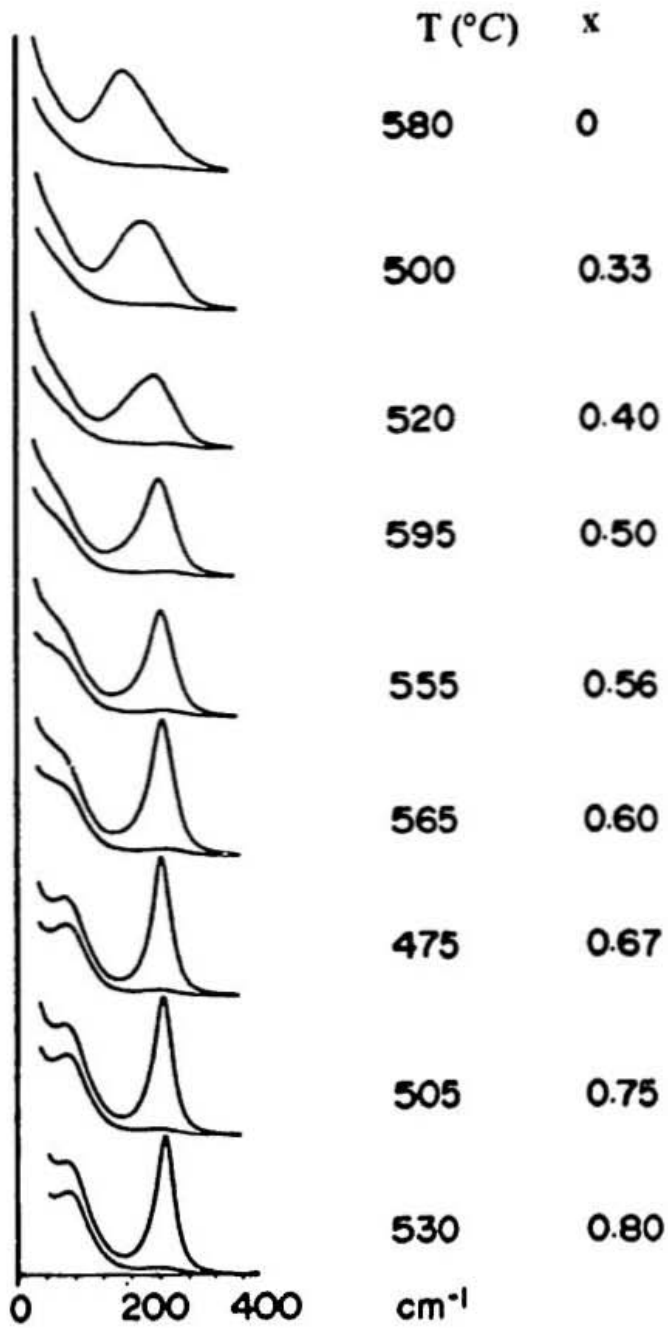

Fig. 7.1

$I(\nu)$ Raman spectra for the molten $CdCl_2/CsCl$ system. Slits 2 cm^{-1}. **X** - the mole fraction of $CsCl$; T - sample temperature.

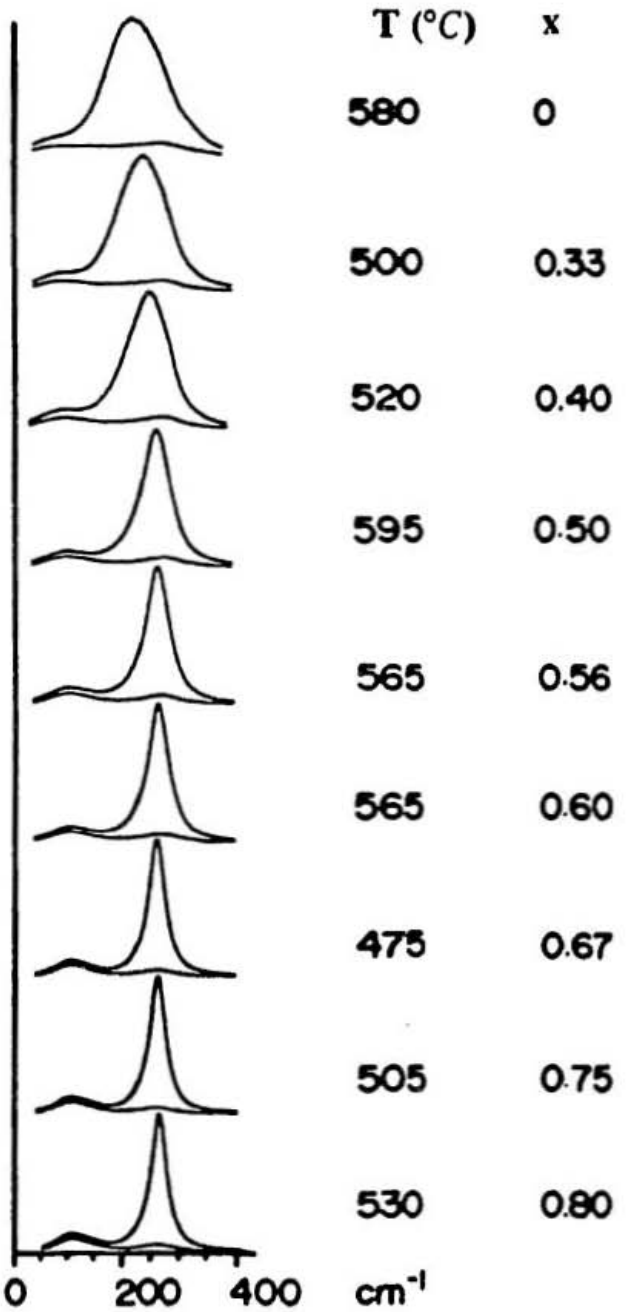

Fig. 7.2

R(v) Raman spectra for the molten $CdCl_2/CsCl$ system. **X** - the mole fraction of *CsCl*; T - sample temperature.

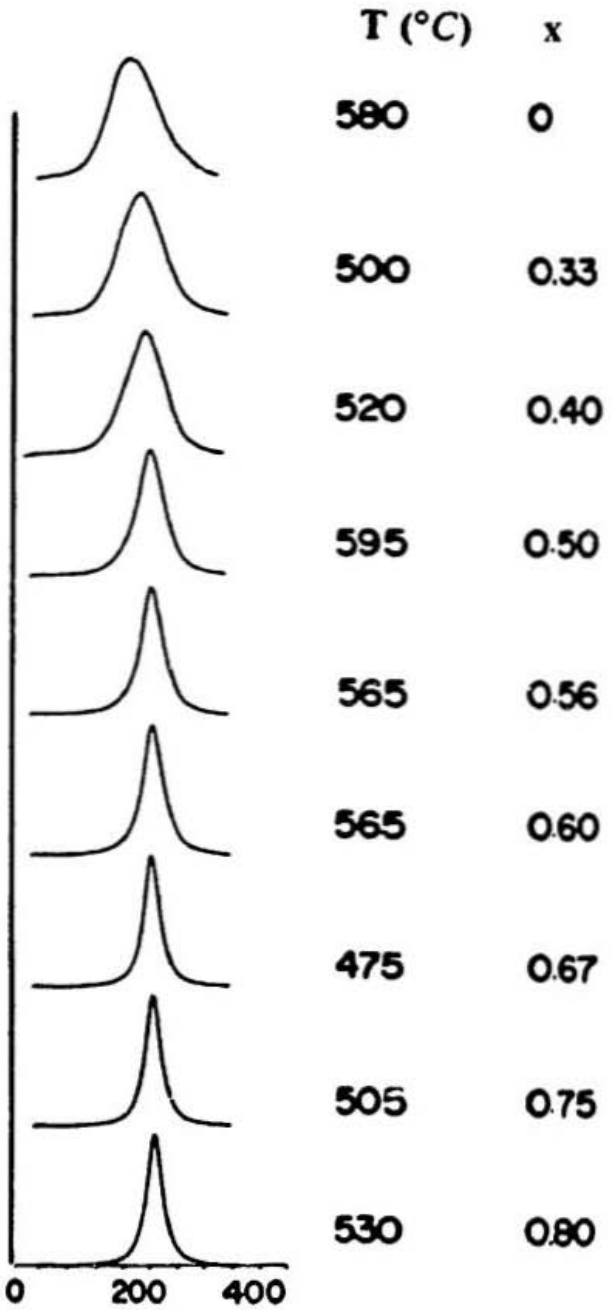

Fig. 7.3

Isotropic Raman spectra ($R_{\parallel}$ - 1.33 $R_{\perp}$) for the molten $CdCl_2/CsCl$ systems. **x** - the mole fraction of $CsCl$; T - sample temperature.

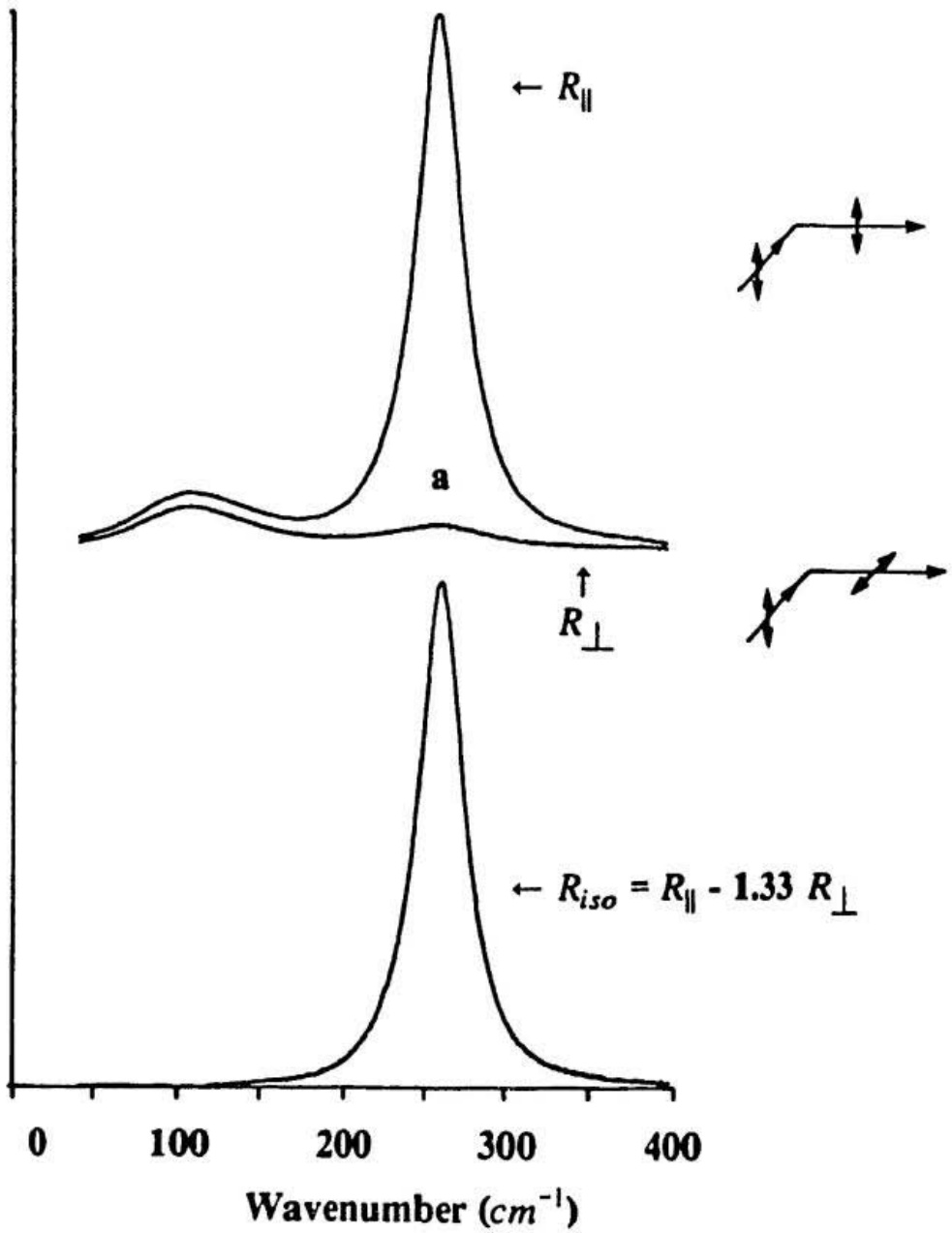

Fig. 7.4

A example of the method to obtain the isotropic spectrum (the example is for the Cs_2CdCl_4 melt). **a** The intensity at 261 cm^{-1} in $R_{\perp}$ is due to ν_3.

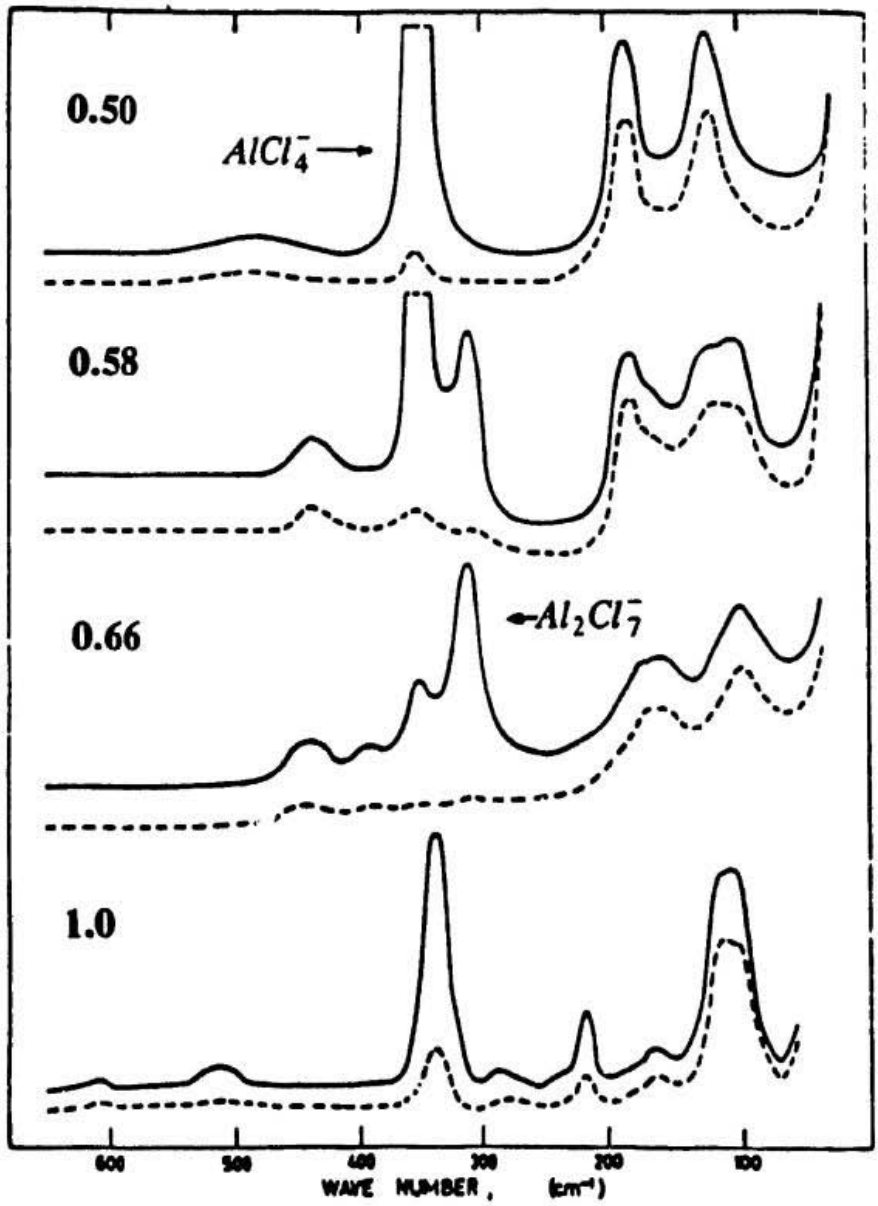

Fig. 7.5

Raman spectra for the $AlCl_3/KCl$ melts [Øye 1971].

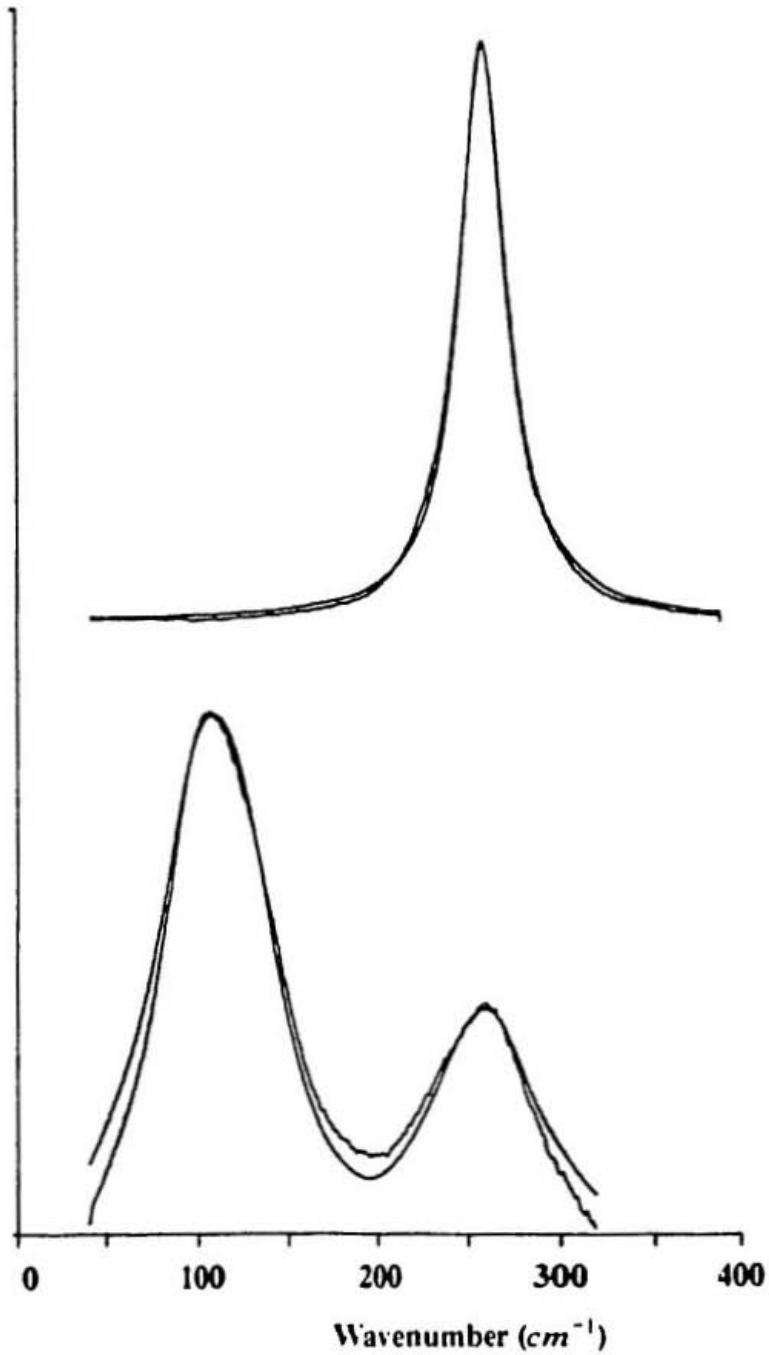

Fig. 7.6

Band resolution for the isotropic (top) and depolarized (bottom) spectra for the Cs_2CdCl_4 melt. The smooth line is the best fit curve calculated with a Lorentzian function for isotropic spectrum (top) and a product function for depolarized spectrum (bottom).

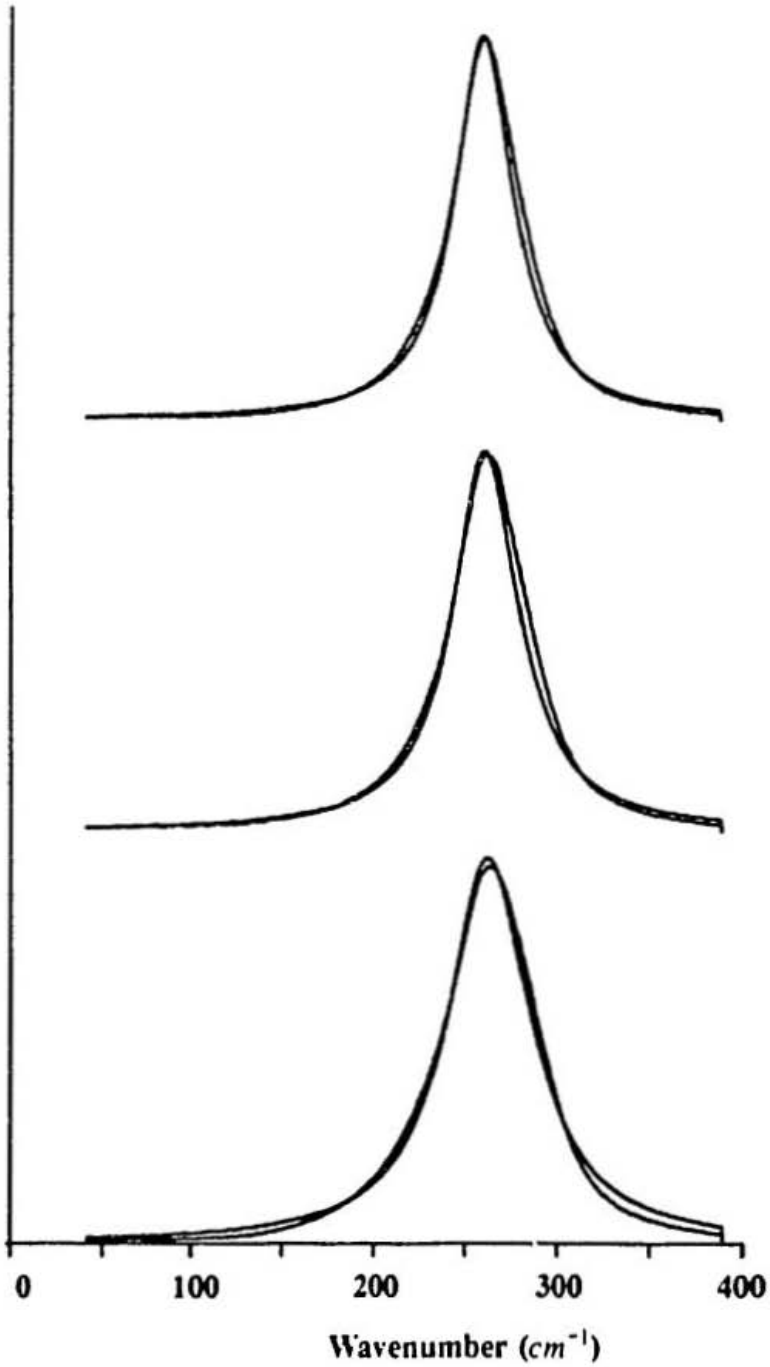

Fig. 7.7

Band resolution for the isotropic spectra of the $CdCl_2/CsCl$ melts with x = 0.60 (top), 0.56 (middle) and 0.50 (bottom). The smooth line is the best fit curve calculated with a Lorentzian function for each of the spectra.

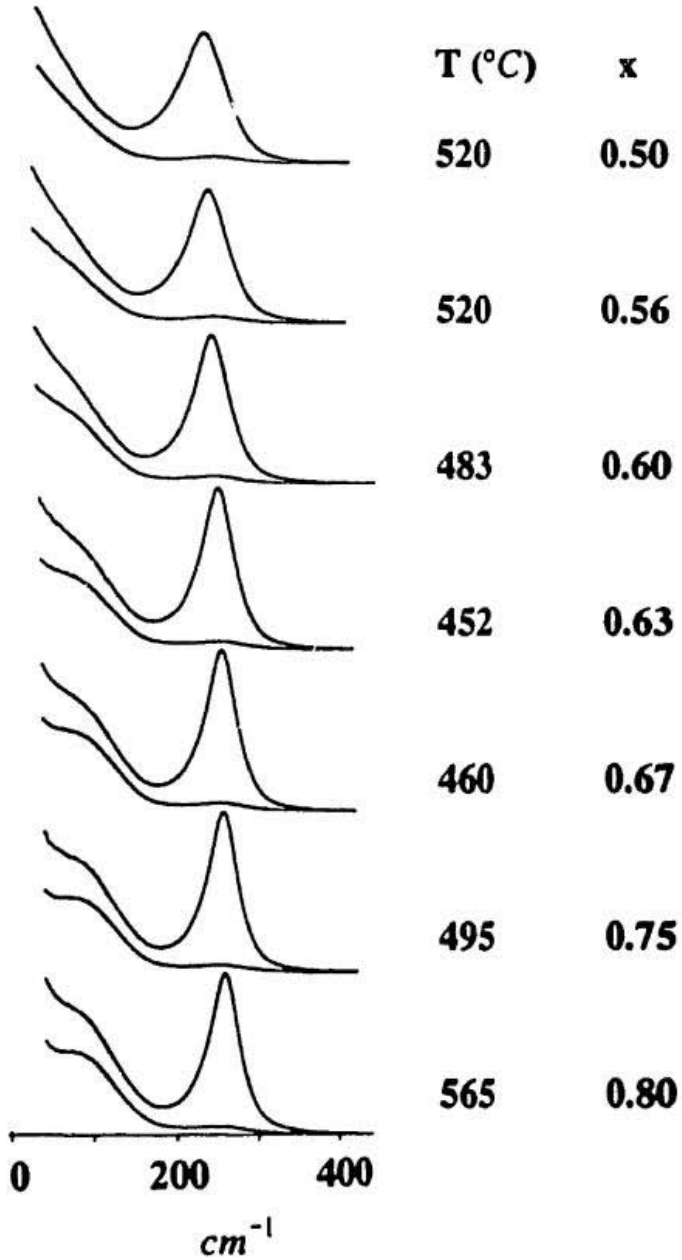

Fig. 7.8

$I(\nu)$ Raman spectra for the molten $CdCl_2/RbCl$ system. Slits 2 cm^{-1}. **x** - the mole fraction of $RbCl$; T - sample temperature.

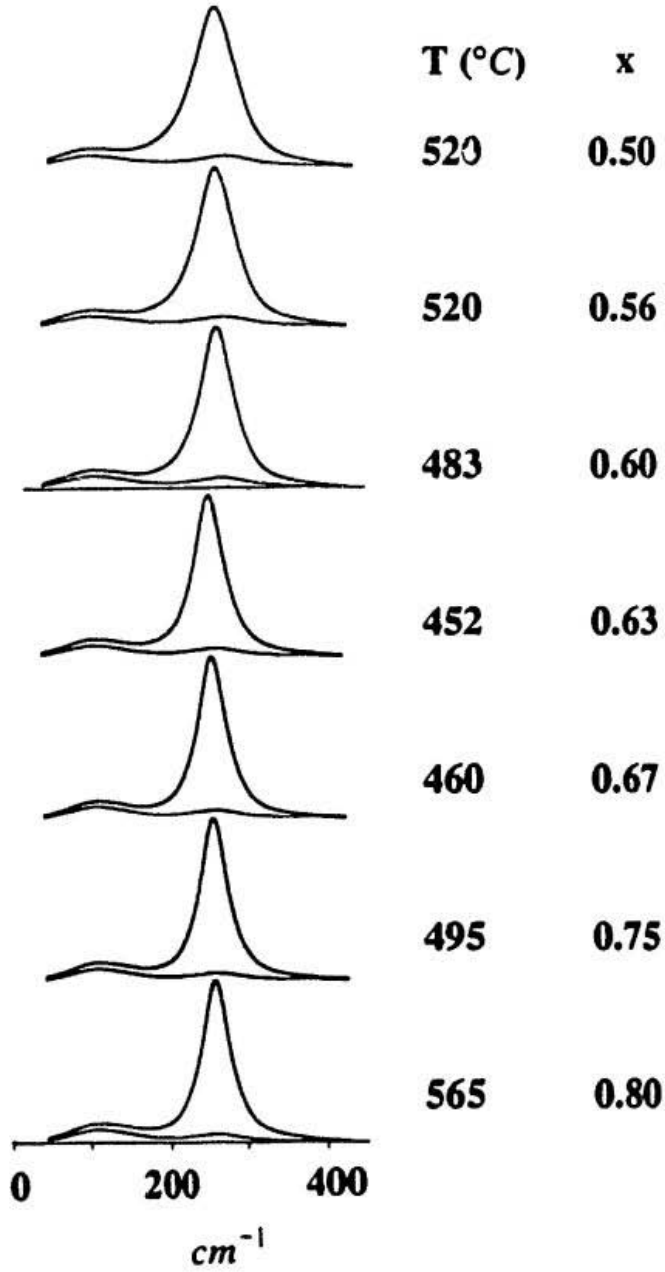

Fig. 7.9

$R(\nu)$ Raman spectra for the molten $CdCl_2/RbCl$ system. **X** - the mole fraction of $RbCl$; T - sample temperature.

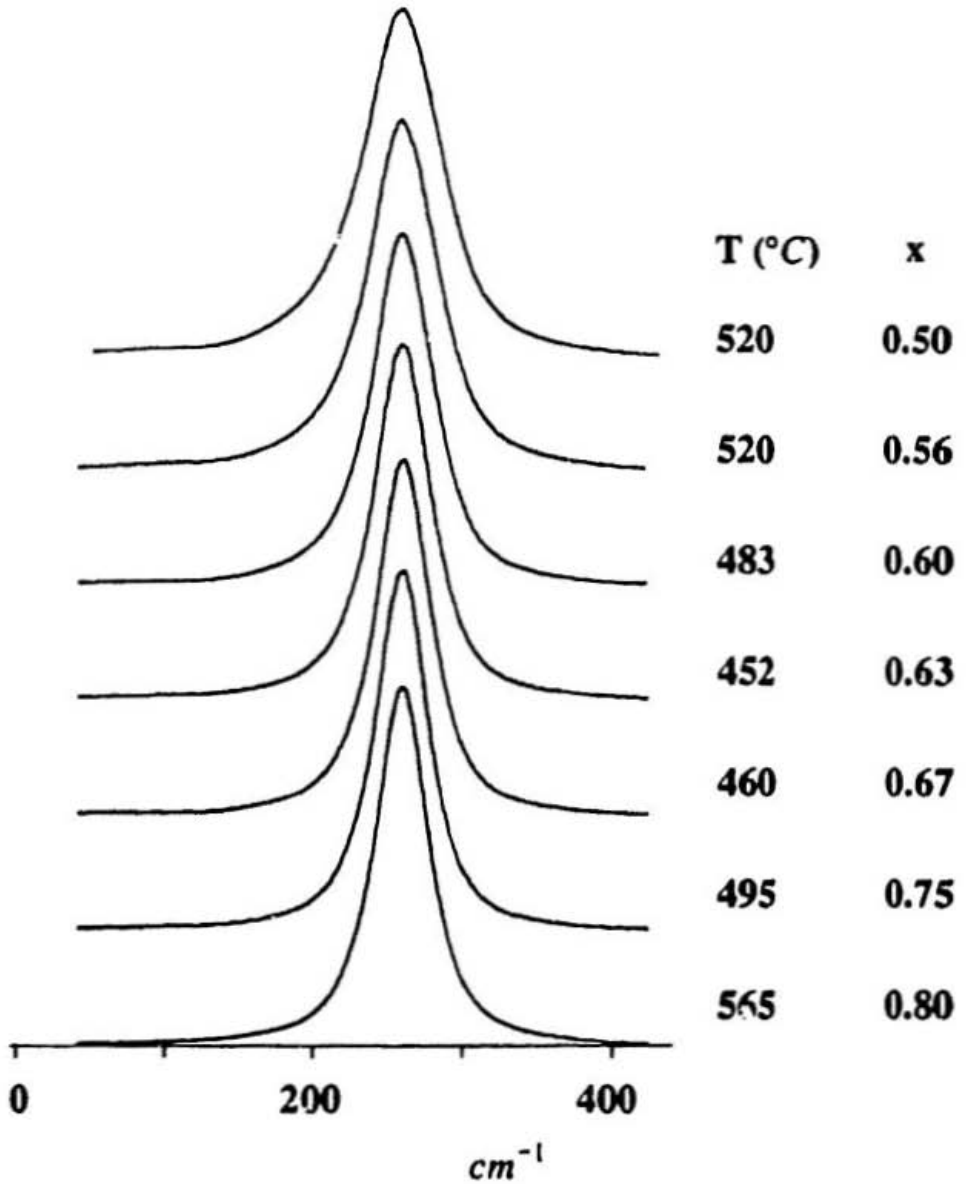

Fig. 7.10

Isotropic Raman spectra ($R_{\parallel}$ - 1.33 $R_{\perp}$) for the molten $CdCl_2/RbCl$ system. **X** - the mole fraction of $RbCl$; T - sample temperature.

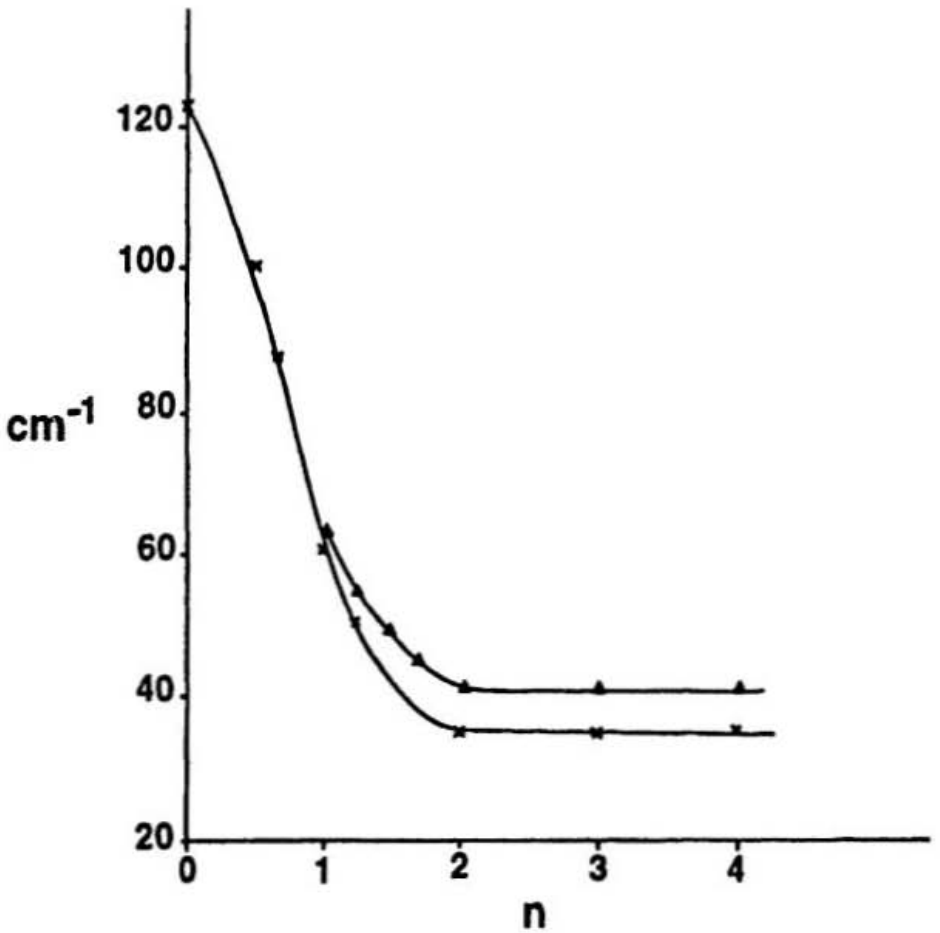

Fig. 7.11

Plots of FWHH vs. compositions for the $CdCl_2/CsCl$ (x line) and the $CdCl_2/RbCl$ (▲ line) molten systems. n = Cl^-/Cd^{2+}.

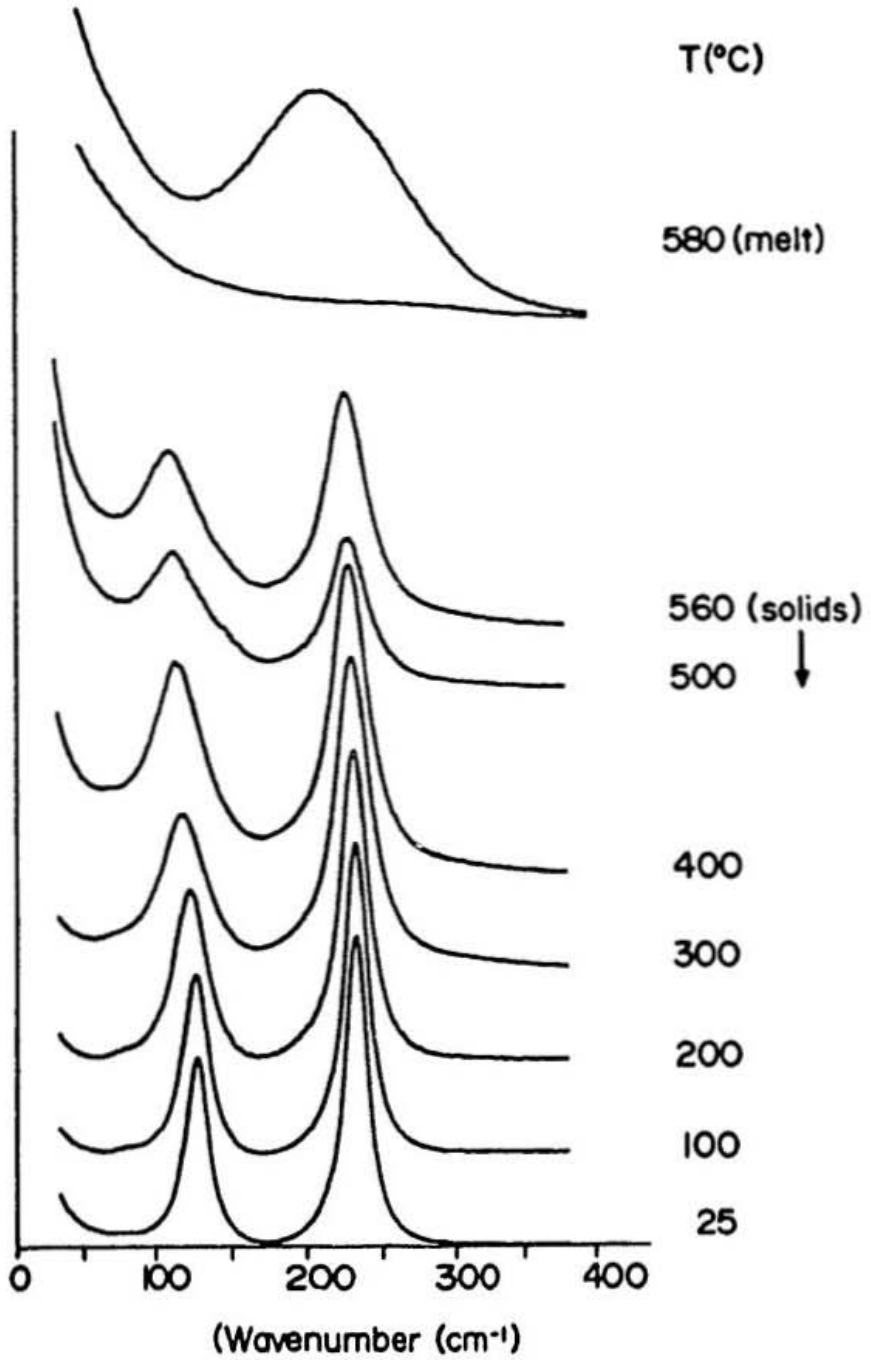

Fig. 7.12

Raman spectra, $I(\nu)$, for solid $CdCl_2$ at different temperatures at the temperatures as indicated. Slits 2 cm^{-1}.

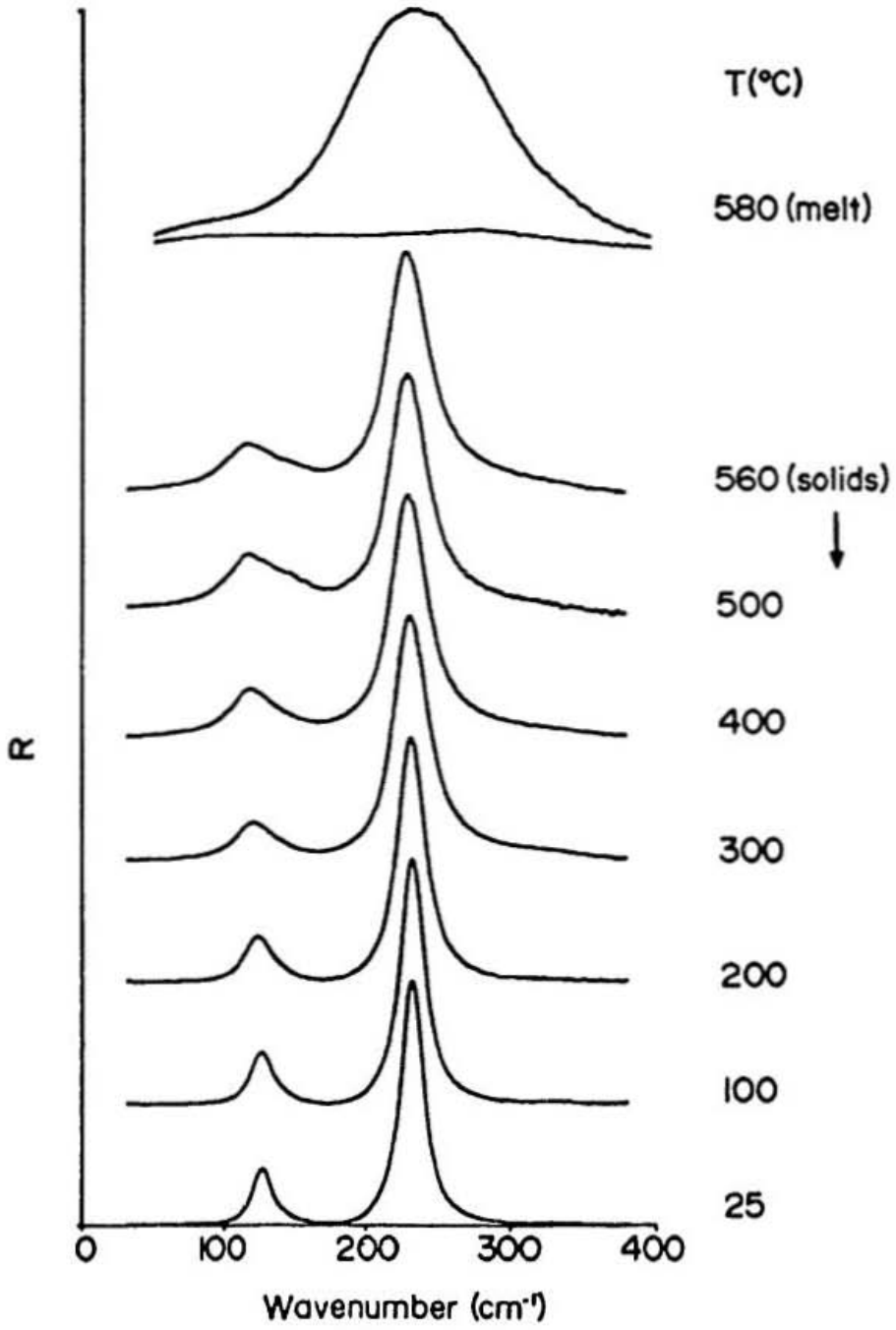

Fig. 7.13

Raman spectra, $R(\nu)$, for solid $CdCl_2$ at different temperatures at the temperatures as indicated. Slits 2 cm^{-1}.

Chapter 8

RAMAN STUDIES OF THE $PbCl_2$/CsCl SOLID SYSTEM

8.1 Introduction

In the previous chapters, Raman studies of the structural properties of cadmium chloride alkali metal chlorides have been discussed in detail. Lead chloride is an ionic crystal but has a special character of the electrical conductivity due only to the movement of chlorides [Mendes-Filho 1979]. From the point of view of the electrical conductivity lead chloride was considered as a typical anionic-conductor with transference number $t_+ = 0$, $t_- = 1$ and $t_e = 0$ for all temperatures up to the melting point at 510°C [Melo 1979]. The ionic motion was explained by the Schottky mechanism through the mobility of anion vacancies [De Vries 1963, Simkovich 1963, Mott 1957]. The Raman modes of $PbCl_2$ at room temperature were divided into two classes reflecting the special, different motions of the Pb^{2+} and Cl^- ions, one involving motions of the lead ions at frequencies below 100 cm^{-1}; and the other involving motions of the chloride ions corresponding to frequencies greater than 100 cm^{-1} [Ozin 1970].

In the solid state $PbCl_2$ exhibits a higher electrical conductivity [De Vries 1963, Simkovich 1963, Julião, 1973]. At room temperature the ionic conductivity of solid $PbCl_2$ is around 10^{-6} $ohm^{-1}cm^{-1}$. This is halfway, on the logarithmic scale, between the low ionic conductivity of solid NaCl at room temperature and the high conductivity of superionic conductors, e.g. $RbAg_4I_5$ [Mendes-Filho 1979].

However, in the molten state it was reported that the $PbCl_2$ melt has a different effect of pressure on the electrical conductivity compared to the $CdCl_2$ melt [Cleaver 1990]. The $PbCl_2$ melt was found to have a reduction of conductivity with pressure but, in an opposite way, the conductivity of the $CdCl_2$ melt increases with pressure.

The electrical conductivity is related to the number of the current-carrying ions in a

system, hence related to the inability to form stable complex ions in melts. It is interesting to compare the structures, and the kinetic and thermodynamic stability of the complex ions in both the solid and molten states for these two kind of MX_2 salts, $CdCl_2$ and $PbCl_2$.

Many previous studies have been performed on pure $PbCl_2$ [e.g. Ozin 1970, De Vries 1963, Simkovich 1963, Julião 1973, Mendes-Filho 1979, Oberschmidt 1980, Melo 1984, Zelezny 1988] and the lead chloride alkali metal chlorides molten systems [e.g. Balasubrahmanyam 1963, Maroni 1971]. The formation of the complex ions in the lead chloride alkali metal chloride melts has been suggested previously [e.g. Lantratov 1953, 1960; Yoshida 1973; Boardman 1949; Barton 1959; Balasubrahmanyam 1964], but relatively few studies have been reported on the lead chloride alkali metal chlorides solid systems [Oyamada 1974]. In this chapter the $PbCl_2$/CsCl solid systems with different compositions will be discussed.

8.2 Results and Discussion

8.2.1 Compound formation

A thermodynamic study suggested that three compounds, Cs_4PbCl_6, Cs_2PbCl_4 and $CsPbCl_3$, formed in the $PbCl_2$/CsCl binary system [Struktur 1952]. The phase diagram suggested by Struktur is presented in fig. 8.1. However an earlier phase equilibrium study gave a phase diagram with compounds of different compositions [Gromakov 1950].

The Raman spectra obtained from several samples with different compositions for $PbCl_2$/CsCl at room temperature are presented in fig 8.2 (mole fraction of CsCl, x, from 0.83 to 0.60) and fig 8.3 (x from 0.50 to 0). Two compounds, Cs_4PbCl_6 and $CsPbCl_3$, have been identified by the present Raman studies.

Cs_4PbCl_6:

Raman spectra for samples with x = 0.83 and 0.80 are essentially identical (fig. 8.2). The characteristic Raman spectra suggest the formation of a compound Cs_4PbCl_6. An intense band centered at about 201 cm^{-1} at room temperature was observed in the Pb-Cl symmetrical vibrational region of the Raman spectrum of Cs_4PbCl_6 characteristic of a discrete octahedral $PbCl_6^{4-}$ species.

Cs_4PbCl_6 is an incongruent compound. The peritectic reaction was suggested to be [Struktur 1952]:

$$Cs_4PbCl_{6(s)} = CsCl_{(s)} + liquid$$

Compared to K_4CdCl_6 and Rb_4CdCl_6, the peritectic reaction of Cs_4PbCl_6 is much faster. The preparation of this compound is relative easy. In principle, the sample with composition x = 0.80 quenched from the melt to room temperature should give a mixture of compounds Cs_4PbCl_6, $CsPbCl_3$ and CsCl. Since $CsPbCl_3$ was found to have a poly-domain structure [Hidaka 1983], no characteristic Raman bands in the Pb-Cl symmetric stretching region and no intense peaks in the external, low frequency region were observed in

the present study. CsCl gave only weak second order scattering in the 150 cm^{-1} region. Therefore both the fast and slowly cooled x = 0.80 samples gave similar Raman spectra.

$CsPbCl_3$:

Similar Raman spectra were observed for the samples with composition 0.50 < x < 0.80 (fig. 8.2). The relative intensity (relative to the Rayleigh background scattering at low frequencies) of the characteristic bands due to the octahedral $PbCl_6^{4-}$ species decreased with the decrease of the mole fraction of CsCl (fig. 8.2). At x = 0.50 the characteristic bands due to $PbCl_6^{4-}$ disappeared completely (fig. 8.3) and only a weak peak at about 57 cm^{-1} and a broad band at 113 cm^{-1} were detected and attributed to $CsPbCl_3$. No intense bands were observed in the Pb-Cl symmetric vibration region for the x = 0.50 sample (fig. 8.3). When the composition of CsCl further decreased, a set of the bands due to pure $PbCl_2$ appeared. The relative intensity of the bands due to $PbCl_2$ increased with the decrease of x. These results suggest the formation of the compound $CsPbCl_3$ with only two weak Raman bands at room temperature. No other compounds were identified in the $PbCl_2$ rich samples.

$CsPbCl_3$ was found to be a congruent compound. Both the fast and slowly cooled x = 0.50 samples gave similar Raman spectra. The result is in good agreement with Struktur's work [Struktur 1952].

The compound Cs_2PbCl_4 suggested by Struktur [Struktur 1952] was not identified in the present Raman studies. The spectrum of a sample with the composition x = 0.67 suggests that this sample is a mixture of the compounds Cs_4PbCl_6 and $CsPbCl_3$ (fig. 8.2, x = 0.67).

8.2.2 Structures and Properties

8.2.2.1 Cs_4PbCl_6

An early X-ray study [Ducloux 1924] reported that Cs_4PbCl_6 is isostructural with K_4CdCl_6, space group $R\bar{3}c$ (D^6_{3d}): a = 13.187 and c = 16.641 Å; z = 6. Discrete octahedral $PbCl_6^{4-}$ species were proposed. However another X-Ray measurement [Petrov 1987] indicated that Cs_4PbCl_6 is monoclinic, space group B2/b with a 13.449, b 9.417, c 13.181 Å, and γ 91.61° . The Pb atom was found to be octahedrally coordinated to six Cl atoms to form a discrete octahedral $PbCl_6^{4-}$ species.

Raman spectra of solid Cs_4PbCl_6 at 77K (fig. 8.4a) and at room temperature (fig. 8.4b) are presented. The peak positions of the bands are listed in table 8.1. The characteristic Raman spectra suggest that Cs_4PbCl_6 contains discrete octahedral $PbCl_6^{4-}$ species. The ν_1 mode, totally symmetric Pb-Cl vibration, appeared at about 201 cm^{-1} at room temperature and at about 202 cm^{-1} at 77K. Broad bands centered at 98 and 116 cm^{-1} were attributed to the ν_5 and ν_2 modes respectively. At 77K the corresponding broad bands resolved into six peaks at 83, 93, 100.5, 108, 119.5 and 131.5 cm^{-1} respectively.

The octahedral $PbCl_6^{4-}$ species appeared to be present in solid Cs_4PbCl_6 at all temperatures. The Raman spectra obtained from Cs_4PbCl_6 over a wide temperature range from 25°C to above the melting point are presented in fig. 8.5. The solid sample at different temperatures gave similar spectra which indicate that there is no structural phase transition within this temperature range.

Usually a peak shifts to a lower frequency with an increase of temperature in the absence of a structural phase transition. An interesting result of the present study is the fact that the ν_1 mode of the Pb-Cl stretching vibration of the $PbCl_6^{4-}$ species shifted slightly to higher frequencies at higher temperatures. The center frequencies at corresponding temperatures were found to be:

T(°C)	25	100	200	300	350	400	450	500
ν_1 (cm^{-1})	201	201	201.5	201.5	202	202.5	204	207

In the molten state, this peak shifted abruptly to about 236 cm^{-1} at 560°C. The large shift of the ν_1 frequency from the solid to the melt suggests a change of the coordination structure of the complex ion. Discrete tetrahedral $PbCl_4^{2-}$ species were found to be present in the molten samples with $x \geq 0.67$. The Raman spectra of the $PbCl_2$/CsCl molten systems with different compositions will be discussed in chapter 9.

8.2.2.2 $CsPbCl_3$

Room temperature

At room temperature, the structure of $CsPbCl_3$ has orthorhombic symmetry, space group Pbnm (D_{2h}^{16}) [Hidaka 1983]. It was reported that $CsPbCl_3$ has a poly-domain structure caused by the antiferrodistorted transitions. The distribution of the domains was found to be strongly dependent on the size of the sample and on the cooling or heating rate when the transitional temperature is surpassed [Hidaka 1983].

The Raman spectrum obtained from $CsPbCl_3$ at room temperature is presented in fig. 8.4d. No intense bands in the Pb-Cl symmetric stretching region but two broad weak bands at about 57 and 113 cm^{-1} were observed. A weak peak at 36 cm^{-1} was due to a plasma line. The characteristic spectrum suggests a disordered poly-domain structure.

A previous Raman measurement was performed in a temperature range from -165°C to 25°C [Hirotsu 1971]. Two broad bands centered at about 60 and 117 cm^{-1} were observed at room temperature. There were no more peaks observed up to 600 cm^{-1} at 25°C. The present Raman study is in agreement with Hirotsu's work.

Below room temperature

Below room temperature, EPR measurements [Cape 1969, Cohen 1971] indicated that a structural phase transition took place at about 190K. The X-ray, neutron diffraction, NQR and Raman scattering measurements confirmed that a second-order transition occurred at about 200K [Hidaka 1983]. It was reported that below 200K $CsPbCl_3$ has monoclinic symmetry, space group $P2_1/c$ (C_{2h}^5) [Hidaka 1983]. But Raman studies performed by Hirotsu [Hirotsu 1971] over a temperature range from -165°C to 25°C suggested that no phase transitions occurred in $CsPbCl_3$ below room temperature.

The Raman spectrum obtained from $CsPbCl_3$ at 77K is presented in fig. 8.4c. The peak frequencies are listed in table 8.1. The Raman spectrum is consistent with Hirotsu's result obtained at 108K [Hirotsu 1971] (table 8.1) and with Hidaka's result obtained at 113K [Hidaka 1983] in the low frequency region. Four more weak peaks at about 150.5, 162, 185.5 and 200 cm^{-1} were observed in the present study. In the present study it was not possible to study the sample over a temperature range from 77 to 300K to investigate possible phase transitions. However the fact that the Raman spectrum for $CsPbCl_3$ at 77K is so different from that at 298K suggests a significant structural change.

Above room temperature

Many previous studies (NQR, elastic, optical, X-ray, neutron diffraction, Raman, EPR and theoretical) have been performed on solid $CsPbCl_3$ above room temperature. It was reported that $CsPbCl_3$ undergoes three phase transitions occurring at 37, 42 and 47°C [e.g. MΦller 1957, 1959, 1960; Sakudo 1969; Natarajan 1971; Hirotsu 1970, 1971; Fujii 1974; Aleksandrov 1976; Cohen 1971; Imaoka 1972; Harada 1976; Sakata 1978; Chabin 1980a, 1980b].

Temperature dependent Raman spectra obtained from $CsPbCl_3$ above room temperature are presented in fig. 8.6. Almost identical spectra were observed at room temperature and at 35°C (fig. 8.6). The broad band at about 113 cm^{-1} at room temperature shifted slightly to 112 cm^{-1} at 35°C. When the temperature increased to 50°C, another broad,

high frequency band appeared at about 136 cm^{-1} (fig. 8.6). This result indicates that $CsPbCl_3$ has a different crystal structure at room temperature and above 50°C. Because there were no intense characteristic bands in the Pb-Cl symmetric stretching region and the peak intensities of the lattice modes were very weak, the present Raman measurements could not give information about the possible individual structural phase transitions at 37, 42 and 47°C respectively.

For the molten salt at 630°C, an intense polarized band at about 241 cm^{-1}, a broad depolarized band at 100-120 cm^{-1} and a depolarized band on the low frequency shoulder of the intense polarized band appeared in the spectrum. The result suggests the formation of a complex ion in the molten state. The structure of the complex ion will be discussed in detail in chapter 9.

8.2.2.3 $PbCl_2$

Lead chloride is orthorhombic with four formula units in the primitive cell [Wyckoff 1965c]; space group Pnma (D_{2h}^{16}). Factor group analysis based on the D_{2h} group predicts 36 normal modes [Mendes-Filho 1979] with the distribution as follows:

$$\Gamma_{tot} = 6A_g + 6B_{1g} + 3B_{2g} + 3B_{3g} + 3A_u + 3B_{1u} + 6B_{2u} + 6B_{3u}.$$

The 18 Raman active modes are:

$$\Gamma_{Raman} = 6A_g + 6B_{1g} + 3B_{2g} + 3B_{3g}.$$

Raman measurements have been performed previously on the single crystals of $PbCl_2$ [Isupova 1968, Ozin 1970, Willensen 1971, Sadoc 1971, Mendes-Filho 1979, Melo 1979]. Detailed spectra in all polarizations and the assignments (table 8.2) for the 18 Raman modes were reported.

The Raman spectrum of a powder sample of $PbCl_2$ has been obtained at 77K in the present study (fig. 8.7 and 8.8). The peak frequencies are listed in table 8.2. The results are in excellent agreement with previous Raman studies obtained from the single crystals of $PbCl_2$ although some peaks overlapped to form broad bands in the present study.

Raman spectra of the powder sample of $PbCl_2$ over a temperature range from 77K to above the melting point are presented in figs. 8.7 and 8.8 (reduced Raman spectra).

The effect of temperature on the bandwidths is different for the two classes of the Raman modes, i.e. frequencies below 100 cm^{-1} due to motions of the Pb^{2+} ions and frequencies above 100 cm^{-1} due to motions of the Cl^- ions [Ozin 1970]. The widths of the bands with frequencies higher than 100 cm^{-1} were broadened more rapidly than those of the bands with frequencies lower than 100 cm^{-1} with the increase of the temperature. The result can be observed clearly in the reduced Raman spectra (fig. 8.8).

The peak frequencies decreased slightly with the increase of the temperature below the melting point. In the melt at 521°C (melting point 501°C) the frequency of the most intense band increased sharply to 210 cm^{-1} (figs. 8.7 and 8.8) due to the formation of the shorted-lived, bridge $PbCl_4^{2-}$ units (the spectrum of the melt will be discussed in chapter 9).

Table 8.1

The Raman frequencies (cm^{-1}) of solids Cs_4PbCl_6 and $CsPbCl_3$ at several temperatures.

Cs_4PbCl_6			$CsPbCl_3$			
77K	298K		77K	108K [a]	293K [a]	298K
40 (vw)[b]			33(w)	41	60(vw)	57(vw)
67(w)			41.5(w)	46	117(br)	113(br)
83(w)			50(w)	56		
93(w)	98(br)	ν_5	69.5(s)	77		
100.5(m)			87(s)	94		
108(vw)			108(s)	115		
119.5(s)	116(s)	ν_2	118.5(s)	125		
131.5(m)			150.5(w)			
168.5(br)			162(w)			
202(s)	201(s)	ν_1	185.5(w)			
			200(w)			

a - Ref. [Hirotsu 1971].

b vw - very weak; w - weak; m - medium; s - strong; br - broad.

Table 8.2

The Raman frequencies (cm^{-1}) of solid $PbCl_2$

a	b	c	d	this work	assignments
86	27	23	25	22	B_{1g}
35?	32	28	28	29	B_{2g}
18	38	36	36	40.5	A_g
26	27?	37	43		B_{1g}
35	60	56	62	63	A_g
100?		85	88	89	B_{1g}
156	62	61	107	108	A_g
126	131		124	125	B_{1g}
156?	127	123	132	132(br)[e]	B_{3g}
86	133	129	133		B_{2g}
	148	143	148	150.5(br)	A_g
	159	159	160	161(br)	B_{1g}
	160	158	162		A_g
	182	179	181	182(br)	A_g
		175	181		B_{3g}
		177	183		B_{1g}
134	179	180	184		B_{2g}
			194		B_{1g}

a - Ref. [Ozin 1970]

b - Ref. [Willensen 1971]

c - Ref. [Sadoc 1971]

d - Ref. [Mendes-Filho 1979]

e - br - Broad

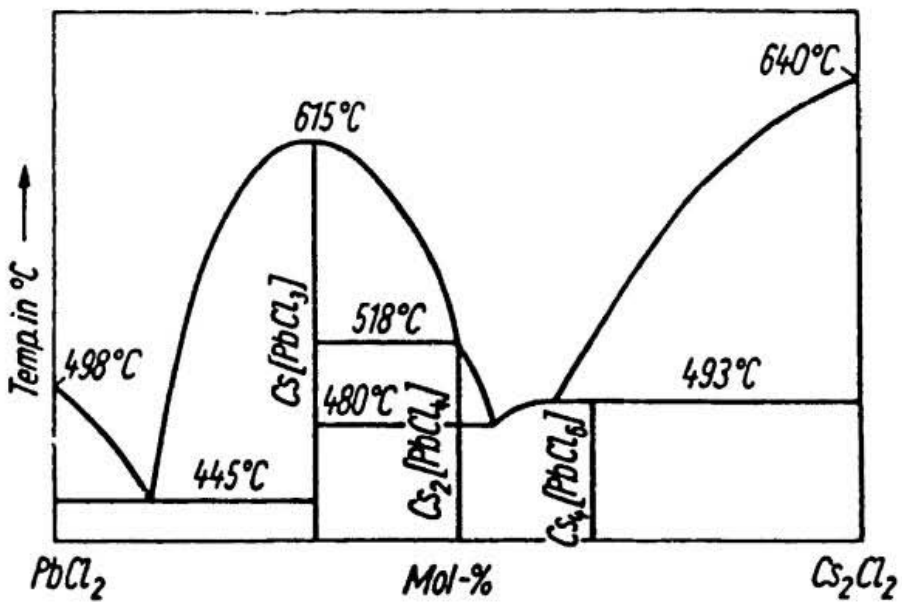

Fig. 8.1

The phase diagram of the $PbCl_2$/CsCl binary system. Copied from Ref. [Struktur 1952].

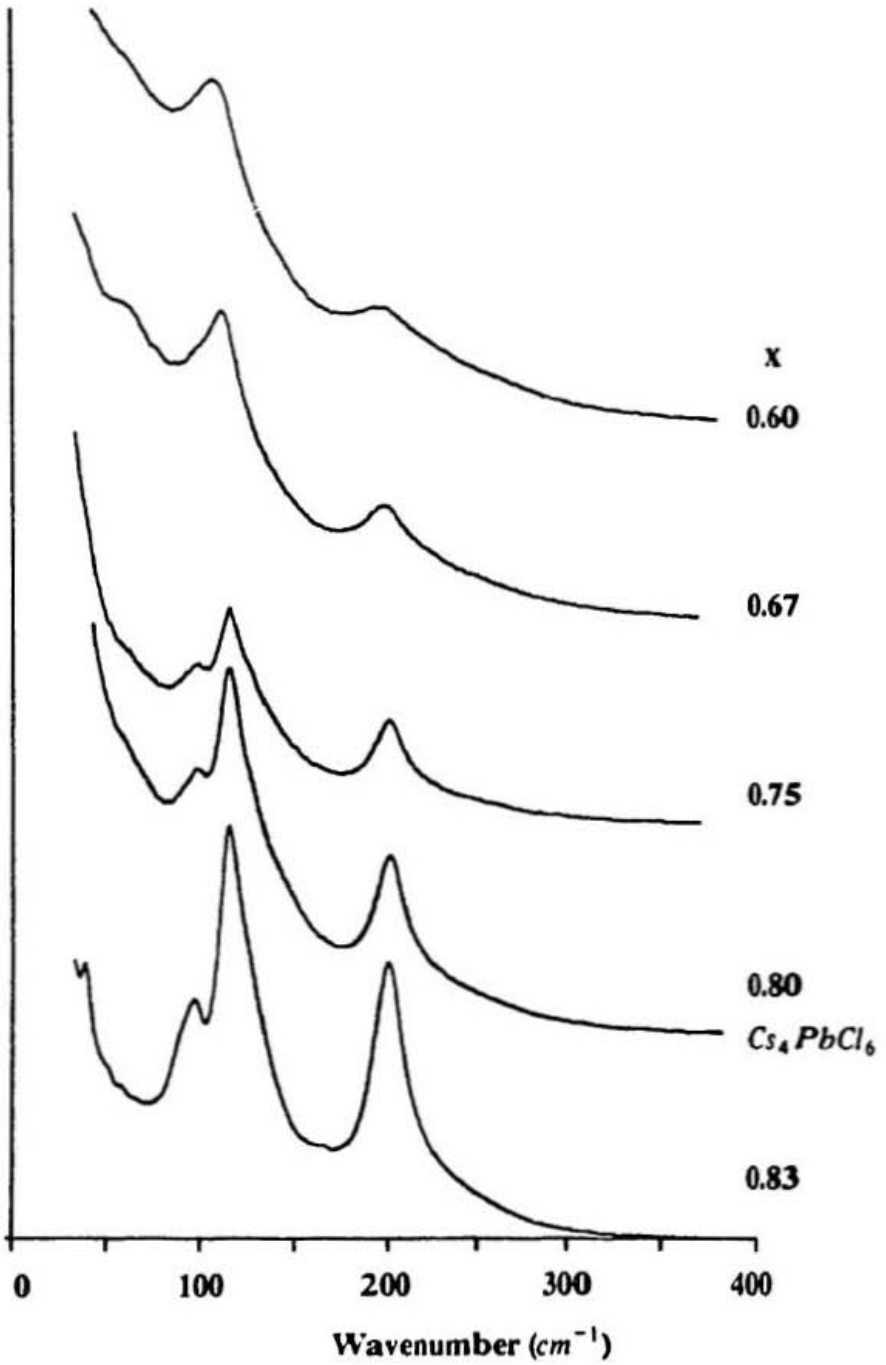

Fig. 8.2

The Raman spectra observed for the $PbCl_2/CsCl$ solid systems with x from 0.83 to 0.60. **x** - the mole fraction of CsCl. 25°C.

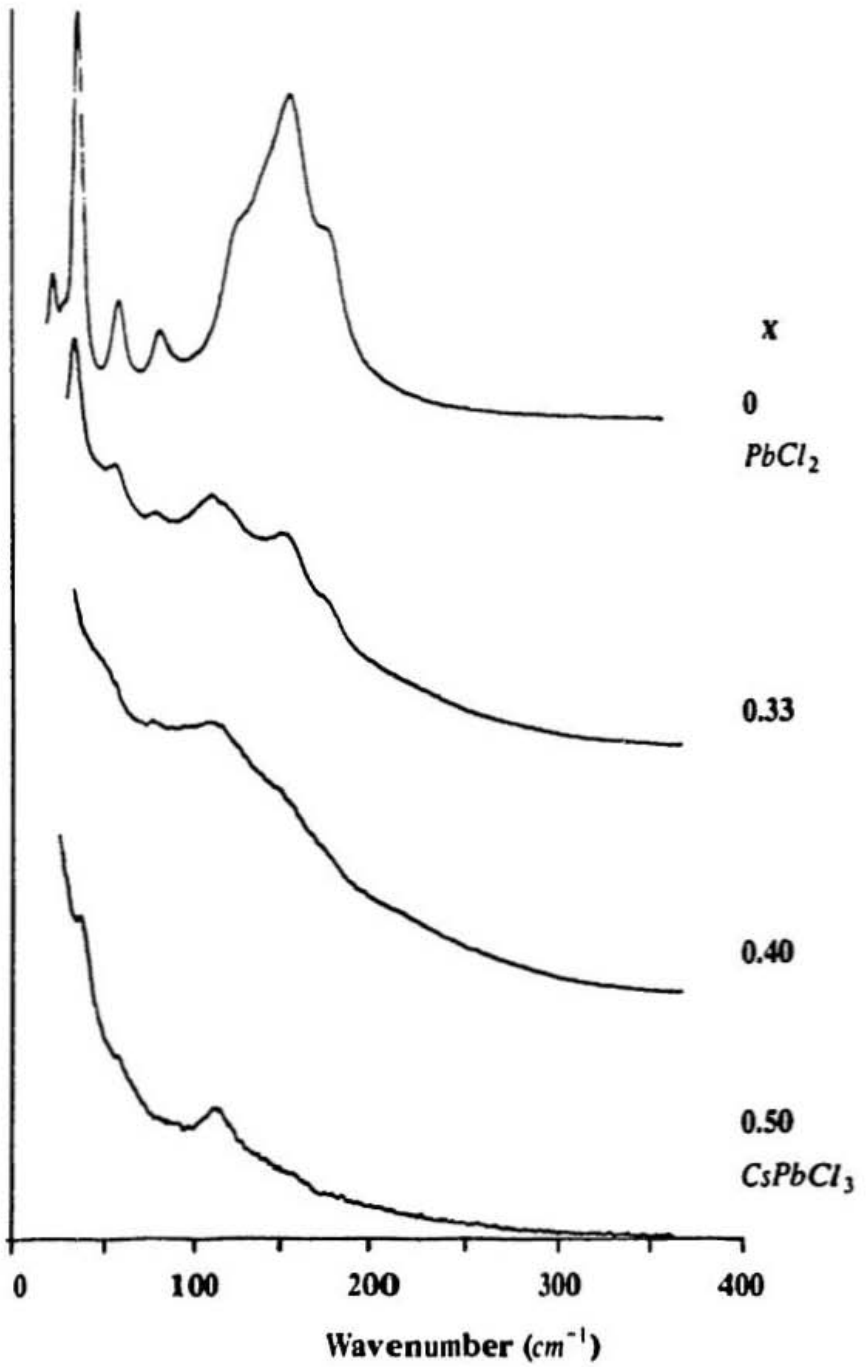

Fig. 8.3

The Raman spectra observed for the $PbCl_2/CsCl$ solid systems with x from 0.50 to 0. X - the mole fraction of CsCl. 25°C.

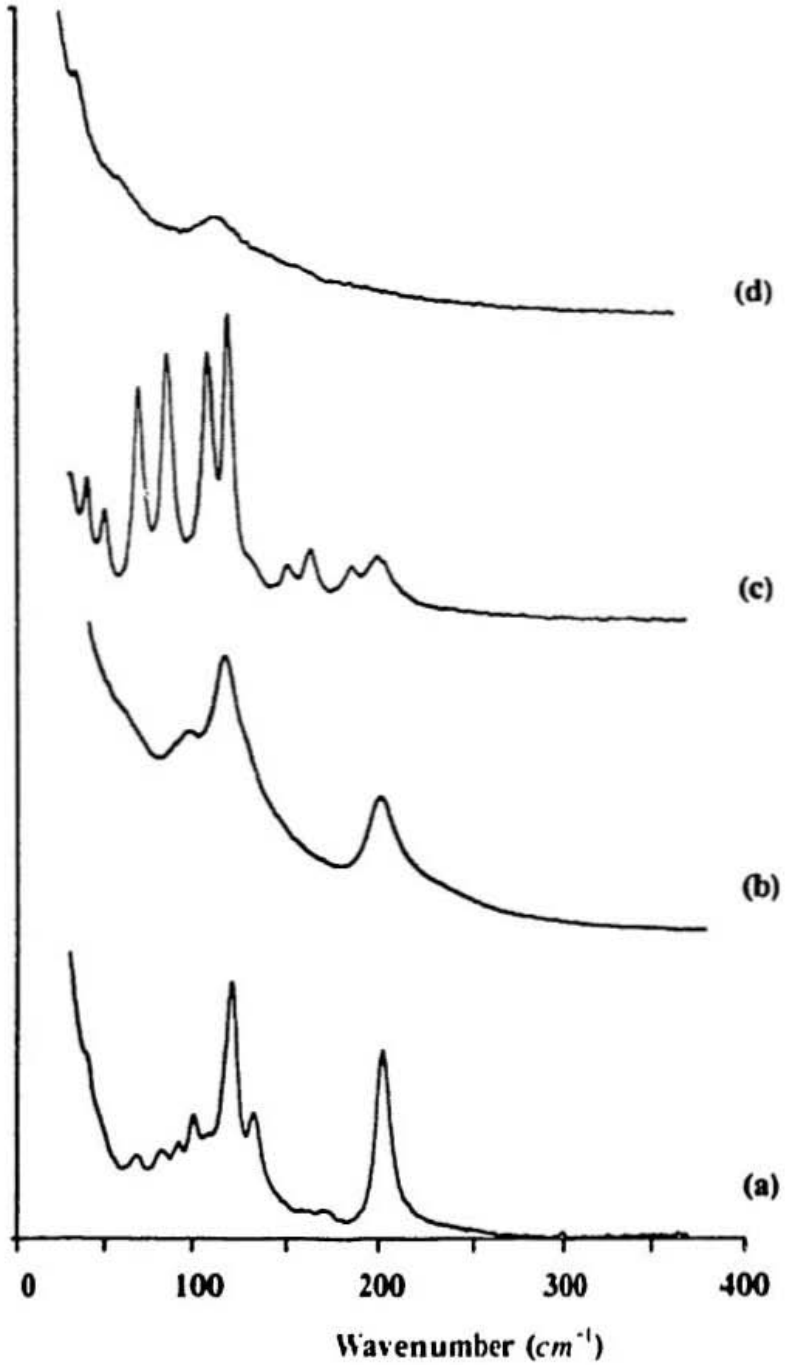

Fig. 8.4

Raman spectra of the compounds Cs_4PbCl_6 and $CsPbCl_3$ at room temperature and 77K. (a): Cs_4PbCl_6 77K; (b): Cs_4PbCl_6 298K; (c): $CsPbCl_3$ 77K; (d) $CsPbCl_3$ 298K.

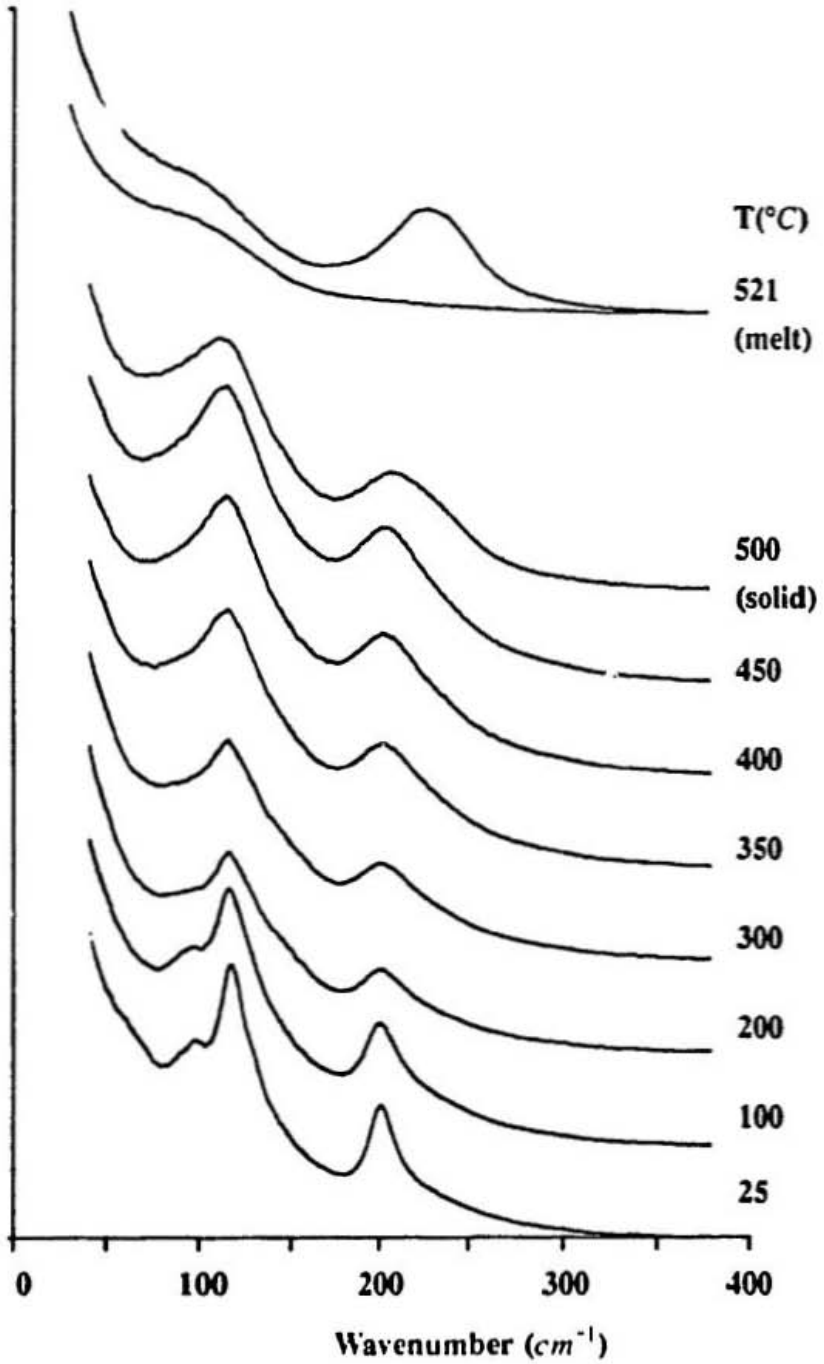

Fig. 8.5

Raman spectra of Cs_4PbCl_6 at different temperatures at the temperatures as indicated.

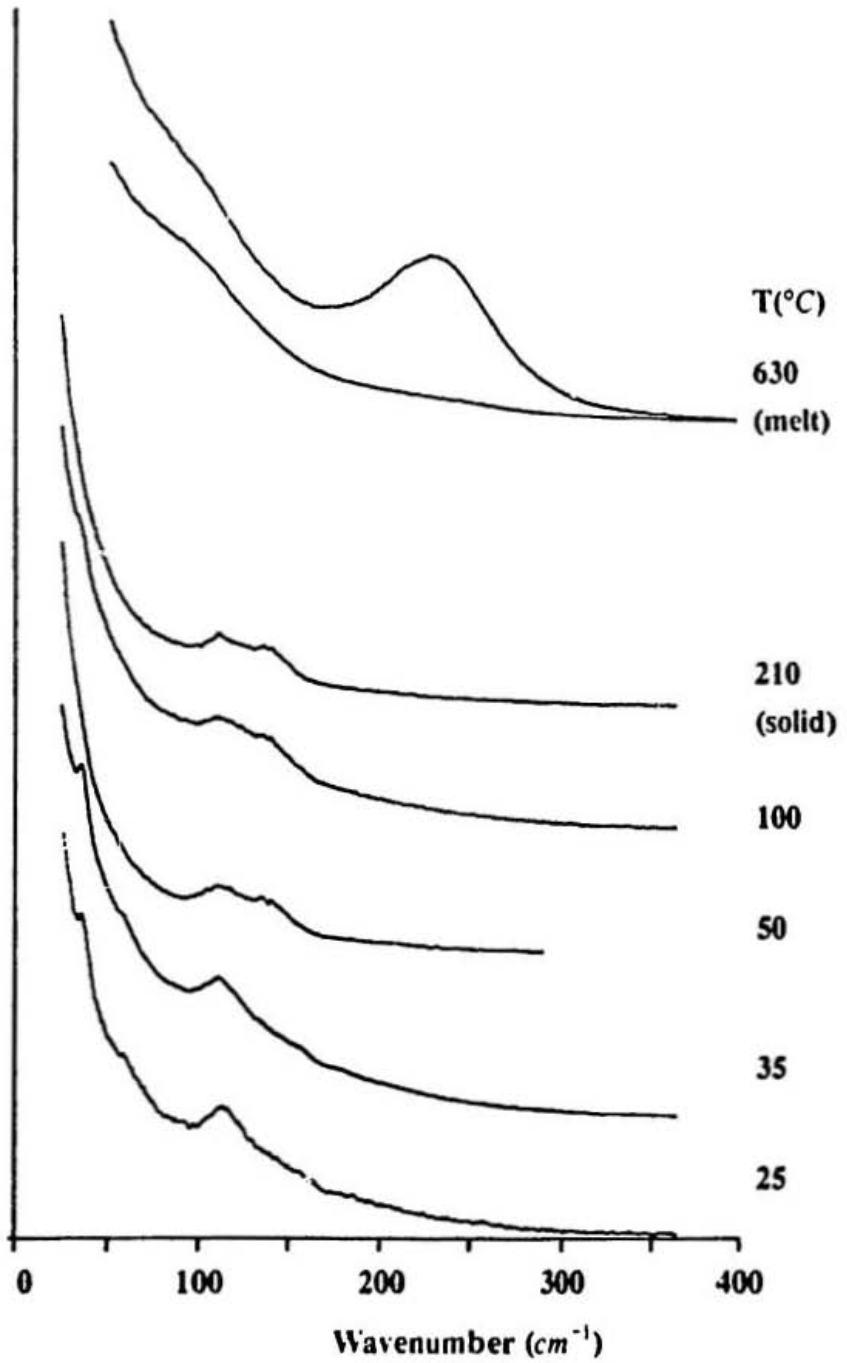

Fig. 8.6

Raman spectra of $CsPbCl_3$ at different temperatures at the temperatures as indicated. Green line (514.5 nm) of Argon ion laser was used.

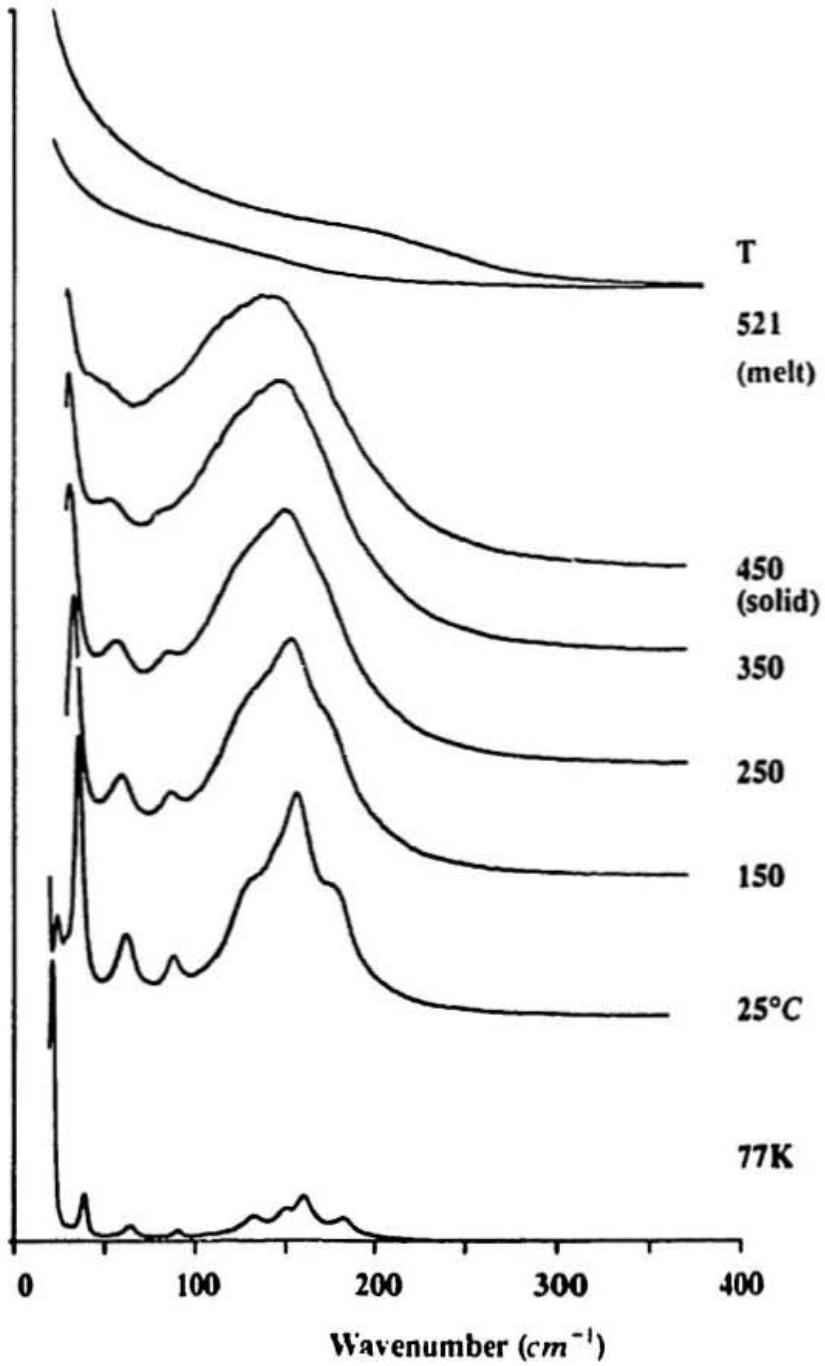

Fig. 8.7

Raman spectra, $I(\nu)$, of $PbCl_2$ at different temperatures at the temperatures as indicated.

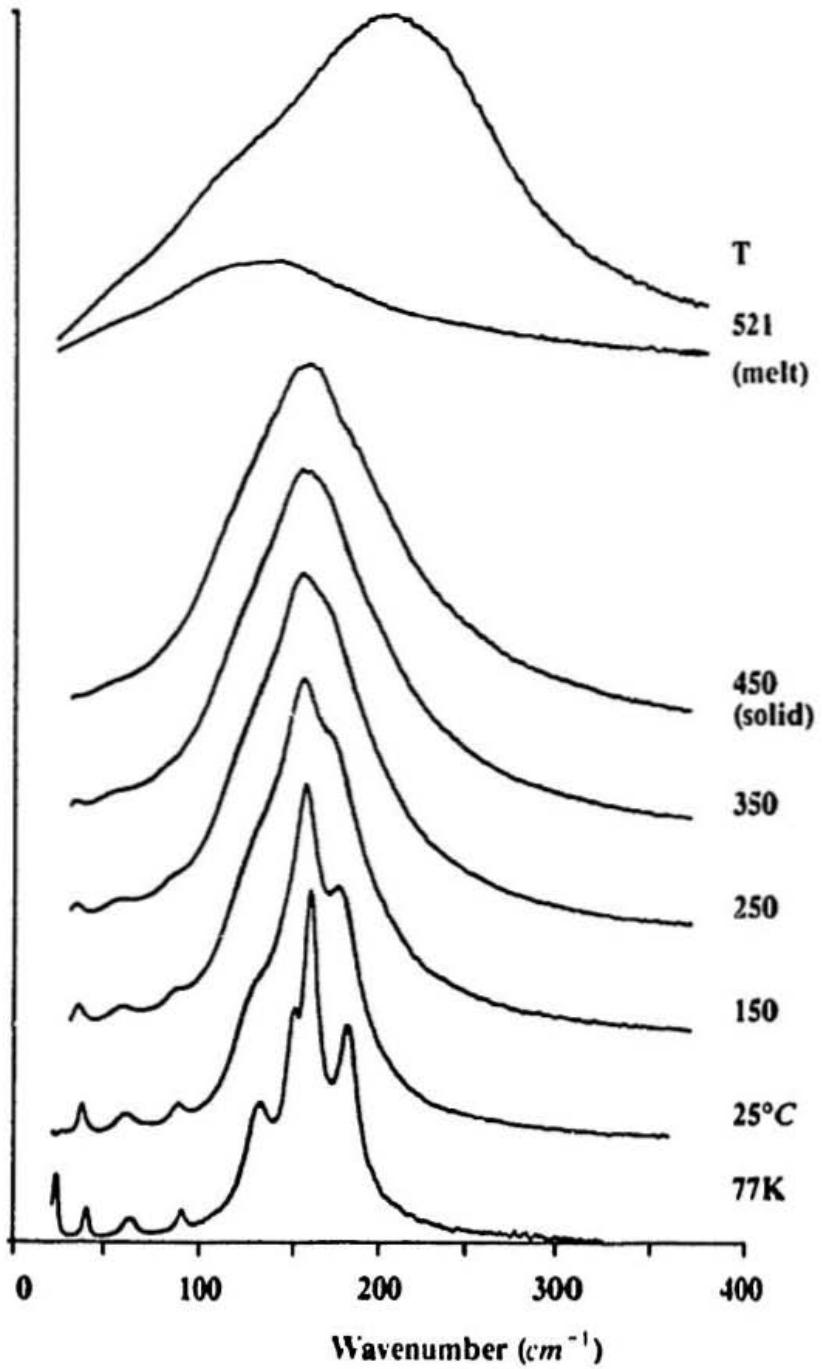

Fig. 8.8

Raman spectra, $R(\nu)$, of $PbCl_2$ at different temperatures at the temperatures as indicated.

Chapter 9

RAMAN STUDIES OF THE $PbCl_2$/CsCl MOLTEN SYSTEM

9.1 Introduction

For the MX_2/AX (A, alkali ions; X, halides) molten systems, the vibrational spectra obtained from the mixtures rich in AX have been normally interpreted in terms of "complex-ion species". The most commonly discussed species is the MX_4^{2-} tetrahedral complex. In the $CdCl_2$/CsCl and $CdCl_2$/RbCl melts, discrete $CdCl_4^{2-}$ species exist in the $x \geq 0.67$ melts, even tetrahedral local structures have been suggested to be present in the $CdCl_2$ rich melts and pure $CdCl_2$ melt [Takagi 1989] as discussed in chapter 7.

Lead chloride is an ionic crystal with high ionic conductivity arising from the mobility of the chloride ions [Oberschmidt 1980]. It was reported that the conductivity data exhibited two activated regions and an anomalous rise at about 765K before melting.

Electrical conductivity measurements as a function of pressure on the $PbCl_2$ and $CdCl_2$ melts have been performed recently [Cleaver 1990]. The conductivity of the $CdCl_2$ melt was found to increase with pressure. The predominant effect of pressure was suggested to cause dissociation of molecule $CdCl_2$ or complex ions. In contrast, the $PbCl_2$ melt showed a reduction of conductivity with pressure. The main effect of pressure was suggested to reduce the mobility of the ions in the $PbCl_2$ melt. It seems that it is interesting to study the structures of these two kind of melts with different effects of the pressure on the conductivity.

Previous Raman studies indicated that the molten lead chloride did not exhibit any Raman bands [Balasubrahmanyam 1963, Maroni 1971], while additions of alkali metal chlorides (e.g. KCl) to the $PbCl_2$ melt a single polarized band was observed in the region from 200 - 240 cm^{-1} [Maroni 1971]. Raman studies by Balasubrahmanyam et al. [Balasubrahmanyam 1963] suggested the existence of the $PbCl_3^-$ species with pyramidal

structure (C_{3v}) in the $2PbCl_2$-KCl and $PbCl_2$-KCl melts and a distorted tetrahedral structure for the $PbCl_4^{2-}$ ion in $PbCl_2$-2KCl. In 1974, Raman measurement by Oyamada [Oyamada 1974] suggested a $PbCl_3^-$ ion-like local structure in the molten state and a chain structure of the $PbCl_3^-$ ions due to the addition of KCl. In $PbCl_2$-Cl^- aqueous solutions, spectroscopic measurements did not permit positive identification of $PbCl_3^-$ and $PbCl_4^{2-}$, but the spectra [Haight 1965] observed from $PbCl_2$ in 10 and 11 M hydrochloric acid suggested that there existed $PbCl_6^{4-}$ species by analogy with observations on $BiCl_6^{3-}$ spectra [Haight 1964]. It seems that Pb^{2+} may have weaker ability than Cd^{2+} to form a complex ion with the Cl^- ion [Haight 1965]. Most previous studies suggested the $PbCl_3^-$ complex in the $PbCl_2/ACl$ molten mixtures [Balasubrahmanyam 1963, Maroni 1971, Oyamada 1974].

In the present study Raman measurements have been performed on the $PbCl_2$/CsCl molten systems with a wide range of concentrations of the CsCl in order to analyze the coordination properties of the Pb^{2+} ion. The reduced spectrum is especially useful in this case because of the strong Rayleigh background scattering.

9.2 Results and Discussion

The polarized and depolarized spectra obtained from the molten $PbCl_2/CsCl$ mixtures and pure $PbCl_2$ melt are presented in fig. 9.1. The reduced $R(\nu)$ spectra are presented in fig. 9.2 and the isotropic spectra based on the polarized and depolarized reduced spectra ($R_{\parallel}$ - 1.33 $R_{\perp}$) in fig. 9.3. The center frequencies and the full width at half height (FWHH) of the bands based on the isotropic spectra and corresponding compositions of the melts are listed in table 9.1.

9.2.1 x ≥ 0.67 systems

The melts with compositions x ≥ 0.67 gave almost identical Raman spectra (figs. 9.1-9.3). For the x = 0.75, 0.80 and 0.83 samples, an intense polarized band at about 236 cm^{-1}, a broad depolarized band at about 110-120 cm^{-1} and a depolarized band in the low frequency shoulder (~ 220 cm^{-1}) of the intense polarized band were observed. The spectrum of the x = 0.67 sample was found to be similar to those of the x = 0.75, 0.80 and 0.83 samples. The peak position of the intense band for the x = 0.67 sample slightly shifted from 236 to 237 cm^{-1}. But for the x = 0.60 sample a relative large shift of the frequency of the corresponding band (from 236 to 240 cm^{-1}) was observed.

Similar results were obtained from the measurements of the bandwidths. The halfwidths of the intense polarized bands for the x = 0.75, 0.80 and 0.83 samples were found to have the same value of about 58.5 cm^{-1} (table 9.1). The corresponding band was slightly broader (60.5 cm^{-1}) for the x = 0.67 sample while the band became as broad as 64 cm^{-1} for the x = 0.60 sample.

These results indicate that the x ≥ 0.67 melts contain the same complex species. The fact that the Raman spectra for the x ≥ 0.67 samples are essentially identical suggests that the maximum coordination number of the lead ion is four. The slight difference of the spectra obtained from the x = 0.67 and the x = 0.75, 0.80 and 0.83 samples probably arose from a little error in composition for the x = 0.67 sample due to the sublimation of

$PbCl_2$ through the process of the sample preparation. Compared to CsCl $PbCl_2$ is much easier to sublime at high temperatures.

The characteristic Raman spectra obtained from the $x \geq 0.67$ melts suggest a tetrahedral structure of the $PbCl_4^{2-}$ species. Group theory predicts nine optic normal modes: $A_1(\nu_1)$, $E(\nu_2)$ and $2F_2(\nu_3, \nu_4)$. All the vibrational modes are Raman active. For an unperturbed tetrahedral species, four Raman lines are expected. Usually the frequencies of these normal modes increase in the order $\nu_2 < \nu_4 < \nu_1 < \nu_3$. Normally the ν_2 and ν_4 modes overlap in the spectrum of the high temperature molten state with heavier central atom, M of a tetrahedral MX_4 molecule. As expected ν_2 and ν_4 modes gave a broad depolarized band centered at about 115 cm^{-1} for the $PbCl_4^{2-}$ species (figs. 9.1-9.3). The strong polarized band at 236 cm^{-1} was attributed to the symmetric stretching, ν_1, vibration. The low frequency depolarized shoulder of the intense ν_1 band was assigned to the ν_4 mode.

Normally the ν_3 mode appears in the high frequency side of the ν_1 band. The $\nu_1(A_1)$ and $\nu_2(E)$ are associated with the vibrations of breathing and bending of the tetrahedral species respectively and are independent of the mass of the central atom. However, the $\nu_3(F_2)$ and $\nu_4(F_2)$ modes represent the vibrations in which both the central atom and chlorides are displaced. Therefore vibrational frequencies of the ν_3 and ν_4 modes depend on the mass of the central atom. For a MCl_4^{2-} species, the heavier the M atom, the smaller the frequency interval between the ν_3 and ν_1 modes. It is even possible that the ν_4 mode will have a lower frequency than ν_1. For example, the ν_3 mode may appear on the low frequency side of the ν_1 band for the tetrahedral $CdCl_4^{2-}$ species in the solid state. The metastable Cs_3CdCl_5 contains discrete $CdCl_4^{2-}$ species with the ν_1 frequency 275 cm^{-1} and ν_3 261 cm^{-1} at 25°C [Chapter 4 in this thesis]; $(NEt_4)_2CdCl_4$ contains $CdCl_4^{2-}$ species with the ν_1 frequency 265 cm^{-1} and ν_3 250 cm^{-1} [Davies 1971]. The tetrahedral $CdCl_4^{2-}$ species exist in the $CdCl_2$/CsCl or $CdCl_2$/RbCl melts. The ν_1 (261 cm^{-1}) and ν_4 (260 cm^{-1}) were found to have almost identical frequencies [chapter 7].

Detailed normal mode calculations have been performed in the present study for a model tetrahedral MCl_4 molecule to illustrate the effect of the change of the mass of the central atom M on the ν_1, ν_2, ν_3 and ν_4 frequencies for a fixed set of force constants based on CCl_4.

Table 9.2 lists the vibrational frequencies for various isotopic CCl_4 molecules. It can be seen that the ν_1 and ν_2 modes have the same values for CCl_4 with the different isotopic carbon atoms and the same isotopic chloride atoms. The ν_3 and ν_4 (especially ν_3) frequencies decrease and the frequency interval between ν_3 and ν_1 decreases as the mass of the isotopic carbon atom increases (table 9.2).

Normal mode calculations for the model tetrahedral MCl_4 molecule were based on the data of CCl_4 as listed in table 9.2. Force constants were calculated from the known vibrational frequencies of the different isotopic CCl_4 molecules. These force constants were then used to evaluate the frequencies of a hypothetical set of MCl_4 molecules with different masses of the central M atoms. The calculated frequencies are listed in table 9.3. The frequency interval between the ν_3 and ν_1 modes decreases as the mass of the central M atom increases. When the mass of the central atom is about 72u the ν_3 frequency (454 cm^{-1}) is lower than the ν_1 frequency (462.5 cm^{-1}). Although in real molecules the force constants must be changed for different MCl_4 molecules the present calculation does illustrate the effect of change in the mass of the central atom.

As early as in the 1940's [Herzberg 1945, Hildebrand 1947, Neu 1948], Raman spectra of a large number of tetrahedral MCl_4^{2-} compounds were measured. The distance from the central atom to the halogen atom was plotted versus the Raman frequencies ν_1, ν_2, ν_3 and ν_4 (fig. 9.4, redrawn from ref. [Neu 1948]). The decrease in the frequency interval between ν_1 and ν_3 was found to decrease with the increase in the M-Cl bond distance. It is also clear that the frequency interval between ν_1 and ν_3 decreases with an increase in the mass of M. Also Raman measurements [Neu 1948] for liquid $PbCl_4$ showed the ν_1 band at 327 cm^{-1} and ν_3 at 348 cm^{-1}. The frequency interval between

these two modes is only 21 cm^{-1} for $PbCl_4$, but is as large as 312.5 cm^{-1} for $^{12}C^{35}Cl_4$ and 322 cm^{-1} for $^{12}C^{37}Cl_4$. Since liquid $PbCl_4$ has totally different force constants compared to the $PbCl_4^{2-}$ species in the molten phase with Cs^+, it is reasonable to propose that the ν_3 frequency of $PbCl_4^{2-}$ in the $PbCl_2/CsCl$ molten mixture is lower than the ν_1 frequency.

9.2.2 Pure $PbCl_2$ and x < 0.67 systems

For the x < 0.67 melts, the bandshape and the band position were found to change gradually with the change of the composition (figs. 9.1-9.3, table 9.1). The frequency of the intense polarized band increased to a maximum value (241 cm^{-1}) for the x = 0.50 melt, then gradually decreased to 219 cm^{-1} for pure $PbCl_2$. The FWHH of this band increased gradually from 60.5 cm^{-1} for the x = 0.67 melt to 128 cm^{-1} for pure $PbCl_2$.

Two depolarized bands at about 100-120 cm^{-1} and a depolarized shoulder on the low frequency side of the intense polarized band were observed from all these spectra. Similar to the $CdCl_2$/CsCl and $CdCl_2$/RbCl melts [chapter 7], the isotropic spectrum of the x < 0.67 melt has a very symmetric band.

These results suggest that the complex ion in the x < 0.67 melts has a similar tetrahedral configuration as for the x ≥ 0.67 melts but the discrete $PbCl_4^{2-}$ species exists only in the x ≥ 0.67 melts. The measurements of the FWHH and the result of the band resolution indicate that $PbCl_3^-$ is not present as a discrete stable species. The FWHH of the intense band for the x = 0.67, 0.60 and 0.50 samples are about 60.5, 64 and 66 cm^{-1} respectively (table 9.1). If $PbCl_3^-$ was a stable species, there should be two species, $PbCl_4^{2-}$ and $PbCl_3^-$, in the x = 0.60 sample. The FWHH of the intense polarized band should be at least 66 cm^{-1} (for $PbCl_3^-$ species). The band resolution for these three melts indicates only one component in the frequency region of this isotropic band (fig. 9.5).

Although the frequency of the intense ν_1 band reaches a maximum value for the x = 0.50 melt (table 9.1) the $PbCl_3^-$ species can not be justified. A number of the molten

MCl_2/ACl systems have been studied previously. The Raman frequency of the polarized band was found to have a maximum value for the melt with x = 0.50 mole fraction of ACl, but the MCl_3^- species was not suggested, for examples, the $CdCl_2/ACl$ system as discussed in this thesis and the $MnCl_2/CsCl$ system [Shabana 1985]. The increase in the frequency for the x = 0.67 to 0.50 samples may be due to the presence of the Pb^{2+} ions as first neighbors to the $PbCl_4^{2-}$ as the concentration of $PbCl_2$ increases. There is no evidence to suggest a polynuclear species similar to $Al_2Cl_7^-$. The lifetime of any possible polynuclear species must be too short to detect by Raman method.

The calculated lifetimes of the complex ions in these melts based on the formula: $\Gamma_i^{-1} = \pi c \tau_v$ [chapter 2], where Γ_i is the FWHH of the isotropic band and τ_v is the vibrational correlation time, are listed in table 9.1. The values of the lifetimes of the complex ions in the $x \geq 0.67$ melts are almost identical (0.18 ps), then decrease with an increase in the concentration of $PbCl_2$ in the $x < 0.67$ melts.

In conclusion the Raman results suggest that the tetrahedral $PbCl_4^{2-}$ species exists in the $x \geq 0.67$ melts with a long lifetime and that the short-lived tetrahedral local units with fast-exchange chloride bridge structures exist in the $x < 0.67$ melts.

Many previous Raman measurements have been performed on the pure $PbCl_2$ melt. No Raman bands were observed by Balasubrahmanyam and Nanis [Balasubrahmanyam 1963] and Maroni [Maroni 1971]. Oyamada [Oyamada 1974] observed two Raman bands at 120 cm^{-1} (depolarized) and at 205 cm^{-1} (polarized) which were attributed to the $PbCl_3^-$ ion-like local structure. A Raman study of $PbCl_2$ as a function of temperature [Mendes-Filho 1979] indicated that the spectrum of solid $PbCl_2$ at high temperature resembled the structureless spectrum of the melt. In the present study of the melt, the reduced spectrum shows a quite broad depolarized band centered at about 140 cm^{-1} and an intense polarized band centered at about 210 cm^{-1}. In the $I(\nu)$ spectrum, it is difficult to determine the central position of the polarized band because of the strong background scattering (fig. 9.1), but the isotropic spectrum ($I_{\parallel} - 1.33 I_{\perp}$) shows the polarized band

centered at about 182 cm^{-1}.

In the spectra of the MCl_2 melts and the alkali halide ionic melts, the relative intensity of the polarized optic mode compared to background scattering reflects the ability of metal cations to form complex ions with halides. For example, a well resolved strong peak has been observed in the polarized spectrum of pure molten $MgCl_2$ [Huang 1976, Bunten 1984], or $CdCl_2$ [chapter 7]. For alkali halides, e.g. $NaCl$ [Mitchell 1983, Giergiel 1984], there was no strong peak, only a broad band in the spectrum. It was reported that there was no complex ion formation in molten NaCl. For some MCl_2 melts, for example, $CaCl_2$, $SrCl_2$ and $BaCl_2$, the spectra showed incompletely resolved shoulders [Bunten 1984]. Neutron diffraction results [Edwards 1978] suggested that the correct description of the structure of the $BaCl_2$ melt was in terms of Ba^{2+} and Cl^- rather than $BaCl^+$ complex and Cl^- ions. The Raman spectrum observed for pure $PbCl_2$ in the present work (fig. 9.1) indicates that the relative intensity of the peak at about 182 cm^{-1} compared to the background scattering is between those of the corresponding bands for $MgCl_2$ and $BaCl_2$. The results suggest that the ability to form complex species for Pb^{2+} is stronger than Ba^{2+} ion but weaker than Mg^{2+} and Cd^{2+}. Further the lifetime of a discrete $CdCl_4^{2-}$ species (0.38 ps, chapter 7) is much longer than that of a discrete $PbCl_4^{2-}$ species (0.18 ps). Perhaps the fact that the Pb^{2+} ion has a weaker ability to form a stable discrete complex ion compared to the Cd^{2+} ion in the melt results in a different effect of pressure on the conductivity for these two melts [Cleaver 1990].

Table 9.1

The center frequencies (cm^{-1}) and FWHH based on the isotropic spectra of the polarized intense bands for the $PbCl_2/CsCl$ molten system.

composition (mole fraction of CsCl)	frequency (cm^{-1})	FWHH (cm^{-1})	τ_1 (ps)	temperature (°C)
0.83	236	58.5	0.18	590
0.80	236	58.5	0.18	585
0.75	236	58.5	0.18	560
0.67	237	60.5	0.18	570
0.60	239	64.0	0.17	632
0.50	241	66.0	0.16	630
0.40	240	77.0	0.14	600
0.33	235	81.5	0.13	580
0	219	128	0.08	521

Table 9.2

The unperturbed vibrational frequencies (cm^{-1}) of isotopic CCl_4

	ν_1	ν_2	ν_3	ν_4	$\nu_3 - \nu_1$
$^{12}C^{35}Cl_4$	462.5	219	775	315	312.5
$^{13}C^{35}Cl_4$	462.5	219	750	314	288.5
$^{12}C^{37}Cl_4$	450	213	772	307	322
$^{13}C^{37}Cl_4$	450	213	747	306	297

Table 9.3

The frequencies (cm^{-1}) of a model tetrahedral MCl_4 molecule obtained from the normal mode calculations based on the force constants of the CCl_4 molecule.

mass of M	ν_1	ν_2	ν_3	ν_4
12	462.5	219	775.5	315
24	462.5	219	594	302
36	462.5	219	524.5	289
48	462.5	219	488.5	278
60	462.5	219	467.5	268
72	462.5	219	454	259.5

The calculated fore constants (mdyne/A) of the CCl_4 molecule are: A_1: $f_r + 3f_{rr} = 4.4088$; E: $d^2(f_\alpha + f_{\alpha\alpha'} - 2f_{\alpha\alpha}) = 1.0273$; F_2: $f_r - f_{rr} = 1.4982$, $2^{1/2}d(f_{r\alpha} - f_{r\alpha'}) = 1.5570$, $d^2(f_\alpha - f_{\alpha\alpha'}) = 3.7011$.

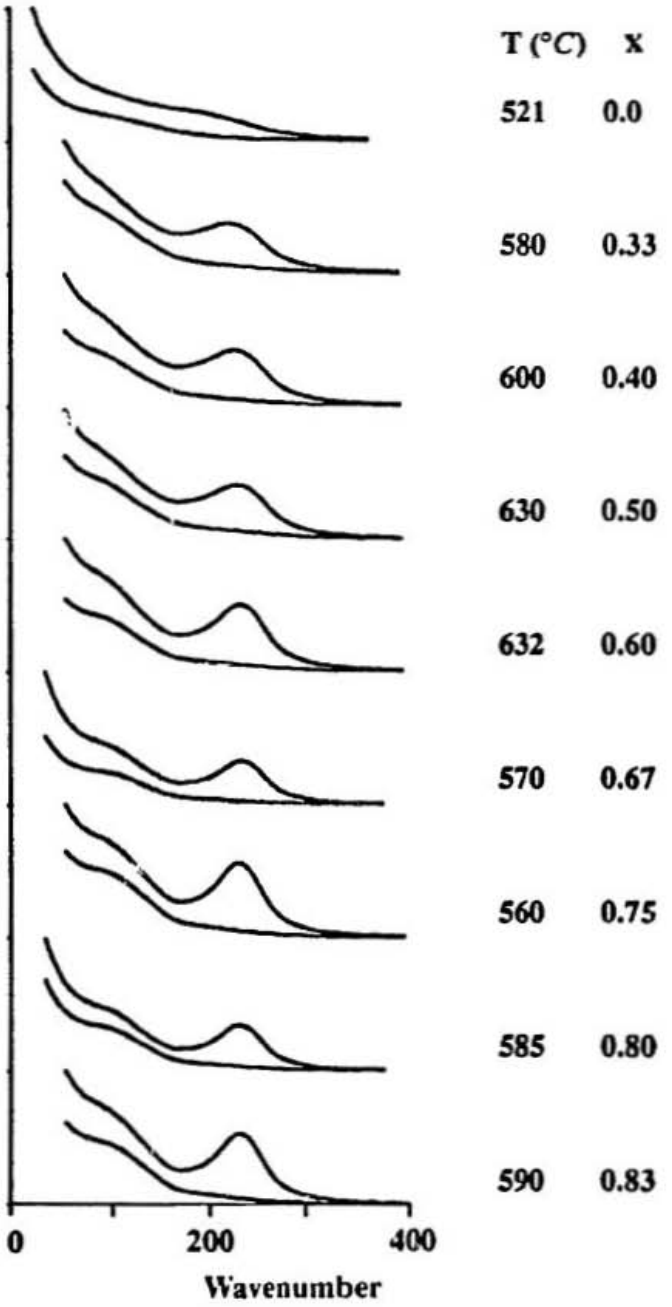

Fig. 9.1

Raman spectra observed from the molten $PbCl_2/CsCl$ system. **X** - the mole fraction of CsCl, **T** - sample temperature.

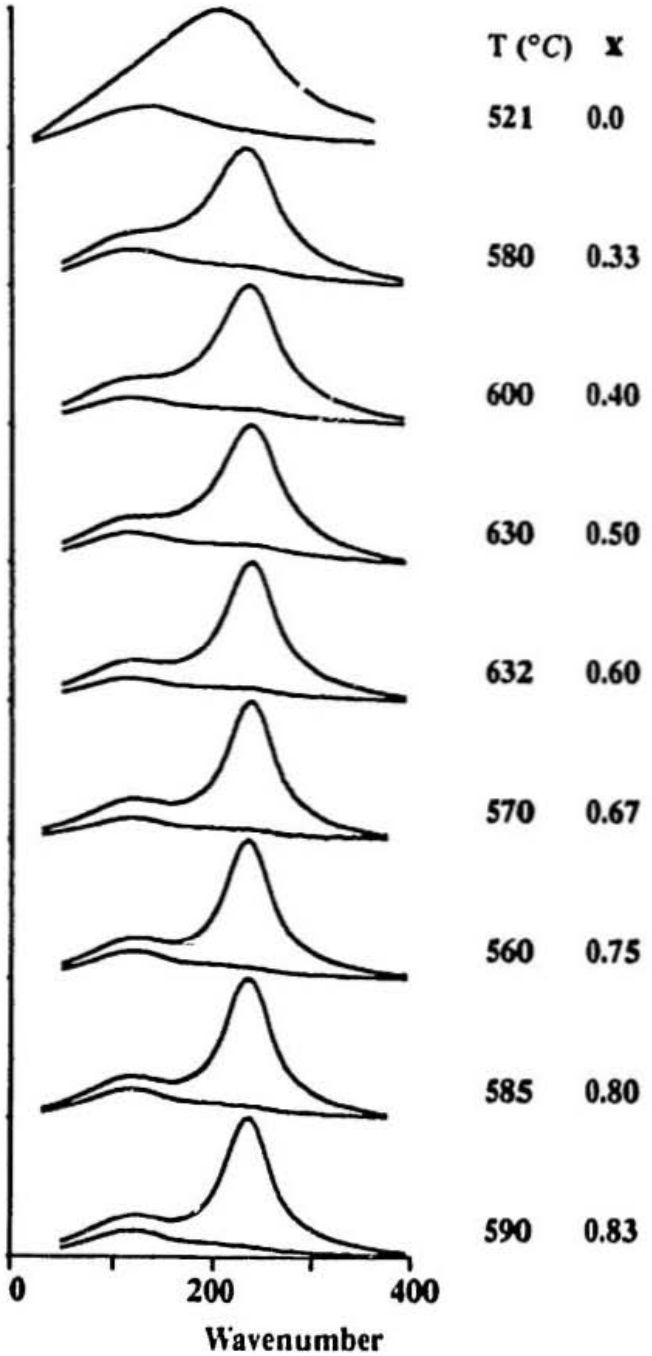

Fig. 9.2

The $R(\nu)$ Raman spectra for the $PbCl_2/CsCl$ molten system. **X** - the mole fraction of $CsCl$; **T** - sample temperature.

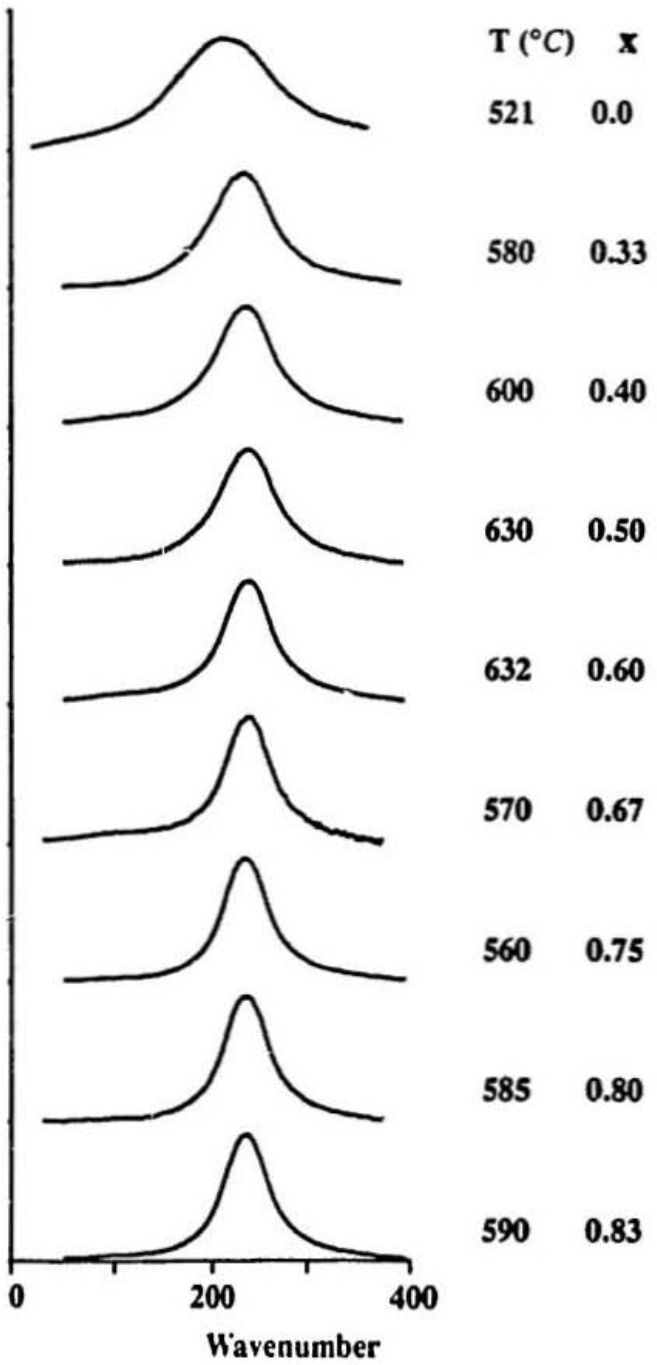

Fig. 9.3

Isotropic reduced Raman spectra ($R_{\parallel}$ - 1.33 $R_{\perp}$) for the molten $PbCl_2/CsCl$ system. **X** - the mole fraction of $CsCl$; **T** - sample temperature.

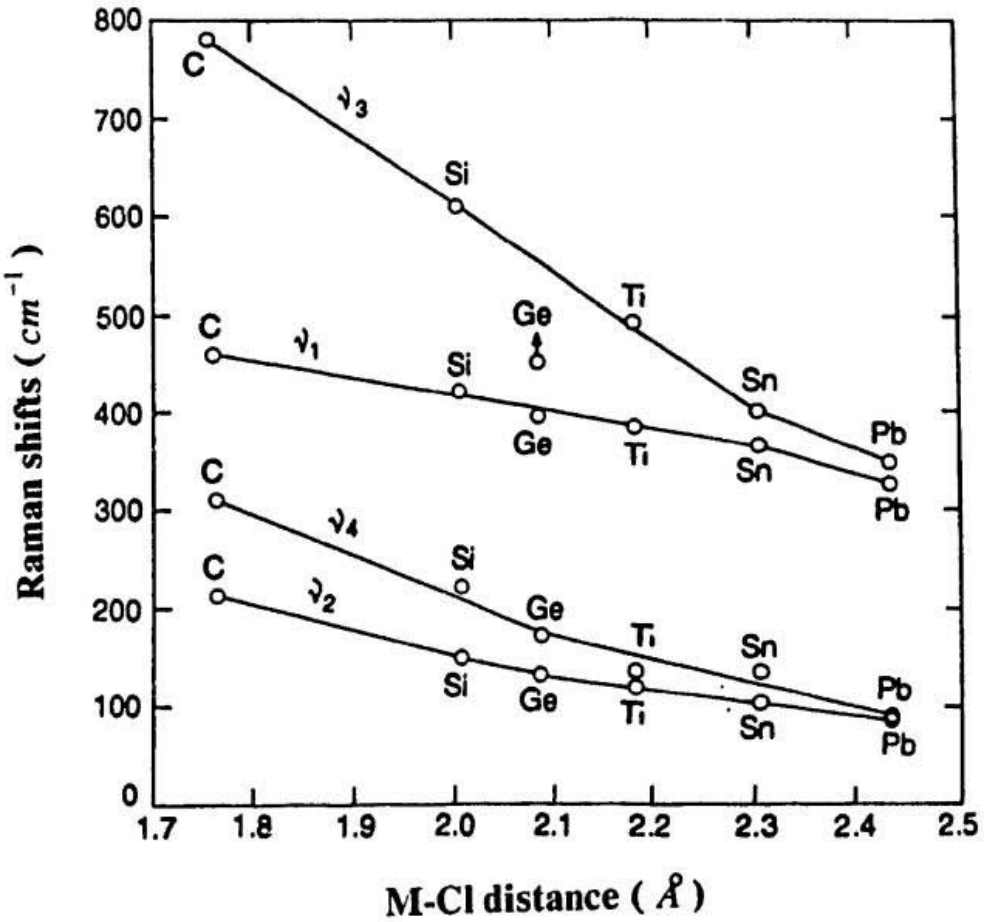

Fig. 9.4

The plot of the characteristic vibrational frequencies of tetrahedral MCl_4 molecules verse the M-Cl distance. Redrawn from Ref. [Neu 1948].

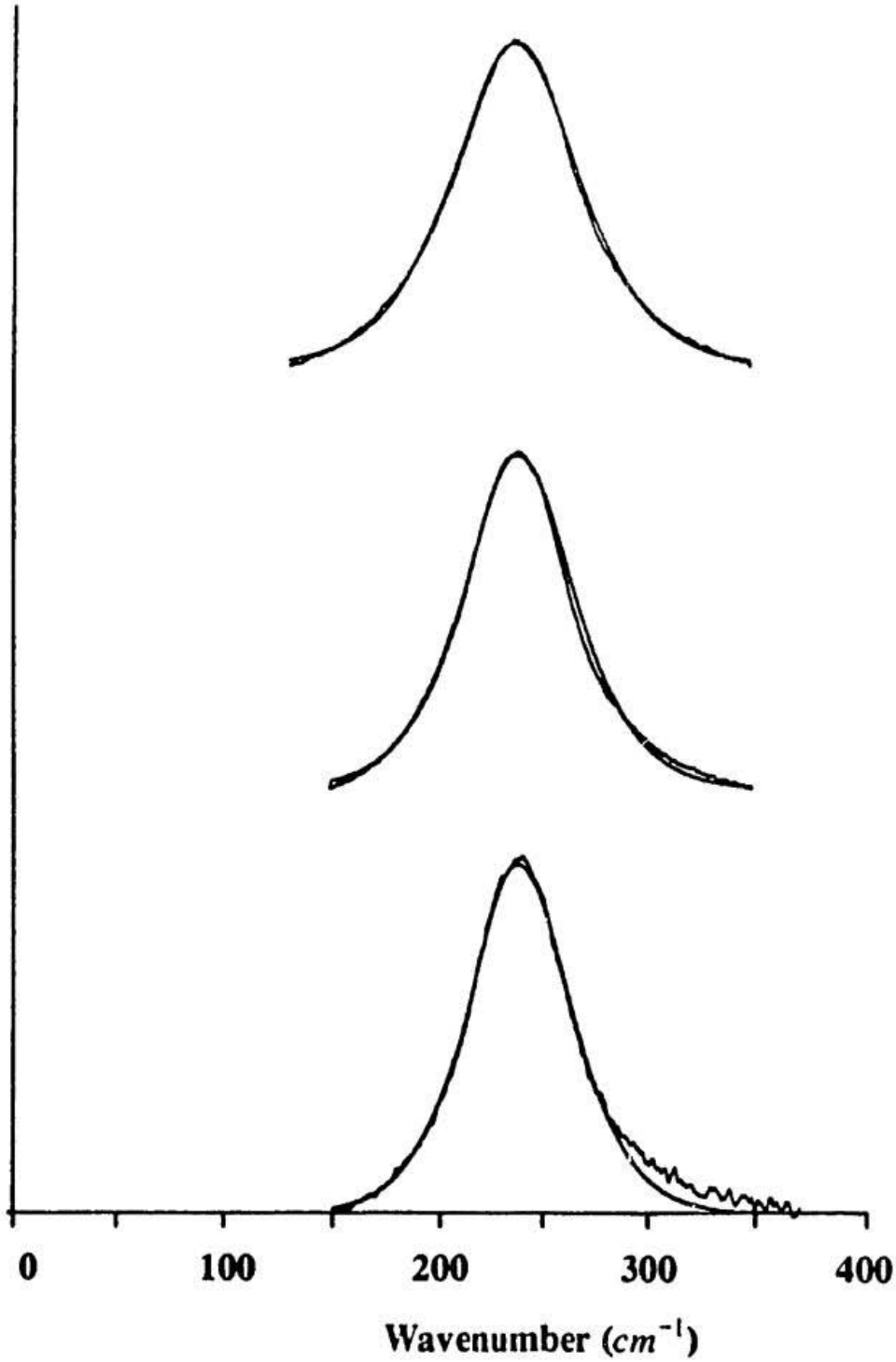

Fig. 9.5

The band resolution of the isotropic Raman spectra for the $PbCl_2$/CsCl melts with x = 0.50 (top), 0.60 (middle) and 0.67 (bottom). The smooth line is the best fit curve calculated with a product function for each of the spectra.

Chapter 10

STRUCTURAL PHASE TRANSITION IN $LiCsCO_3$ AND PHASE EQUILIBRIUM IN THE Li_2CO_3/Cs_2CO_3 SYSTEM

10.1 Introduction

Molten alkali metal carbonate mixtures have been found to be suitable for use as electrolytes for high temperature fuel cells and batteries. A study of the structural and dynamical properties of the alkali metal carbonates in both the solid and molten states was initiated.

The local structures of these melts can not be determined easily by X-ray diffraction studies because of the large contribution of the intra-ionic C-O and O-O interactions within the CO_3^{2-} ion dominate the experimentally obtained diffraction patterns. Ab inito calculations have been attempted to obtain this information [Habasaki 1990].

Phase diagrams of the most binary carbonate systems have been obtained by several methods e.g. DTA, X-ray and conductivity measurements [Janz 1963, Christmann 1978, 1979, Bale 1982, Dissanayake 1986]. But few phase equilibria studies have been performed for the Cs_2CO_3/A_2CO_3 (A, other alkali metal ions) binary systems.

Although the alkali metal carbonates are chemically simple compounds, many have complicated structures at room temperature and have been found to undergo one or several SPTs (structural phase transition) in the solid states. Raman measurements by Maciel and Ryan [Maciel 1981a] indicated that a feature of the α phase in K_2CO_3 was a very broad low frequency band which suggested that the system was highly anharmonic. A soft librational mode of the CO_3^{2-} ion at the α - β transition was observed in the β phase of K_2CO_3 [Maciel 1981a]. The same authors [Maciel 1981b, 1981c] observed the temperature dependence phonons in the Raman spectrum of the incommensurate γ-Na_2CO_3 phase. It was reported that two soft modes were observed at the α-β transition and two

additional lines in the γ phase were assigned to couple amplitude modes that arose from the coupling of the acoustic and librational branches at $q \sim q^*$.

Wolff [Wolff 1987] has discussed the α-β phase transition of the alkali carbonates. The hexagonal structure common to the α -A_2CO_3 phase (A = Na, K, Rb) transformed into the β-phase structure by rotations of the anions which act as hinges between parallel AO_3 columns. It was reported that the SPT may still occur in the mixed salts $ABCO_3$ (A, B = alkali metal ions) [Wolff 1987]. For example, thermal analysis and X-ray diffraction suggested that $LiNaCO_3$ [Christmann 1978] presented three crystalline forms.

Raman studies have been performed on the Li_2CO_3/A_2CO_3 (A = Cs, Rb, K and Na) and Na_2CO_3/K_2CO_3 systems in this program in order to obtain more information about:

i) the possible SPT in the compounds formed in these binary systems;

ii) the effect of the alkali metal ions on the structures and properties of the carbonate salts in both the solid and molten systems;

iii) the structure and properties of a pure A_2CO_3 salt which may be deduced by the studies of the $ABCO_3$ salt (An excellent example of this kind of studies is the studies of the mixed $ABNO_3$ in order to understand the ferroelectric behavior of KNO_3 [Yanagi 1963, Kawabe 1964, 1965, Yoshida 1960, Sawada 1961, Tanisaki 1961, Shinnaka 1962, Dork 1964].).

In this chapter, results of the Li_2CO_3/Cs_2CO_3 system will be discussed (only the Li_2CO_3/Cs_2CO_3 solids and Li_2CO_3/K_2CO_3 melts will be discussed in this thesis). The framework of the phase diagram and the properties of the mixed system, especially the structural phase transition in the $LiCsCO_3$ compound will be reported.

10.2 Results and Discussion

For an alkali metal carbonate salt, the vibrational spectrum of the solid state can be explained in terms of the CO_3^{2-} ions perturbed by a crystal field. An unperturbed carbonate ion has D_{3h} symmetry. Group theory predicts six optic normal modes, i.e. A_1' (ν_1), 2E' (ν_3 and ν_4) and A_2'' (ν_2). $\nu_1(A_1')$ is Raman active, symmetric stretching mode at about 1063 cm^{-1} [Herzberg 1945]; $\nu_2(A_2'')$ infrared active, out of plane deformation at about 880 cm^{-1}; $\nu_3(E')$ and $\nu_4(E')$ both infrared and Raman active, antisymmetric stretch and bend at about 1400 cm^{-1} and 700 cm^{-1}, respectively.

10.2.1 Compound formation

Raman spectra with the frequencies scanned from 30-1800 cm^{-1} have been obtained for several fused Li_2CO_3/Cs_2CO_3 samples in different compositions from x = 0.25 to 0.75 (x, mole fraction of Cs_2CO_3) at room temperature. The ν_1 regions of these spectra are presented (fig. 10.1). The characteristic peak frequencies of the ν_1 bands and the corresponding compounds identified are listed (table 10.1). Only one compound $LiCsCO_3$ with 0.50 mole fraction of Cs_2CO_3 was identified. $LiCsCO_3$ was found to be a congruent compound and formed eutectic mixtures with Li_2CO_3 or Cs_2CO_3. The slowly cooled low temperature solid exhibited a characteristic ν_1 band at 1052 cm^{-1} at room temperature. The sample quenched from the melt to room temperature gave a metastable form of $LiCsCO_3$ with a characteristic ν_1 band of CO_3^{2-} at 1060 cm^{-1} (table 10.1). The slowly cooled sample was found to undergo a SPT at about 435°C. The SPT was reversible during the heating and cooling cycle. The SPT in $LiCsCO_3$ still took place in the mixtures of $Li_2CO_3/LiCsCO_3$ or $Cs_2CO_3/LiCsCO_3$. The framework of the phase diagram suggested by the present Raman study is shown in fig. 10.2.

10.2.2 Phase transition in $LiCsCO_3$

$LiCsCO_3$ exhibited only one SPT at about 435°C in a temperature range from 77K to the melting point (about 595°C). When the sample was heated to above the transition temperature (not necessarily to a molten state), then was quenched to room temperature, the phase transition was not observed and the metastable HTP (high temperature phase) was identified. The metastable phase was stable at room temperature for a long time. In our laboratory, the sample remained as the metastable HTP at least one year at room temperature. When the metastable solid was maintained at about 150°C for about 24 hours the Raman spectrum showed a new, small peak at about 1052 cm^{-1} due to the LTP (low temperature phase) and a very strong peak at 1059 cm^{-1} due to the metastable phase in the ν_1 region. After about 48 hours at 150°C, the relative intensities of the bands at 1059 and 1052 cm^{-1} were almost identical. The rate of the phase transition increased as the temperature increased. At about 400°C, it took only about 42 minutes before the metastable HTP transformed completely to the LTP.

A plot of the relative intensity of the band at about 1049 cm^{-1} (peak maximum of the ν_1 band due to LTP) versus time during the SPT at 400°C is presented in fig. 10.3. The data as shown in fig. 10.3 were obtained in the following way. First, the sample was heated to ~ 440 °C for about 30 minutes to convert the sample to the HTP. A Raman measurement was performed in the ν_1 region to make sure that the LTP transformed completely to the HTP (only one ν_1 peak observed at ~1055 cm^{-1} due to the HTP). Second, the spectrometer was fixed at about 1049 cm^{-1} (peak maximum of the ν_1 band due to the LTP) and the Raman intensity data were recorded as a function of time when the temperature controller was re-set to 400°C. The high relative intensity at t = 0 was due to the ν_1 band for the HTP. Although the ν_1 band of the HTP centered at about 1055 cm^{-1}, the distribution of the intensity of this band as a function of the frequency in the ν_1 region gave intensity at 1049 cm^{-1} and caused a high relative intensity at 1049 cm^{-1} for t = 0 (fig. 10.3). At $0 < t \leq 14$ minutes the relative intensity decreased with time. Both the ν_1 bands

due to the LTP and the HTP contributed to the intensity at 1049 cm^{-1} and the intensity decrease indicates that the SPT started. The value of the intensity reached a minimum at about t = 14 minutes, then increased with time. At t ≈ 42 minutes the intensity reached a maximum value, then remained constant (fig. 10.3). Under these conditions the SPT completed at t ≈ 42 minutes. Raman measurement then confirmed that the ν_1 band centered at about 1055 cm^{-1} due to the metastable HTP disappeared completely and was replaced by the band at 1049 cm^{-1}. It should be noted that the real time it takes to transform the metastable HTP into the LTP at 400°C should be longer than the experimental value (about 42 min.) obtained by this method because the average temperature would be higher than 400°C as the furnace cooled naturally from 440°C to 400°C.

10.2.2.1 Temperature dependent Raman spectra of $LiCsCO_3$

Raman spectra of the solid $LiCsCO_3$ at 77K and at room temperature over a frequency region from 30-1800 cm^{-1} are presented in figs. 10.4 (LTP) and 10.5 (LTP) respectively. Peak frequencies are collected in table 10.2. The structure of the compound $LiCsCO_3$ is unknown so detailed assignments are not possible.

Raman spectra of the solid $LiCsCO_3$ as a function of temperature in the low frequency external modes region, the ν_1, ν_3 and ν_4 regions are presented in figs. 10.6, 10.7, 10.8 and 10.9 respectively. The complete spectra over a frequency region from 30-1800 cm^{-1} for $LiCsCO_3$ at the temperatures just below (430°C) and above (440°C) the phase transition point (~ 435°C) are presented in fig. 10.10 (430°C bottom, 440°C top) and the peak frequencies are collected in table 10.2.

Below 430°C, the ν_1 frequency decreased gradually as the temperature increased from 1054 cm^{-1} at 77K (fig. 10.4 LTP) to 1049 cm^{-1} at 430°C (fig. 10.7, LTP). At 440°C, the ν_1 frequency increased abruptly to 1055 cm^{-1} (fig. 10.7 HTP). The result indicates that the compound $LiCsCO_3$ has two different crystal structures at 430 and 440°C. Similar results were observed in the external modes, ν_3 and ν_4 regions.

In the external mode regions, at 77K eleven peaks were observed (table 10.2, fig. 10.4). The frequencies of these bands decreased and the bandwidths increased as the temperature increased. At 25°C ten bands with a broad band centered at 149 cm^{-1} and at 430°C six bands including three broad bands at 104, 133 and 203 cm^{-1} were observed (fig. 10.6). When the LTP transformed to the HTP at 440°C, a dramatic change occurred. Only four bands including a broad band at 150 cm^{-1} were observed at 440°C (fig. 10.6).

In the ν_3 region four peaks at 1384, 1404, 1472 and 1496 cm^{-1} (fig. 10.4 LTP) were observed for the sample at 77K. These bands shifted to the lower frequencies at 1382, 1402, 1468 and 1491 cm^{-1} at 25°C (fig. 10.5 LTP) and 1372, 1392, 1455 and 1478 cm^{-1} at 430°C (fig. 10.8) respectively. But at 440°C, only two broad bands centered at about 1419 and 1431 cm^{-1} were observed (fig. 10.8).

In the ν_4 region three bands centred at 687, 716 and 723 cm^{-1} at 77K (fig. 10.4 LTP). At 430°C the frequency of the band at 687 cm^{-1} decreased slightly to 686 cm^{-1} (fig. 10.9) and the bands at 716 and 723 cm^{-1} collapsed into a broad band centered at 712 cm^{-1}. At 440°C, only one broad band at about 701cm^{-1} (fig. 10.9) was observed.

The analysis above indicates that the information about the SPT obtained from the spectra in the external, ν_1, ν_3 and ν_4 regions is consistent. Careful experiments indicated that the SPT occurred at about 435°C.

10.2.2.2 Raman spectra of the stable and metastable $LiCsCO_3$ at low temperatures

The SPT in $LiCsCO_3$ took place at about 435°C. The SPT was reversible for the slowly heating and cooling cycles and was kinetically sluggish. When the molten sample was quenched to room temperature, a metastable modification formed. The similarity of the spectra obtained from the stable HTP solid phase at 440°C and the metastable phase at 25°C and 77K suggests that the metastable phase at low temperatures retains the crystalline structure of the stable HTP. The Raman spectra of the metastable HTP have been obtained at 298K and 77K. Because the higher resolution of a band at low temperatures

compared at 440°C, the analysis of these spectra obtained at low temperatures can provide more information about the SPT.

Raman spectra obtained from the stable LTP and the metastable HTP of $LiCsCO_3$ at 77K and 25°C over a frequency region from 30 to 1800 cm^{-1} are presented in figs. 10.4 and 10.5 and the expanded ν_1, ν_4 and external regions are presented in figs. 10.11, 10.12 and 10.13 respectively. The peak frequencies are collected in table 10.2.

The symmetric stretching mode appeared at a higher characteristic frequency for the metastable HTP than for the stable LTP. The ν_1 bands centered at 1054 and 1062.5 cm^{-1} in the spectra of the LTP and the metastable HTP at 77K respectively. While the corresponding bands slightly shifted to 1052 and 1060 cm^{-1} at 25°C (table 10.2).

In the alkali metal carbonate series, the ν_1 frequency tends to decrease as the mass of alkali metal increases from ~1089.5 cm^{-1} (Li_2CO_3) to ~ 1040.5 cm^{-1} (Cs_2CO_3). For $LiCsCO_3$ solid, the ν_1 frequency decreases as the metastable HTP transforms to the stable LTP. It suggests that the relative position between the CO_3^{2-} ion and the Li^+ ion (and Cs^+ ion) must be changed. Probably the distance between Li^+ and CO_3^{2-} decreases and results in the increase in the ν_1 frequency. This result indicates that the mechanism of this SPT may be associated with a rotation of the CO_3^{2-} ion in the unit cell.

In the ν_3 region the same number of the peaks were observed for both the solid phases at 77K (fig. 10.11) with peak frequencies 1384, 1404, 1472 and 1496 cm^{-1} for the LTP and 1432, 1440, 1453 and 1513 cm^{-1} for the metastable HTP respectively. However two evident differences are:

i) The magnitude of the ν_3 splitting for the LTP (1496 - 1382 = 112 cm^{-1}) is larger than that for the metastable phase (1513 - 1432 = 81 cm^{-1}). Especially the first three peaks are very close in the spectrum of the metastable phase compared to that for the LTP (fig. 10.11).

ii) The relative intensities of the corresponding peaks are different for the two solid phases, especially the relative intensity of the fourth peak in the spectrum of the metastable HTP is much weaker than the corresponding peak in that of the LTP (fig. 10.11).

In the region, there are three bands at 687, 716 and 723 cm^{-1} for the LTP, but two bands at 695 and 705 cm^{-1} for the metastable HTP at 77K (fig. 10.12, table 10.2). The relative intensity of the first peak at 687 cm^{-1} is much higher than that of the second and third peaks at 716 and 723 cm^{-1} for the LTP, while the relative intensity of the second peak at 705 cm^{-1} is slight higher than that of the first peak at 695 cm^{-1} for the metastable HTP (fig. 10.12).

Similar results can be obtained from the analysis of the spectra in the ν_3 and ν_4 regions obtained from the two solid phases at 25°C (figs. 10.11 and 10.12).

In a solid state the vibrational spectrum of a molecule in a site of low symmetry will depend on how the molecule interacts with its surrounding. Qualitatively, the effects of a low site symmetry are of two general types: (1) change in selection rules and (2) splitting of degeneracies. The results for both the HTP and LTP suggest a low site symmetry because it appears as if the degeneracy of the E' modes is lifted. In addition the fact that there are four bands in the ν_3 and ν_4 regions suggests that the number of formula units in the unit cell is four or more (if the crystal is centrosymmetric).

Maciel et al. [Maciel 1981b] examined the phase transition in crystalline Na_2CO_3 by Raman measurement. It was reported that the internal vibrational modes were little affected by the crystalline environment which could be seen in two ways: (a) their frequencies were only slightly shifted from the free-ion values e.g. ν_1 (free-ion) = 1063 cm^{-1} and ν_1 (Na_2CO_3) = 1072 cm^{-1}; (b) the optical selection rules were essentially those of the free ion, e.g. ν_1 is Raman active only. It was also confirmed by the fact that the planar configuration of the CO_3^{2-} ion survives successive phase transition in Na_2CO_3

[Hogervorst 1979]. The present Raman results indicate that the internal vibrational modes are more affected by the crystalline environment.

Raman spectra for the external mode regions also provide direct information about the SPT. Usually the change of a spectrum in the external mode region is much more sensitive to a SPT than that in the internal mode regions because the external modes directly arise from the interaction among the different molecular/ionic/atomic units. Sometimes the internal modes are little affected by a crystalline environment, but possible changes of the external modes region may still reflect the different structures of the solids. Most previous studies of SPTs were based on the analysis of the spectra in the external mode regions [Scott 1974, 1983].

At 77K eleven bands appeared for the LTP, but only five bands were observed for the metastable HTP in the region 30-250 cm^{-1} (fig. 10.13). The number of the bands and the peak positions were changed after the SPT.

10.2.3 Phase transition in $LiCsCO_3$ in the $LiCsCO_3/Li_2CO_3$ or Cs_2CO_3 mixtures

Similar Raman measurements have been performed on several $LiCsCO_3/Li_2CO_3$ and $LiCsCO_3/Cs_2CO_3$ eutectic mixtures. Several major characteristic properties are summarized:

a) Whether or not the SPT took place in $LiCsCO_3$ was independent on the concentration of the Li_2CO_3 or Cs_2CO_3 in these mixtures. In those mixtures with common CO_3^{2-} anions, the extra Li^+ or Cs^+ ion (relative to the composition of the compound $LiCsCO_3$) did not affect whether or not the SPT took place. The result further suggests that the SPT is associated with the rotation of the CO_3^{2-} ions.

b) The transition temperature depended on the concentration of the $LiCsCO_3$. Table 10.3 lists the transition points for four samples. The transition temperature slightly decreased as the concentration of $LiCsCO_3$ decreased.

c) The eutectic mixture quenched from the melt gave a mixture of the metastable $LiCsCO_3$ and Li_2CO_3 or Cs_2CO_3 depended on the composition. Raman spectrum exhibited two sets of the peaks due to the metastable $LiCsCO_3$ and Li_2CO_3 or Cs_2CO_3. At 25°C in the ν_1 region two peaks at 1060 cm^{-1} (due to metastable $LiCsCO_3$) and 1089.5 cm^{-1} (due to Li_2CO_3) or 1040.5 cm^{-1} (due to Cs_2CO_3) were observed (table 10.1). The slowly cooled eutectic mixtures gave a mixture of the stable $LiCsCO_3$ with characteristic frequency at 1052 cm^{-1} at 25°C and Li_2CO_3 or Cs_2CO_3 (table 10.1). As an example the Raman spectra in the external modes, ν_1 and ν_4, and ν_3 regions obtained from both the fast and slowly cooled x = 0.67 samples at 25°C are shown in figs. 10.14-10.16 respectively. Two sets of the bands due to the metastable $LiCsCO_3$ and Cs_2CO_3 for the fast cooled sample but two sets of bands for the stable $LiCsCO_3$ and Cs_2CO_3 for the slowly cooled sample were observed. Samples cooled at intermediate rates could give sets of bands due to the metastable HTP, the LTP and the excess Cs_2CO_3. In the early stages of the study the variation in the spectra for different samples cooled at different intermediate rates was the source of considerable conclusion.

d) the peak frequencies for the metastable HTP and LTP of $LiCsCO_3$ were almost independent of the concentration of the $LiCsCO_3$, but, of course, the relative intensities of the peaks were changed as expected.

10.3 Conclusion

a) In the Li_2CO_3/Cs_2CO_3 binary system, only one congruent compound $LiCsCO_3$ with mole fraction 0.50 of Cs_2CO_3 was identified. This compound was found to melt at about 595°C. $LiCsCO_3$ could form eutectic mixtures with Li_2CO_3 or Cs_2CO_3.

b) The quenched Li_2CO_3/Cs_2CO_3 sample gave a metastable compound $LiCsCO_3$ or an eutectic mixture of the metastable $LiCsCO_3$ and Li_2CO_3 or Cs_2CO_3 depended on the composition. The metastable $LiCsCO_3$ could be stable at room temperature for a long time.

c) $LiCsCO_3$ took place a SPT at 435 ± 5°C in the temperature range from 77K to the melting point. The SPT was found to be kinetically sluggish. The rate of the phase transition increased as the temperature increased. The mechanism of this SPT is suggested to be associated with the rotation of the CO_3^{2-} ion in the unit cell.

d) In the $LiCsCO_3/Li_2CO_3$ (or Cs_2CO_3) eutectic mixtures, the SPT for $LiCsCO_3$ still occurred. However, the transition temperatures decreased as the concentration of Li_2CO_3 (or Cs_2CO_3) increased. The vibrational frequencies of the CO_3^{2-} ions in $LiCsCO_3$ for both the metastable HTP and LTP were almost independent of the concentration of the $LiCsCO_3$ in these mixtures.

Table 10.1

Raman frequencies (cm^{-1}) in the ν_1 region for the Li_2CO_3/Cs_2CO_3 binary system at 300K.

composition (mol fraction of Cs_2CO_3)	frequencies (cm^{-1})and phases			
	Li_2CO_3	$LiCsCO_3$		Cs_2CO_3
		stable	metastable	
0.25	1089.5	1051.5	1060	—
0.33	1089.5	1052	1060	—
0.40	1089.5	1051.5	1060	—
0.44	1089.5	1052	1060	—
0.50	—	1052	1060	—
0.57	—	1052	1060	1040.5
0.60	—	1052	1060	1040.5
0.67	—	1052	1060	1041
0.75	—	1052	1060	1041.5

Table 10.2

Raman frequencies (cm^{-1}) for $LiCsCO_3$ in the LTP and the metastable HTP at 77K, 300K, and 703K (LTP) and 713K (HTP).

LTP			HTP			
77K	298K	703K	77K	298K	713K	
52	51	45	55.6	51	45	
60.5	59	55.5	64	60	57.5	
69	66.5	60	102	91.5	74	
107.5	104.5		151	140		
116		104(br)*	171.5	160	150(br)	
125	119(br)					
134.5	131					
150	145.5	133(br)				
163.5	157					
198	191	203(br)				
240	232					
687	686.5	686	695	695	701(br)	ν_4
716	718(br)	712(br)	705	705		
723						
1036	1034		1043	1040		$\nu_1\ C^{13}O^{16}O_2^{2-}$
1054	1052	1049	1062.5	1060	1055	ν_1
1384	1382	1372	1432	1427	1419(br)	ν_3
1404	1402	1392	1440	1435		
1472	1468	1455	1453	1443	1431(br)	
1496	1491	1478	1513	1503		
1750	1747	1749(br)	1749(br)	1752	1747	$2\nu_2$
1753	1750					

* - broad band

Table 10.3

The phase transition temperatures for the compound $LiCsCO_3$ in the Li_2CO_3/Cs_2CO_3 binary system

composition (mole fraction of Cs_2CO_3)	temperature (°C)
0.40	392 ± 10
0.50	435 ± 5
0.60	410 ± 10
0.75	380 ± 10

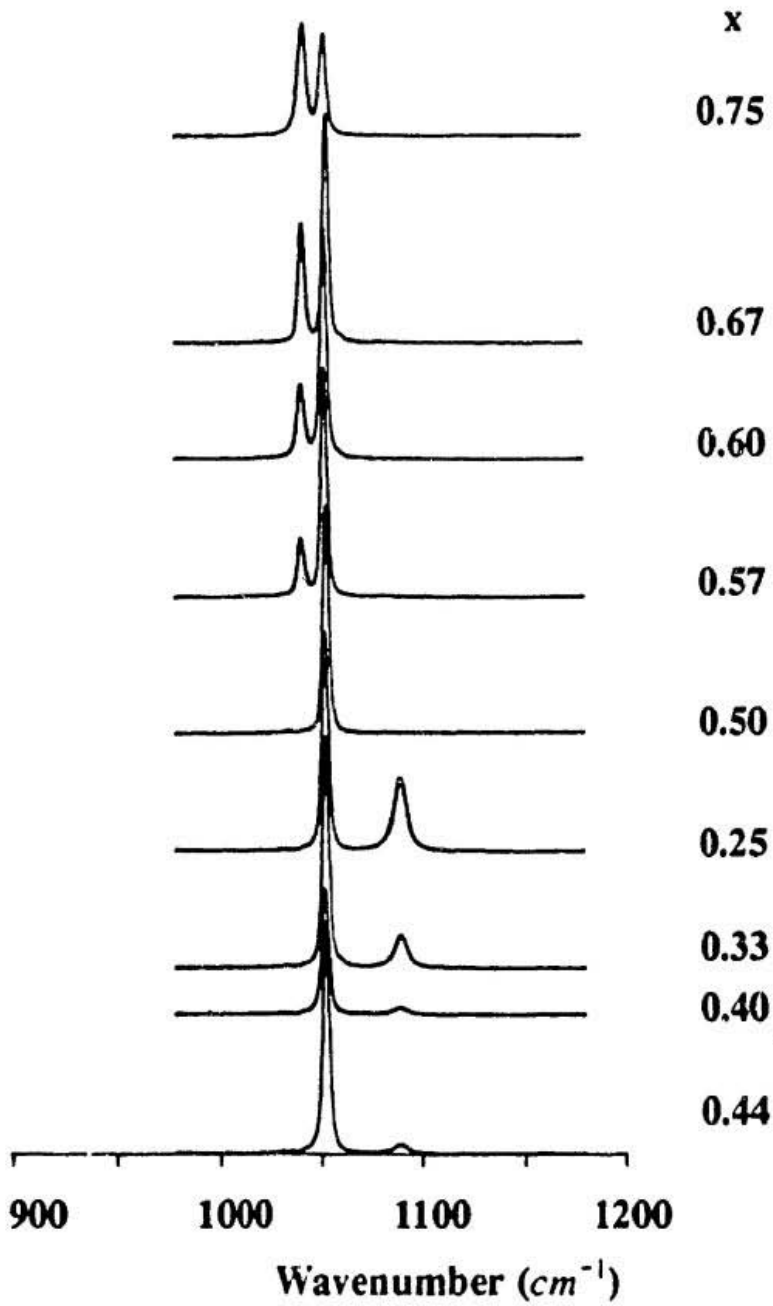

Fig. 10.1

Raman spectra in the ν_1 region for several fused Li_2CO_3-Cs_2CO_3 samples (slow cooled) with the compositions as indicated. Slits 2 cm^{-1}; 25°C. **x** - the mole fraction of Cs_2CO_3.

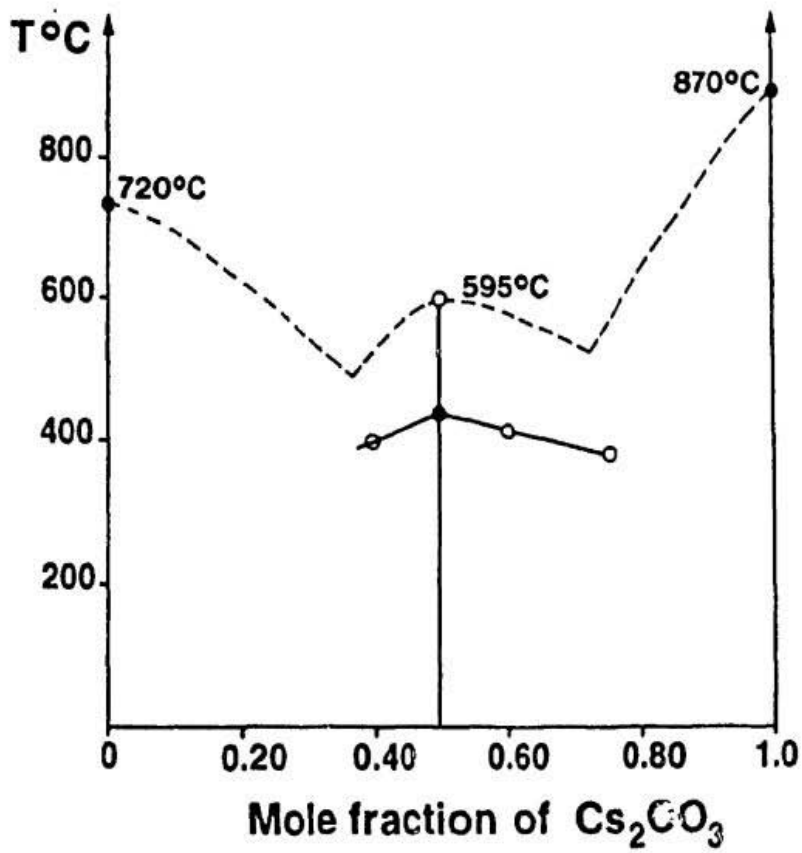

Fig. 10.2

The framework of the phase diagram for the Li_2CO_3/Cs_2CO_3 binary system. M.P.: Li_2CO_3 Ref. [Dean 1978]; Cs_2CO_3 Ref. [Wittorf 1904]; $LiCsCO_3$ Ref. [this work].

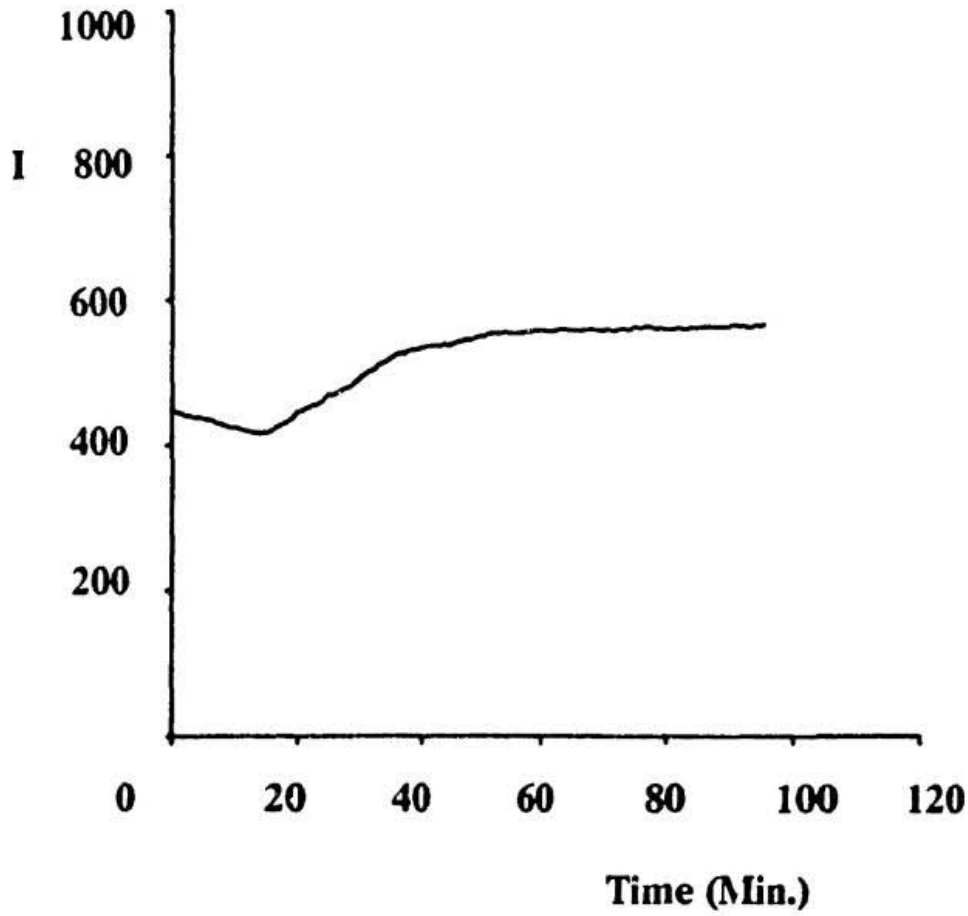

Fig. 10.3

The plot of the intensity of the ν_1 band due to the LTP during SPT in $LiCsCO_3$ vs. time. Slits 2 cm^{-1}; 400°C.

Fig. 10.4

Raman spectra obtained from the stable (bottom) and metastable (top) $LiCsCO_3$. 77K; Slits 2 cm^{-1}.

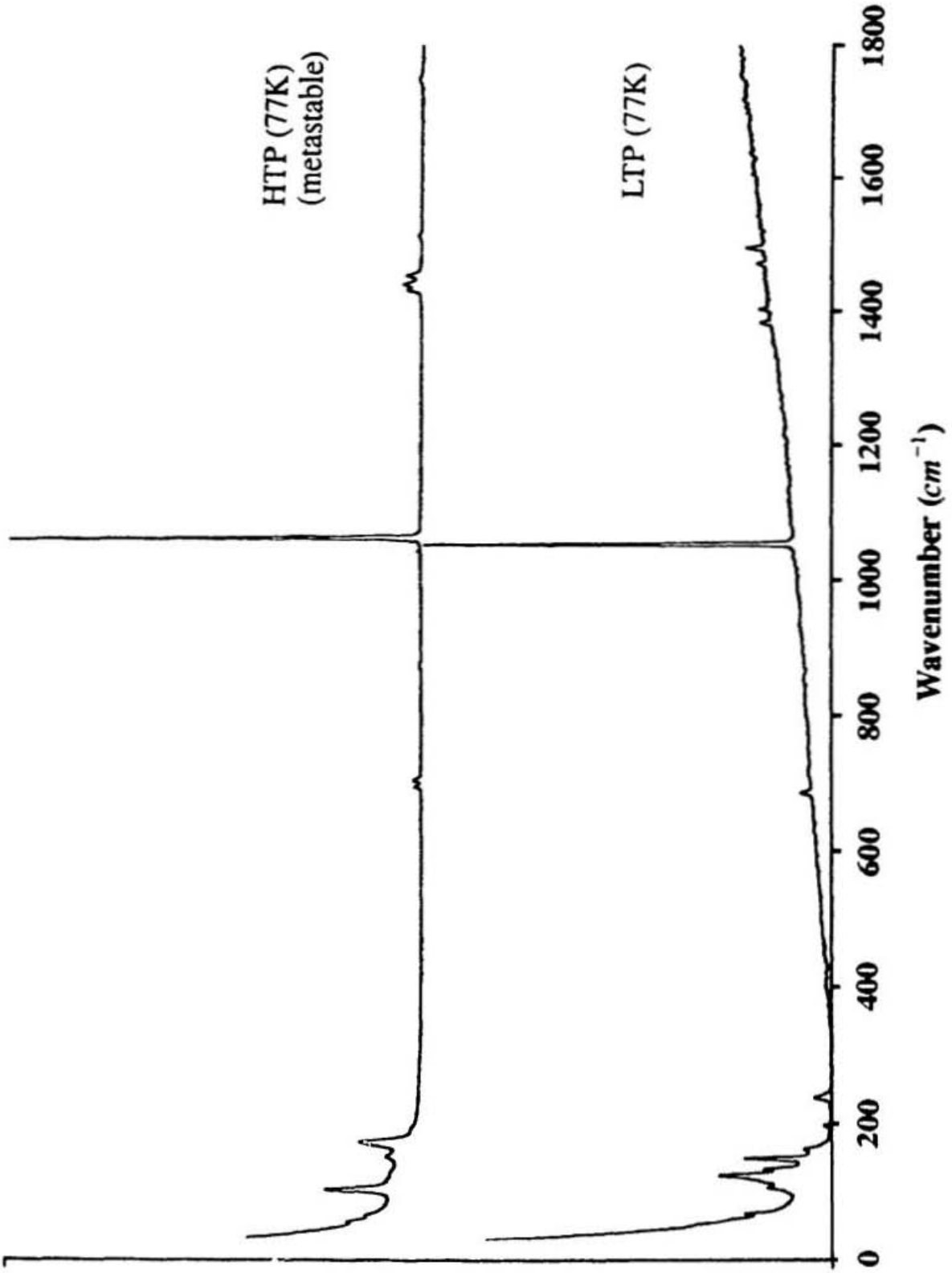
HTP (77K)
(metastable)
LTP (77K)
0
200
400
600
800
1000
1200
1400
1600
1800
Wavenumber (cm^{-1})

Fig. 10.5

Raman spectra obtained from the stable (bottom) and metastable (top) $LiCsCO_3$. 25°C; Slits 2 cm^{-1}.

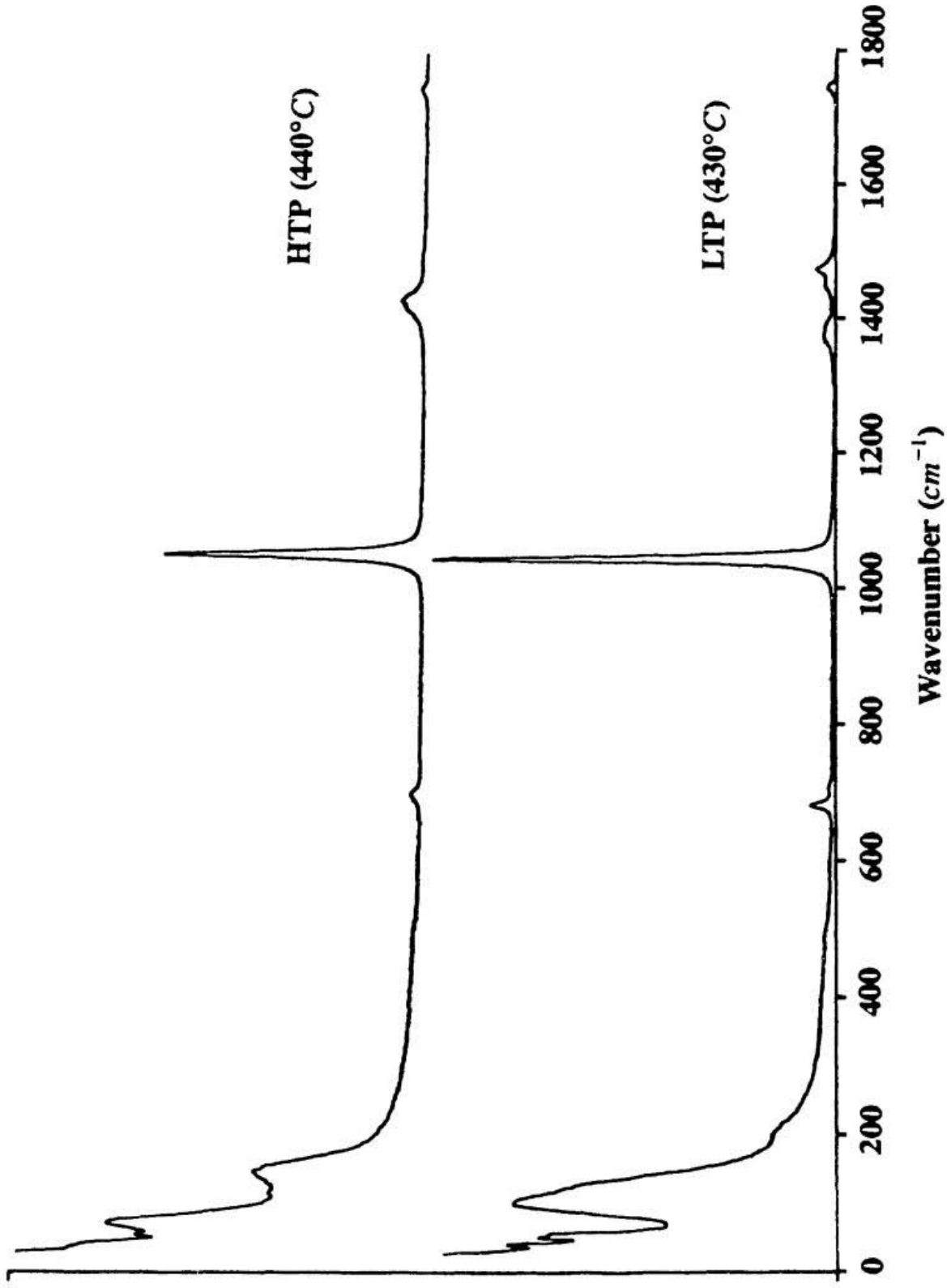
HTP (440°C)
LTP (430°C)
0
200
400
600
800
1000
1200
1400
1600
1800
Wavenumber (cm^{-1})

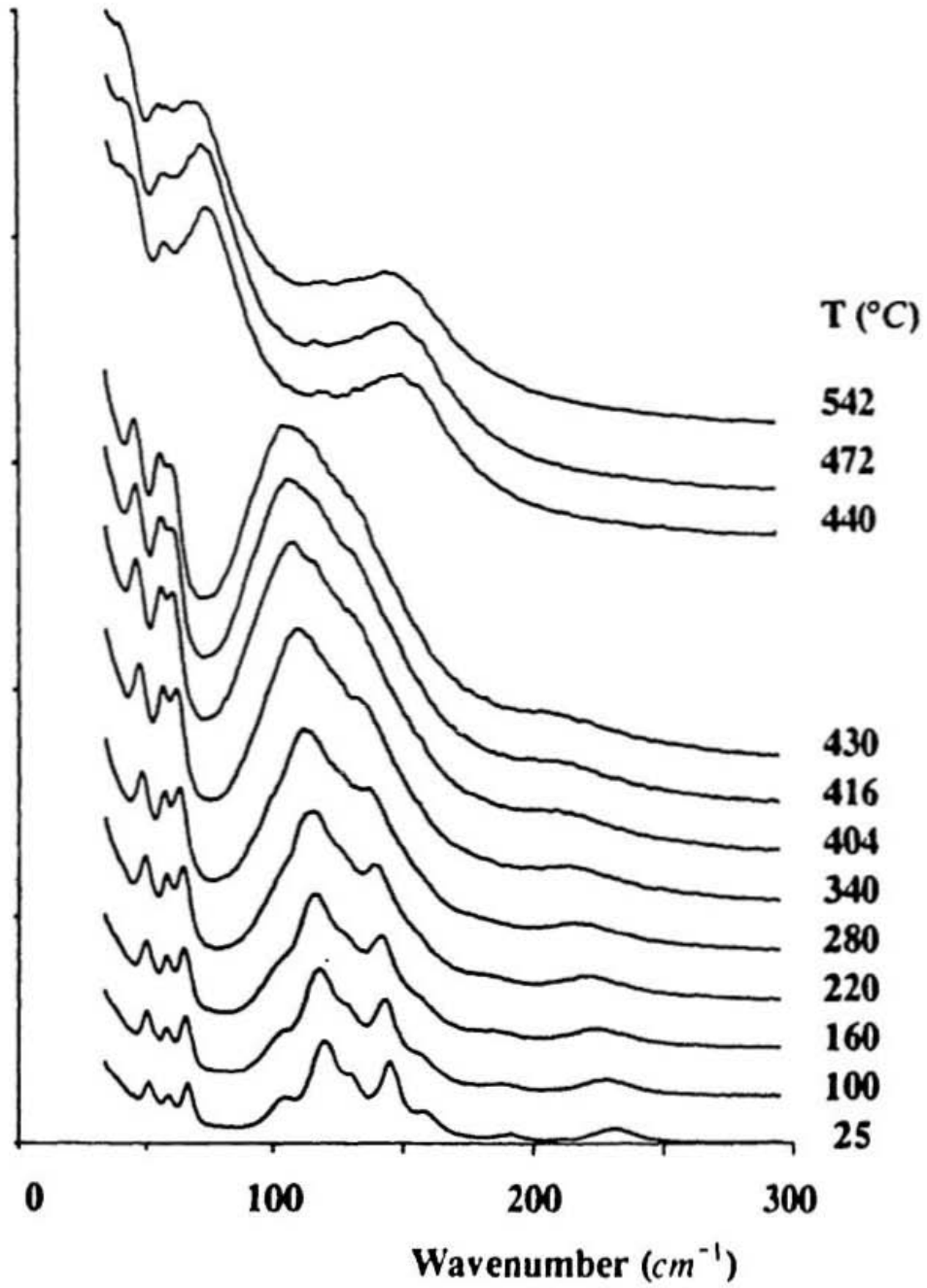

Fig. 10.6

Raman spectra in the external mode region for the $LiCsCO_3$ system at different temperatures at the temperatures as indicated. Slits 2 cm^{-1}.

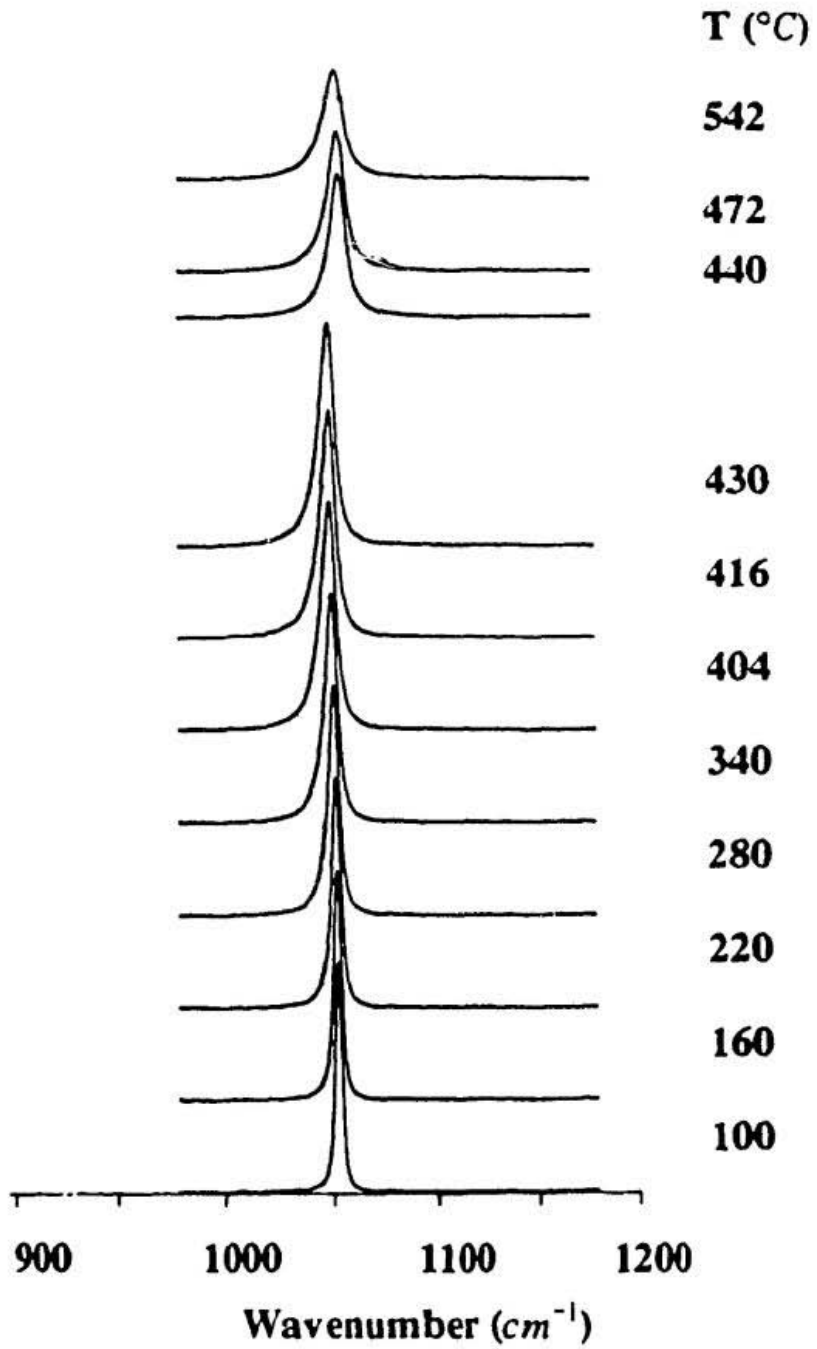

Fig. 10.7

Raman spectra in the ν_1 region for the $LiCsCO_3$ system at different temperatures at the temperatures as indicated. Slits 2 cm^{-1}.

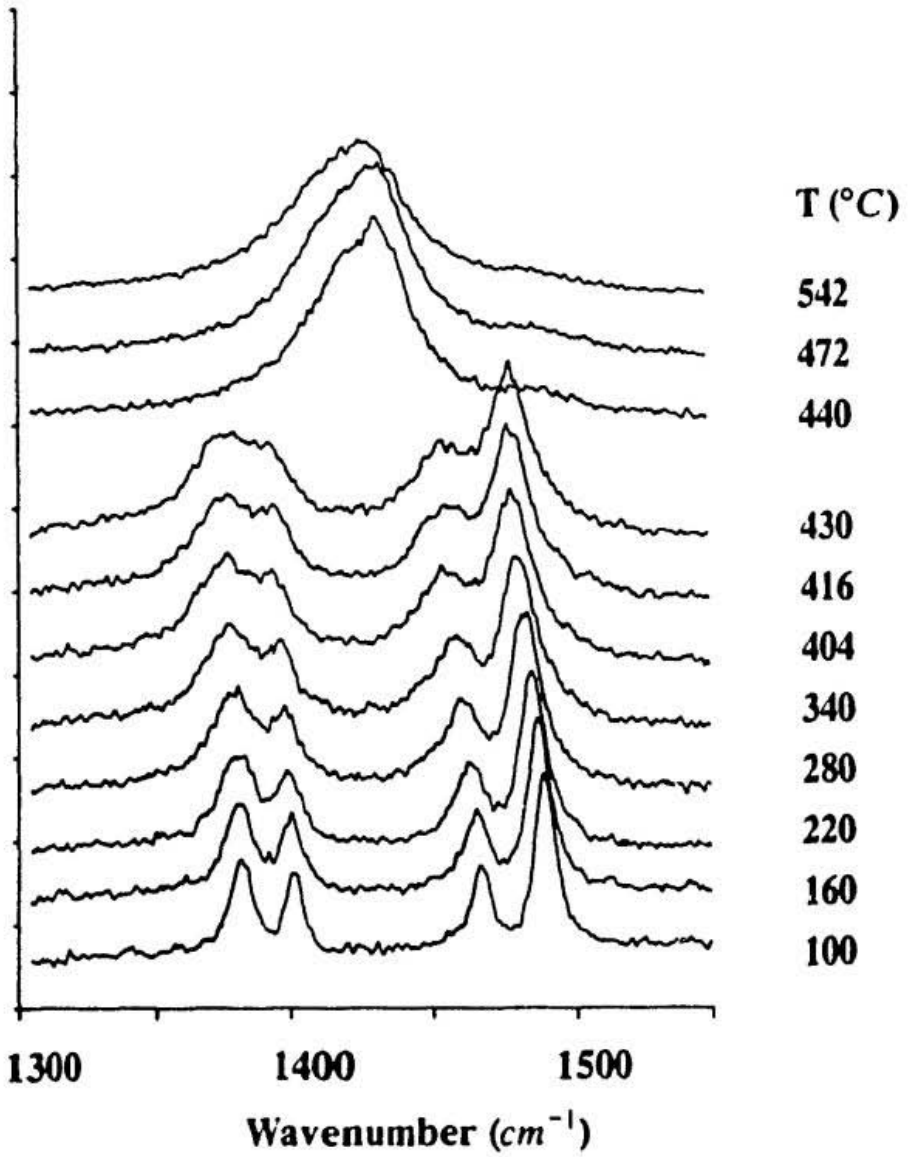

Fig. 10.8

Raman spectra in the ν_1 region for the $LiCsCO_3$ system at different temperatures at the temperatures as indicated. Slits 2 cm^{-1}.

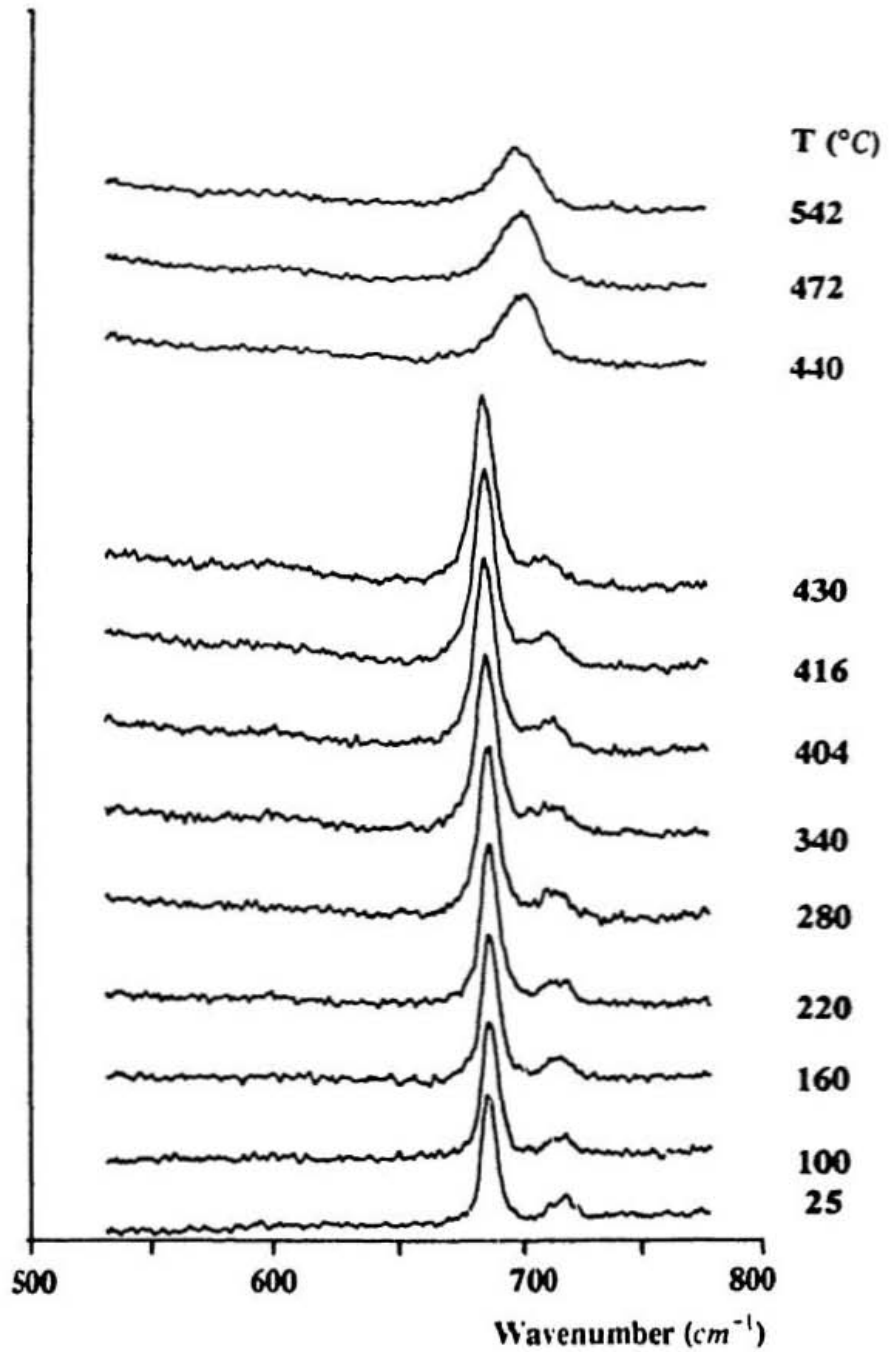

Fig. 10.9

Raman spectra in the ν_4 region for the $LiCsCO_3$ system at different temperatures at the temperatures as indicated. Slits 2 cm^{-1}.

Fig. 10.10

Raman spectra obtained from $LiCsCO_3$ at the temperatures just below (430°C, bottom) and above (440°C, top) the phase transition point (435°C). Slits 2 cm^{-1}.

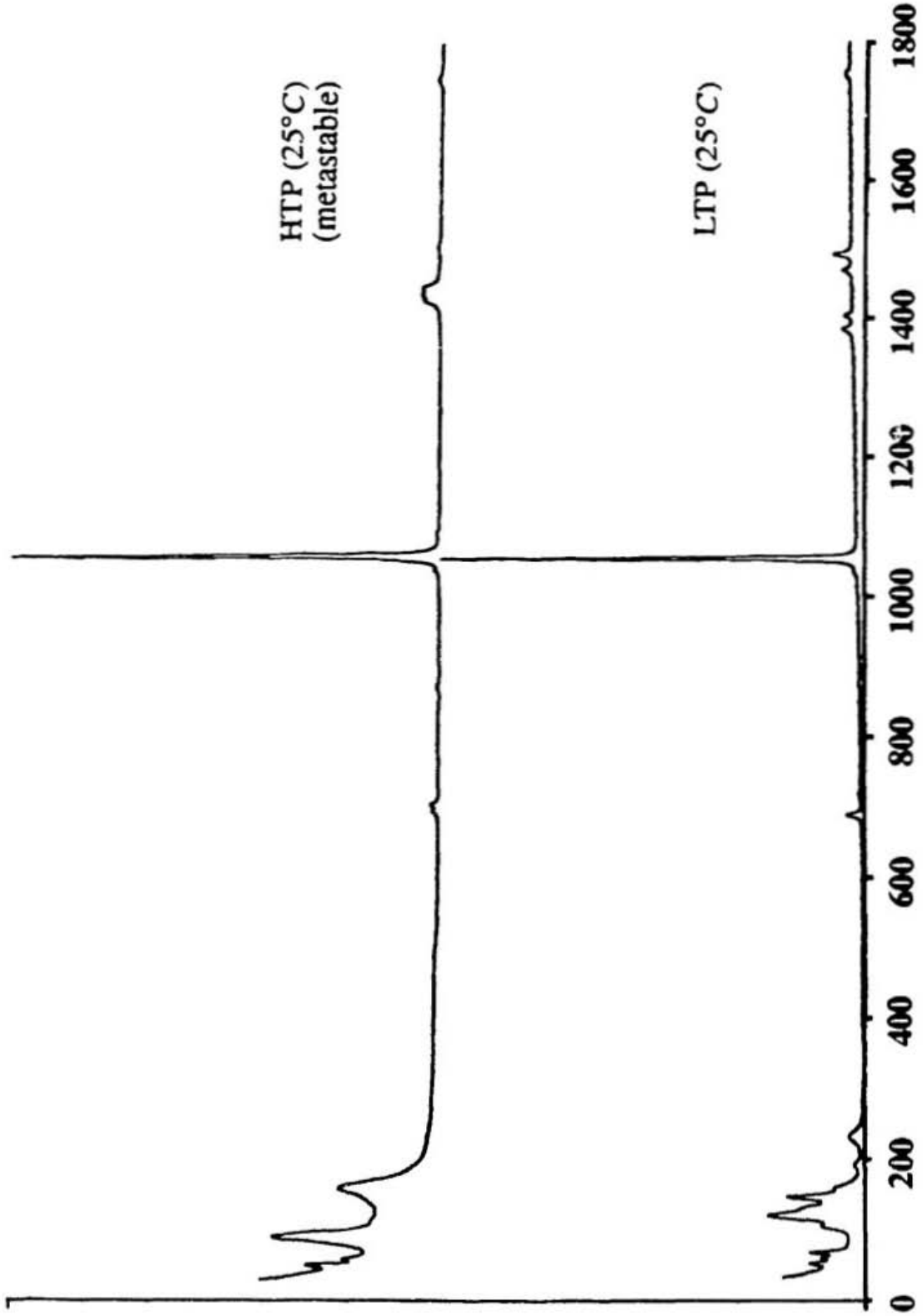
HTP (25°C)
(metastable)
LTP (25°C)
0
200
400
600
800
1000
1200
1400
1600
1800
Wavenumber (cm^{-1})

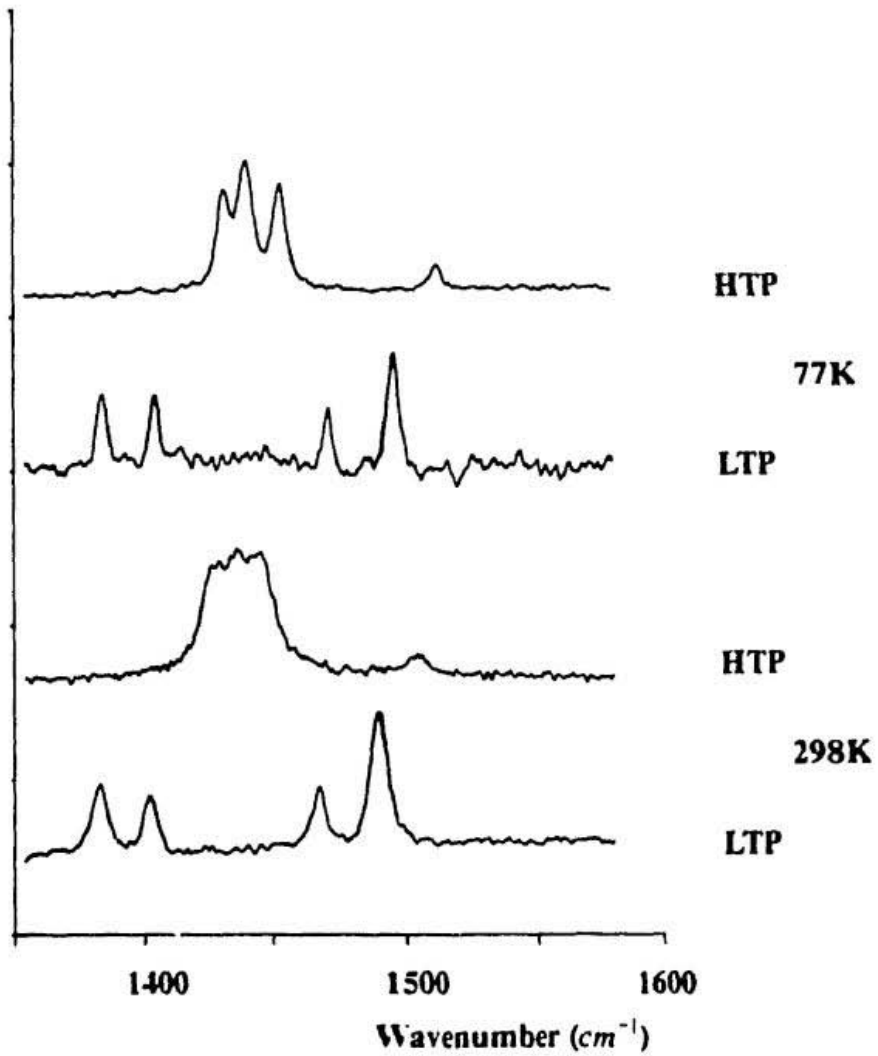

Fig. 10.11

Raman spectra in the ν_1 region for $LiCsCO_3$ in the LTP (slow cooled) and the metastable HTP (fast cooled) at 77K and 298K. Slits 2 cm^{-1}.

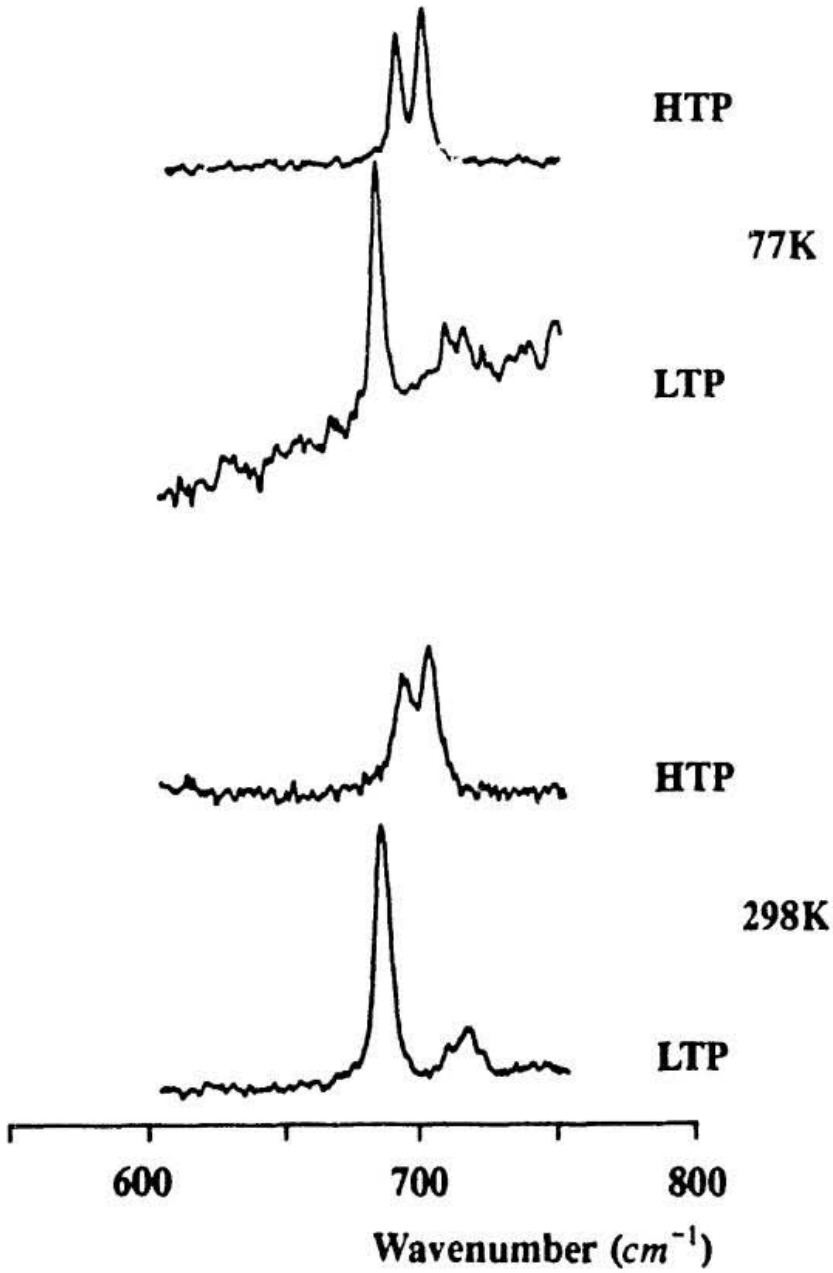

Fig. 10.12

Raman spectra in the ν_4 region for $LiCsCO_3$ in the LTP (slow cooled) and the metastable HTP (fast cooled) at 77K and 298K. Slits 2 cm^{-1}.

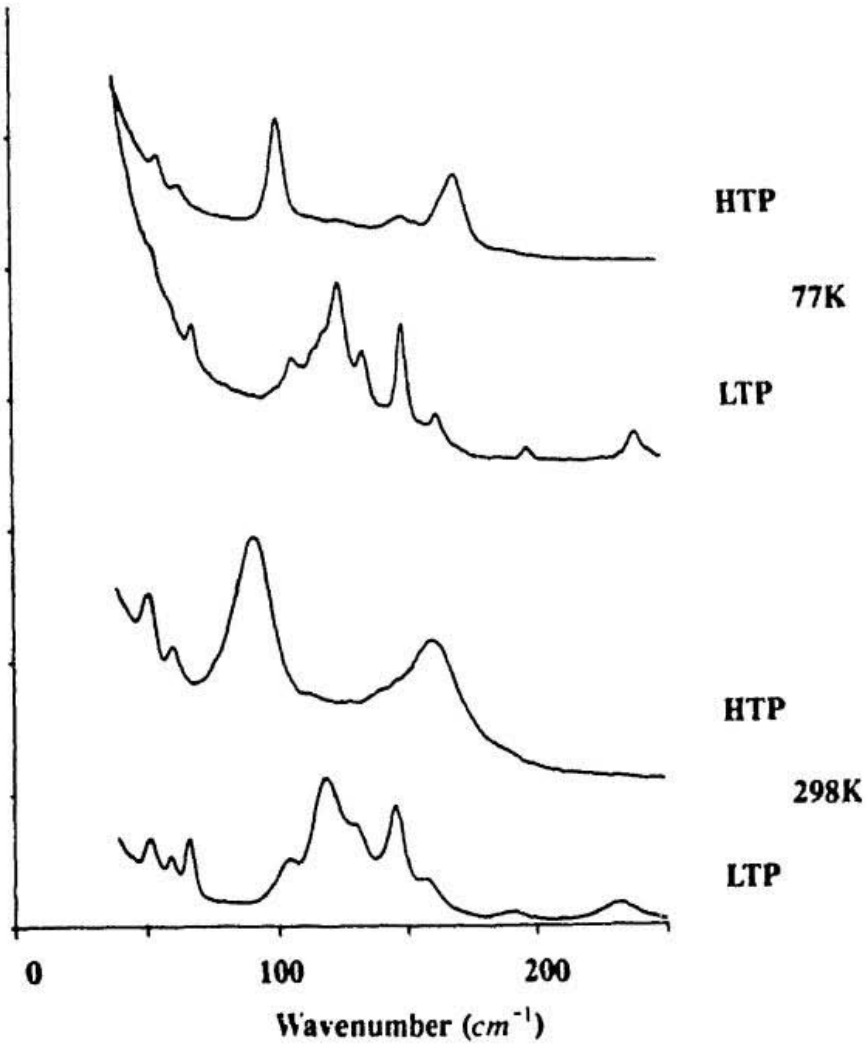

Fig. 10.13

Raman spectra in the external mode region for $LiCsCO_3$ in the LTP (slow cooled) and the metastable HTP (fast cooled) at 77K and 298K. Slits 2 cm^{-1}.

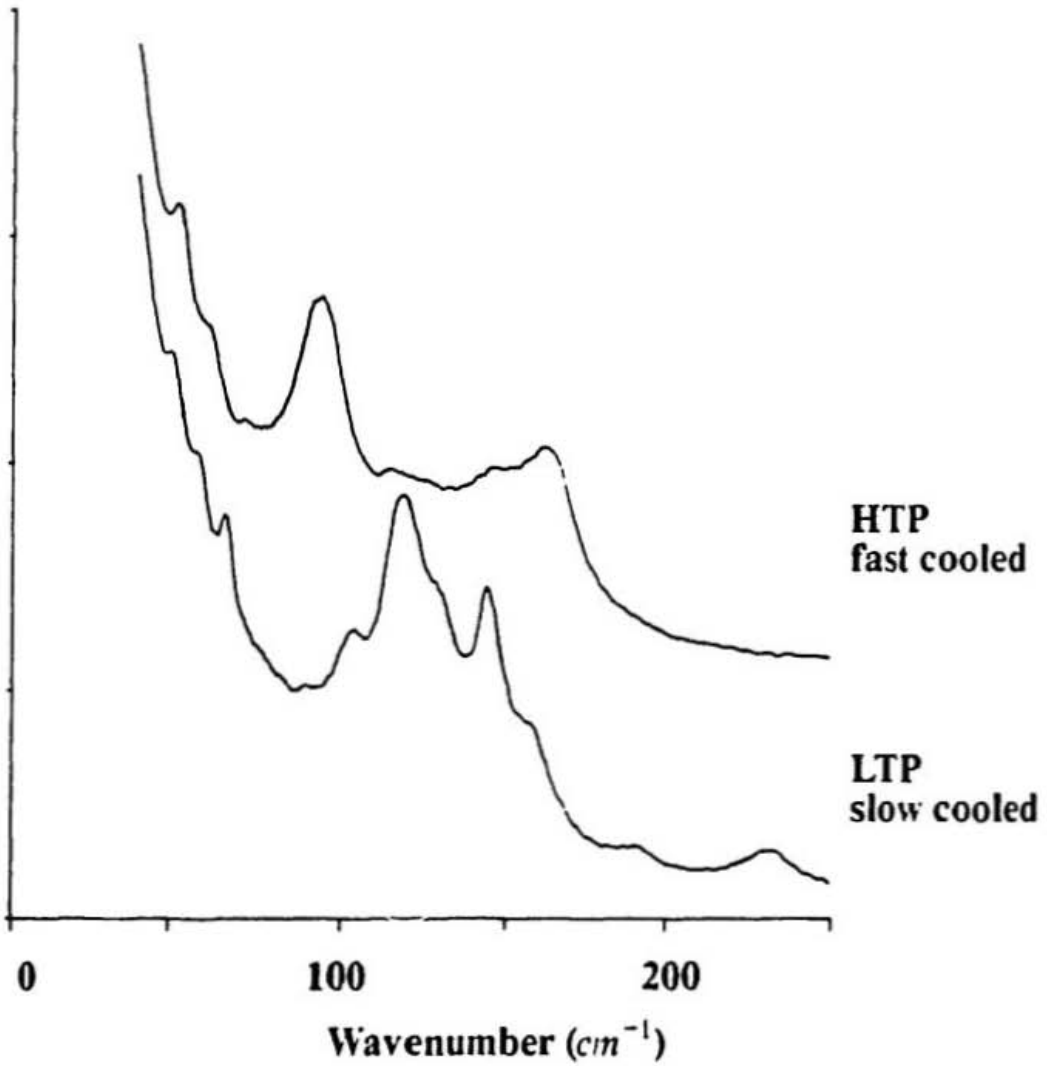

Fig. 10.14

Raman spectra in the external mode region for the $LiCsCO_3$ + Cs_2CO_3 mixture (mole ratio of Cs_2CO_3 and Li_2CO_3 is 0.67); 25°C; Slits 2 cm^{-1}.

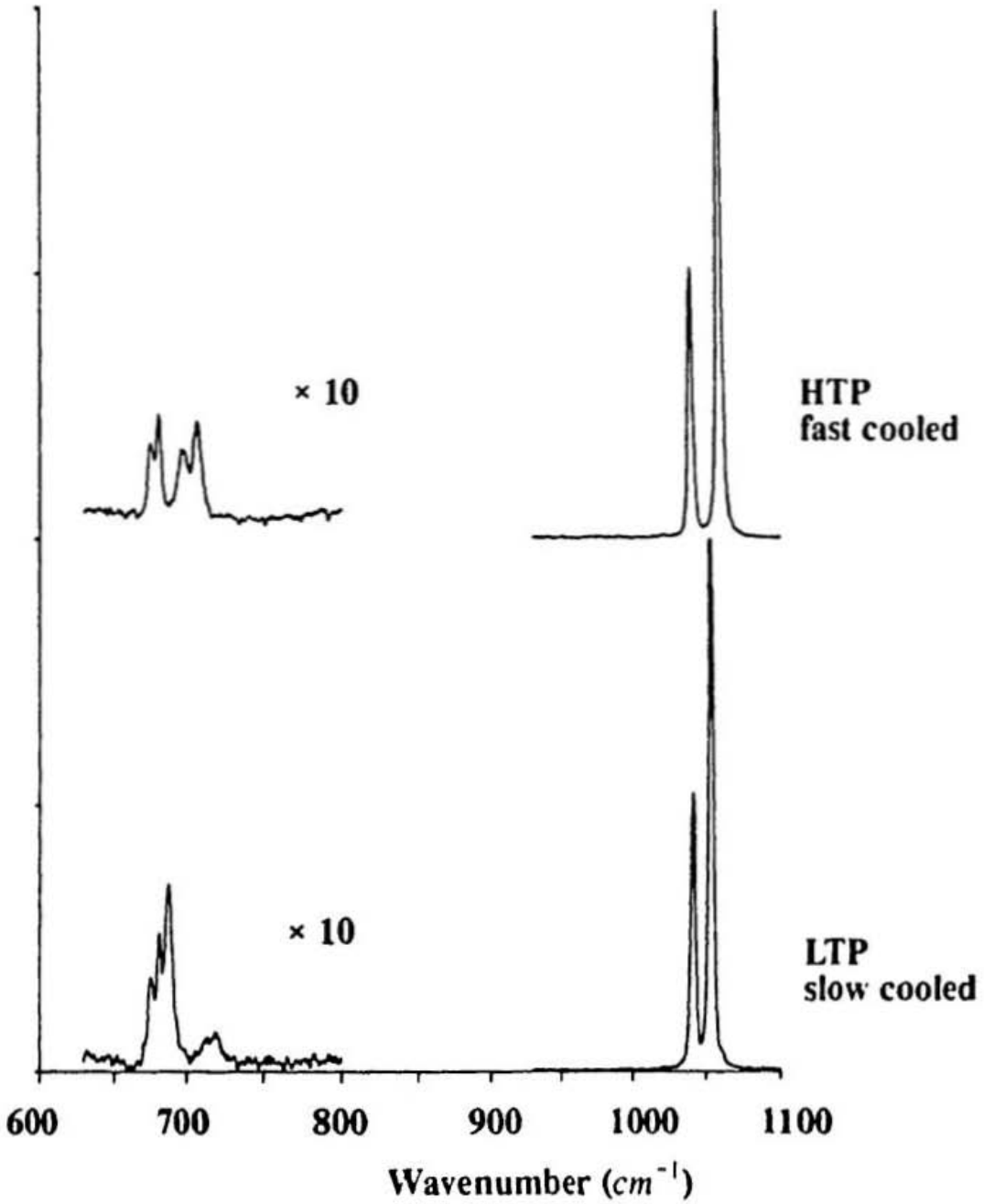

Fig. 10.15

Raman spectra in the ν_1 and ν_4 regions for the $LiCsCO_3$ + Cs_2CO_3 mixture (mole ratio of Cs_2CO_3 and Li_2CO_3 is 0.67); 25°C, Slits 2 cm^{-1}.

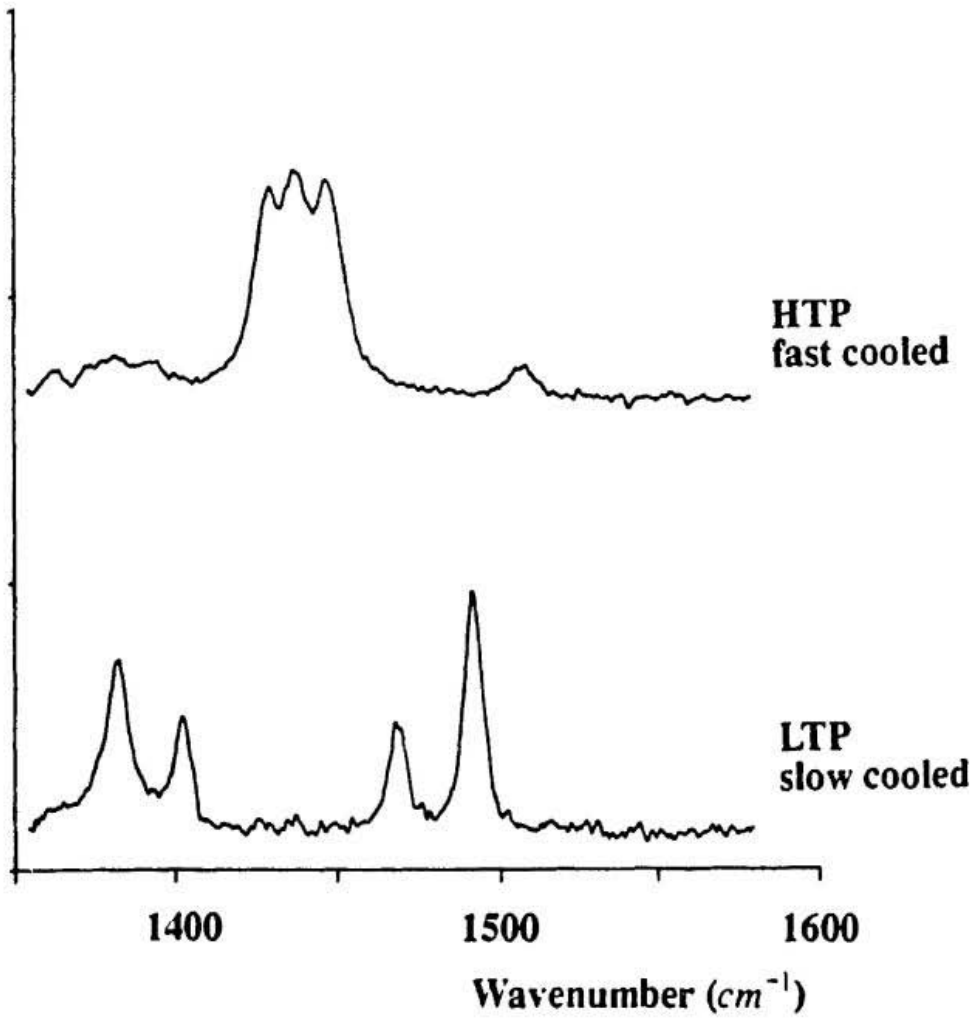

Fig. 10.16

Raman spectra in the ν_1 region for the $LiCsCO_3 + Cs_2CO_3$ mixture (mole ratio of Cs_2CO_3 and Li_2CO_3 is 0.67); 25°C; Slits 2 cm^{-1}.

Chapter 11

RAMAN STUDIES OF THE MOLTEN Li_2CO_3/LiCl AND Li_2CO_3/K_2CO_3 SYSTEMS

11.1 Introduction

Molten carbonate fuel cell is considered as a promising power-generating device for the effective utilization of fossil fuel energy by gasification [Liebhafsky 1968]. Carbonate mixtures are the only electrolytes which are invariant with respect to the electrochemical combustion of the hydrogen and carbon monoxide. The carbonate ion itself takes part in the reactions and the melt remains constant in composition by a continuous transfer of the carbonate ion from cathode to anode [Selman 1981]. A variety of electrolyte mixtures of alkali carbonates have been employed in molten carbonate fuel cells mainly because of the lower melting points of the eutectic mixtures. It was found that there is a trend of preferred composition of the molten mixtures [Selman 1981]. It seems important to investigate the properties of the mixed carbonates. Therefore the study of the local structure of the CO_3^{2-} ion in the molten mixture was initiated.

Raman spectroscopy has proven to be a powerful method to study the structure and physical and chemical properties of molten salts but few Raman measurements have been performed on the molten carbonate salts [Maroni 1970b, Bates 1972 and Matsumoto 1990]. The major problems arise from the experimental difficulties due to the high corrosiveness against glass, the high melting points and chemical decomposition.

As part of the program to study the molten carbonate salts, Raman measurements have been performed on the Li_2CO_3/LiCl and Li_2CO_3/K_2CO_3 melts.

11.2 Results and discussion

11.2.1 Li_2CO_3/LiCl melt

Polarized ($I_{\parallel}$) and depolarized ($I_{\perp}$) Raman spectra in a frequency range from 50 - 1800 cm^{-1} of molten Li_2CO_3/LiCl with the molar ratio 1:1 at 610°C are presented in fig. 11.1 (bottom). The isotropic spectrum, $I_{iso} = I_{\parallel} - 1.33I_{\perp}$, was produced from the corresponding polarized and depolarized spectra (fig. 11.1 top). The reduced polarized ($R_{\parallel}$, fig. 11.2 bottom) and depolarized ($R_{\perp}$, fig. 11.1 bottom) spectra are also shown. The 10 times scale expanded $R_{\parallel}$ spectrum in the frequency regions, 50-900 cm^{-1} and 1200-1800 cm^{-1}, is presented in fig. 11.2 (top). The positions and assignments of the bands observed are collected in table 11.1. The present Raman data are in good agreement with previous Raman studies by Bates et al. [Bates 1972] on the Li_2CO_3/LiCl melt and by Matsumoto et al. [Matsumoto 1990] on the pure Li_2CO_3 melt.

In the ν_4 region, a weak depolarized band centered at about 706 cm^{-1} was observed (figs. 11.1 and 11.2). In the ν_3 region two weak broad depolarized bands at about 1419 and 1514 cm^{-1} were observed (figs. 11.1 and 11.2). While only a very weak depolarized band at 872 cm^{-1} was observed in the ν_2 region. The $2\nu_2$, overtone, centered at about 1750 cm^{-1}. As expected the $2\nu_2$ band was polarized (figs. 11.1 and 11.2).

In the ν_1 region a strong polarized band at 1074.5 cm^{-1} appeared. The isotropic and anisotropic components of this ν_1 band were curvefitted by a Lorentzian function respectively (fig. 11.3). The depolarization ratio, $\rho = R_{aniso}/R_{iso}$, was calculated to be about 0.045. This is in excellent agreement with Matsumoto's result. It was reported that the depolarization ratio at the peak intensity of the ν_1 band is 0.044 for pure Li_2CO_3 melt at 750°C [Matsumoto 1990]. The full width at half height (FWHH) is about 24 cm^{-1} for the isotropic component of the ν_1 band, while it is about 38 cm^{-1} for the anisotropic component of this band. The additional bandwidth of the anisotropic component results from the reorientational motion of the CO_3^{2-} ion.

In the region from 50 to 600 cm^{-1} two broad components centered at about 200 and 400 cm^{-1} were observed (fig. 11.4b). The low frequency component at 200 cm^{-1} has been assigned to a mode associated with reorientational motions of a planar carbonate ion in a cation cage. A similar band was reported in molten nitrates [Brooker 1983]. This band (200 cm^{-1}) should be depolarized (fig. 11.4b). The intensity detected in the 200 cm^{-1} region of the R_{iso} spectrum probably arose from reflected background light (fig. 11.4c). The polarized band at about 400 cm^{-1} has been assigned to the symmetric stretching motions of Li^+ against Cl^- over a wide range of coordinations and environments (fig. 11.4a, b, c). Previous Raman studies indicated that the broad Raman band of molten alkali halides was highly polarized [e.g. Clarke 1972c, Giergiel 1984 and Raptis 1987]. The spectrum of the Li_2CO_3/K_2CO_3 melt showed only the feature at about 200 cm^{-1} (fig. 11.4d, e, f).

11.2.2 Li_2CO_3/K_2CO_3 melt

Polarized ($I_{\parallel}$) and depolarized ($I_{\perp}$) Raman spectra in a frequency range 50-1800 cm^{-1} of the molten Li_2CO_3/K_2CO_3 mixture with molar ratio 1:1 of Li and K at 570°C are presented in fig. 11.5. The corresponding isotropic spectrum, $I_{iso} = I_{\parallel} - 1.33I_{\perp}$, is also presented (fig. 11.5 top). The reduced polarized ($R_{\parallel}$) and depolarized ($R_{\perp}$) spectra are presented in fig. 11.6 (bottom). The peak frequencies and assignments are listed in table 11.1.

The position of the ν_4 band of the CO_3^{2-} ion shifted from 706 cm^{-1} for the Li_2CO_3/LiCl melt to about 696 cm^{-1} for the Li_2CO_3/K_2CO_3 melt. Similar shift in the ν_1 region was observed. Two broad, overlapped, weak and depolarized bands centered at about 1384 and 1493 cm^{-1} in the ν_3 region. The central frequency of the $2\nu_2$, overtone, was found to be about 1753 cm^{-1}.

In the ν_1 region, a strong polarized band at 1057.5 cm^{-1} was observed. The result of the curvefit with a Lorentzian function for the isotropic and anisotropic components of

the ν_1 band fig. 11.7) indicates that the depolarization ratio, $\rho = R_{max}/R_{max}$, is about 0.13. Compared to the diluted Li_2CO_3 in the LiCl melt the depolarization ratio of the ν_1 band of the CO_3^{2-} ion in the Li_2CO_3/K_2CO_3 molten mixture is much higher and may be due to stray light or a calibration factor. The FWHH of the isotropic (24 cm^{-1}) and anisotropic (39 cm^{-1}) components of the ν_1 band are almost identical with those for the Li_2CO_3/K_2CO_3 and Li_2CO_3/LiCl melts.

A significant result is the detection of the band due to the rotational oscillation motion of the CO_3^{2-} ion at about 145 cm^{-1} which was observed clearly in the depolarized spectrum of the Li_2CO_3/K_2CO_3 melt (fig. 11.4d).

Raman measurements indicate that the molten Li_2CO_3/LiCl and Li_2CO_3/ K_2CO_3 mixtures exhibited similar Raman spectra in the internal mode regions except for the slightly different peak positions. The characteristic bands observed from these two melts indicate no significant perturbation of the CO_3^{2-} ion in these molten mixtures. The fact that the anisotropic component of the ν_1 band is much broader than the isotropic component suggests a relatively long relaxation time for the reorientional motion of the CO_3^{2-} ion. The interaction between the CO_3^{2-} ions and alkali metal ions does not appear to be very strong.

Table 11.1

The Raman frequencies (cm^{-1}) of the molten Li_2CO_3/LiCl and Li_2CO_3/K_2CO_3 mixtures.

Li_2CO_3/LiCl	Li_2CO_3/K_2CO_3	assignments
610°C	570°C	
200(w, dp)*	145(w, dp)	
400(w, p)		
706(w)	696(w)	$\nu_4(E')$
872(vw)		$\nu_2(A_2'')$
1074.5(s, p)	1057.5(s, p)	$\nu_1(A_1')$
1419(w)	1384(w)	$\nu_3(E')$
1514(w)	1493(w)	
1750(m, p)	1753(m, p)	$2\nu_2$

* w = weak; vw = very weak; m = medium; s = strong; p = polarized.

Fig. 11.1

Polarized ($I_{\parallel}$), depolarized ($I_{\perp}$) (bottom), and isotropic (I_{iso}) (top) Raman spectra of the molten Li_2CO_3/LiCl mixture. 610°C; Slits 2 cm^{-1}.

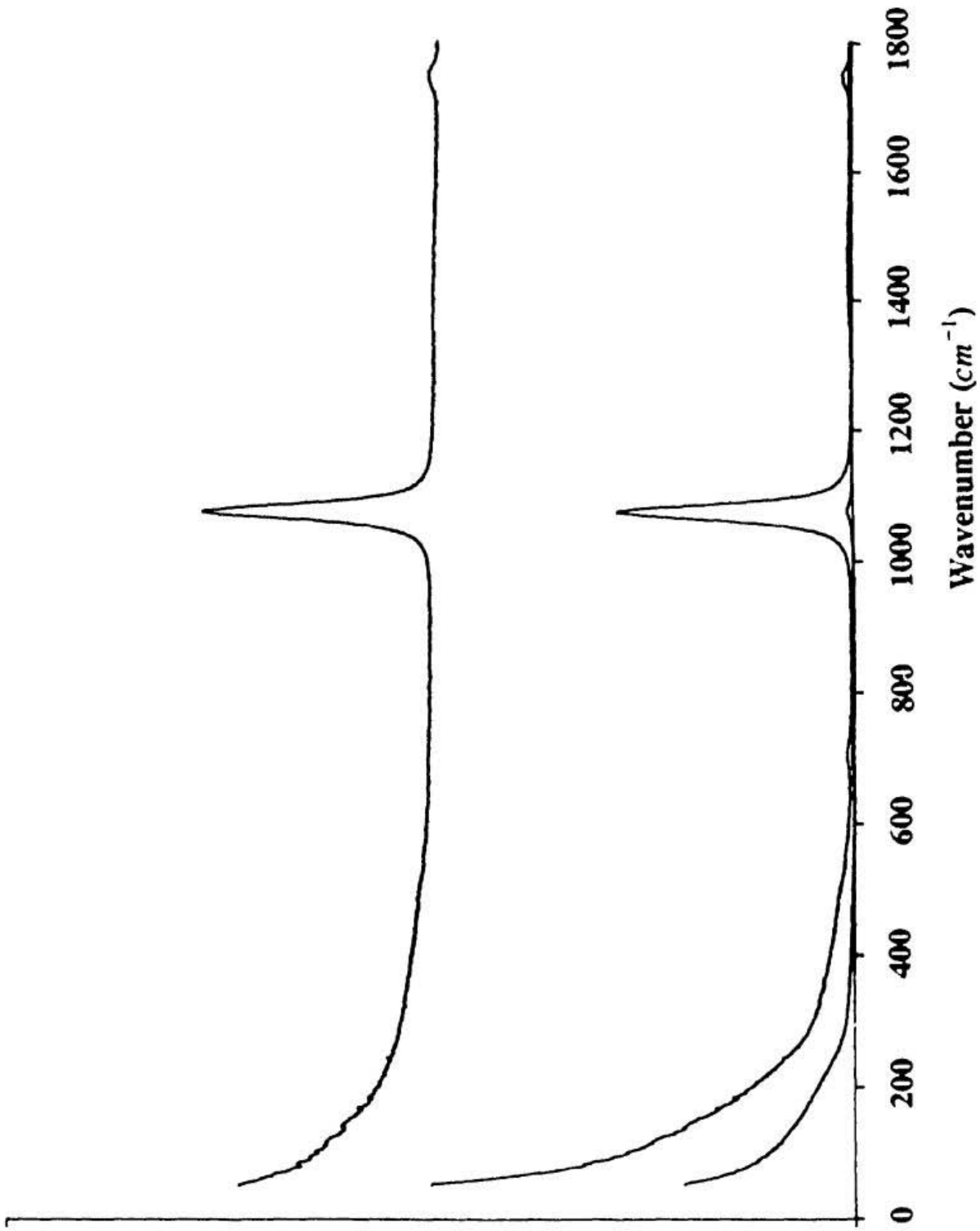
0
200
400
600
800
1000
1200
1400
1600
1800
Wavenumber (cm^{-1})

Fig. 11.2

Polarized ($R_{\parallel}$), depolarized ($R_{\perp}$) (bottom), and ten times scale expanded $R_{\parallel}$ (top) Raman spectra of the molten Li_2CO_3/LiCl mixture. 610°C; Slits 2 cm^{-1}.

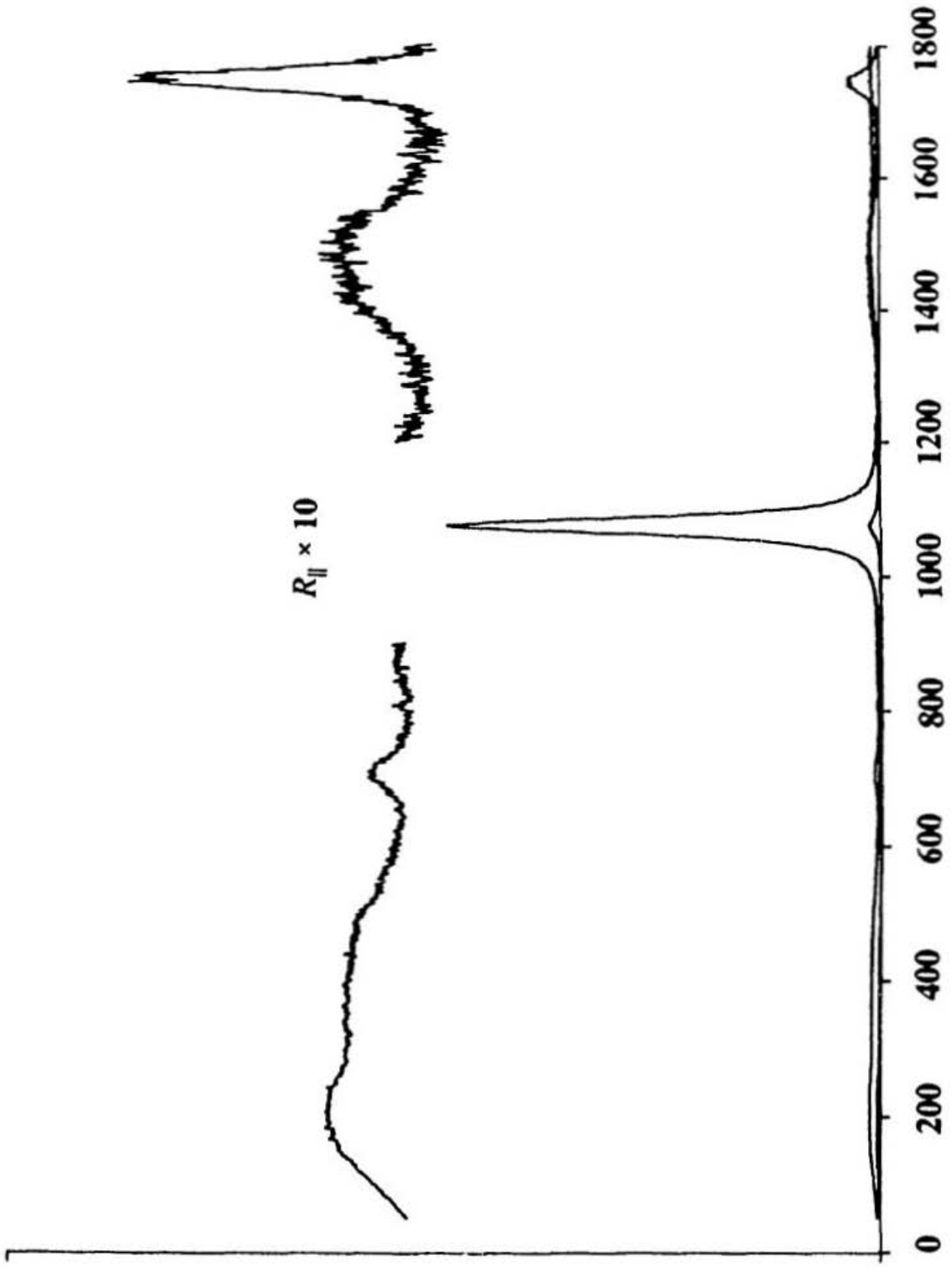
$R_{\parallel} \times 10$
0
200
400
600
800
1000
1200
1400
1600
1800
Wavenumber (cm^{-1})

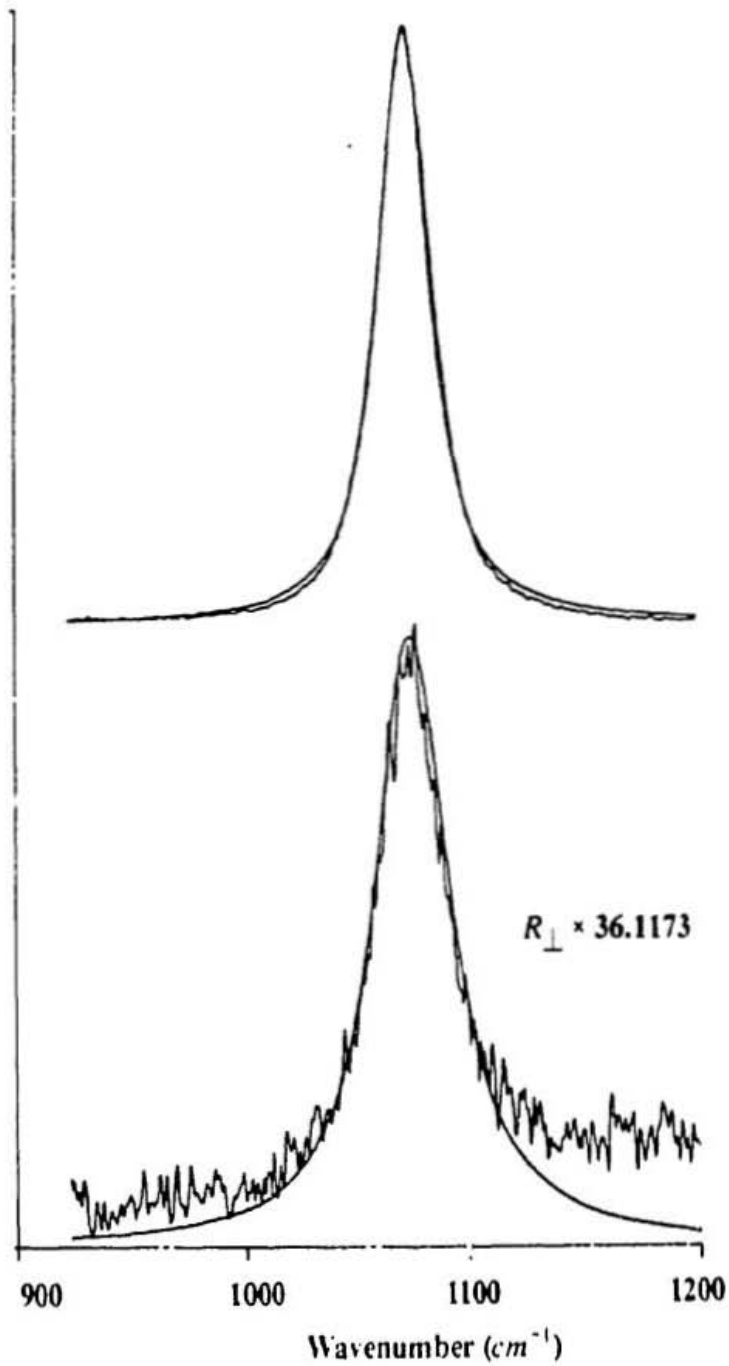

Fig. 11.3

Curvefit for the isotropic (R_{iso}) and anisotropic (R_{anis}) components of the ν_1 band for the Li_2CO_3/LiCl melt by a Lorentzian function (smooth lines).

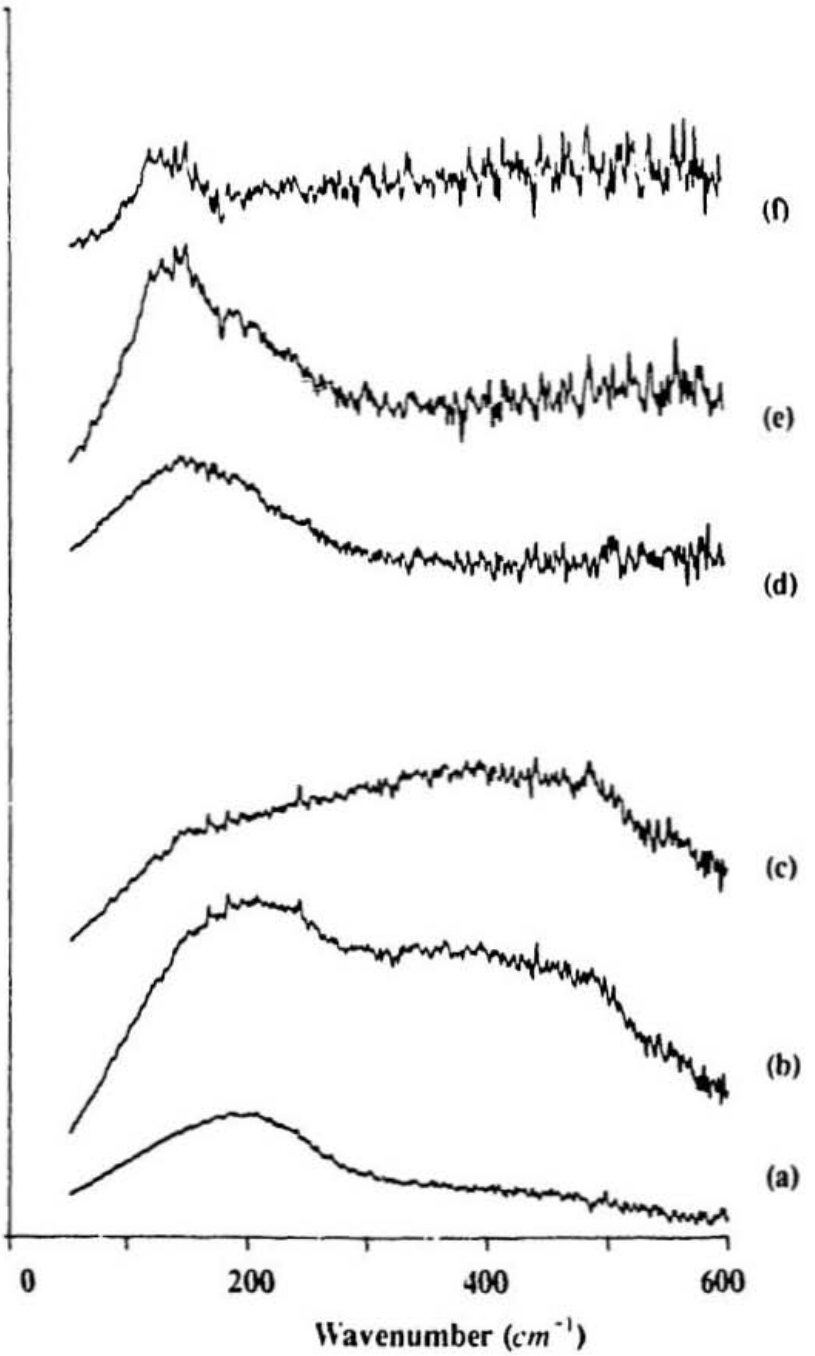

Fig. 11.4

The ten times scale expanded reduced Raman spectra of the molten Li_2CO_3/LiCl and Li_2CO_3/K_2CO_3 melts. Li_2CO_3/LiCl: (a) $R_{\perp}$, (b) $R_{\parallel}$, (c) R_{iso}; Li_2CO_3/K_2CO_3: (d) $R_{\perp}$, (e) $R_{\parallel}$, (f) R_{iso}.

Fig. 11.5

Polarized ($I_{\parallel}$), depolarized ($I_{\perp}$) (bottom), and isotropic (I_{iso}) (top) Raman spectra of the molten Li_2CO_3/K_2CO_3 mixture. 570°C; Slits 2 cm^{-1}.

* scattering from stray light

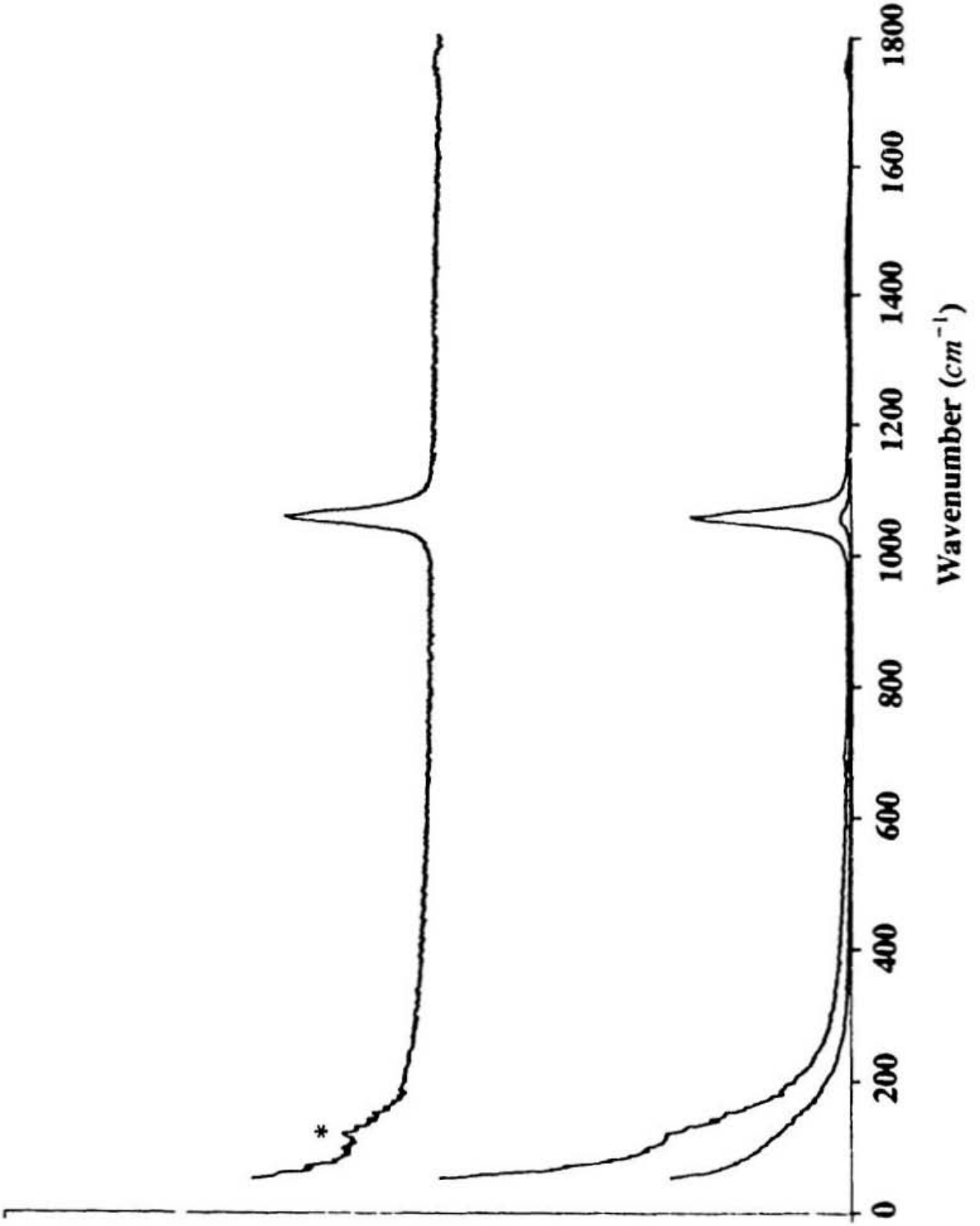
*
0
200
400
600
800
1000
1200
1400
1600
1800
Wavenumber (cm^{-1})

Fig. 11.6

Polarized ($R_{\parallel}$), depolarized ($R_{\perp}$) (bottom), and ten times scale expanded $R_{\parallel}$ (top) Raman spectra of the molten Li_2CO_3/K_2CO_3 mixture. 570°C; Slits 2 cm^{-1}.

* scattering from stray light

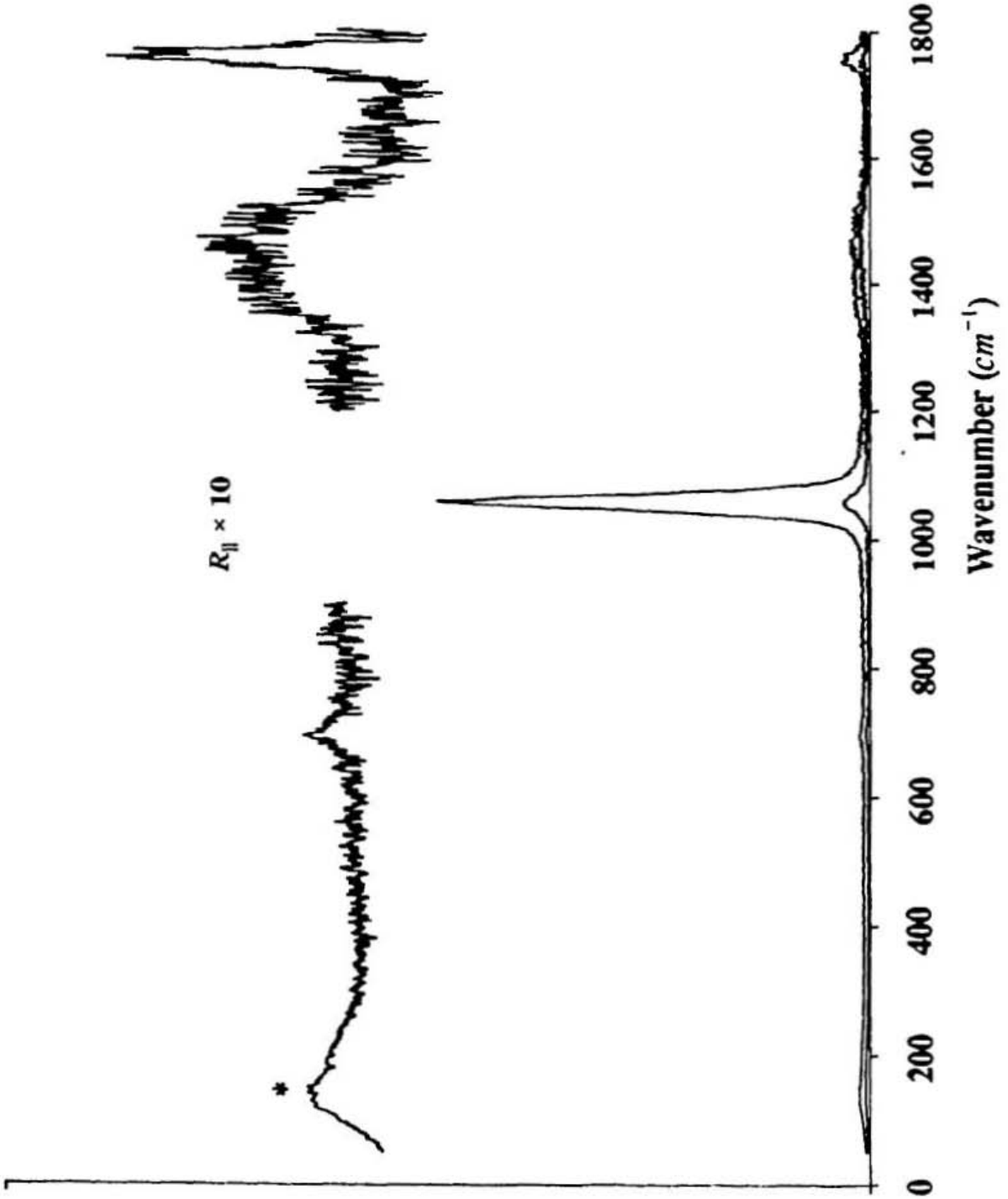
$R_{\parallel} \times 10$
*
0
200
400
600
800
1000
1200
1400
1600
1800
Wavenumber (cm^{-1})

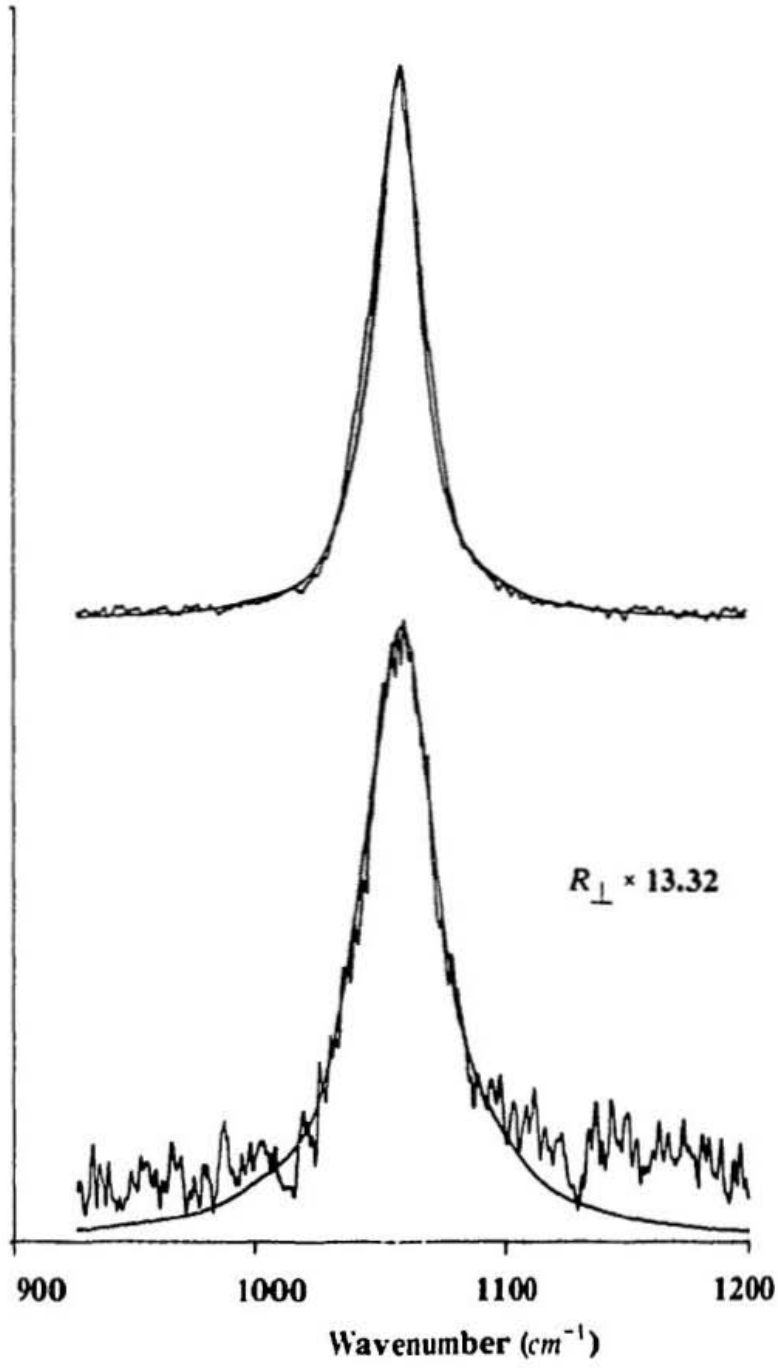

Fig. 11.7

Curvefit for the isotropic (R_{iso}) and anisotropic (R_{aniso}) components of the ν_1 band for the Li_2CO_3/K_2CO_3 melt by a Lorentzian function (smooth lines).

References

Adams, D.M. and Newton, D.C., *J. Chem. Soc. A* 3499 (1971).

Agrawal, B.S., Kirby R.D. and Hardy, J.R., *Phys. Rev.* **B11**, 5153 (1975).

Aleksandrov, K.S., Besnosikov, B.V. and Posdnjakova, L.A., *Ferroelectrics* **12**, 197 (1976).

Aleksandrov, K.S., *Ferroelectrics* **20**, 61 (1978).

Aleksandrov, K.S., Emelyanova, L.S., Misyul, S.V., Melnikova, S.V. Gorev, M.L., Kokov, I.T. and Schäfer, A.D., *Japanese J. of Applied Phys.* **24**, 399 (1985a).

Aleksandrov, K.S., Emelyanova, L.S., Misyul, S.V. and Kokov, I.T., *Solid State Communications* **53**, 835 (1985b).

Aleksandrov, K.S., Kokov, I.T., Mel'nikova, S.V. Misyul, S.V. and Flerov, I.N., *Sov. Phys. Solid state* **30 (12)**, 2098 (1988).

Anderson, A., Lo, Y.W. and Todoeschuck, J.P., *Spectroscopy Letters* **14(2)**, 105 (1981).

Balasubrahmanyam, K. and Nanis, L., *J. Chem. Phys.* **40**, 2657 (1964).

Bale, C.W. and Pelton, A.D., *Calphad* **6**, 255 (1982).

Balz, D., *Naturwissenschaften* **40**, 241 (1953).

Barr, R.M. and Goldstein, *J. Chem. Soc. Dalton*, 1180 (1974).

Barton, J.L. and Bloom, H., *Trans. Faraday Soc.* **55**, 1792 (1959).

Bates, J.B., Brooker, M.H., Quist, A.S. and Boyd, G.E., *J. Phys. Chem.* **76**, 1565 (1972).

Belyaev, I.N., Lesnykh, D.S., Doroshenko, A.K. and Eikhenbaum, I.G., *Zh. Prikl. Khim.* **45**, 665 (1972).

Bergerhoff, G. and Schmitz - Dumont, O., *Z. Anorg. Chem.* **284**, 10 (1956).

Bhagavantam, S. and Venkatarayudu, T., *Proc. Indian Acda. Sci. Sect.* **A9**, 224 (1939).

Bhagavantam, S., *Proc. Indian Acda. Sci. Sect.* **A13**, 543 (1941).

Bhagavantam, S. and Venkatarayudu, T., *Theory of Groups and its Application to Physical Problem* Audhra University, Waltair, India (1962).

Bhagavantam, S. and Venkatarayudu, T., *Theory of Groups and its Application to Physical Problem* Academic Press, New York and London (1969).

Biggin, S. and Enderby, J.E., *J. Phys. C: solid state phys.* **14**, 3577 (1981a).

Biggin, S. and Enderby, J.E., *J. Phys. C: solid state phys.* **14**, 3129 (1981b).

Biggin, S., Cummings, S., Enderby, J.E. and Blander, M., Proc. of the Fifth Int. Symp. on molten salts, las, vegas, NV. October 13-18, 1985. V80-1, The Electrochemical Society, Inc, Pennigton, NJ, Eds, M.-L. Saboungi, et al. pp81 - 96 (1986).

Blinc, R., Zeks, B. and Kind, R., *Phys. Rev. B* **17**, 3409 (1978).

Boardman, N.K., Dorman, F.H. and Heymann, E., *J. Phys. Chem.* **53**, 375 (1949).

Bohac, P., Gäumann, A. and Arend, H., *Mat. Res. Bull.* **8**, 1299 (1973).

Brandenberger, E., *Experientia* **3**, 149 (1947).

Brasseur, H. and Pauling, L., *J. Amer. Chem. Soc.* **60**, 2886 (1938).

Bredig, M.A., in *Molten Salts*, G. Mamantov, Ed. Marcel Dekker, New York, 1969.

Briat, B., Vervoitte, A., Canit, J.C. and Francke, E., *Solid State Commun.* **50**, 229 (1984).

Brooker, M.H., *J. Chem. Phys.* **63**, 3054 (1975).

Brooker, M.H., *J. Phys. Chem. Solids* **39**, 657 (1978).

Brooker, M.H. and Huang, C-H., *Mat. Res. Bull.* **15**, 9 (1980).

Brooker, M.H. and Perrot, M., *J. Chem. Phys.* **74**, 2795 (1981).

Brooker, M.H. and G.N. Papatheodorou, *Advance in Molten Salt Chemistry* vol. 5 , Editor, G. Mamanton, Elsevier, Amsterdam 1983 pp. 26-183.

Brooker, M.H., *The Chemical Physics of Solvation*, Ulstrup, J., Dogonadze, R.R., Kálmán, E. and Karnyshev, A.A., Eds., Elsevier, Netherlands, 1986, chapt. 4

Brooker, M.H., Nielsen, O.F. and Praestgaard, E., *J. Raman Spectroscopy* **19**, 71 (1988).

Brooker, M.H., Hancock, G., Rice, B.C. and Shapter, J., *J. Raman Spectroscopy* **20**, 683 (1989).

Bues, W., Z *anorg. allgem. Chem.* **279**, 104 (1955).

Bues, W., Demiray, F. and Φye, H.A., Z *Phys. Chem.* **84**, 18 (1973).

Bunten, R.A.J., McGreevy, R.L., Mitchell, E.W.J., Raptis, C. and Walker, P.J., *J. Phys. C: solid state phys.* **17**, 4705 (1984).

Cach, R., Tomaszewski, P.E. and Bornarel, J., *J. Phys. C:* **18**, 915 (1985).

Cape, J.A., White, R.L. and Feigelson, R.S., *J. Appl. Phys.* **40**, 5001 (1969).

Chabin, M. and Gilletta, F., *J. Appl. Cryst.* **13**, 533 (1980a).

Chabin, M. and Gilletta, F., *J. Appl. Cryst.* **13**, 539 (1980b).

Chang, J.R. and Mcpherson, G.L. *Inorg. Chem.* **14**, 3079 (1975).

Chang, I.F. and Mitra, S.S., *Adv. Phys.* **22**, 359 (1971).

Christian, J.W. and Vitek, *Rep. Prog. Phys.* **33**, 307 (1970).

Christmann, M., Sadeghi, N. and Papin, G., *Revue de Chimie Minrale* **t.15**, p312 (1978).

Christmann, M. and Papin, G., *Revue de Chimie Minrale* **16**, 485 (1979).

Clarke, J.H.R., Hartley, P.J. and Kuroda, Y., *J. Phys. Chem.* **76**, 1831 (1972a).

Clarke, J.H.R., Hartley, P.J. and Kuroda, Y., *Inorg. Chem.* **11**, 29 (1972b).

Clarke, J.H.R. and Woodcock, L.V., *J. Chem. Phys.* **57**, 1006 (1972c).

Clarke, J.H.R. and Hartley, P.J., *J. Phys. Chem.* **78**, 595 (1974).

Cleaver, B. and Kumar, S.P., *J. Chem. Soc. Faraday Trans.* **86**, 123 (1990).

Cochran, W., *Adv. Phys.* **9**, 387 (1960).

Cochran, W., *Adv. Phys.* **10**, 401 (1961).

Cohen, M.I., Young, K.F., Chang, Te-Tse and Brower, W.S., *J. Appl. Phys.* **42**, 5267 (1971).

Cotton, F.A., *Chemical Applications of Group Theory*, Wiley - interscience, New York (1990).

Cristol, B., Houriez, J. and Balesdent, D., *Thermochimica Acta* **23**, 337 (1978).

Damen, T.C., Porto, S.P.S. and Tell, B., *Phys. Rev.* **142**, 570 (1960).

Damen, T.C., Porto, S.P.S. and Tell, B., *Phys. Rev.* **144**, 771 (1966).

Davies, J.E.D. and Long, D.A., *J. Chem. Soc. A* 2054 (1968).

Davies, J.E.D. and Long, D.A., *J. Chem. Soc. (A)*, 1273 (1971).

De Vries, K.J. and Vansanten, J.H., *Physica* **29**, 482 (1963).

Dean, J.A., *Lange's Handbook of Chemistry*, Editor Dean, J.A., MaGraw-Hill, twelfth edition, 1978.

Denbeigh, K., *The Principles of Chemical Equilibrium* 2, Cambridge Press, 1968.

Dergurov, E.P., *Doklad. Adad. Nauk. S.S.S.R.* **64**, 517 (1949).

Dissanayake, M.A.K.L. and Mellander, B.E., *Solid State Ionics* **21**, 279 (1986).

Donnay, J.D.H. (Ed.) *Crystal Data-Determinative Tables* (2nd Ed.). Am. Cryst. Assoc. 1963.

Dork, R.A., Schubring, N.W. and Nolta, J.P., *J. Appl. Phys.* **35**, 1984 (1964).

Drobasheva, T.I., Ilyasov, I.I. and Tokman, I.A., *Rus. J. Inorg. Chem.* **16**, 517 (1971).

Ducloux, E.H., *Mikrochemie* **2**, 108 (1924).

Edwards, F.G., Enderby, J.E., Howe, R.A. and Page, D.I., *J. Phys. C: solid state phys.* **8**, 3483 (1975).

Edwards, F.G., Howe, R.A., Enderby, J.E. and Page, D.I., *J. Phys. C: solid state phys.* **11**, 1053 (1978).

Enderby, J.E., North, D.M. and Eglestaff, P.A., *Phil. Mag.* **14**, 961 (1966).

Fateley, W.G., McDevitt, N.T. and Bentley, F.F., *Appl. Spectrosc.* **25**, 155 (1971).

Fateley, W.G., Dollish, F.R., McDevitt, N.T. and Bentley, F.F., *Infrared and Raman Selection Rules for Molecular and Lattice Vibrations: The Correlation Method* Wiley-Interscience, New York (1972).

Ferrari, A. and Baroni, A., *R. C. Accad. Lincei* **6**, 48 (1927).

Ferraro, J.R. and Zjomek, J.S., *Introductory Group Theory and its Application to Molecular Structure*, Plenum Press, New York (1975).

Filippov, V.K., Yakimov, M.A. and Tam, C.T., *Z. Neorg. Khim.* **18**, 2269 (1973).

Fonseca, C.H.A., Rigeiro, G.M., Grazzinelli, R. and Chares, A.S., *Sol. St. Commun.* **46**, 221 (1983).

Forland, T. in *Fused salts*, B.R. Sundheim, Ed. McGraw - Hill, New York, 1964, p63

Fujii, Y., Hoshino, S., Yamada, Y. and Shirane, G., *Phys. Rev.* **B9**, 4549 (1974).

Gibbons, C.S., Reinsborough, V.C. and Whitla, W.A., *Can. J. Chem.* **53**, 114 (1975).

Giergiel, J., Subbaswamy, K.R. and Eklund, P.C., *Phys. Rev.* **B29**, 3490 (1984).

Gilbert, B., Mamantov, G. and Begun, G.M., *Inorg. Nucl. Chem. Lett.* **10**, 1123 (1974).

Gilbert, B., Mamantov, G. and Begun, G.M., *J. Chem. Phys.* **62**, 950 (1975).

Godeffroy, R., *Berichte D. Chem. Ges.* **8**, 9 (1875).

Gorban, I.S., Korenyuk, P.I. and Kutovoi, S.Yu. (Kie. Gos. Univ. Kiev. USSR), *Ukr. Fiz. Zh.* **35**, 366 (1990) (Russ. Ed).

Gordon, R.G., in *Advance in Magnetic Resonance*, Vol. 3, John Waugh, Academic press, 1968.

Gromakov, S.D., *Zhur. Fiz. Khim.* **24**, 641 (1950).

Habasaki, J., *Mol. Phys.* **69**, 115 (1990).

Haight, G.P., Spring, C.H. and Heilmann, O.J., *Inorg. Chem.* **3**, 195 (1964).

Haight, G.P. and Peterson, J.R., *Inorg. Chem.* **4**, 1073 (1965).

Halford, R.S., *J. Chem. Phys.* **14**, 8 (1946).

Harada, J., Sakata, M., Hoshino, S. and Hirotsu, S., *J. Phys. Soc. Jpn.* **40**, 212 (1976).

Heine, V., *Group Theory in Quantum Mechanics - An Introduction to its PresentUsage*, international monographs in pure and applied mathematics, Pergamon press, London (1960).

Herzberg, G., *Molecular Spectra and Molecular Structute: II Infrared and RamanSpectraofPolyatomicMolecules*, D. Van Nostrand Company, Inc., Princeton, New York (1945).

Hidaka, M., Wood, I.G., Wanklyn, B.M.R. and Garrakd, B.J., *J. phys. C: solid state phys.* **12**, 1799 (1979a).

Hidaka, M., Garrakd, B.J. and Wanklyn, B.M.R., *J. Phys. C: solid state phys.* **12**, 2737 (1979b).

Hidaka, M., Okamoto, Y. and Zikumayu, Y., *Phys. Stat. Sol. (a)* **79**, 263 (1983).

Hildebrand, I.H., *J. Chem. Phys.* **15**, 727 (1947).

Hiraishi, J., Taniguchi, N. and Takahashi, H., *J. Chem. Phys.* **65**, 3821 (1976).

Hirotsu, S., *J. Phys. Soc. Jpn.* **28**, 185 (1970).

Hirotsu, S., *J. Phys. Soc. Jpn.* **31**, 552 (1971).

Hodges, C.H., *Phys. Rev.* **187**, 994 (1969).

Hofmann, F., *Neues Jahrb. Min. Abt. A, Beil. Bd.* **55**, 149 (1926-27).

Hogervorst, A., Peterse, W.J.A.M. and Wolff, P.M. de, *AIP conf. Proc.* **53**, 217 (1979).

Holm, J.L., Holm, B.J., Rinnan, B. and Groenvold, F., *J. Chem. Thermodyn.* **5**, 97 (1973).

Horning, D.F., *J. Chem. Phys.* **16**, 1063 (1948).

Huang, C.H. and Brooker, M.H., *Chem. Phys. Lett.* **43**, 180 (1976).

Imaoka, K., Modorikawa, M., Ishibashi, Y. and Takagi, Y., *J. Appl. Phys. Jpn.* **11**, 120 (1972).

Inman, D. and Bockris, J.O'M., *Trans. Faraday Soc.* **57**, 2308 (1961).

Inman, D., *Electrochim. Acta* **10**, 11 (1965).

Iskandarov, K.I., and Ilyasov, I.I., *Zh. Neorg. Khim.* **21**, 1581 (1976).

Isupova, L.A. and Sobolev, E.V., *Zh. Strukt. Khim.* **9**, 324 (1968).

Janz, G.J. and Lorenz, M.R., *J. Chem. Eng. Data* **9**, 1419 (1963).

Johnston, D.F., *Rep. Prog. Phys.* **23**, 66 (1960).

Jones, H., in *Molecular Dynamics and Structure of Solids* p. 1. N.B.S. special publication (1969).

Julião, J.F., *Rev. Bras. Fisica* **3**, 17 (1973).

Kato, T., Umeura, J. and Kakenaka, T., *Mol. Phys.* **36**, 621 (1978).

Katsumata, K., Tire, T., Tanimoto, M. and Yoshizawa, H., *Phys. Rev.* **B25**, 428 (1982).

Kawabe, U., Yanagi, T. and Sawada, S., *J. Phys. Soc. Japan* **19**, 767 (1964).

Kawabe, U., Yanagi, T. and Sawada, S., *J. Phys. Soc. Japan* **20**, 2059 (1965).

Kind, R., Plesko, S. and Roos, J., *Phys. Stat. Sol.(a)* **47**, 233 (1978).

Kittel, C., *Introduction to solid state physics*, John Wiley and Sons, New York (1986).

Kohles, N., Theuerkaufer, H., Strobel, K., Geick, R. and Treutmann, W., *J. Phys. C: Solid State Phys.* **15**, L137 (1982).

Kuok, M.H., *J. Raman Spectroscopy* **14**, 264 (1983).

Lantratov, M.F. and Alabyshev, A.F., *J. Appl. Chem. USSR* **26**, 235 (1953).

Lantratov, M.F. and Moiseeva, O.F., *Zh. Fiz. Khim.* **34**, 171 (1960).

Lefebvre, J., Fouret, R. and Zeyen, C.M.E., *J. Physique* **45** (1984)

Lemos, V., Centoducatte, R., Melo, F.E.A., Filho, J.M., Moreira, J.E. and Martins, A.R.M., *Phys. Rev.* **B37**, 2262 (1988).

Lemos, V., Gomes, P.A.P., Melo, F.E.A., Filho, J.M. and Moreira, J.E., *J. Raman Spectroscopy* **20**, 155 (1989).

Li, Y.Y., *Sol. St. Commun.* **51**, 355 (1984).

Liebhafsky, H.A. and Cairns, E.J., *Fuel Cells and fuel Batteries*, Wiley, New York (1968), Chapters 2 and 13.

Long, D.A., *Raman Spectroscopy*, McGraw-Hill, New York 1977.

Lumsden, J., *Discuss. Faraday Soc.* **32**, 138 (1961).

Lund, P.A., Nielsen, O.F. and Praestgaard, E., *Chem. Phys.* **28**, 167 (1978).

MacGillavry, C.H., Nijveld, S. Dierdorp, S. and Karsten, J., *Rec. Trav. Chim.* **58**, 193 (1939).

Maciel, A., Ryan, J.F. and Walker, P.J., *J. Phy. C: solid state Phys.* **14**, 1611 (1981a).

Maciel, A. and Ryan, J.F., *J. Phys. C: solid state Phys.* **14**, L509 (1981b).

Maciel, A. and Ryan, J.F., *Journal DE Physique* C6-725, 1981

Margaca, F.M.A., McGreevy, R.L. and Mitchell, E.W.J., *J. Phys. C: solid state phys.* **17**, 4725 (1984).

Maroni, V.A. and Hathaway, E.J., *Electrochim. Acta* **15**, 1837 (1970a).

Maroni, V.A. and Cairns, E.J., *J. Chem. Phys.* **52**, 4915 (1970b).

Maroni, V.A., *J. Chem. Phys.* **54**, 4126 (1971).

Mathieu, J.P., *Spectres De Vibration et Symetrie*, Herman et cie, Paris (1945).

Matsumoto, M., Okazaki, S. and Okada, I., *J. Chem. Phys.* **92(2)**, 1515 (1990).

McGreevy, R.L. and Mitchell, E.W.J., *J. Phys. C: solid state phys.* **15** 5537 (1982).

Melo, F.E.A., Garrett, K.W., Mendes-Filho, J., Moreira, J.E. and Gurney, R.W., *Electronic Processes In Ionic Crystals* p54, Clarendon Press, Oxford (1957).

Melo, F.E.A., Garrett, K.W., Mendes-Filho, J. and Moreira, J.E., *Solid State Communication* **31**, 29 (1979).

Melo, F.E.A., Mendes-Filho, J., Moreira, J.E., Lemos, V. and Cerdeira F., *J. Raman Spectroscopy* **15**, 128 (1984).

Mendes-Filho, J., Melo, F.E. and Moreira, J.E., *J. Raman Spectroscopy* **8**, 199 (1979).

Mitchell, E.W.J., Poncet, P.F.J. and Stewart, R.J., *Phil. Mag.* **34**, 721 (1976).

Mitchell, E.W.J. and Raptis, C., *J. Phys. C: solid state phys.* **16**, 2973 (1983).

Møller, Chr. Knakkergaard, *Nature (London)* **180**, 981 (1957).

Møller, Chr. Knakkergaard, *Mat. Fys. Medd.* K. Dan Vindesk. Selsk **32** No. 2. 1959. IP Møller, Chr. Knakkergaard, *Mat. Fys. Medd.* K. Dan Vindesk. Selsk **32** No. 15. 1960.

Møller, Chr. Knakkergaard, *Acta Chem. Scand.* **A31**, 669 (1977).

Murphy, W.F., Brooker, M.H., Nielsen, O.F., Praestgaard, E. and Bertie, J.E., *J. Raman Spectroscopy* **20**, 695 (1989).

Mustajoki, A., *Ann. Acda. Sci. Fenn.* AVI No. 6., 1957 [Chem. Abs. 52:5111f].

Náray-Szabo, St., *Structure Reports* **11**, 454 (1947 -1948).

Narayanan, P.S., Ramdas, S. and Rao, C.N.R., *Phys. Lett.* **29A**, 528 (1969).

Natarajan, M. and Prakash, B., *Phys. Stat. Sol. (a)* **4**, K167 (1971).

Narayanan, P.S., *Ind. J. Pure Appl. Phys.* **10**, 514 (1973).

Natarajan, M., Howard - Lock, H.E. and Brown, I.D., *Can. J. Chem.* **56**, 1192 (1978).

Neu, J.T. and Gwinn, W.D., *J. Amer. Chem. Soc.* **70**, 3463 (1948).

Newns, D.M. and Staveley, L.A.K., *Chem. Rev.* **66**, 267 (1966).

Nielsen, O.F., Lund, P.A. and Praestgaard, E., *J. Chem. Phys.* **75**, 1585 (1981).

Oberschmidt, J. and Lazarus, D., *Phys. Rev.* **B21**, 5813 (1980).

Oyamada, R., *J. Phys. Soc. of Japan* **36**, 903 (1974).

Ozin, G.A., *Can. J. Chem.* **48**, 2931 (1970).

Perrot, M., Brooker, M.H. and Lascombe, J., *J. Chem. Phys.* **74**, 2787 (1981).

Perry, C.H. and Agrawal, E.K., *Solid State Commun.* **8**, 225 (1970).

Person, Willis B. and Zerbi, G., *Vibrational intensities in Infrared and Raman Spectroscopy* , Elsevier scientific publishing company, Amsterdam - Oxford - New York 1982

Petrov, V.V., Bogdanova, A.V., Bagina, M.A., Zavodnik, V.E., Gladyshevskii, E.I., Pecharskii, V.K. and Mokraya, I.R., *Kristallografiya* **32(2)**, 495 (1987).

Placzek, G., Rayleigh-streuung und Raman-effekt, in Handbuck der Radiologie vol. VI, Ed. by E. Marx, Akademische verlagsgesellschaft, Leipzig, 1934

Ramakrishnan, V., Nayar, V.U. and Aruldhas, G., *Infrared Phys.*, **25**, 607 (1985).

Raman, C.V. and Krishnan, K.S., *Nature* **121**, 501 (1928).

Raman, C.V. and Nedungadi, T.M.K., *Nature (lond.)* **145**, 147 (1940).

Rangaprasad, *Pramana* **11**, 81 (1978).

Raptis, C. and Mitchell, E.W.J., *J. Phys. C: solid state phys.* **20**, 4513 (1987).

Reinsborough, V.C. and Wetmore, F.E.W., *Austral. J. Chem.* **20**, 1 (1967).

Reisman, A., *J. Amer. Chem. Soc.* **80**, 3558 (1958).

Rimbach, E., *Berichte D. Chem. Ges.* **35**, 1298 (1902).

Rousseau, D.L., Bauman, R.P. and Porto, S.P.S., *J. Raman Spectroscopy* **10**, 253 (1981).

Ruddlesden, S.N. and Popper, P., *Acta Cryst.* **11**, 54 (1958).

Rytter, E., *Aluminium, Gallium and Indium Halide Complexs*, Institutt for Uorganisk Kjemi, Norges Tekniske HΦgskole, Universitetet I Trondheim. 1974.

Rytter, E., Φye, H.A., Cyvin, S.J., Cyvin, B.N. and Klaeboe, P., *J. Inorg. Nucl. Chem.* **35**, 1185 (1973).

Sadoc, A. and Guillo, R., *C. R. Acad. Sci.* **273**, 203 (1971).

Sahni, V.C. and Roy, A.P., *Phys. Status Solidi* **75**, K31 (1976).

Sakata, M., Harada, J., Rouse, K.D. and Cooper, M.J., *Acta Cryst.* **A34**, S284 (1978).

Sakudo, T., Unoki, H., Fujii, Y., Kobayashi, J. and Yamada, M., *Phys. Lett.* **A28**, 542 (1969).

Sawada, S., Nomura, S. and Fujii, S., *J. Phys. Soc. Japan* **13**, 1549 (1958).

Sawada, S., Nomura, S. and Asao, Y., *J. Phys. Soc. Japan* **16**, 2486 (1961).

Scherer, J.R., In *Advance in Infrared and Raman spectroscopy*, vol. 5, Clark, R.J.H. and Hester, R.E. Eds, Heyden, London, Chapter 3, p149, 1978.

Schonland, D., *Molecular Symmetry*, Van Nostrand, London (1965).

Scott, J.F., *Reviews of Modern Physics* **46**, 83 (1974).

Scott, J.F., *Light scattering near phase transition* Chapter 5 Edited H.Z. Cummins and A.P. Levanyuk 1983

Seifert, H.J. and Koknat, F.W., Z *Anorg. Allg. Chem.* **341**, 269 (1965).

Seifert, H.J. and Koknat, F.W., Z *Anorg. Allg. Chem.* **357**, 314 (1968).

Seifert, H.J., Preuss, N. and Sandrock, J., *Experientia, Suppl.* **37**, 23 (1979).

Seifert, H.J. and Thiel, G., *Thermochimica Acta* **100**, 81 (1986).

Selman, J.R. and Maru, H.C., *Advances in molten salt chemistry*, Ed. Mamantov, G. and Braunstein, J. v. **4**, p159, 1981.

Shabana, A.A.A.A., "*Raman Spetroscopy Studies of Manganese Chloride - Alkali metal Chloride systems* Ph.D thesis in Memorial University of Newfoundland, St. John's, NF, Canada. 1985

Sharma, D.P., *Pramana* **13**, 223 (1979).

Sherwood, P.M.A., *Vibrational Spectroscopy of Solids* Published by the Syndics of the Cambridge university press, London 1972.

Shinnaka, Y., *J. Phys. Soc. Japan* **17**, 820 (1962).

Shiroishi, Y., *J. Phys. Soc. Japan* **40**, 911 (1976).

Shuker, R. and Gammon, R.W., *J. Chem. Phys.* **55**, 4784 (1971).

Siegel, S. and Gebert, E., *Acta Cryst.* **17**, 790 (1964).

Simkovich, G., *J. Phys. Chem. Solids* **24**, 213 (1963).

Smith, H.M.J., *Phil. trans.* **A241**, 105 (1948).

Snyder, R.G. and Scherer, J.R., *J. Polymer Sci.* **18**, 421 (1980).

Struktur, Z. and Schmitz-Dumont, O., *Angew. Chem.* **64**, 613 (1952).

Stucky, G.D., *Acta Cryst.* **B24**, 330 (1968).

Swanson, H.E., McMurdie, H.F., Morris, M.C. and Evans, E.H., *Standard X-ray Diffraction Powder Patterns*, U.S. Nat. Bureau of standards, Monograph No. 25, Sec. 5 (1967).

Takagi, Yoshiki, Itoh, Noriko and Nakamura, Tetsur, *J. Chem. Soc. Faraday Trans. I* **85(3)**, 493 (1989).

Tanaka, M., Balasubrahmanyam, K. and Bockris, J.O'.M., *Electrochim. Acta* **8**, 261 (1963).

Tanisaki, S., *J. Phys. Soc. Japan* **16**, 579 (1961).

Tanisaki, S., Mashiyama, H., Hasebe, K., Shiroishi, Y. and Sawada, S., *Acta Crystallogr.* **B36**, 3084 (1980).

Teeters, D. and Frech, R., *Phys. Rev.* **B26**, 5877 (1982a).

Teeters, D. and Frech, R., *Phys. Rev.* **B26**, 4132 (1982b).

Teeters, D., *J. Chem. Phys.* **76**, 799 (1982c).

Timmermans, J., *J. Phys. Chem. Solids* **18**, 53-61 (1961).

Tinkham, M., *Group Theory and Quantum Mechanics* International series in pure and applied physics, McGraw - Hill, New York (1964).

Torsi, G., Mamantov, G. and Begun, G.M., *Inorg. Nucl. Chem. Letters* **6**, 553 (1970).

Toupry-Krauzman, N. and Poulet, H., *J. Raman spectroscopy* **7**, 1 (1978).

Toupry, N., Poulet, H., Postollec, M.Le, Pick, R.M. and Yvince, M., *J. Raman spectroscopy* **14**, 166 (1983).

Wells, A., *Structural Inorganic Chemistry* 5th Ed. Clarendon press, Oxford, (1984).

Welsh, H.L., Crawford, M.F., and Scott, G.D., *J. Chem. Phys.*, **16**, 97 (1948).

Wilkinson, G.R., *In the Raman Effect* vol. 2 Edited by Anderson, A., Marcel Dekker, New York 1973 Chapt. 1

Willensen, B., *J. Inorg. Nucl. Chem.* **33**, 3963 (1971).

Wilson, E.B., Decuis, I.D. and Cross, P.C., *Molecular Vibrations*, McGraw-Hill Book Company, Inc., New York (1955).

Winston, H. and Halford, R.S., *J. Chem. Phys.* **17**, 607 (1949).

Wittorf, N.M.V., *Z Anorg. Ch.* **39**, 195 (1904).

Wolff, P.M. de and Tuinstra, F., *Zeitschrift fr Kristallographie* **179**, 241 (1987).

Woodward, L.A., in *Raman Spectroscopy*, Szymanski, H.A. Ed. Plenum Press, New York 1967

Wyckoff, R.W.G., *Crystal Structure* **v. 2** Second Edition Interscience Publishers, a division of John Wiley and Sons, New York, London, Sydney (1965a).

Wyckoff, R.W.G., *Crystal Structure* **v. 3** Second Edition Interscience Publishers, a division of John Wiley and Sons, New York, London, Sydney (1965b).

Wyckoff, R.W.G., *Crystal Structure* **v. 1** Second Edition Interscience Publishers, a division of John Wiley and Sons, New York, London, Sydney (1965c).

Yie, S.S., *Acta Phys. Sinica* **33**, 235 (1983).

Yanagi, T. and Sawada, S., *J. Phys. Soc. Japan* **18**, 1228 (1963).

Yanagi, T., *Proc. Phys. Soc.* **82**, 954 (1963).

Yoshida, I. and Sawada, S., *J. Phys. Soc. Japan* **15**, 199 (1960).

Yoshida, S. and Oyamada, R., *Denki Kagaku* **41**, 221 (1973).

Zbinden, R. *Infrared Spectroscopy of high Polymers*, Academic Press, New York and London (1964).

Zelezny, V., Simon, P., Gervais, F. and Barta, C., *J. Phys. C: solid state phys.* **21**, 4727 (1988).

Zhang, Ming-sheng, Katiyar, R.S. and Scott, J.F., *Ferroelectrics* **74**, 309 (1987).

Фуе, H.A., Rytter, E., Klaeboe, P. and Cyvin, S.J., *Acta Chem. Scand.* **25**, 559 (1971).